D 2024

U.PORTO
FEUP FACULDADE DE ENGENHARIA
UNIVERSIDADE DO PORTO

INNOVATIVE STRATEGIES FOR THE PRODUCTION OF SOLKETAL BASED ON THE SIMULATED MOVING BED REACTOR TECHNOLOGY

ISABELLA CORRÊA

TESE DE DOUTORAMENTO APRESENTADA
À FACULDADE DE ENGENHARIA DA UNIVERSIDADE DO PORTO EM
PROGRAMA DOUTORAL DE ENGENHARIA QUÍMICA E BIOLÓGICA

Doctoral Program in Chemical and Biological Engineering

Innovative strategies for the production of solketal based on the simulated moving bed reactor technology

Dissertation presented to the Faculty of Engineering of the University of Porto for the PhD degree in Chemical and Biological Engineering

by

Isabella Pires Ferreira Corrêa

Supervisor:

Prof. Dr. Alírio Egídio Rodrigues

Co-supervisor:

Dr. Rui Pedro Vieira Faria

LSRE – Laboratory of Separation and Rection Engineering

Associated laboratory LSRE-LCM

Department of Chemical Engineering, Faculty of Engineering of the University of Porto

2024

This work was supported by national funds through FCT/MCTES (PIDDAC): LSRE-LCM, UIDB/50020/2020 (DOI: 10.54499/UIDB/50020/2020) and UIDP/50020/2020 (DOI: 10.54499/UIDP/50020/2020); and ALiCE, LA/P/0045/2020 (DOI: 10.54499/LA/P/0045/2020). This research was also funded by project PTDC/QEQ-ERQ/2698/2014 – POCI-01-0145-FEDER-016866 - funded by FEDER funds through COMPETE2020 - Programa Operacional Competitividade e Internacionalização (POCI) and by national funds through FCT - Fundação para a Ciência e a Tecnologia, I.P.

Isabella Corrêa gratefully thanks FCT for the Doctoral Grant (2020.07258.BD) through NORTE2020 — Programa Operacional Regional do Norte from the FSE — Fundo Social Europeu of the UE.

Acknowledgments

To God, the ultimate source of wisdom and knowledge, the first acknowledgment. I am thankful for His inspiration and for guiding my mind and heart in this research.

I am deeply thankful for my supervisor, Professor Alírio Rodrigues, for the unwavering support. His immense knowledge is truly inspiring, and his guidance shaped me professional and personally. I am privileged for having the chance of hearing so many Life Stories, being part of his team and be one of the many people that have been impacted through his history.

I am also sincerely grateful for my inspiring co-supervisor, Dr. Rui Faria. His dedication, attention, patience and intelligence are beyond words. Beyond co-supervisor, he is a true friend.

I am blessed for being included in LSRE, a group with so many spirited and smart people. Especial thanks to Professor Alexandre Ferreira and Professor Ana Mafalda Ribeiro for the advice and fruitful discussions, notably for Alexandre's sensitivity and Mafalda's pragmatism.

My dear friends – Rute, Albertina, Rafael, Ana, Pedro and Paulo – thank you for always offering help, advice, coffee, laughs, ideas, and, most importantly, unconditional support. They made my days happier and my challenges easier, I am genuinely grateful for that.

To my QSA family, thanks for the patience, advice, moments of fun and continuous presence.

I owe my deepest gratitude to my parents, Alexandre and Fátima. The Thesis reflects the values and resilience they taught me. Thanks for the love, patience, support, and wisdom, that have guided me throughout my life. To my siblings, Mariana and Victor, thank you for continually teaching me to be better. I could not reach this goal without my Family. My heartfelt thanks to Fernanda, a friend like a sister. Her encouragement and positivity have lifted me since we met. Her faith in me has been invaluable.

My last acknowledgement, one of the most important, to my wonderful husband, Arthur, a pillar in my life. Besides the practical support, he is unstoppable motivating and loving me. Having him by my side has been a blessing, making this journey even more meaningful.

"33 O the depth of the riches and the wisdom and knowledge of God! How inscrutable are his judgments! How unsearchable are his ways! 34 For, 'Who has known the mind of the Lord? Who has been his counsellor?' 35 Or, 'Who has given him anything and made him pay it back?' 36 ***For from him and through him and to him are all things. To him be the glory forever! Amen.****"*

Romans 11:33-36

Resumo

Para garantir a sustentabilidade económica e ambiental da indústria do Biodiesel, esforços têm sido feitos para utilizar glicerol, um subproduto, como matéria-prima. Uma alternativa promissora é o Solketal, uma substância que pode ser usada como aditivo de combustíveis por sua capacidade de aumentar a octanagem, melhorar as propriedades do fluido quando em baixas temperaturas e reduzir emissão de fumo e particulados, consequentemente reduzindo a poluição atmosférica. O Solketal é sintetizado a partir da reação de ketalização entre glicerol e acetona na presença de um catalisador ácido. Água é gerada como subproduto da reação.

O desenvolvimento de processos para valorização do glicerol tem como objetivo evitar produção de resíduos e reduzir a emissão de gases de efeito estufa, mas a produção enfrenta alguns desafios, como limitação na taxa de reação, no equilíbrio de conversão e na transferência de massa. O Reator de Leito Móvel Simulado, uma tecnologia de Intensificação de Processos melhorada por adsorção reativa, é uma alternativa promissora para a produção de solketal por ketalização. Ela promove o deslocamento do equilíbrio de reação em favor da formação dos produtos por remover água do meio reacional. O processo pode atingir produtividades ainda maiores quando utilizados modos de operação não convencionais, como o Multifeed SMBR, em que glicerol e acetona são alimentados à unidade por correntes diferentes e independentes, e a estratégia de modulação de concentração da corrente de alimentação, conhecida como ModiCon, em que a concentração da corrente de alimentação é modulada durante o time switch. Essas estratégias aumentam o contacto entre os reagentes e, consequentemente, a taxa de reação e aumentam a pureza dos produtos.

O primeiro passo do projeto consiste em coletar os dados do equilíbrio de adsorção pela Metodologia de Análise Frontal, e ajustar os resultados à Isoterma de Equilíbrio de Adsorção de Langmuir. Em seguida, a síntese de solketal é conduzida no reator adsortivo de leito fixo

para coletar os dados de reação/adsorção e validar o modelo matemático que é usado para simular os processos SMBR convencional e não convencional. Os experimentos foram feitos em uma faixa de temperatura para avaliar as condições ótimas do processo. Uma metodologia de otimização abrangente foi desenvolvida com o objetivo de identificar o melhor conjunto de parâmetros experimentais para realizar a síntese de solketal no SMBR.

Para avaliar a viabilidade prática da produção de solketal no SMBR, experimentos foram conduzidos na nova planta piloto que foi construída no âmbito da Tese, com um design versátil que permite a validação da operação convencional e a prova de conceito das inovativas operações não convencionais. O software para controle e automação foi desenvolvido em LabVIEW ®.

Abstract

To ensure the economic and environmental sustainability of the Biofuel Industry, efforts have been made to utilize glycerol, a commonly produced by-product, as a raw material. One promising development is Solketal, a substance used as a fuel additive due to its ability to enhance octane number, improve liquid properties at low temperatures, and reduce gum formation and particle emissions, thereby mitigating atmospheric pollution. Solketal is synthesized through the ketalization reaction of glycerol with acetone in the presence of an acid catalyst, with water as the by-product.

While the development of an effective process to valorise glycerol aims to prevent waste and decrease fossil fuel emissions, the production of solketal from crude glycerol presents challenges such as limited reaction rate, equilibrium conversion, and mass transfer. The Simulated Moving Bed Reactor (SMBR), a sorption-enhanced reactive Process Intensification technology, is a promising alternative for solketal production via ketalization. It facilitates the equilibrium shift toward the product by removing water from the reaction medium. The process can achieve even higher production yields under non-conventional operation modes, as the Multifeed SMBR, in which glycerol and acetone are fed to the unit by independent streams, and the feed stream concentration modulation strategy, known as ModiCon, in which the feed stream concentration is modulated during the time switch. These strategies increase the reactants contact, consequently, the overall reaction rate, and increase the products' purity.

The project's first stage involves collecting adsorption equilibrium data using the Frontal Analysis Methodology and fitting the results to the multicomponent Langmuir adsorption equilibrium isotherm. Subsequently, solketal synthesis is conducted in a fixed-bed adsorptive reactor to gather reaction/adsorption data and validate the fixed-bed model used to simulate conventional and non-conventional SMBR processes. Experiments are performed across a

range of temperatures to assess optimal process conditions. A comprehensive optimization methodology was developed and applied to all the modes of operation aiming to find the best set of operational parameters to perform solketal synthesis on the SMBR.

To assess the practical viability of solketal production in the SMBR, experiments are carried in a new pilot-scale unit assembled under the scope of the Thesis. with a versatile design that enables the validation of the conventional operation and the proof-of-concept of the innovative non-conventional SMBR operations. The control and automation software was developed in LabVIEW ®.

Table of Contents

List of Figures

List of Tables

Chapter 1

Relevance and Motivation, Objectives and Outline

1.1. Relevance and Motivation

Relying on petroleum as the primary source of energy is a risky strategy for countries that are unable to exploit it, as this makes their entire economy susceptible to market volatilities. Furthermore, the growing environmental concerns highlight the adverse effects of using this source of energy incautiously. Since 57% of the global oil demand and 20% of the global CO_2 emissions are accounted for the road transportation system, replacing the traditional fossil fuels for biofuels is a significant step towards energy independence and environmental preservation, once they are renewable, nontoxic, and highly degradable; they produce no sulphur and no net CO_2 and release less hydrocarbons and nongaseous emissions [1, 2].

In view of the above mentioned, global biodiesel production has been growing as never seen before, encouraged by government policies, fiscal incentives, and emissions laws to control air pollution. As consequence, there has been the collateral effect of generating massive amounts of crude glycerol, since this is the main by-product of the industrial biodiesel production. The positive effect of minimizing CO_2 emissions using biofuels is jeopardized by the fact that the waste generated by this industry represents a major environmental drawback. The strategy of viewing “waste as a resource” led the scientific community to propose numerous processes that use glycerol as raw material. Some of the products derived from glycerol and their respective synthesis routes are exhibited in Figure 1.1.

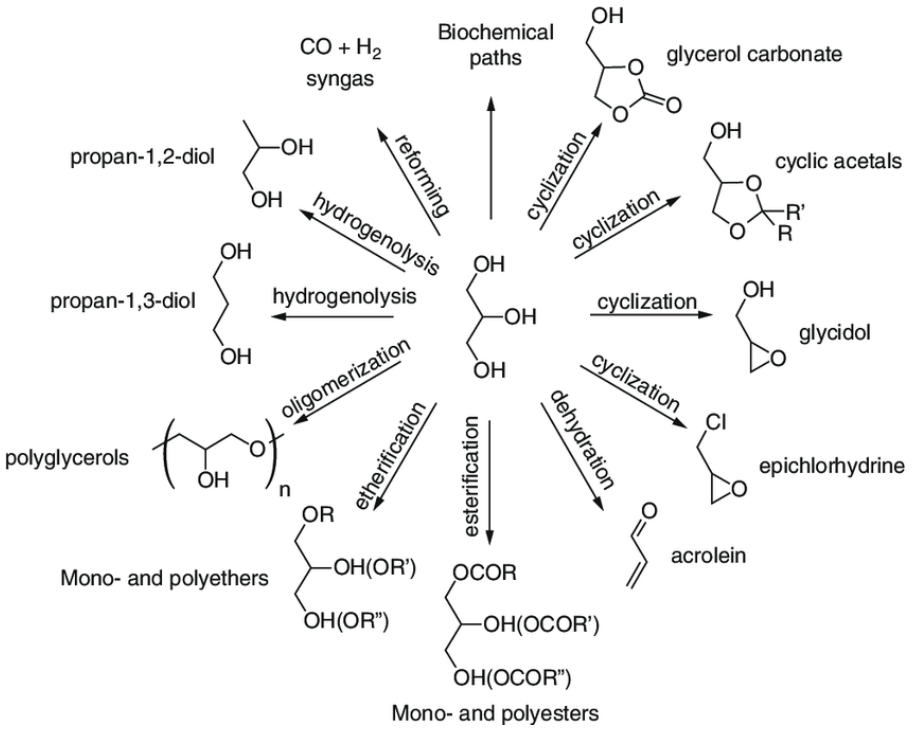

Figure 1.1. Glycerol valorisation reactions (reprinted from Springer Nature, Juan A. Cecilia, Cristina García-Sancho, Pedro J. Maireles-Torres et al., Industrial Food Waste Valorization: A General Overview, 253–277, Copyright 2021, with permission from Elsevier) [3].

Solketal, the product of the reaction of glycerol and acetone, stands out as a promising fuel additive with the capability of enhancing fuel octane number and oxidation stability, diminishing particle emissions and gum formation, and enhancing properties at low temperatures. The reaction conforms to several of the Green Chemistry principles, as all the reactants are from renewable sources, the reaction is catalysed by a heterogeneous catalyst and performed under mild conditions, the chemicals involved present relatively low toxicity, and the by-product of the reaction is water. The synthesis is even more environmentally beneficial if carried in a Simulated Moving Bed Reactor (SMBR), a Process Intensification strategy.

Process Intensification (PI) is one of the most promising approaches to attain environmental sustainability at the industrial level. According to Stankiewicz and Moulijn, two of the pioneers of PI, by definition, PI is an engineering strategy for the development of new equipment and

techniques expected to spawn in "substantially smaller, cleaner, safer and more energy-efficient technologies" [4, 5]. The SMBR is a multifunctional reactor where both reaction and separation occur in the same unit, therefore an excellent example of an energy-efficient process. This technology is versatile, and several non-conventional operations had already been proved to greatly enhance the productivity and the purity of the products in its precursor, the Simulated Moving Bed (SMB), a unit developed for intensifying separation processes.

Taking even further the concept of PI, the present Thesis proposes the investigation and development of non-conventional SMBR operating modes. These modified processes aim to enhance the reactants contact to overcome the reaction's thermodynamic and kinetic limitation. By introducing one more feed stream in the unit, the Multifeed SMBR, one intends to promote the counter-current contact of the reactants to increase the overall reaction rate and the conversion yield. As for the ModiCon, where the strategy is to modulate the feed concentration, the objective is to manipulate the velocity of the concentration fronts to obtain purer products. Both innovative methods achieved good results in the SMB, but literature regarding this topic on the SMBR is scarce or non-existent. Solketal as a product and the SMBR as technology are both worthwhile alternatives to make biofuel industry even better economically and environmentally.

1.2. Objectives and Outline

The present Thesis' main goal is to develop a technology to surpass the growing glycerol gut, a major environmental and economical challenge for the biodiesel industry, by producing solketal. To this end, the SMBR Process Intensification strategy is deeply investigated as an alternative to valorise glycerol through its use as raw material in the synthesis of this auspicious green fuel additive. Innovative non-conventional operations for the SMBR are designed and

validated, which is of outstanding scientific value since the literature on this topic is scarce and these sorption-enhanced strategies are versatile to the synthesis of countless other compounds.

The Thesis comprises eight chapters that describe the acquisition and analysis of fundamental data, the use of these data to implement the SMBR, the investigation of the non-conventional operating modes and finally the discussion of the large-scale implementation of a process to produce Solketal.

In Chapter 1, the motivation and relevance of the proposed objective are exposed, and it is detailed the general outline of this work.

In Chapter 2, a literature review on the current and prospected global energy requirements, on the biofuel market share and on the valorisation of glycerol is presented, in the light of environmental preservation. Details on Solketal characteristics, history, and most recent studies on its synthesis, both in batch and fixed-bed, are provided, along with a review of the published reaction's thermodynamic and kinetic data. Then, the Process Intensification strategies to produce Solketal are summarized, focusing on the SMBR, with a dedicated section to explain its working principles and how far it can get in terms of PI, especially when exploring the non-conventional operating modes. Since one of the outputs of this work is to propose an industrial alternative to produce Solketal, an overview of the processes published in the literature and most relevant patents is presented.

The dynamic study of the solketal synthesis is described and discussed in Chapter 3. Multicomponent adsorption isotherms were measured, and reaction experiments were performed using a fixed-bed adsorptive reactor (FBAR) packed with Amberlyst-35, the ion-exchange resin selected to act as adsorbent and catalyst. Therefore, the best operating conditions to be implemented in the SMBR were assessed. A mathematical model able to describe the synthesis on the FBAR was developed and validated.

The process' scale-up to the SMBR is presented in Chapter 4. Based on the mathematical model developed in the previous chapter, an extrapolated SMBR model was designed to simulate the behaviour of the solketal production on a new unit. Due to the poor performance of solketal synthesis on the Conventional SMBR, the non-conventional operation Multifeed SMBR is proposed in Chapter 5. A thorough discussion on the main process struggles and on the concepts that make this non-conventional strategy perform much better is presented. Also, an optimization methodology developed in the scope of this Thesis specifically for the Multifeed SMBR is presented.

Based on the same principles that make the Multifeed SMBR perform much better than the Conventional operation, the ModiCon SMBR is another non-conventional strategy that is presented in Chapter 6. As it will be shown, it can reach even higher productivities than the first non-conventional strategy, at a cost of a more difficult optimization.

Chapter 7 was developed in form of the operation manual of the new SMBR of the LSRE-LCM. The description of the design, assembly, and operation of the SF-SMB(R) is presented. This unit is built to be versatile to conventional and non-conventional operations, and the details on each mode of operation are specified in this chapter.

Finally, in Chapter 8 the experimental validation of the models developed throughout the Thesis takes place on the new flexible SMBR unit built under the scope of the present Thesis, the SF-SMB(R). Also, it shows the proof-of-concept of the ground-breaking non-conventional operations, the Multifeed SMBR and the ModiCon.

Chapter 9 summarizes the main achievements of the Thesis, and the conclusions and suggestions for future work.

1.3. References

1. Rashid, M.H., *Power electronics handbook*. 4th ed. 2017: Butterworth-Heinemann. 1522.
2. Atabani, A.E., A.S. Silitonga, I.A. Badruddin, T. Mahlia, H. Masjuki, and S. Mekhilef, *A comprehensive review on biodiesel as an alternative energy resource and its characteristics.* Renew. Sust. Energ. Rev., 2012. **16**(4): p. 2070-2093.
3. Cecilia, J.A., C. García Sancho, P. Maireles-Torres, and R. Luque, *Industrial Food Waste Valorization: A General Overview*. 2019. p. 253-277.
4. Stankiewicz, A. and J.A. Moulijn, *Process Intensification: Transforming Chemical Engineering.* Chem. Eng. Prog., 2000. **96**: p. 22-33.
5. Reay, D.R., Colin; Harvey, Adam, *Chapter 2 - Process intensification – an overview*, in *Process Intensification*, D. Reay, C. Ramshaw, and A. Harvey, Editors. 2008, Butterworth-Heinemann: Oxford. p. 21-45.

Chapter 2

State of the Art

ADAPTED FROM: Corrêa, I.; Faria, R.P.V.; Rodrigues, A.E. Continuous Valorization of Glycerol into Solketal: Recent Advances on Catalysts, Processes, and Industrial Perspectives. *Sustain. Chem.* **2021**, *2*, 286-324. https://doi.org/10.3390/suschem2020017

2.1. Introduction

The growing interest in processes that can combine economical savings and environmental preservation has driven not only research groups but also industry to find alternative technologies and methods that conform to Green Chemistry principles [1]. It was not a tough challenge to combine the interests of society, industry, and scientific groups when it has become clear that applying these principles is economically profitable [2]. The first concepts regarding Green Chemistry arose in 1990 and, since its creation, it has been based on improving design to reduce consumption of raw materials rather than treating waste [2, 3]. Anastas and Warner introduced, in 1998, the guidelines necessary to redesign processes and products systematically, more known as The Twelve Principles of Green Chemistry [3].

Even before the introduction of the concepts of Green Chemistry, stimulated by the international petroleum crisis from the 1970s, the search for renewable energy sources led to the discovery of biofuel as the most promising alternative to the use of fossil fuels, since it is appropriate for the transportation sector, responsible for 57% of the global oil demand and for 24% of direct CO_2 emissions [4, 5]. Considering the significant share of the transportation sector on the Greenhouse Gases emissions and on the air quality of cities, replacing fossil fuel with biofuel emerges as a promising alternative to diminish emissions, specially where the renewable alternative does not seem to be extensively applied, for instance, in jet and maritime fuel.

Biodiesel manufacture is a well-established process with billions of gallons produced yearly; however, it still has room for improvements to maximize the economic value and minimize the environmental impact, especially in what concerns diminishing waste production [6, 7]. Avoiding the generation of waste is so relevant that it has been highlighted as one of the main issues since the first discussions about environmental preservation. In 1980, Roger Sheldon proposed a metric to measure the production efficiency taking into account the amount of waste

generated, the E-factor [8]. The first principle of Green Chemistry, indeed, is waste preservation [3]. The main biodiesel production process is the catalysed transesterification of triglycerides with an alcohol (mainly methanol and ethanol), generating an ester (biodiesel) and glycerol (by-product) (Figure 2.1) [9].

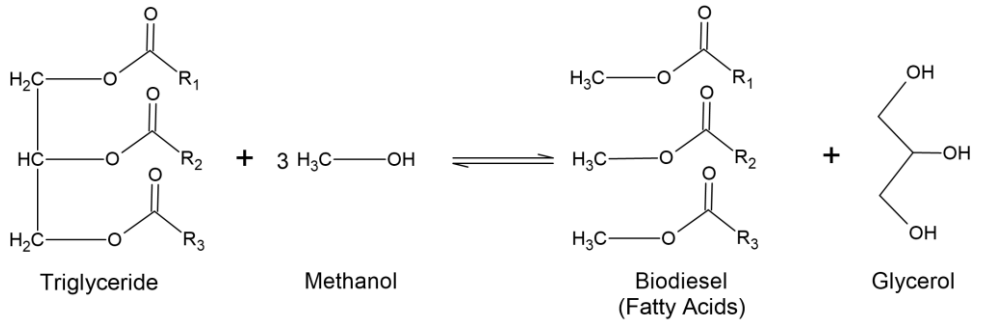

Figure 2.1. Biodiesel production with glycerol as by-product.

The primary environmental disadvantage of the biodiesel industry is the massive amount of glycerol generated as by-product, at a rate of 10–12% and a purity of about 50–55% [10]. Since 68% of the glycerol supply comes from the biodiesel industry, the expected growth in the supply of this commodity follows the biofuel industry tendency, with a predicted growth rate of 5.2% until 2027. [4, 11]. In fact, the side production of glycerol, viewed as a problem in the past, helped to alleviate the economic pressure over biodiesel plants as a consequence of the demand reduction by the COVID-19 pandemic, because as less biodiesel was produced, the market felt glycerol supply pressure, and its prices rose to levels not seen in years. However, it is relevant to note that this effect was not due to a lack of glycerol on the market, but due to logistics problems caused by the mobility restrictions. Therefore, glycerol is considered a safe chemical in terms of supply and it is produced at a much faster pace than the new applications to absorb it [4, 11].

Many alternatives have been studied to avoid treating this chemical as waste [12]. The alternatives are particularly interesting if crude glycerol can be used, without the need of purifying it [13]. Refined glycerol has found numerous applications in cosmetics,

pharmaceuticals, and food industries for years. By 2019, this segment accounted for 65.1% of the glycerol market [14, 15]; however, traditional markets are not able to absorb crude glycerol from biodiesel plants, both because of its low purity and the amount generated [13].

One of the most promising chemicals derived from glycerol is solketal (2,2-Dimethyl-4-hydroxymethyl-1,3-dioxolane), an oxygenated cyclic ketal with two methyl groups. It is produced by the reaction of glycerol with acetone in the presence of an acidic catalyst, with water as the by-product (Figure 2.2). It is an emerging fuel additive by reason of improving fuel's octane number, enhancing liquid properties at low temperatures, reducing gum formation, thus aiding maintenance and cleanliness of engines, and reducing particle emission, which diminishes atmospheric pollution [10,19,20]. Its potential use as a fuel additive for the aviation industry (accountable for 2% of the global CO_2 emissions) is noteworthy because of its icing inhibition and de-icing properties, improving the storage stability of aviation fuels [16-18].

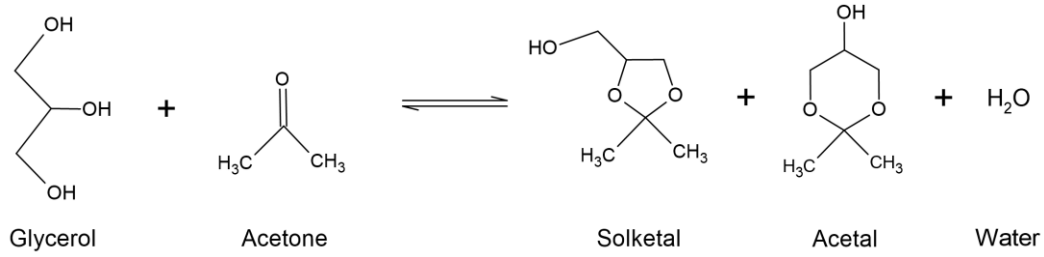

Figure 2.2. Glycerol reaction with acetone to produce solketal and water.

Glycerol valorisation into solketal is appealing from the environmental and economical perspectives [19]. The reaction conforms to several of the Green Chemistry principles, as all the reactants can be obtained from renewable sources, the reaction can be catalysed by a heterogeneous catalyst and performed under mild conditions, the chemicals involved present relatively low toxicity and the by-product of the reaction is water. Furthermore, by using it as fuel additive, this chemical is reinserted in the biofuel production chain, constituting a mass and energy closed flow that complies with the Circular Economy Model and improves the

carbon footprint and life cycle parameters. Economically, the by-product is valorized and capitalized on, once the selling price of crude glycerol is US$210–390/ton (pre-pandemic scenario) and of solketal is around US$3000/ton, clearly enhancing the industry profitability [14,24,25].

Over the years, especially from 2015 on, numerous technologies have been proposed for the synthesis of solketal, notably concerning the use of heterogeneous catalysts and continuous processes. This chapter summarizes these new catalysts and the Process Intensification strategies that have been investigated for solketal production. Moreover, it is aimed to explore the kinetic models commonly proposed and explain the reasons why different models better describe the reaction behaviour for each type of catalyst. Furthermore, the works and the patents with proposed industrial plants for the production of this chemical are exposed, discussed, and compared to appoint solutions for the implementation of large-scale processes. The chapter also briefly discusses the biofuel and glycerol markets.

2.2. Biodiesel Production and Glycerol Market

The International Energy Agency (IEA) foresee a global energy demand growth of 9% annually between 2019 and 2030 if the policies in the field are kept unchanged, slightly slower than in the pre-pandemics scenario when the expected growth rate was 12% [20]. Nevertheless, it is imperative to invest in the use of renewable feedstocks, one of the most disseminated principles of Green Chemistry, to control global warming [3].

Considering the significant share of the transportation sector on the oil demand (almost 60%, as previously stated), COVID-19 mobility restrictions deeply affected the petroleum market, returning the oil consumption to the levels of 2012 [4]. The expected demand drop for gasoline, diesel, and jet fuel is 9%, 6%, and 26%, respectively, and numerous predictions foresee a

smaller growth in the oil demand than expected prior to the COVID-19 crisis and an anticipation to reach the oil demand plateau, as can be seen in Figure 2.3 [4, 14, 20].

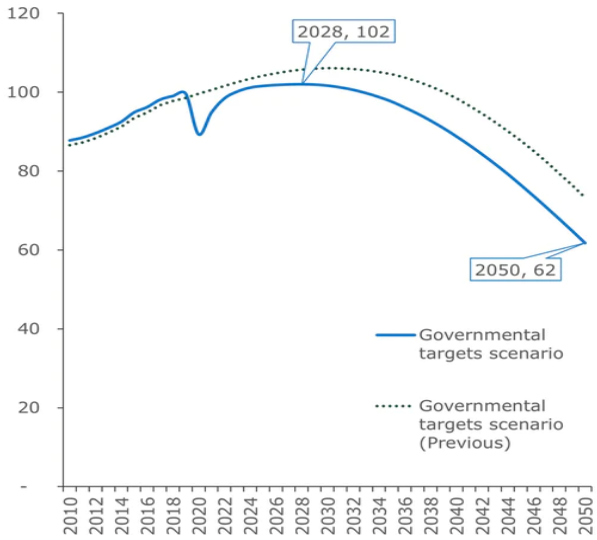

Figure 2.3. Global oil demand forecast (adapted; Source: Rystad Energy research and analysis) [14].

The new scenario also impacts biofuel consumption once they are blended with fossil fuels. Thus, a production contraction of 13% is expected, returning to the 2017 levels [14, 21]. The pressure on the biofuel industry is not expected to diminish in the following years because of the lower oil prices caused by the demand reduction and the delay in the adoption of blending mandates to enable the fossil fuel industry to recover [4]. Nevertheless, the predictions for the biofuel industry are still optimistic, as the demand for biofuel is estimated to grow anually at a rate of 5.5% from 2023 to 2030, mainly explained by the increasing awareness of the environmental concerns and by the desire to avoid relying on the petroleum industry [22].

The environmental benefits of using biodiesel over traditional fossil fuels are noteworthy: it is renewable, biodegradable, and non-toxic; it reduces CO, hydrocarbon (HC), and nongaseous emissions; it produces no sulphur and no net CO_2 (on a life cycle basis); and usually, it has a higher cetane number and better lubricant properties, which is beneficial for the maintenance

of the engine [10, 23]. Furthermore, biodiesel plants are often local, which reduces transport costs, create jobs, and aid local economies [23]. Nonetheless, biodiesel also presents some disadvantages: it emits higher levels of nitrogen oxides; engines may perform worse in severe winter temperatures when compared to petrodiesel and require adaptations for the use of biodiesel; the energy content is lower than petrodiesel; and biodiesel can present considerable variations depending on which raw material is used to manufacture it. Part of these disadvantages, however, such as performance in cold weather and less energy content, is dampened with the use of fuel additives, such as solketal [23].

The decline in the CO_2 emissions caused by the slowdown of the economy and by the mobility restrictions reached 5.4%, a level that would enable to stay below the 1.5 °C warming limit defined in the Paris Agreement [24]. Nearly half of the decrease in emissions is accounted for surface transportation. This new scenario is, at the same time, challenging, because it reveals the magnitude of the changes that would have to be established to control the emissions, and appealing, as it disclosed part of the path that governments, companies, and citizens would have to follow to control global warming [20].

The biofuel industry is divided into two main products: ethanol and biodiesel. The primary use of ethanol is as a blending agent, as it has the capacity of increasing fuel oxygen content, which enhances the combustion process and releases less CO and HC into the atmosphere [25]. Since ethanol is mainly employed as a blending agent for gasoline, mostly used in passengers' cars, its market has felt more the effects of the pandemic, with a demand reduction of 15% [21]. As for biodiesel, it is primarily used for rail transport of goods, a less-affected sector when compared to personal mobility, with an estimated contraction of 6% [21]. The aviation and marine sectors are the less developed in terms of using renewable sources of energy, responsible for less than 0.01% in 2018 [26]. The US production predictions for all types of

biofuels is exhibited in Figure 2.4, in which the "other biofuels" category refers to the fuels of the aviation and marine sectors.

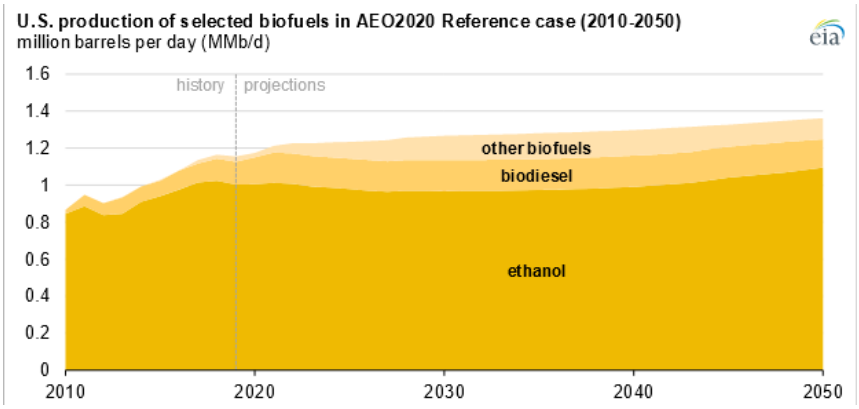

Figure 2.4. Predictions for the US production market of biofuels (Source: U.S. Energy Information Administration, Annual Energy Outlook 2020) [26].

The global glycerol supply is secure, as this chemical has been, for years, more produced than demanded. The main segments that exploit glycerol are personal care and chemical intermediates, the difference between them is that the first requires refined glycerol, and in many applications of the second, less purified glycerol can be used [11]. Due to its physicochemical properties (colourless, odourless, viscous, biodegradable, and non-toxic liquid) and three hydroxyl groups that can be easily replaced by other groups, glycerol is a reactive molecule frequently used as a platform chemical [12, 27].

There has been occurring an intensive search for alternative glycerol valorisation routes. The use of refined and crude glycerol has been reported for the production of biofuels, as hydrogen, ethanol, and methanol [16,37,39]; fuel additives, as glycerol ethers, esters, and formal (mix of solketal and acetal) [16,19,40]; and as a precursor for several other chemicals that can compete with petroleum products [15,18,37,39]. Another alternative for the valorisation of glycerol is its conversion through biotechnological processes, such as fermentation and anaerobic digestion, because of their capacity to absorb crude glycerol. The literature is substantial in

fermentation processes with different types of microorganisms that can generate hydrogen, methane, ethanol, and numerous other chemicals [16,20,39].

2.3. Solketal

2.3.1. Solketal Properties

Solketal (CAS 100-79-8) has low viscosity at room temperature (~11 cP) and freezing, boiling, and flash points of about −26 °C, 190 °C, and 80 °C, respectively. The density is 1.06 g/cm3 and the vapor pressure is 107.32 mmHg. It has low toxicity, slight odour, and it is non-irritant for humans; due to these characteristics and to the renewable origin, it is considered an environmentally friendly substance. It is completely miscible in water and in most organic compounds, which endows its solvent capacity [28, 29].

2.3.2. Solketal Uses

Owing to the high compatibility and miscibility of solketal, the major application is as a solvent in resins, paints coatings, and cleaning agents, also because it can influence film-formation and drying time [28]. Its low toxicity and solubility in body fluids enable it to be used also as a solvent in medicaments (i.e., driving agent), and as a precursor of other chemicals of medical interest [30].

Nevertheless, the most studied solketal application is as fuel additive. Melero et al. [31] studied the benefits of adding oxygenated compounds in biodiesel and if the blends would be under the EN 14214 standard. Solketal has the positive effect of diminishing biodiesel viscosity and the negative effect of increasing fuel density, fundamental properties for the correct operation of engines. Because of the amount of saturated fat in biodiesel, it presents poor cold properties, a problem proved to be aided by adding solketal to the fuel [31]. Giraldo et al. also attested the positive effect of using this ketal on diminishing the cloud point (the temperature

at which wax crystals begin to form) and pour point (the temperature at which the fuel no longer flows) [23].

Another parameter analysed was the flash point ("the lowest temperature at which a volatile substance evaporates to form an ignitable mixture with air in the presence of an igneous source," according to Isac-García et al.), in which the addition of solketal decreased the properties' value [31, 32]. Conversely, Alptekin registered higher flash point of the biodiesel blend and higher brake specific fuel consumption (measure of the fuel efficiency—rate of fuel consumption divided by the power produced) due to the low energetic efficiency of solketal. Despite that, CO_2, CO, and THC (total hydrocarbon) emissions were lower [33]. Mota et al. [34] tested the addition of solketal in gasoline and concluded that it improved octane number and reduced gum formation, results confirmed by Ilgen et al. [35].

2.4. Solketal Synthesis

The reaction between acetone and glycerol is a process that adheres to the Green Chemistry principles because it is a condensation reaction, an example of atom economy, and it is a catalytic conversion [36]. According to Anastas and Warner, catalysis can improve energy efficiency, avoid the use of reactants in great excess, and enhance product selectivity [2]. The reaction produces two ketal species, one five-membered ring (solketal) and one six-membered ring (5-hydroxy-2,2-dimethyl-1,3-dioxane), with much higher selectivity for the first (99:1 molar ratio in recent studies), further explained by the mechanism of the reaction described in Section 2.4.2 [9, 36]. The reaction has a low equilibrium constant; therefore, it is thermodynamically limited. To obtain high conversion yields, it is necessary to shift the reaction in favour of product formation by either removing water or by adding acetone in excess [36].

2.4.1. History

The first solketal synthesis dates back to 1895 when it was obtained by the reaction of glycerol with acetone under acidic conditions (hydrogen chloride catalyst) in a batch reactor [37]. Years after that, the process was repeated varying the reaction medium (addition of anhydrous sodium sulphate) and the operating conditions, using different equipment, solvents (petroleum ether), and catalysts (p-toluenesulfonic acid-pTSA) [36, 38]. At that time, the reaction with pTSA resulted in high conversion (87–90%); however, acetone was used in great excess and a long reaction time was necessary, which made the production in large scale unviable. New routes for solketal synthesis were deeply investigated only when the massive glycerol generated by the biofuel industry became a problem and society turned its attention to the Green Chemistry concepts [36].

In the following years, new approaches were proposed to obtain higher productivity in less time. Initially, the reaction was mainly made with homogeneous catalysts, as the pTSA was also used by Newman and Renoll back in 1945, and strong acids such as sulfuric, hydrochloric, hydrofluoric, and phosphoric acids [39]. Some authors registered good solketal yields (88 and 90% with pTSA as the catalyst). Despite that, the long reaction times were still a problem that rendered the process discouraging; moreover, acetone in excess was still required, and often a strategy to remove water from the reaction medium was applied, as the use of desiccants, entrainers, or molecular sieves [21,50,52]. Furthermore, the problems related to the use of homogenous catalysts are well known: difficult separation from the products, equipment corrosion, and serious concerns about effluent disposal [7, 39]. The use of heterogeneous catalysts, as was later proposed, conforms to some of the Green Chemistry principles: less hazardous chemical synthesis, safer solvents, and auxiliary, inherently safer chemistry to accident prevention [2].

There has been an extensive study of alternative heterogeneous catalysts, with emphasis on zeolites, acidic resins, and montmorillonite [8,10,48,54]. The performance of several zeolites under different conditions revealed that beta zeolites can achieve the highest conversion rates [9, 40-43]. The resins tested, mainly Amberlyst-15, 35, and 36, showed satisfactory activity as a catalyst in the conversion of glycerol to solketal. Moreover, they can be used as adsorbent, which may help to overcome the thermodynamic limitation of glycerol conversion when used in multifunctional reactors [10,55,58,59]. Since the hybrid solid must perform two tasks, catalysis and adsorption, besides considering the catalytic activity in the reaction of glycerol with acetone, the adsorbent must have a strong affinity to water. Interesting results about the use of ion exchange resins in the synthesis of oxygenated compounds have been reported in several studies, especially because of their affinity with water [44].

Da Silva et al. [43] compared the performance of the three types of heterogeneous catalysts mentioned above. The study was conducted in a batch reactor at 373 K and the authors stated that Amberlyst-15 achieved the highest conversion (95%) in only 15 min of reaction. Zeolite beta and Montmorillonite K-10 achieved conversions up to 90%, but only after 40 min. Other zeolites tested, namely ZSM5 and USY, presented poor catalytic activity due to the small pore diameter of the first that impair the reaction from occurring inside the pores and to the hydrophilic character of the second, responsible for retaining the water formed as by-product inside the pores and deactivating the acid sites [43]. From the three types of catalysts, despite the low cost of Montmorillonite K-10, zeolites and ion exchange resins have been preferred due to the higher conversion rates with the same catalyst load [58,59,61].

Nanda et al. stated that the catalyst acidity and acetone to glycerol molar ratio have a great influence on the reaction (kinetics and conversion), but the physical characteristics of the resin, such as pore volume and particle size, have a negligible effect on catalysts activity [36]. Nonetheless, Faria et al. studied the effect of the particle size of Amberlyst-15 for a similar

reactive system and concluded that the reaction occurs under diffusion-controlled regime; therefore, the internal mass transfer resistances effectively influence the catalytic activity, which makes particle size a relevant parameter [45].

The limited miscibility between acetone and glycerol is one of the obstacles of this reactive system [36]. To overcome this challenge, the most common solutions are using acetone in great excess and applying auxiliary solvents that enhance the miscibility of the system. For the solvent selection, Faria et al. developed a methodology to determine the most appropriate solvent for reactive-adsorptive processes considering properties that directly affect the system as miscibility, reactivity, adsorption, and kinetics. The method also evaluates environmental aspects as lethal dose (LD50), NFPA health hazard classification, octanol−water partition coefficient, and persistence time [45]. According to this methodology, solvents that are reactive to any of the reagents at the operating conditions cannot be used and the interaction of the solvent with the catalyst is a key factor [9].

Different production processes were proposed for the synthesis of solketal in batch and continuous modes of operation (most of the studies about batch processes), especially in what concerns surpassing the thermodynamic limitation. This can be done by either removing one of the products from the reaction medium, typically water, or by adding acetone in excess. In batch processes, a major issue is reaction rate drop when the equilibrium is nearly reached, being necessary to stop the synthesis to collect and purify the products, then clean and refill the reactor to restart the process. Depending on the catalyst, some sort of regeneration may be required after each run [36].

When operating in batch, water removal can be accomplished by the use of entrainers, as previously mentioned [38]. The open literature reports the use of benzene, petroleum ethers, and chloroform; however, the problem faced in this operation is the relatively low boiling point of acetone, which often was removed from the reaction medium even before the entrainers [36,

46]. Another alternative explored was the use of desiccants with a role in catalysis as well (sodium sulphate and phosphorus pentoxide). Experiments confirmed the economic unfeasibility of this option due to the high solid consumption, together with some environmental concerns, due to waste generation [36, 46]. Furthermore, technologies as membrane sieves, membrane batch reactors, and modified batch operations were experimented and achieved good conversion yields, but in all cases, acetone in great excess was necessary [36]. Because of the already mentioned miscibility issues, Royon et al. tested the use of supercritical acetone to improve the contact of the reagents, yet the low conversion yields reached were discouraging [47].

The results reported for the continuous processes are encouraging, showing much higher efficiency, with solketal being produced in less time [36]. Among the numerous advantages of studying continuous processes, the one that needs to be highlighted is the possibility of scaling up the process to the industrial level [44]. The most explored technology for the large-scale production of basic chemicals and intermediates is the catalytic fixed-bed reactor; thus, this operation is the most applied in studies concerning the continuous reaction of glycerol [48]. Most of the research on the field is recent and more details are provided in Section 2.4.2. .

One of the first continuous operations proposed for the solketal synthesis was actually a semi-continuous counter-current distillation reaction, investigated by Clarkson et al. [49], where glycerol was fed in batch and acetone in continuous, and the reaction was catalysed by Amberlyst-DPT. Using acetone to glycerol molar ratio of 2, the authors registered a conversion of 98%, but the temperature had to be carefully monitored since providing much heat removes acetone from the reaction medium and low temperatures affect the conversion due to glycerol's miscibility [49]. The studies on continuous operations also considered the use of homogeneous catalysts, such as the synthesis in a Continuous Microwave Reactor proposed by Cablewski et al. with pTSA as catalyst (84% conversion yield) [50] and in a module of several continuous

glass flow reactors connected in series with sulfuric acid as catalyst (98–99% conversion with acetone to glycerol molar ratio between 8 and 14 and 69% with acetone: glycerol molar ratio of 4) [51]. The main disadvantages, however, are related to the use of the homogenous catalysts, as already mentioned.

2.4.2. Catalyst Study

Recent Advances on Catalysts

Most of the recent studies on solketal synthesis comprise the development of heterogeneous catalysts or homogeneous catalysts that can be recovered, as seen in Table 2.1, where the most recent studies on catalysts performance are summarized. Despite being a relatively simple reaction, the reaction of glycerol with acetone faces the previously mentioned challenges: thermodynamic limitation and mass transfer resistance.

From the catalyst development point of view, to overcome the mass transfer resistance, it is preferable to avoid microporous catalysts [52]. As for the thermodynamic limitation, by exploiting the differences in affinity with the solid phase, water separation may be promoted, and the direct reaction can be fostered. This can be accomplished by using hybrid solids with higher affinity to water than to solketal, such as ion exchange resins; therefore, the by-product is adsorbed and the direct reaction is favoured [11,70,71]. Furthermore, the catalyst must be water tolerant to preserve the active sites along the reaction and it must remain active after more than one cycle, ideally with large production capacity [43, 53].

Table 2.1. Summary of the recent investigations (from 2015 on) on catalysts for the synthesis of solketal.

Author	Catalyst	Acidity (mmol/g_{cat})	Reaction Conditions	Results (%)	Reusability	Ref.
Homogeneous Catalysts						

Esposito, 2019	Iron (III) Complex $FeCl_3$ (1-NO_2) 0.05 mol% (glycerol)	N.A. [1]	G:A = 1:4 T = - t = 90 min	X_{gly} > 99% Sel ≥ 98.5%	N.A. [1]	[54]
Da Silva, 2020	Fe $(NO_3)_3$ 9·H2O 0.30 mol% [2]	N.A. [1]	G:A = 1:20 T = 298 K t = 60 min	X_{gly} = 98% Sel = 97%	Four cycles without significant activity loss.	[55]
Zeolites						
Manjunathan, 2015	H-Beta 5 wt% (glycerol)	1.51	G:A = 1:2 T = 301 K t = 60 min	X_{gly} = 86% Sel = 98.5%	One cycle without significant activity loss.	[56]
Rossa, 2017	H-Beta 5 wt% (glycerol)	0.094	G:A = 1:4 T = 333 K t = 60 min	X_{gly} = 72.62% Sel = 98.3%	A 22% decrease on the activity after the first use. Activity remained until the fourth cycle.	[57]
Kowalska-Kus, 2017	MFI Beta MOR 1 wt% (glycerol)	0.369 0.388 0.55	G:A = 1:1 T = 343 K t = -	X_{gly} = 85, 85, 80% Sel < 99% Y_{solk} ≈ 80%	N.A. [1]	[52]
Talebian-Kiakalaieh, 2019	HR/Y-W20 10 wt% (glycerol)	1.806	G:A = 1:10 T = 313 K t = 90 min	X_{gly} = 100% Sel = 97.9% Y_{solk} = 97.9%	Four cycles without significant activity loss.	[58]
Rahaman, 2020	OTS-HY 5 wt% [2]	0.552	G:A = 1:12 T = 303 K t = 60 min	X_{gly} = 89% Sel = 95%	N.A. [1]	[59]
Ion Exchange Resins						
Esteban, 2015	Lewatit GF101 0.5 wt% [2]	5.11	G:A = 1:12 T = 313 K T = 240 min	X_{gly} = 96% Y_{solk} ≈ 80%	N.A. [1]	[60]

Cornejo, 2019	Purolite CT275 5 wt% (glycerol)	5.2	G:A = 1:12 T = 323 K T = 300 min	X_{gly} = 93%	N.A. [1]	[61]
Moreira, 2019	Amberlyst-35 0.5 wt% (reactants)	5.08	G:A = 1:2 T = 303 K T = 480 min Solv. = Ethanol	X_{gly} = 70%	N.A. [1]	[9]
Sulistyo, 2020	Indion 225 Na 5 wt% [2]	N.A. [1]	G:A = 1:5 T = 328 K T = 180 min	X_{gly} = 31.9%	N.A. [1]	[62]
Clays						
Timofeeva, 2017	HNO_3 Modified montmorillonite clay 5 wt% (glycerol)	0.015 [3]	G:A = 1:2.5 T = 298 K T = 15 min Solv.= acetonitrile	X_{gly} = 94% Sel = 95.4%	Three cycles without significant activity loss.	[63]
Amri, 2019	HCl activated clay 5 w/v% (reactants)	0.0065 [3]	G:A = 1:6 T = 298 K T = 60 min Solv. = Isopropanol	Y_{solk} = 69.3%	Significant activity loss in the second cycle.	[64]
Metal Oxides						
Zhang, 2015	M-$NiAlPO_4$ 4 wt% (glycerol)	0.12	G:A = 1:8 T = 353 K T = 60 min	Sel = 75.1% Y_{solk} = 75.4%	Three cycles without significant activity loss. Activity decreased from the fourth cycle on.	[65]
Gadamsetti, 2015	MoPO/SBA-15 2.7 wt% (reactants)	≈ 1	G:A = 1:2 T = 301 K T = 60 min	X_{gly} = 100% Sel = 98%	A 30% activity loss after the first cycle. Activity remained until de fourth cycle (Xgly = 100, 70, 68, and 62%).	[66]
	1Nb:0.05Al	0.094	G:A = 1:4	X_{gly} = 84%		[67]

Rodrigues, 2016	2.7 wt% (glycerol)		T = 323 K T = 360 min	Sel = 98%	Four cycles without significant activity loss.	
Ionic Liquid						
Gui, 2016	1-(4-sulfonylbu-tyl)triphenylpho sphonium methanesulfonat e 2.7 mol% (glycerol)	N.A. [1]	G:A = 1:15 T = 298 K T = 30 min	X_{gly} = 96% Sel = 98.5%	Four cycles without significant activity loss.	[68]
Ji, 2020	[P $(C_4H_9)_3C1_4H_{29}$] [TsO] 5 wt% (glycerol)	N.A. [1]	G:A = 1:6 T = 303 K t = 30 min	Y_{solk} = 86%	Ten cycles without significant activity loss.	[69]
Sulfonated Carbon based						
Gonçalves, 2016	GC-1:2 3 wt% (glycerol)	3.8	G:A = 1:4 T = 298 K t = 240 min	X_{gly} = 82% Sel = 95%	A 10% activity loss after five cycles.	[70]
Fernández, 2019	Cel-215-2 M-20 h-S Glu-195-20 h-S 1 wt% (glycerol)	5.43 3.42	G:A = 1:7 T = 298 K t = 120–240 min	Ysolk = 80 − 86% Y_{solk} = 80 − 86%	Stable for 60 h of operation. No information on the recycle.	[71]
Ballotin, 2020	BS9.2 0.6 wt% [2]	0.3	G:A = 1:10 T = 298 K t = 120 min	X_{gly} = 93% Sel = 98%	A 4% activity loss after four cycles.	[72]
Kaur,2021	AAC-CC 3wt.% [2]	N.A. [1]	G:A = 1:8 T = 373 K t = 120 min	X_{gly} = 80.3%	Less than 5% activity loss after three cycles.	[73]

Saikia, 2022	C-SO_3H 7 wt% (glycerol)	4.56	G:A = 1:5 T = 343 K t = 10 min	X_{gly} = 97.1% Sel = 100%	Steady and mild decrease in glycerol conversion until the fifth cycle (82.1%).	[74]
Silica based						
Roncaglia, 2021	Silica sulfuric acid (SSA - $H_2SO_4 \cdot SiO_2$) 1.5 mol% (glycerol)	3.0	G:A = 1:4 T = 328 K t = 210 min	Y_{solk} = 96%	Five cycles without significant activity loss.	[75]
Zhou, 2021	*p*-phenolsulfonic acid on modified SiO_2 (PSF/K-SiO_2) 5 wt% (glycerol)	2.6	G:A = 1:10 T = 328 K t = 360 min	X_{gly} = 86.3% Sel = 97.7%	Five cycles without significant activity loss.	[76]
Chansorn, 2022	SNSs-*g*-PMVP/PTA 5 wt% [2]	4.501	G:A = 1:8 T = 343 K t = 60 min	X_{gly} = 94% Y_{solk} = 97%	Two cycles without significant activity loss. A 24% activity loss after the second cycle.	[77]
Others						
Sandesh, 2015	Heteropoly acids $(C_3H_7)_4N^+$/PWA 3 wt% (reactants)	0.6	G:A = 1:6 T = 303 K t = 120 min	X_{gly} = 94% Sel = 98% Y_{solk} = 93%	A 5% activity loss after three cycles.	[78]
Li, 2019	Layered crystalline α-zirconium phosphate 5 wt% (glycerol)	1.3	G:A = 1:10 T = 323 K t = 180 min	X_{gly} = 85.7% Sel = 98.3%	Four cycles without significant activity loss. Activity decreased until the fifth cycle.	[79]
Vannucci, 2020	Sulfated zirconium oxide	0.09	G:A = 1:8 T = 313 K t = 280 min	$X_{gly} \approx$ 80%	A 16% activity loss after four cycles.	[80]

	0.3 wt% (glycerol)					
Sulistyio, 2020	Basolite F300 1 wt% (glycerol)	N.A. [1]	G:A = 1:4 T = 323 K t = 60 min	X_{gly} ≈ 84.3%	N.A. [1]	[81]
Da Silva, 2020	Tin (II) silicotungstate acid salt 0.01 mol% [2]	1.3	G:A = 1:4 T = 298 K t = 120 min	X_{gly} ≈ 74% Sel > 98% Y_{solk} = 73%	"No decrease in the catalytic activity was found."	[72]
Podolean, 2020	Germanosilicate zeolite 5 wt% (glycerol)	N.A. [1]	G:A = 1:5 T = 298 K t = 180 min	X_{gly} = 56% Sel = 98%	Six cycles without significant activity loss. Stable up to 12 h on stream.	[82]
Li, 2020	Zirconium organophosphonate 5 wt% [2]	1.12	G:A = 1:10 T = 313 K t = 360 min	X_{gly} = 90.2% Sel = 98.5%	A 2.7% activity loss after five cycles. Stable up to 10 h on stream.	[83]
Hussein, 2020	Gallosilicate 10 mg	0.39	G:A = 1:4 T = 353 K t = 180 min	X_{gly} = 34% Sel > 95%	Seven cycles without significant activity loss. Stable up to 6 h on stream.	[84]
Vivian, 2021	Gallosilicate 3.2 wt% (glycerol)	N.A. [1]	G:A = 1:4 T = 323 K t = 60 min	X_{gly} = 43% Sel = 93%	Four cycles without significant activity loss.	[85]
Santos-Vieira, 2021	Triphosphonic Coordination Polymers with Eu^{3+} (UAV-63) and La^{3+} (UAV-20) 5 wt% (glycerol)	N.A. [1]	G:A = 1:10 T = 298 K t = 360 min	X_{gly} = 84% Sel = 96% X_{gly} = 56% Sel = 82%	"For UAV-63 there was a slight conversion decrease, from 84% to 69%, while for UAV-20 the conversion remained constant in consecutive runs."	[86]

Rodrigues, 2021	Activated carbon activated by HNO_3 3 wt% (glycerol)	5.1	G:A = 1:4 T = 328 K t = 60 min	X_{gly} = 91% Sel = 97%	Four cycles with 8% activity loss. [87]
Dashtipour, 2022	Mil-118-SnO_2 20 wt% (glycerol)	0.338	G:A = 1:10 T = - t = 240 min	X_{gly} = 76% Sel = 97%	Four cycles without significant activity loss. [88]
Julião, 2022	HPA ($H_3[PW12O40]$ (PW12)) 3 wt% (glycerol)	N.A. [1]	G:A = 1:15 T = 298 K t = 4.8 min	X_{gly} = 99.2% Sel = 97%	N.A. [1] [89]

1 Not available. 2 Not stated whether in relation to glycerol or to total reactants. 3 Bronsted Acidity.

Iron (III) complexes homogeneous catalysts were investigated due to their potential to be recovered and their low cost, desirable characteristics for an industrial scale process. Esposito et al. tested several types of iron (III) catalysts in an apparatus where water was removed by molecular sieves to shift the reaction equilibrium towards product formation. They concluded that $FeCl_3$(1-NO_2) had the better performance, achieving almost total glycerol conversion and 100% selectivity to solketal [54, 90]. Da Silva et al. compared different transition metal salts and found the best result for $Fe(NO_3)_3 \cdot 9H_2O$, also converting almost all of the glycerol and achieving selectivity of 95%. Then, the authors compared the result with the conversions of Brønsted acid catalysts (pTSA and H_2SO_4) and confirmed that the iron (III) salt is more efficient probably because besides polarizing acetone's carbonyl group, it releases H^+ ions in the reaction medium, therefore acting like Lewis and Brønsted acid simultaneously [55]. Another conclusion of the articles is the high catalyst efficiency, once a small catalyst load leads to great conversion values [54, 55].

Ionic Liquids (ILs), as iron (III) catalysts, combine the advantages of homo- and heterogeneous catalysts, although their major drawback is usually the high cost. Ji et al. avoided this problem by exploring the tributyl (tetradecyl)phosphonium p-toluenesulfonate (TPTT), an inexpensive IL. The researchers obtained high solketal yield (85.9%), also with a high reaction rate, because the reaction was not impaired by internal mass transfer resistance; however, the authors had to use acetone in excess, probably to diminish external mass transfer resistance. The results are in line with the ones obtained previously by Gui et al. (X_{gly} = 96%) with 1-(4-sulfonylbutyl) triphenylphosphonium methanesulfonate. The second study used almost half of the catalyst load, but more than doubled the acetone to glycerol ratio. The ILs of both studies were recovered and used in several cycles without losing the catalytic activity, an important characteristic for the industrial application [68, 69].

One of the main reasons that make zeolites so deeply studied is their versatility, once the acidity, pore size distribution, and crystallite size can be relatively easily manipulated under adequate treatment [91]. Nowadays, many researchers compare the performance of the modified zeolites (usually called Hierarchical—H—due to the presence of more than one type of pore) with their respective Parent (P) zeolites to assess the effect of the changes on the catalytic activity. Manjunathan et al. studied the effects of dealuminating, increasing crystallite size, and preparing copper ion exchange zeolites and concluded that the highest conversion (86%) was attained by H-Beta zeolite with enlarged pores, small crystallite size (low diffusion path length), and higher amount of strong acidic sites. The dealumination led to a decrease in strong acidic sites that reduced glycerol conversion [56]. The findings of Rossa et al., also with H-Beta, agree with this previous study. Furthermore, Rossa et al. attributed the activity reduction along with the number of recycles to the blockage of the acidic sites by the water molecules formed inside the pores, but not to the deactivation of the surface acidic sites, once the hydrophobicity of the zeolite impaired water to approach to the surface of the catalyst [57].

This statement is contrary to what Silva et al. reported in a similar study with the same catalyst, where it was affirmed that the hydrophobic zeolite environment expels off from the pores the water formed, preserving the acid sites, besides preventing water diffusion from the medium to the interior of the pores [91]. The hydrophobicity is related to the silicon to aluminum ratio, which is also related to the porosity and to the acidity of the catalyst, thus selecting the parent zeolites and the adequate treatment is a convoluted process [43, 52]. Nonetheless, the good conversion achieved with modified zeolites, with reactions performed under mild conditions and with reasonable amounts of acetone makes the use of zeolites favorable for industrial application [69,75,76].

An interesting zeolite modification proposed by Rahaman et al. is grafting an organosilane surfactant (n-octadecyltrichlorosilane – OTS) to the HY catalyst so that it assists on the emulsion formation between the reactants. This avoids the need of a solvent to aid their miscibility. With this modified catalyst, the authors attained a conversion of 89% at 303K, against a conversion of only 28% attained by using the unmodified HY [59].

Talebian-Kiakalaieh et al. synthesized a NaY zeolite supported over heteropoly acid to enhance its acid strength and active sites. The zeolite went over a dealumination process to enlarge its pores and create the mesoporous structure, the downside is the consequent reduction in the total acidity. Nonetheless, 98% glycerol conversion and 96.6% selectivity were achieved, and the authors affirmed that the mesoporosity and the acidity are the main parameters that affect the catalytic activity and stability [58]. Sandesh et al. also explored the potential of heteropoly acids and reported the use of $(C_3H_7)_4N^+$/PWA to achieved 94% glycerol conversion and 98% selectivity for solketal. These results are attributed to its acidity and to its pseudo liquid behaviour: the polar reactants absorb into the polyanion space of the catalyst, contact the active sites, react, and then the products desorb [78].

Recently, studies comprise a variety of ion exchange resins, as this type of catalyst is particularly interesting for glycerol ketalization because of its affinity with water. From Table 2.1, one may conclude that the mass transfer hinders the use of this type of hybrid solid, once acetone in large excess is necessary to attain conversions as high as 90% when selected a solvent-free environment [60, 61]. To overcome this issue, Moreira et al. opted for using ethanol as solvent to enhance the reactants miscibility and the result was promising, achieving conversions almost 20% higher than the industrial process used nowadays (i.e., 52.55% with pTSA), accordingly to Rossa et al. [9, 57].

One of the main advantages that renders clays a relevant alternative for industrial application is their low cost. The latest studies focus on modifying its textural and acid properties to enhance its conversion and selectivity. Timofeeva et al. studied the modification of montmorillonite with nitric acid (HNO_3) and Amri et al. the modification of a natural clay with hydrochloric acid (HCl). Both systems used solvents (acetonitrile and isopropanol, respectively) in the reaction medium and mild conditions (273 K and ambient pressure). The first study presents better conversion values, 94%, with a lower catalyst loading, probably due to its higher density of strong acidic sites, together with the fact that it was more stable in terms of catalyst deactivation [63, 64]. The mild conditions used, the results attained, and the catalyst cost makes the research on modified clays promising; however, further studies on the reaction kinetics must be performed.

The metal oxides' catalysis is similar to the zeolite's; therefore, the surface area, the size of the pores, and the strength of the acidic sites play major roles in the conversion and selectivity to solketal [67]. Zhang et al. investigated the effect of introducing a heteroatom in the structure of a metal oxide and concluded that Ni promoted the highest solketal yield (75.44%), a fact that they attributed to the larger surface area of M-NiAlPO4, which increased the number of surface-exposed Ni atoms responsible for the stronger acidity of the catalyst [65]. Gadamsetti

et al. and Rodrigues et al. found that molybdenum and niobium have high activity to glycerol conversion to solketal in similar systems, but the first presented better results because, besides the total conversion of glycerol, the reaction was performed under milder conditions [66, 67]. There are numerous similar studies in the literature, many of them with low selectivity to solketal which were not included as inputs to Table 2.1 [92, 93].

A noteworthy new green catalyst was proposed by Gonçalves et al., a carbon-based solid prevenient from biodiesel waste acidified by sulfuric acid (H_2SO_4). The catalysts were prepared with different amounts of sulfuric acid and the one that performed better (X_{gly} = 82%) was the GC-1:2 (i.e., 1:2 mol carbon-based material:acid), besides being more stable at higher temperatures (373 K). Doping the catalyst with higher sulphur concentrations does not make difference in its structural properties [70]. Similarly, Ballotin et al. produced a sulfonated catalyst based on bio-oil with amphiphilic characteristics: hydrophobic carbon matrix with hydrophilic oxygen and sulfonic surface groups. The system was kept under mild conditions, without solvent, and the catalyst was in emulsion. The conversion was up to 98% with a large excess of acetone [72]. A similar conversion was attained by Saikia et al. for a cellulose-based catalyst, 97.1%. The authors performed a microwave-assisted reaction and, due to that, could achieve such high conversion under atypical short reaction time, only 10 minutes [74].

The sulfonation strategy was also used by Vannucci et al.; however, the matrix was zirconium oxide. Despite achieving good conversion yields of 80%, the previous materials are more appealing environmentally because they are obtained from renewable sources and are more resistant to recycle [80]. Using a similar strategy of acidifying a carbon-based material, Rodrigues et al. [87] proposed treating the yeast biomass waste prevenient from ethanol production to transform it in an activated carbon and then treat it with nitric acid (HNO_3). This acid catalyst achieves a conversion of up to 91% and could be used at least for four cycles, proving to be an environmentally appealing strategy to produce solketal.

The growing number of studies investigating alternative catalysts evidence the potential and the relevance of solketal on the market, but it also reveals how far the industrial process applied nowadays is from the optimum. Many research works disclose promising catalysts that attain high glycerol conversions and that can be recycled; however, almost none assess the viability of using them on larger than laboratory scale. Furthermore, only a few assess the impacts of the impurities of crude glycerol over the catalysts or suggest pre-treatments for this reactant. There is also a lack of thermodynamic and kinetic study for several of the mentioned catalysts, fundamental data to deliberate whether the catalyst is appropriate for industrial application. Therefore, the development of new catalysts must be supported by data that disclose their capacity to be used on a large scale.

Kinetics and Mechanisms of Reaction

Solketal synthesis is a relatively simple reaction, with controlled potential hazards; therefore, it could be carried in less carefully designed reactors when compared to inflammable or explosive reactions. However, since it is also a limited reaction, to make it industrially viable, it is necessary to rely on kinetic and thermodynamic data to design efficient equipment. The most-cited kinetic models in the open literature are the Pseudo-homogeneous (PH), Langmuir-Hinshelwood-Hougen-Watson (LHHW), and Eley-Rideal (ER).

The simplest approach is the Pseudo-homogeneous (PH) model, based on Power Laws and often referred to with this term. It considers a reversible reaction of first order in each species with virtually no adsorption of the species on the catalyst; therefore, the reaction would occur exclusively in the fluid phase [9, 60]. It is usually represented by the following expression:

$$\Re = k\ (C_{gly}C_{acetone}\ -\ \frac{C_{solketal}C_{water}}{K_{eq}}) \tag{2.1}$$

where C represents the concentration of each species, k the reaction kinetic constant, and K_{eq} the thermodynamic equilibrium constant.

In the Langmuir-Hinshelwood-Hougen-Watson (LHHW), the mechanism comprises three steps: (i) adsorption of acetone and glycerol on the catalyst surface; (ii) a bimolecular reaction of adjacent molecules occurs to form a short-lived hemiketal (rate-controlling step), followed by two reactions that originate solketal and water; finally, (iii) both products desorb from the surface of the catalyst [9, 60]. The usual equation is:

$$\Re = k\frac{C_{glycerol}C_{acetone} - \frac{C_{solketal}C_{water}}{K_{eq}}}{(1 + K_{water}C_{water})^2} \quad (2.2)$$

where K_{water} is the adsorption equilibrium constant for water. Equation 2.2 is a simplification of the actual rate law, as the adsorption of water is usually much stronger than the other compounds; therefore, these terms are neglected in the denominator [9, 60].

The Eley-Rideal (ER) model considers that only one of the molecules adsorb into the catalyst surface, while the other reacts directly from the fluid phase. It is expressed as follows:

$$\Re = k\frac{C_{glycerol}C_{acetone} - \frac{C_{solketal}C_{water}}{K_{eq}}}{1 + K_{water}C_{water}} \quad (2.3)$$

All the studies reviewed report the use of one of these three models. Table 2.2 summarizes the recent literature (from 2015 on) on kinetic studies for solketal synthesis over a range of catalysts.

Table 2.2. Summary of the recent investigations on the kinetic study of solketal synthesis.

Author	Catalyst	E_A (kJ·mol^{-1})	Other Parameters [1,2,3,4,5]	Ref.
Pseudo-homogeneous (PH)				
Rossa, 2017	Zeolite H-Beta	44.77 ± 1.2	$\overleftarrow{E_A}$ = 41.40 ±1.80 kJ·mol^{-1} K_{eq} = 0.52 (313 K)	[57]
Dmitriev, 2018	Sulfuric acid	87.1	$\overleftarrow{E_A}$ = 101.67 kJ·mol^{-1} K_{eq} = 0.77 (303 K)	[94]

Cornejo, 2019	Purolite® CT275	39.78 ± 0.34	$k = (4.800 \pm 0.030).\ 10^{-3}$ $L^2\ mol^{-1} \cdot g_{cat}^{-1} \cdot min^{-1}$ (298 $\Delta H = -6.605 \pm 0.168$ kJ· mol^{-1}	[61]
Amri, 2019	HCl activated clay	65.4	$\overleftarrow{E_A} = 70.65$ kJ· mol^{-1} $K_{eq} = 0.3931$ (313 K)	[64]
Ji, 2020	Ionic Liquid	28.2	$K_{eq} = 0.4703$ (298 K)	[69]
Vannucci, 2020	Sulfated zirconium oxide	88.1 ± 8.9	$k = 0.11516 \pm 0.0093$ $mol \cdot g_{cat}^{-1} \cdot min^{-1}$ $\Delta H = -11.6 \pm 1.1$ kJ· mol^{-1} $\Delta G = 4.0 \pm 0.1$ kJ· mol^{-1}	[80]
Taddeo, 2021	Iron(III) Complex $FeCl_3(1\text{-}NO_2)$	13	$\overleftarrow{E_A} = 64$ kJ·mol^{-1}	[95]
Langmuir-Hinshelwood−Hougen−Watson (LHHW)				
Moreira, 2019	Sulphonic Ion Exchange Resin Amberlyst-35	69.0 ± 6.6	$k = 0.492 \pm 0.093$ $mol \cdot g_{cat}^{-1} \cdot s^{-1}$ $K_{water} = 14.4 \pm 3.1$ $\Delta H = -20.1 \pm 1.1$ kJ·mol^{-1} $\Delta G = 1.4 \pm 0.3$ kJ· mol^{-1}	[9]
Sulistyo, 2020	Metal Organic Framework Basolite F300	15.7	$K_{eq} = 6.345$ (at 303 K) $K_{water} = 1.029$ $\Delta H = -29.7176$ kJ· mol^{-1} $\Delta G = -4.8675$ kJ· mol^{-1}	[81]
Li, 2020	Cation Exchange Resin NKC-9	44.3	$\overleftarrow{E_A} = 47.23$ kJ· mol^{-1} $K_{eq} = 0.9690$ (323 K) $K_{water} = 0.7511$	[96]
Eley–Rideal (ER)				
Esteban, 2015	Ion Exchange Resin Lewatit GF101	124.0 ± 12.9	$\overleftarrow{E_A} = 127.3 \pm 12.6$ kJ mol^{-1} $K_{eq} = 0.3679$ $K_{water} = 128.0 \pm 21.4$	[60]

Sulistyo, 2020	Ion Exchange Resin	21.2	$K_{acetone} = 0.62$ $K_{solketal} = 0.03$	[62]

1 $\overleftarrow{E_A}$: reverse reaction activation energy. 2 K_{eq}: equilibrium constant. 3 ΔH: enthalpy 4 ΔG: reaction Gibbs free energy. 5 K_i: adsorption equilibrium constant of species *i*.

Being mindful that there is no adsorption onto the catalyst in homogeneously catalysed reactions, it is intuitive to think the PH model, which does not consider the adsorption of molecules, describes well this type of process. Dmitriev et al. proposed a mechanism (Figure 2.5) for the reaction with sulfuric acid (strong Brønsted acid) as a catalyst comprising a nucleophilic addition of glycerol to the carbonyl group of acetone, forming a semiketal. Then, the ring closure takes place, forming a carbenium ion (limiting step). Finally, the H+ ion is released and solketal is formed [94].

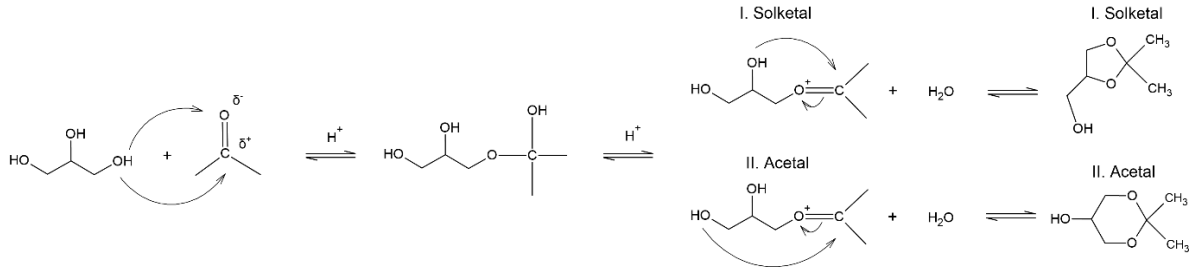

Figure 2.5. Plausible mechanism of reaction catalysed by sulfuric acid (based on [94]).

It is important to notice, however, that the mechanism proposed by Dmitriev et al. is unprobable since the protonation of the oxygen from the carbonyl group, promoted by the ions of the acidic medium, is what impels the nucleophilic attack, similar to what is proposed by Nanda et al., described in Figure 2.6 [36].

With ionic liquid as the catalyst, Ji et al. obtained activation energy of 28.2 kJ· mol^{-1}. The authors highlighted the high activity of this catalyst, tested for the first time in the study [69]. Taddeo et al. proposed a mechanism with two steps to describe the formation of solketal: first, the coordination of the carbonyl oxygen of acetone with the metal centre, then the nucleophilic

attack of a glycerol oxygen molecule to the carbonylic carbon of the coordinated acetone, followed by ring closure, forming solketal, and releasing of a molecule of water. This mechanism is generally accepted for solketal formation with Lewis acid catalysts (Figure 2.6). The authors reported the lowest activation energy of 13 kJ·mol^{-1} (Table 2.2), a result that may be supported by da Silva et al. in a study where they affirm that Lewis acid catalysts are more effective than Brønsted acid catalysts for this ketalization [55, 95]. Nevertheless, it is notable that this is a very low value for the reaction.

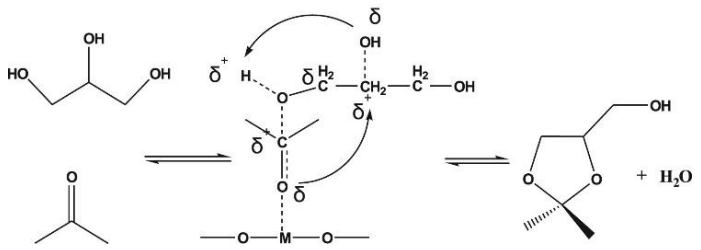

Figure 2.6. Mechanism of reaction of Lewis acid catalysts (reprinted from Renewable and Sustainable Energy Reviews, 56, Nanda, M.R.; Zhang, Y.; Yuan, Z.; Qin, W.; Ghaziaskar, H.S.; Xu, C., Catalytic conversion of glycerol for sustainable production of solketal as a fuel additive: A review,1022–1031, Copyright 2021, with permission from Elsevier) [36].

Despite using a sulphonic ion exchange resin Purolite® CT275, contrary to other authors, Cornejo et al. opted for using the PH model, which they named Low Range Adsorption in their study. After testing ER and LHHW, the authors affirmed the adsorption term was zero in the modelling studies, which justifies the choice for the model that does not consider adsorption of water. They reported smaller activation energy than other authors usually found for this type of catalyst, 39.78 ± 0.34 kJ·mol^{-1} [61].

Vannucci et al. explained their choice for the PH model instead of the LHHW model: water does not affect the number of active sites of the sulphated zirconium oxide, because, in the presence of water, the Lewis acid sites (Zr (IV) species) are converted to Brønsted acid sites. Therefore, the LHHW equation can be simplified to the PH equation [80].

The comparison of the studies that used the LHHW model reveals that the reaction conducted by Sulistyo et al. with MOF Basolite F300 would be the easiest to carry, analysing solely the activation energy estimated by the authors [81]. Basolite F300 is a highly active Lewis acid catalyst; therefore, the explanation for this low activation energy value (i.e., 15.7 $kJ \cdot mol^{-1}$) may also be explained by da Silva et al., who showed a higher activity of Lewis acid catalysts when compared to Brønsted acid catalysts [55]. Moreira et al. and Li et al. reached approximate values using different ion exchange resins as catalyst, 69.0 and 44.3 $kJ \cdot mol^{-1}$, and the latter found that the reverse reaction is less favourable than the forward reaction. As for K_{water}, it is notable that Amberlyst-35 has much more affinity to this compound [9, 96].

Esteban et al. compared the PH, LHHW, and ER models and concluded that the latter provided the best fit, considering that the rate law is zero order for the reactants. However, the activation energy was high (over 120 $kJ \cdot mol^{-1}$) compared to the remainder estimations in Table 2.2 [60]. Conversely, using the same model but with a rate law of the first order for the reactants, Sulistyo et al. found a slightly lower value with Indion 225 Na [62]. As previously stated, this is probably due to the different characteristics of the catalysts.

The generally accepted mechanism for the solketal synthesis using Brønsted acid catalysts is shown in Figure 2.7.

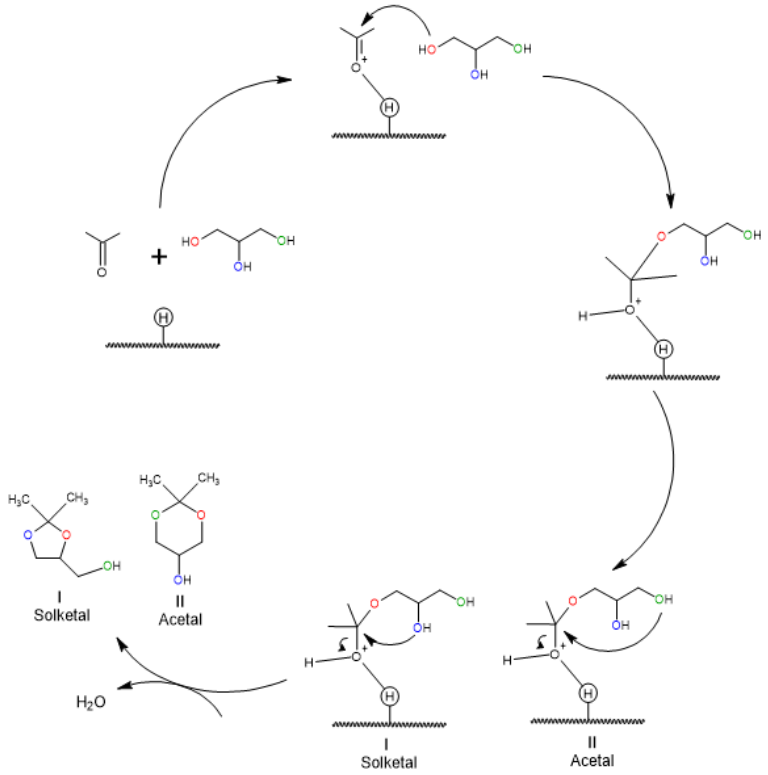

Figure 2.7. Mechanism of reaction of Brønsted acid catalysts.

The difference between the reaction catalysed by Brønsted and Lewis acids is that for the first, a short-lived hemiketal is formed and suffers a nucleophilic attack from one of the hydroxyl groups of glycerol to its central carbon, leading to the formation of solketal or the six-membered ring ketal (2,2-dimethyl-1,3-dioxan-5-ol). For Lewis catalysts, the metal site coordinates and activates the carbonyl group of acetone, followed by an attack from the glycerol alcoholic group to this carbonyl and a consequent bond forming between the carbonyl oxygen atom and the secondary carbon atom of glycerol. Finally, dehydration occurs to form the five-membered ring [36, 80].

The products of the reaction are a five-membered ring (solketal) and a six-membered ring (5-hydroxy-2,2-dimethyl-1,3-dioxane), with much higher selectivity for the first compound [9, 36]. This is probably due to the more likely acetone attack on the end-chain hydroxyl group than on the middle-chain hydroxyl group [9]. Additionally, the most energetically favourable product is the five-membered ring, because one of the methyl groups of the six-membered ring

is in the axial position of the chair conformation, an unstable position due to the steric repulsion between the methyl group and the hydrogens bonded to the carbons of the ring [40].

Recent Advances on the Continuous Process

Among the continuous process strategies studied, the fixed-bed reactor stands-out owing to its relatively simple operation under mild conditions, the use of heterogeneous catalysts, and the possibility of coupling other processes (as downstream distillation separation), or unit operations (as adsorption or membrane permeation). Most of the recent studies still relied on ion exchange resins and hierarchical zeolites. The latest developments and tests on conventional continuous processes are summarized in Table 2.3.

Table 2.3. Summary of the recent investigations on the continuous synthesis of solketal.

Author	Catalyst	Catalyst Loading	Reaction Conditions	Results	Ref
Fixed-bed					
Dmitriev, 2016	KU-2-8 Cation-Exchange Resin	205 g	G:A = 1:5 T = 308 K P = N.A. Solv. = Ethanol Space time = 1.45 h	X_{gly} = 65%	[97]
Oliveira, 2016	Amberlyst-15	7 g	G:A = 1:20 T = 323 K P = 1 bar Solv. = DMF Space time = 0.2 h	X_{gly} = 96% Sel = 94%	[98]
Guidi, 2016	Amberlyst-36	0.09 g_{cat}/g_{gly}	G:A = 1:4 T = 298 K; 373 K P = 10 bar Solv. = Methanol	X_{gly} = 95% Sel > 99%	[99]
	AlF3·3H2O	0.067 g_{cat}/g_{gly}		X_{gly} = 80%	

			WHSV [1] = 2 h^{-1}	Sel > 99%	
Konwar, 2018	Lignosulfonate-based macro/mesoporous solid protonic acids	0.5 g	G:A = 1:8 T = 313 K P = 1 bar Solv. = Ethanol Space time = 0.25 h	X_{gly} = 92% Sel = 99.5%	[100]
Cornejo, 2019	Purolite CT275	N.A. [2]	G:A = - T = 323 K P = High pressure [2] Solvent Free Space time = -	X_{gly} = 91% Sel > 99.5%	[61]
Domínguez-Barroso, 2019	Monolithic structured carbon-based functionalized with sulfonic acid	0.345 g_{cat}/g_{gly}	G:A = 1:8 T = 330 K P = N.A. Solvent Free WHSV 1 = 2.9 h^{-1}	X_{gly} = 99% Sel > 99%	[101]
Kowalska-Kus, 2019	ZSM5(P) [3] ZSM5(H) [3] Beta(P) [3] Beta(H) [3] Mordenite(P) [3] Mordenite(H) [3]	0.083 g_{cat}/g_{gly}	G:A = 1:3 T = 323 K P = 1 bar Solv. = Methanol WHSV 1 = 3.4 h^{-1}	X_{gly} = 35% X_{gly} = 90% X_{gly} = 90% Sel > 97% X_{gly} = 90% Sel > 97% X_{gly} = 86% Sel = 97% X_{gly} = 86% Sel = 97%	[102]
Fernández, 2019	Sulfonated hydrothermal carbons (SHTC)	0.00085 g_{cat}/g_{gly}	G:A = 1:9 T = 298 K P = 1 bar Solv. = Ethanol	Prod = 2048 $mmol_{solketal}$ $g_{catalyst}^{-1}$ h^{-1} [4]	[71]

			Space time = 1 min		
Moreira, 2019	Amberlyst-35	25 g	G:A = 1:2 T = 313 K P = N.A. Solv. = Ethanol Space time = 0.25 h	X_{gly} = 81%	[10]
Kowalska-Kus, 2020	ZSM5 (H) [3] Beta(P) [3] USY(P) [3]	0.083 g_{cat}/g_{gly}	G:A = 1:3 T = 323 K P = 1 bar Solv. = Methanol Space time = 5 min	X_{gly} = 85% Sel > 95% X_{gly} = 69% Sel > 95% X_{gly} = 85% Sel > 95%	[102]
Capillary Microreactor					
Huang, 2020	ZSM5 Film	0.050 g_{cat}/g_{gly}	G:A = 1:2 T = 323 K P = N.A. Solvent Free Space time = 2.86 min	Y_{solk} = 30%	[103]
Zhang, 2020	ZSM5 Film	4.7 μm film thickness	G:A = 1:8 T = 323 K P = N.A. Solvent Free Space time = 2.86 min	X_{gly} = 62%	[104]
Continuously Stirred Tank Reactor					
Dmitriev, 2018	Sulfuric Acid	0.00066 g_{cat}/g_{gly}	G:A = 1:5 T = 308 K P = N.A. Solvent Free Space time = 1.73 h	X_{gly} = 68.4%	[94]

1 Weight hourly space velocity. 2 Not available. 3. P stands for parent and H for hierarchical. 3 Only result provided.

Nanda et al. and Moreira et al. proposed a similar system for the solketal synthesis in a fixed-bed reactor, both at 313 K, and an acetone to glycerol molar ratio of 2; the first, with the ion-exchange resin Amberlyst-36, achieved a conversion of 74%, and the latter, with Amberlyst-35, achieved a conversion of 81%. It is important to emphasize that these conversion values were obtained under transient operation [10, 39]. Additionally, Nanda et al. achieved a conversion of 94% using optimized conditions and an acetone to glycerol molar ratio of 4, like Guidi et al., who used the same resin under similar reaction conditions [39, 99]. Oliveira et al. also proposed an analogous system, but with the use of Amberlyst-15, and achieved excellent conversion, but the excessive acetone was a problem that could not be overcome [98].

Kowalska-Kuś et al. compared the catalytic performance of three zeolites (H-Beta, H-Mordenite, and H-ZSM5), also in a fixed-bed reactor, with methanol as the solvent in mild conditions, and found conversion about 88%, with an acetone to glycerol molar ratio of 3. The H-ZSM5 was subjected to desilication and acid pre-treatment to enlarge the pores and achieve an acceptable conversion. Moreover, the zeolites presented a loss in their activities over time [102]. The same researchers investigated the performance of zeolites with crude glycerol and achieved good conversion rates after just 1 h of reaction, but there was a fast deactivation of the catalysts and there was almost no conversion after 6 h [102].

Still on a fixed-bed reactor, but with a different type of packing, Domínguez-Barroso et al. built a carbon-based monolithic structure from spiral-wound laminated cellulose, constituting a structured packed reactor. The structure was impregnated with methanesulfonic acid solution with SO_3H to provide the catalyst acidic sites. The authors reported a complete glycerol conversion at WHSV = 2.9 h^{-1} and no catalytic activity loss, which they attributed to the possible hydrophobic character of the monolithic structure [101].

Solketal synthesis was also tested in capillary microreactors with zeolite ZSM5 film, as proposed by Huang et al. and Zhang et al.; however, the results are not encouraging when considering scaling-up the process [103, 104].

Most of the studies on the continuous production of solketal are still done on a very small scale, which inhibits its industrial application, required to solve the problem of the gut of glycerol. Furthermore, many continuous technologies still focus on catalyst performance rather than on intensifying the overall operation by handling the limitations inherent to this reaction.

2.5. Solketal Production

The number of studies on solketal synthesis in the open literature is substantial, with many new catalysts being investigated. However, the number of studies on solketal production at an industrial scale grows at a much slower pace and the literature on large-scale methods for the production of solketal is rather scarce.

Solketal production plants are normally divided into Reaction Section and Separation Section. On a usual flowsheet, there is necessarily a reactor, the type depending on the catalyst and on the process, and a separation unit, usually a sequence of distillation columns. There can also be one or more mixers to homogenize the reactants and a heat exchanger to heat the compounds to the reaction temperature. Usually, a vessel is used to collect the products before the separation section. The recovered eluent and unreacted reactants are often recycled back to the process.

The proposed flowsheets found after an extensive bibliographic search are described with more details in Section 2.5.1. Then, the patented processes that could be industrially implemented are described in Section 2.5.2.

2.5.1. Processes

Zaharia et al. [105] proposed an industrial flowsheet divided into two sections: in the reaction section, solketal production would be carried in a Continuously Stirred Tank Reactor (CSTR) and in the separation section, three distillation columns would purify the products and recycle the unconverted reactants. The proposed flowsheet is exhibited in Figure 2.8. The authors used the kinetic and thermodynamic data from Nanda et al. [39] to estimate the mass and energy balances necessary to process a glycerol stream resultant from a biodiesel plant, aiming to reach a glycerol conversion of 76.5% with Amberlyst-35 as catalyst. The stream is considered pure glycerol and there is no information about its pre-treatment. The flowsheet was designed in Aspen Plus software. The reaction section comprises two mixers, one for each reactant, followed by a heat exchanger to assure the reactor's inlet stream is at 308 K and then the CSTR. The authors proposed that the catalyst could be retained inside the reactor by placing it in a basket or it could be later separated in a cyclone or in a decanting unit. The separation section consists of three distillation columns; in the first, acetone would be separated and recycled, in the second, water would be removed as distillate with 99.9% of purity, and in the third, solketal would be recovered as distillate also with high purity (99.8%) and the unreacted glycerol would be recycled [105].

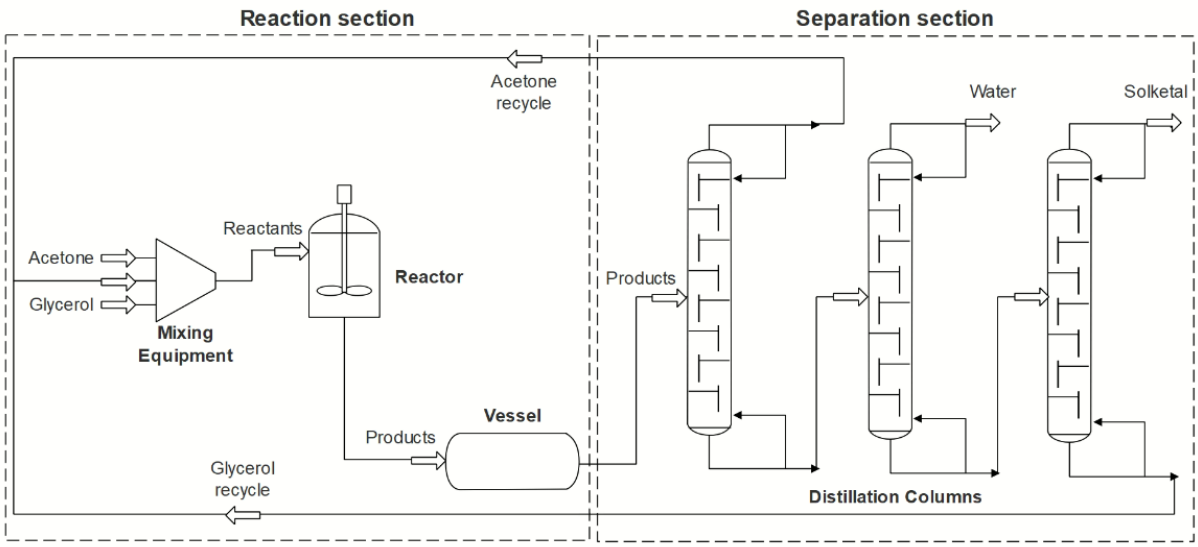

Figure 2.8. Flowsheet of the industrial solketal production plants proposed by Zaharia et al. (without vessel) and Dmitriev et al. (without mixing equipment) [105, 106].

In this study, the economic evaluation is presented; however, the authors have not accounted for the reactants and catalyst costs. Moreover, they have not provided information about glycerol purification costs, which is a necessary step once Amberlyst-35 is deactivated when salts are present in crude glycerol. Thus, considering a payback period of five years, the cost to produce 3720 t of solketal/year was estimated at US$128.50/ton, a much lower value than what was estimated in other studies and which can be considered unrealistic [10,25,120].

Dmitriev et al., one of the few groups that endorsed the use of traditional homogeneous catalysts, performed experiments with H_2SO_4 and a series of heterogeneous catalysts and concluded that H_2SO_4 was the most economically appealing for the industrial production of solketal. The authors proposed a similar flowsheet to Zaharia et al. comprising a CSTR, where the reactants and the catalyst would be directly fed, followed by a vessel to collect the reaction products and then three Rectification Columns with the same separation procedure suggested by Zaharia et al. The neutralization of H_2SO_4 would be carried by adding NaOH in the stream between the vessel and the first column. The authors highlighted that the most energetically

demanding step would be acetone recovery because a large reflux ratio is necessary to assure the water content in the unconverted acetone is low [106].

After stating the many benefits of using heterogeneous catalysts, as higher productivity, no need to purify the products by neutralization, the consequent absence of wastewater due to not needing this step, and the prevented corrosion of the apparatus, the authors counteracted the mentioned benefits. They stated that the low miscibility between acetone and glycerol impairs the reaction; thus, low conversion is attained and there is the need of adding a solvent in the reaction mixture. By using H_2SO_4, there would be no need to use a solvent to enhance the reactants miscibility, which would diminish the equipment costs (no need for a pre-mixer before the reactor) and operational costs (no need to separate ethanol from the products). Additionally, the glycerol recycled back to the reactor has high impurity content, which would quickly deactivate the heterogeneous catalyst and greatly increase the operational costs. The study affirms the proposed flowsheet is simple, reliable, economically efficient and would reach a solketal yield near 100%. No economic evaluation data was provided [106].

Da Silva et al. proposed a similar flowsheet (Figure 2.9) but performed a more meticulous economic analysis. The flowsheet comprises two mixers, one for combining fresh and recycled glycerol, followed by the second mixer where acetone, glycerol from the first mixer, and the Lewis catalyst (solid-supported SnF_2) are added. The second mixer's outlet stream is the inlet of the reactor (generic conversion reaction vessel operating at 298 K and 1 bar), which is expected to reach a glycerol conversion of 80%. The condensate stream with the products, unconverted reactants and catalyst follows to a filter to remove the catalyst. The filter's outlet stream is inserted in the first distillation column to separate the remainder of acetone and water, which is the most energetically demanding step. The bottom stream follows to the second distillation column to obtain high purity solketal (99.6%) and the unreacted glycerol that will be recycled back to the system. Acetone is not recycled [107].

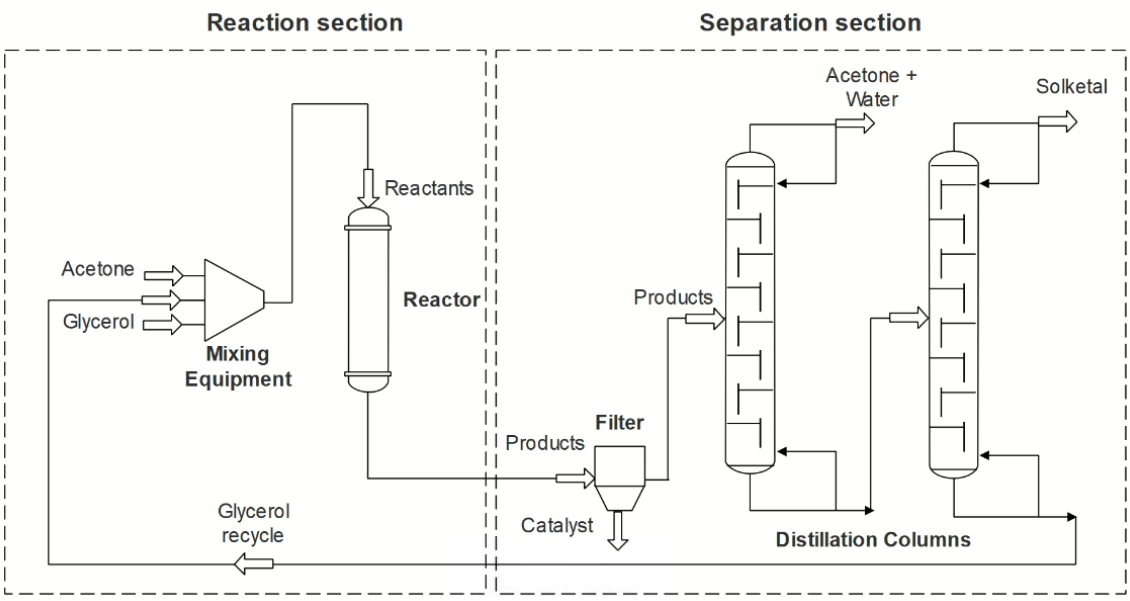

Figure 2.9. Flowsheet of the industrial solketal production plant proposed by da Silva et al. [107].

One of the most significant economic concerns of an industrial plant is the catalyst cost. SnF_2 is highly recoverable and recyclable; therefore, it was assumed to be replaced twice a year, accounting for only 0.005% of the annual operating costs. The other consumables account for nearly 17.50% of the operating costs. The total cost of producing solketal was US$ 1229/ton; thus, when compared to the selling price stated by Al-Saadi et al. of US$ 3000/ton, one can assume implementing a solketal production plant would be highly profitable [107, 108].

Al-Saadi et al. simulated and compared the performance of three industrial flowsheets: (I) a one-stage solketal process plant operated at 8.5 wt% Sulphonic Acid-Functionalized Copolymer catalyst (ST-DVB-SO_3H), 323 K, and a glycerol to acetone molar ratio equal to 1:6, obtaining 87% solketal yield; (II) a similar plant with a glycerol to acetone molar ratio equal to 1:12, obtaining 98% solketal yield; (III) and a two-stage plant with the first step operating at 8.5 wt% ST-DVB-SO_3H, 323 K, and a glycerol to acetone molar ratio equal to 1:10, obtaining 84% solketal yield in the first step, followed by removal of formed water, and another reaction under the same conditions to achieve 98% solketal yield. The two-stage plant

(Figure 2.10) was found to be the most economically appealing, because the separation costs were lower than the one-stage processes, resulting, according to the authors, in a Net Present Value (NPV) 45.7% higher when compared with (I) and 0.57% higher when compared with (II); therefore, (III) will be described further [108].

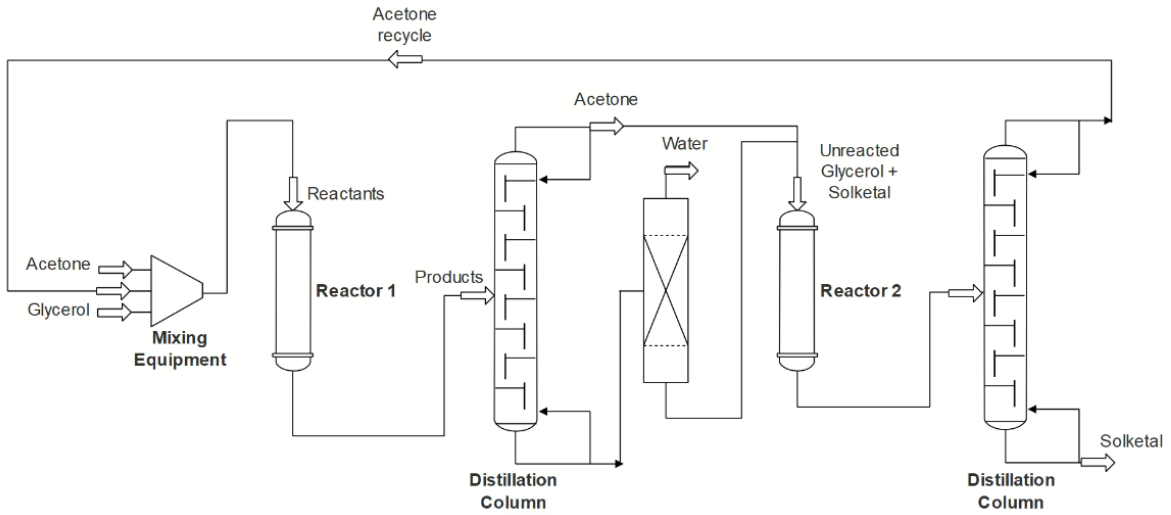

Figure 2.10. Flowsheet of the industrial solketal production plant proposed by Al-Saadi et al. [108].

The flowsheet comprises two mixers, the first to combine recycled and fresh acetone, followed by the second where glycerol is inserted. Then, the stream is heated in a heat exchanger up to the reaction temperature, which occurs in a plug-flow reactor packed with the catalyst. The first reaction's product stream is separated in a distillation column, the acetone recovered as distillate is reinserted in the second reactor and the bottom stream containing glycerol, water, and solketal is fed to a separation unit (not specified), where water is removed. The products stream is cooled in a heat exchanger prior to being fed to the second reactor, where almost all the remainder glycerol is converted. What follows is the second distillation column, where acetone is collected and recycled back to the system and solketal is the bottom product with a content of 98% solketal and 2% glycerol. According to the authors, the separation cost is lower because, in the second reaction, only 0.16% of the products' stream is water. The cost of producing solketal in the described plant, considering a capacity of 100,000

t/years and a 20-year lifetime, was estimated at $ 2058/ton, well below the selling value reported by the authors US$ 3000/ton [108].

An even deeper analysis was proposed by Chol et al. in a study that compared three scenarios comprising the treatment of crude glycerol and its valorisation into solketal and glycerol carbonate. The authors concluded that the most economically advantageous flowsheet performs the valorisation into both products, with glycerol equally divided for both routes [109].

The flowsheet (Figure 2.11) will be briefly described, with more focus on the solketal production steps. Initially, crude glycerol and methanol were fed into a mixer to lower glycerol viscosity so the mixture can undergo a saponification reaction using KOH in the first reactor. The resultant stream was fed to a second reactor to be acidified using HCl before being transferred to a gravity separator for sedimentation, where glycerol (bottom layer) was separated from free fatty acids (light liquids) and vapours. The resultant glycerol was cooled in a heat exchanger prior to solvent extraction using petroleum ether in a liquid-liquid extraction vessel. Petroleum ether was then recovered in a flash separator for reuse and glycerol was neutralized with KOH in another reactor. Then, the resultant glycerol was fed into a membrane separator, where impurities were separated from the glycerol, methanol, and water solution, and in turn, vaporized in a flash separator. Glycerol was cooled and split into two streams. Half of the glycerol was converted into glycerol carbonate by feeding it to a mixer, where it was combined with recovered methanol, then heated and inserted in the reactor with dibutyltin oxide (catalyst) and excess CO_2. The other half of glycerol, i.e., the stream leading to solketal production, was pressurized (12,000 kPa) before being fed into a conversion reactor with acetone and heterogeneous catalyst Amberlyst-15. The reaction was carried at 343 K for 1.5 h. The separation was promoted by a flash separator, where acetone with trace water was vaporized and recovered and the solketal stream was split into pure solketal and a recycle

stream that was sent back to the reactor to improve conversion, since glycerol conversion is only 35% but can be enhanced with product recycle, according to the authors [109].

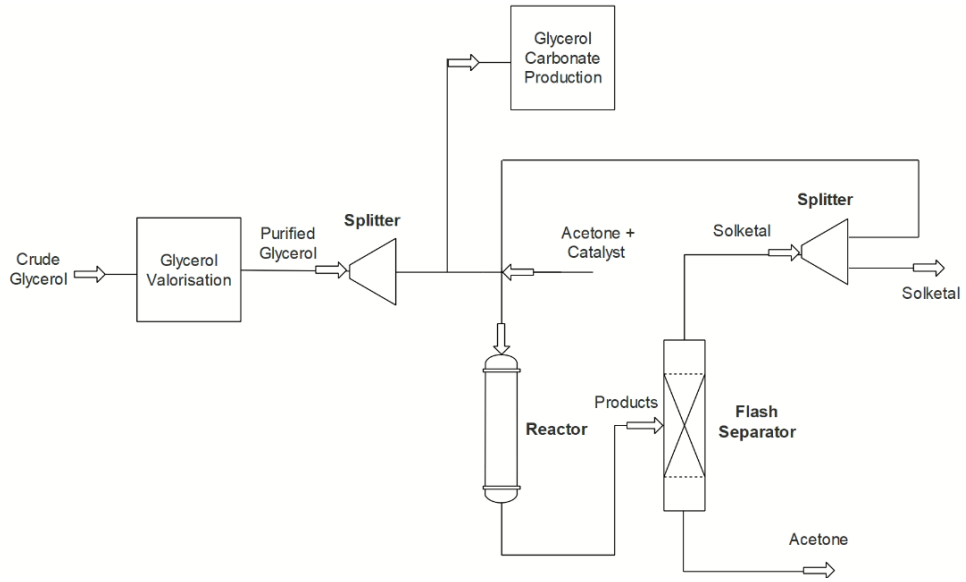

Figure 2.11. Flowsheet of the industrial solketal production plant with glycerol purification proposed by Chol et al. [109].

The economic analysis of implementing this industrial flowsheet is also promising, the cost of treating one ton of crude glycerol would be US$ 5045, while the revenue cost would be US$ 8036, resulting in a profit of almost US$ 3000/ton of glycerol. The total investment cost was expected to be recovered within three years of operation; considering that the first three years would be dedicated to building the facility, complete recovery is made within six years. According to the authors, these margins are decent for a biodiesel plant and the increased profit indicate that it would be worth it investing in crude glycerol purification and valorisation plant [109].

Another project proposed by Al-Saadi et al. is a plant where solketal would be valorised in situ simultaneously to biodiesel production. The authors studied an industrial facility operating at a molar ratio of 7:1:10 acetone:triolein:methanol, 323 K, 1 h of reaction, and 0.5 mol of DBSA (*p*-Dodecylbenzenesulfonic acid) catalyst to oil. The objective was to attain triolein conversion of 98% and glycerol conversion of 82% [108, 110].

The flowsheet (Figure 2.12) comprises one mixer where the catalyst (DBSA) and the oil are fed, parallel to a mixer where fresh acetone, fresh methanol and the recycled streams are inserted. The reactants are preheated and delivered to the reactor (generic conversion reaction vessel). The outlet of the reactor flows to a separator to be divided in a light organic fraction (the 'biodiesel-rich phase') and the heavy more polar fraction (glycerol, catalyst, solketal, unreacted methanol, and water). Then, the light fraction follows to a distillation column to separate acetone in the top and biodiesel in the bottom. The heavy fraction is separated in methanol in the top and low purity solketal in the bottom, and this is the most energetically demanding step. No information is given about the water produced as by-product or the recovery of the catalyst; however, it is stated that methanol and acetone are recycled [108]. Therefore, one can conclude that the flowsheet is not a complete industrial plant, as there are some missing purification steps necessary to attest the process is techno-economically feasible.

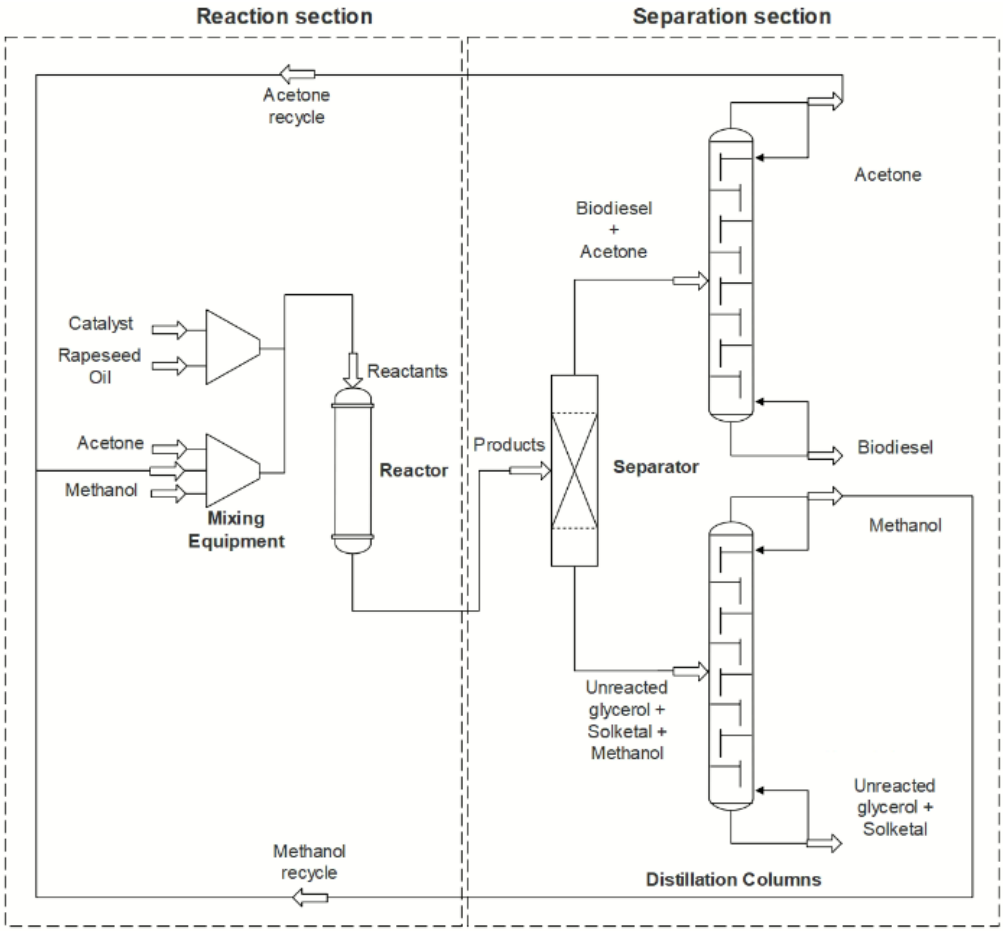

Figure 2.12. Flowsheet of the industrial solketal production plant with glycerol valorisation in situ proposed by Al-Saadi et al. [108].

Nonetheless, the economic analysis was performed considering an oil feed of 100,000 t/year and a plant lifetime of 20 years. Compared to an industrial process producing biodiesel alone, which would cost approximately US$ 927.9/ton of biodiesel, coupling the production with solketal makes the industry more profitable and the cost of producing biodiesel is reduced to US$ 824.8/ton [108].

Bumbac and Banu proposed one of the first industrial flowsheets with an equipment that combines reaction and separation in the same unit, a catalytic distillation (CD) process in a dividing wall column (CDDWC). In practice, one side of the DWC is dedicated to the reaction, and the other to the separation by distillation. At the top and bottom of the CDDWC there are plates, prior to the condenser and the reboiler. To foster the reaction in favour of the products,

the authors used the concept fist proposed by Clarkson et al of using acetone in vapor phase as stripping agent [49], which requires a large excess of acetone. The separation side of the DWC performs the separation of the vapor phase acetone from water, and acetone is recycled back to the process. Solketal is recovered by the bottom stream. Before the CDDWC, the authors include a fixed-bed pre-reactor to avoid the two liquid phases formation in the catalytic zone of the column and the feed is inserted in the reaction side. The authors considered a plant with capacity of processing 24,000 metric tons/year of pure glycerol, however they did not perform the economic evaluation of the process [111].

2.5.2. Patents

A meaningful indication of the industrial relevance of a process or new compound is the number and technological value of the patents developed by major market players. Patent research reveals the most recent advances in a specific field, the development of new technologies, and the relevant course of events concerning the subject searched. Additionally, it reveals the gaps in the literature that can be seen as an opportunity to develop and propose new processes. A good patent is comprehensive; therefore, the claims must be concise but not specific, which explains why most of the patents of solketal production generically mention the production of acetals and ketals [112].

Usually, when a technologically valuable innovative process or product is developed and patented, it is followed by several related patents with lower value when analysed singly [113]. Concerning the use of solketal, it was initially deeply explored as solvent and plastifying agent in paints, films, and cleaning products; therefore, several products with different solketal contents were created and patented. Then, it was discovered to be useful as an antifreezing compound, which drove the research to its use as an additive for aviation fuel. Closely related, solketal use as fuel additive for surface transport was investigated due to the enhancement of

fuel properties. Nowadays, the current trend of solketal application is its use as a biocompatible solvent in medicaments, since it is non-toxic for humans, and it is soluble in body fluids. It is important to highlight that these research fields overlap each other; therefore, the described timeline is a draft of the trend of the new uses of this ketal based on the patents published.

Concerning solketal production, the initial innovation was to carry the process in batch reactors with homogeneous catalyst, which was followed by the study of the performance of different homogeneous catalysts. Then, heterogeneous catalysts were proposed, still in batch, soon upgraded by the use of fixed-bed reactors, which nowadays have been extensively studied. Few patents were published proposing alternative production processes.

A common conclusion to many of the authors that proposed and simulated industrial flowsheets for producing solketal is that the costliest step is the separation in distillation columns to remove the excess of acetone [25,121,122]. In view of that, the focus of several patents is intensifying the process to obtain purer products already in the outlet stream of the reactor or to use different separation technologies. The alternative technologies and the most promising patents (based on the possibility of scaling-up the process to the industrial level) proposed by some of the major players on the market are summarized in Table 2.4.

Table 2.4. Summary of the patents for solketal production.

First Inventor, Publication Date	Patent	Assignee	Catalyst	Reaction	Separation	Ref
Process Intensification Strategies/Non-conventional operation						
Bruchmann, 1999	US5917059A	BASF SE	Homo- or heterogeneous	Reaction vessel with continuous distillation	Not necessary	[46]
Boesch, 2003	US6528025B1	Roche	Heterogeneous	Not specified	Pervaporation unit	[114]

		Vitamins Inc.				
Winkler, 2004	US20040024260A1	Evonik Degussa GmbH	Homo- or heterogeneous	Not specified	At least two-stage pervaporation or vapor permeation	[115]
Dubois, 2008	FR2906246A1	Arkema France SA	Heterogeneous catalyst	Simulated Moving Bed Reactor	Not specified	[116]
Dubois, 2008	FR2906807A1	Arkema France SA	Homo- or heterogeneous	Reactive extraction	Vacuum evaporation	[116]
Haiyu, 2018	CN107698552A	Guangzhou Yintian New Material Co., LTD	Heterogeneous catalyst	Membrane reactor	Not specified	[117]
Haiyu, 2018	CN107652263A	Guangzhou Yintian New Material Co., LTD	Heterogeneous catalyst	Reactive distillation on a shell and tube or column plate device	Not specified	[117]
Yujia, 2020	CN111253359A	China Petroleum & Chemical Corporation	Heterogeneous catalyst	Tank, fixed-bed, moving bed, suspended bed, or slurry bed reactor with tin-titanium-silicon molecular sieve as catalyst	Not specified	[118]
Yujia, 2020	CN111253363A	China Petroleum & Chemical Corporation	Heterogeneous catalyst	Tank, fixed-bed, moving bed, suspended bed, or slurry bed reactor with a mixture of a titanium silicalite and a tin silicalite molecular sieves	Not specified	[119]

Yujia, 2020	CN111253362A CN111253364A	China Petroleum & Chemical Corporation	Heterogeneous catalyst	Tank, fixed-bed, moving bed, suspended bed, or slurry bed reactor with tin-silicon molecular sieve	Not specified	[120]
Traditonal production methods						
Abe, 2004	JP2006273750A	Nippon Oil & Fat Co. Ltd.	Homogeneous catalyst	Reactor with stirring equipment	Distillation column(s)	[121]
Wimmer, 2011	EP2183238A1	Christof International Management GmbH	Heterogeneous catalyst	Plug-flow reactor	Distillation column(s)	[122]
Terrill, 2012	US20120330033A1	Eastman Chemical Co	Homogeneous catalyst	Reaction vessel	Distillation column(s)	[123]
Mastroianni, 2013	US20130178638A1	Rhodia Operations SAS	Homo- or heterogeneous	Reaction vessel or fixed-bed reactor	Distillation column(s)	[124]
Rodrigues, 2013	WO2013045967A1	Rhodia Poliamida e Especialidades Ltd.a	Homogeneous catalyst	Reaction vessel	Decantation, filtration, or centrifugation, followed by liquid-liquid extraction and distillation(s)	[125]
Rodrigues, 2014	US20140235878A1	Rhodia Poliamida e Especialidades Ltd.a	Homogeneous catalyst	Reaction vessel	Distillation column(s)	[126]
Terrill, 2014	US8829206B2	Eastman Chemical Co	Heterogeneous catalyst	Fixed-bed reactor	Distillation column(s)	[127]

Terrill, 2016	US9440944B2	Eastman Chemical Co	Heterogeneous catalyst	Fixed-bed reactor	Distillation column(s)	[128]
Varfolomeev, 2018	RU2625318C2	Institute of Biochemical Physics, Russian Academy of Sciences, in association with Company Tatneft	Homogeneous catalyst	Reaction vessel	Distillation column(s)	[129]

Evidencing the industrial applicability of reactive distillation as a PI strategy, BASF SA and Guangzhou Yintian New Material Co. proposed new methods for producing acetals and ketals. BASF SA patented a process of reaction preferentially in batch with continuous distillation of the azeotrope acetone-water, ideally after the equilibrium was reached, and continuous addition of fresh acetone. The azeotrope would have to be treated by distillation or absorption with desiccants, but the products would be obtained with purities of 95 to 99.5%, high enough for many applications, according to the authors, so further downstream would be unnecessary [46]. Guangzhou Yintian New Material Co. proposed a similar process to the proposed by Clarkson et al. [49, 117].

Aiming to replace the traditional and energy-intensive distillation, Roche Vitamins Inc. and Evonik Degussa presented pervaporation or vapor permeation for downstream separation. The basic flowsheet of the first comprises at least three modules of a reactor with acidic ion exchange resin, followed by a vessel with basic ion exchange resin and then the pervaporation unit. The vessel with the basic ion exchange resin is required for the formation of other acetals and ketals that have acidic compounds as by-product, but not for glycerol ketalization. As for the second, at least two modules of a reactor followed by the pervaporation unit, with more

acetone fed between the first membrane module and the second reactor and, in the end, another module to remove unreacted acetone. The inventors have not specified the type of reactor in which the reaction would be carried; however, both stated the importance of installing a heat exchanger between the reaction and separation sections [114, 115].

Arkema France SA proposed a promising PI strategy based on the separation of water by adsorption in a Simulated Moving Bed Reactor (SMBR). The equipment comprises a series of columns packed with a hybrid acid solid that perform catalysis and selective adsorption of one of the reaction products. There are two inlet streams where the reactants and the eluent are fed and two outlet streams, where the products are withdrawn. Since the thermodynamic equilibrium is surpassed, as water is continuously separated, high conversions are achieved. Nonetheless, a later treatment step is required to remove the eluent from the products, but much less energy-demanding than the traditional separation of unreacted acetone and water [116].

Arkema France SA also invented a reactive liquid-liquid extraction methodology to allow the continuous process and to enhance conversion. During the reaction, part of the fraction containing the cyclic acetal products would be continuously removed from the continuous phase, driving the reaction towards product formation [116].

Relying on another PI strategy, Guangzhou Yintian New Material Co. patented a process in which the reaction occurs in a membrane reactor. The reactants would be continuously fed in a shell and tube membrane reactor with a heterogeneous catalytic layer and the water formed as by-product would permeate in the membrane and be removed from the medium. The benefits of the process are high conversion due to overcoming the thermodynamic limitation, diminished or no need for products downstream separation, that the catalyst is easily recovered, and that wastewater production is avoided [117].

China Petroleum & Chemical Corporation approached the thermodynamic limitation problem by using tin or titanium (or both) silicalite molecular sieves in form of powder mixed

with the heterogeneous catalyst. The invention stated that the preferred types of reactor used would be tank, fixed-bed, moving bed, suspended bed, or slurry bed, but it was not specified whether a downstream separation would be required [118-120].

The other patents exhibited in Table 2.4 are more well-known processes of reaction in tank or fixed-bed reactors with homogeneous or heterogeneous catalyst and separation in distillation columns, each of them with small particularities. These inventions are relevant to the industry once they are the most industrially accepted and supported by years of extensive know-how on the operation.

2.6. Process Intensification

For the solketal synthesis, there are a few registries in the literature about the use of Process Intensification strategies to minimize the mass transfer and thermodynamic limitations, or even to couple biodiesel and ketal production, as listed in Table 2.5.

Table 2.5. Process intensification strategies for the synthesis of solketal.

Author	Catalyst	Catalyst Loading	Reaction Conditions	Results	Observations	Ref.
Microwave Reactor						
Cablewski, 1994	pTSA	0.05 g_{cat}/g_{gly}	G:A = 1:13.5 T = 405 K P = 1 bar Space time = 1.2 h	Y_{solk} = 84%	Continuous process	[50]
Priya, 2017	Copper metal suported on Mordenite	0.43 g_{cat}/g_{gly}	G:A = 1:3 T = 373 K P = 1 bar Space time = 0.25 h	X_{gly} = 95% Sel > 98%	Three cycles without significant activity loss. Activity decreased slightly from the fourth cycle on.	[130]
Reactive Distillation						
	Amberlyst DPT-1		G:A = 1:23.6	X_{gly} = 70%		[49]

			T = 343 K	Sel > 99%		
Clarkson, 2001		0.05 g_{cat}/g_{gly}	Reactive Stages = 10 Space time = 0.5 h/stage		"Only a slight loss of catalytic activity was observed."	
Li, 2022	Seepage packing internals filled with cation Exchange Resin NKC-9	NA	G:A = 1:3 P ≈ 1 bar Reactive Stages = 20 [1] Space time = 20 s Reflux ratio = 2.5	X_{gly} = 85.9%		[96]
Bumbac, 2022	Amberlyst-35	NA	G:A = 1:6 P ≈ 1 bar Reactive Stages = 12 [1] Total reflux	X_{gly} > 99%		[111]
Membrane Reactor						
Roldán, 2009	K10 montmorillonite	0.1 g_{cat}/g_{gly}	G:A = 1:2 T = 333 K P = 1 bar Vaccum = 2 mbar	X_{gly} > 90%	Vapor permeation	[131]
Adsorptive Reactor						
Moreira, 2020	Amberlyst-35	25 g	G:A = 1:2 T = 313 K P = N.A. Solv. = Ethanol Space time = 0.25 h	X_{gly} = 81%		[10]
Reactive coupling						
Eze, 2018	Amberlyst 70-SO3H	9 g	1 glycerol:4 acetone 2;	X_{gly} = 80.6% [2]		[132]

	Amberlyst 70-SO3H Amberlyst A26-OH	30 methanol:1 triacetin:4 acetone 3; 6 methanol:1 triacetin:4 acetone 4 T = 323 K P = N.A. Sol = Methanol Space time = 0.5 h	X_{gly} = 48.5% [3] X_{gly} = 80.6% [4]	Mesoscale oscillatory baffled reactors (meso-OBRs)	
Al-Saadi, 2019	DBSA (*p*-Dodecylbenzenesulfonic acid)	0.5 mol 10 methanol: 1 triacetin: 7 acetone T = 323 K P = N.A. Space time = 8 h	Y_{solk} = 82%	Silica gel added as dehydrating agent to overcome the thermodynamic equilibrium limitation	[110]

1 Number of theoretical stages. 2 Synthesis of only solketal. 3 Synthesis of biodiesel and solketal in one reactor. 4 Synthesis of biodiesel and solketal in two reactors.

Microwave irradiation has been explored as a heating intensification strategy in continuous and batch processes. According to the authors, heat transfer is more efficient because the microwave energy is transferred directly to the reaction molecules; moreover, since there is a faster response in comparison to conventional heating, the process is safer. Cablewski et al. produced solketal with pTSA and high excess of acetone in an apparatus that comprises a reaction coil inside a microwave cavity. The reactants were preheated and fed together with the catalyst continuously. Years later, Priya et al. tested a more environmentally friendly process in batch with several transition metals supported over Mordenite and stated that Cu-MOR performed better, which they attributed to the greater acidity of this catalyst [50, 130].

Reactive distillation is an appealing PI strategy because it tackles the thermodynamic limitation by removing water from the reaction medium at the same time it integrates reaction and separation, eliminating the need for post-treatment processes.

Clarkson et al. proposed to carry the reaction on a multitray reactive distillation column with deep stages containing Amberlyst-DPT in suspension. They proposed a 15 stages column, with 10 reactive stages. Pre-heated glycerol would be fed at the top of the column so it could flow down through all the stages and acetone would be fed at the bottom so it could pass up the column agitating the resin and stripping out the water generated. Solketal would be purified in the bottom three stages and collected with a purity of more than 99% [49].

A similar system was proposed by Li et al., followed by optimization in Aspen Plus software and comparison with a novel equipment, the reactive dividing-wall column (RDWC). The experimental parameters and results are shown in Table 2.5. As for the optimization results considering the energy consumption (reboiler duty), it was found that the ideal scenario is nine theoretical reaction stages, five theoretical rectifying stages, and six stages in the stripping section (solketal purification), with a G:A molar feed ratio of 1:2–3 and a reflux ratio of 2.4. The comparison of the optimized traditional process with the RDWC resulted in a reduction in energy consumption by 13.6%; therefore, the authors address the RDWC as a PI strategy. This column promotes a more efficient purification of the solketal because it simulates a distillation column (II) alongside the reactive distillation column (I) inside the same unit, as seen in Figure 2.13 [96].

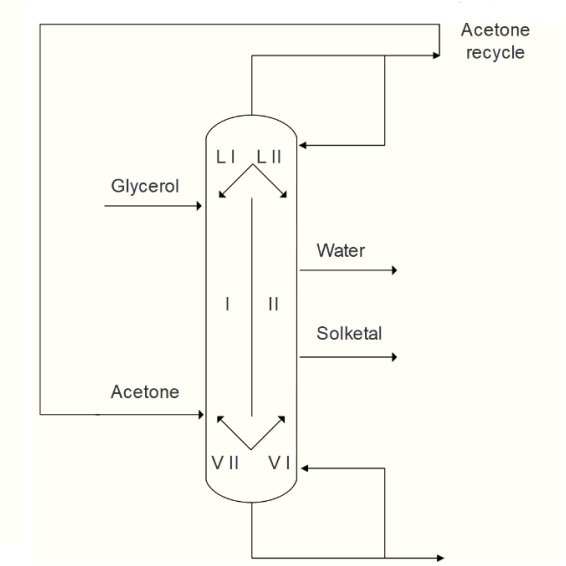

Figure 2.13. Diagram of the reactive dividing-wall column (based on [96]).

Membrane reactors also approach PI by diminishing the thermodynamic limitations, i.e., removing water from the reaction medium. Pervaporation and vapor permeation are already industrially well-established processes for water removal; the challenges faced with the use of these technologies for solketal synthesis are the catalyst activity and the mass transfer limitation. Roldán et al. avoided these problems by using K10 montmorillonite as catalyst dispersed in the reaction medium, thus handling catalysis and water removal separately, and preventing membrane contact with the liquid phase by promoting vapor permeation [131, 133]. Qing et al., on the other hand, used a catalytically active membrane to react glycerol with cyclohexanone in a very similar system to solketal synthesis. The catalyst is constituted of three layers: the top being a catalytic layer, the middle a dense selective layer, and the bottom a porous support layer. The results were promising, and the behaviour may be the same for the reaction of glycerol with acetone [133].

Moreira et al. also explored water removal as a strategy to conform to the PI guidelines. In a simple system already explained in Section 2.4.2, the authors exploit Amberlyst-35 affinity to water to shift the equilibrium toward the formation of solketal, transforming a simple fixed-

bed reactor in an adsorptive reactor [10]. This was a remarkable study in comparison to other studies described Section 2.4.2 because many of the authors that employed fixed-bed columns mentioned the use of acetone as a stripping agent rather than the use of a separation strategy to favour glycerol conversion.

Eze et al. proposed an interesting system where the biodiesel preparation and glycerol conversion would be carried at the same time (reaction coupling) so that the valorisation of glycerol would occur in situ. To do so, the reactions would occur in two oscillatory baffled reactors in series packed with Amberlyst-70. Methanol and triacetin would be fed to the first reactor and the products would follow to the second, where acetone would be fed. A glycerol conversion of 80.6% was achieved [132].

Similarly, Al-Saadi et al. proposed a reaction coupling in batch catalysed by *p*-Dodecylbenzenesulfonic acid (DBSA). This catalyst is a homogeneous strong Brønsted acid chosen because of the surfactant-like nature of the catalyst, the high rate of reaction, and the low corrosivity compared to mineral acid catalysts, according to the authors. The authors compared the effect of feeding acetone at the beginning of the process with feeding when almost complete triacetin conversion would be reached and found that the second strategy is much more efficient, achieving 82% glycerol conversion against 39.5% achieved by the first strategy [110].

2.7. Simulated Moving Bed Reactor

Combining reaction and adsorption, the Simulated Moving Bed Reactor (SMBR) is a cheaper, faster, and safer Process Intensification strategy, which also concurs with the Green Chemistry principle of designing products and processes for energy efficiency [2]. The advantages of using an SMBR unit go beyond the equipment reduction since the limitations of both reaction and separation process can be overcome, surpassing the chemical equilibrium

and avoiding the formation of azeotropes. By removing one of the reaction products, parallel reactions are prevented and purer and more concentrated outlet streams are obtained, which diminishes the use of desorbent and diminishes downstream separation costs [134]. The process is particularly useful for thermodynamically limited reactions, such as the solketal synthesis by ketalization, because it enables the reaction equilibrium to be shifted in favour of product formation by adsorbing one of the reaction products [135].

2.7.1. Separation Principle

Chromatography is a massively used separation technology because it is safe, relatively simple to apply, and very robust. It relies on the difference of affinity between the species that are supposed to be separated and the stationary and mobile phases that are part of the chromatographic column. As one of the species has more affinity with the stationary phase, it takes longer to percolate the column than the species with more affinity with the eluent, this way, the compounds get to the end of the column at different moments [136].

To overcome the obstacles of low productivity and high desorbent consumption associated with traditional batch chromatographic processes, a more economically advantageous process was developed taking advantage of a continuous counter-current operation. The True Moving Bed (TMB) chromatography is a more efficient process derived from the traditional batch chromatography. The movement of the solid enhances the separation: as the fluid phase moves in one direction, carrying the less retained component, which is removed in the raffinate stream, the solid phase moves on the opposite direction, carrying the more retained one, in turn, removed in the extract stream. This operation enhances the productivity maximizing the separation driving forces and the use of the stationary phase and minimizing the desorbent consumption [137]. Besides it enables much more difficult separations that otherwise, with the traditional chromatography, could not be accomplished [138].

The downside of the TMB operation is the movement of particles inside the columns, which could lead to equipment damage and particle breakage due to abrasion, as well as prevent the satisfactory desorption of the adsorbed species. The practical use of continuous counter-current chromatography was made possible by the development of the SMB, which simulates the movement of the stationary and mobile phases by periodically shifting the two inlet (feed and desorbent) and the two outlet (raffinate and extract) ports by one column in the direction of the fluid flow, in a series of columns packed with the adsorbent, in a close loop configuration [44]. The positions of the four streams set the borders between the unit's sections (as seen in Figure 2.14), each of them operating at specific flowrates and where distinct processes conventionally occur.

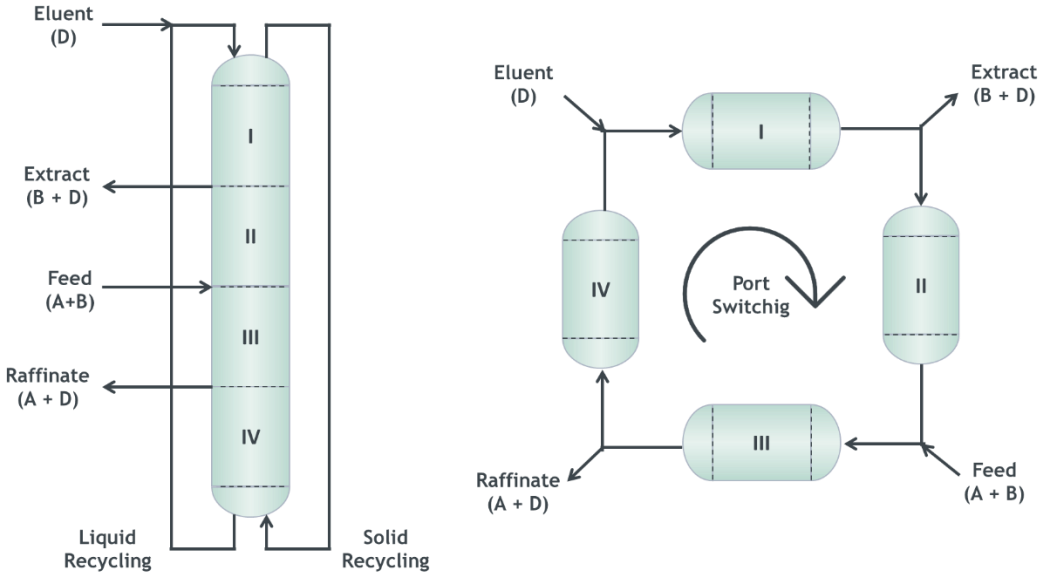

Figure 2.14. Scheme of a) a TMB and b) an SMB.

For the correct operation of an SMB the following steps must simultaneously occur in each section: in Section I the desorption of the most retained species for the regeneration of the solid phase, in Section II, the desorption of the less-retained species to avoid contamination of the extract stream and adsorption of the more-retained species so it can be withdrawn through the extract port, in Section III, the adsorption of the more-retained species to avoid contamination

of the raffinate stream and desorption of the less-adsorbed so it can be withdrawn through the raffinate port and, in Section IV, the desorption of the less-adsorbed species for the regeneration of the eluent [44].

The industrial application of the SMB begun in 1961 in the petrochemical sector with Broughton and Gerhold patent for the *Sorbex* ®, for replacing conventional distillation where the required purity specifications were difficult to achieve [139]. After this first step, there was an outbreak on the research and development of several alternative SMB technologies for petrochemical applications. The second outbreak is marked by the introduction of the SMB on the pharmaceuticals, fine chemicals, biotechnology sectors, especially in what concerns to enantiomer separation, with the use of much smaller equipment [135, 140].

2.7.2. Non-conventional modes of operation

The dissemination of the SMB technology and the need for even more efficient technologies entailed several research groups to scrutinize the SMB operation in the quest for new processes, modes of operation and stationary phases that could be applied to the manufacture of new products or to enhance the productivity of already well-established processes. It was found that the number of degrees of freedom of the conventional process could be manipulated so that the range of potential applications of the SMB could be extended. The non-conventional modes of operation take advantage of the flexibility on the number of sections, the number of inlets and outlets of each Section, the composition of the feed streams, and the variation of the dynamic configuration. The improvement may achieve even better results when two or more non-conventional modes of operation are combined [138, 141-143]. Besides modifying the Conventional SMB, it is also possible to combine the separation by adsorption with other processes, which gives rise to Hybrid-SMB [138]. The most common non-conventional modes of operation and Hybrid-SMB technologies are exhibited in Table 2.6, as follows.

Table 2.6. Non-conventional operations and hybrid technologies based on the SMB chromatography.

Process Name	Characteristic	Main Application/Advantage	Ref.
Dynamic Configuration			
Varicol	Asynchronous shift of the inlet and outlet ports	Units with a reduced number of columns; Increased productivity for the same purity	[144, 145]
Pseudo-SMB	Intermittent introduction of feed and withdrawal of outlet streams	Ternary separation	[146, 147]
Flowrate modulation			
Power Feed	Modulation of the Section flow rates between two consecutive switches	Improve the classical SMB productivity and solvent consumption	[148, 149]
Improved-SMB	Sub-division of the time switch into two intervals: (1) no flow rate in Section IV (no fluid is recycled); (2) all inlet and outlet streams are closed (recycling is restored)	Sugar processing industry; ternary separations	[150, 151]
Partial-Feed	Discontinuous introduction of the feed and changing the raffinate flowrate in order to keep the internal flowrates in Sections I, II and IV constant	Units with reduced number of columns per Section	[152]

Partial-Discard	Selectively collecting the desired fraction of the extract and raffinate streams and discarding the remaining fractions	High product purity; if implemented with Partial-Feed, enhances the overall process performance	[153]
Outlet Swing Stream	Expansion or contraction of the product concentration front by dynamically adjusting the flowrates in Section I and IV and keeping a constant value in Sections II and III	High purity of the target species; low eluent consumption	[154]
Simcon-SMB	Sub-division of the time switch into three intervals: (1) no extract flowrate; (2) conventional operation with all streams active; and (3) no raffinate flowrate	High purity of target species because it slows the migration of the extract front and speeds up the migration of the raffinate tail	[141, 155]
Sequential-SMB	Sub-division of the time switch into three intervals: (1) no outlet streams; (2) no flowrate in Section IV, eluent and raffinate streams restored; and (3) no flowrate in Sections II and IV, all streams restored	Sugar processing industry; lower eluent consumption	[156]

Concentration modulation			
ModiCon	Dynamic variation of the feed concentration throughout the time switch	Target product with an increased purity value, preserving the productivity of the classical SMB	[141, 157, 158]
Enriched Extract	A fraction of the product stream is collected, and the remaining is reintroduced in the system at the same point	Overcomes the classical SMB performance with restrictive purity requirements for the more retained compound	[159, 160]
FeedCol	Pre-separation of the feed on a small chromatographic column (Feed Column)	Reduces impurity near outlet ports; enhance performance of aging and damaged columns	[141, 161]
Backfill	A fraction of the raffinate and extract are reinjected to their corresponding intermediate nodes during the initial and final stages of the time switch, respectively	High purity of the target species	[141, 162]
Gradient operation			
Solvent Gradient	Variation of the composition of the solvent between the two inlet streams	Systems with the adsorption equilibrium strongly dependent on the solvent composition	[163, 164]

Temperature Gradient	Regulation of the temperature in each section, to promote the required variation in the adsorption behaviour	Good for the product purity, even for units with fewer columns	[165]
Alternative SMB configuration			
Reduced number of Sections	Conventionally three-zone open-loop SMB: elimination of Section IV (or, alternatively, Section I) and the recycling stream.	Simplified process control, preventing extract contaminations through the recycling stream and increasing its purity	[166-168]
Extended number of Sections	Introduction of additional outlet streams, for withdrawal of the intermediately adsorbed species, and bypass streams between the sections of interest	Separation of ternary mixtures, with low eluent consumption	[169, 170]
SMB cascades	Multiple sequential SMB	Ternary mixtures separation	
MultiFeed	Introduction of additional feed streams	Increased productivity for the same purity	[135, 154]
Special units			
Supercritical SMB	Use of supercritical fluids as eluent. The eluent is recovered in a cyclone and then cooled down, condensed, and recycled	Easy downstream separation	[47, 171, 172]
Hybrid-SMB			

SMB + Crystallization	Introduction of a crystallization unit in parallel with the SMB for separating the raffinate or extract stream from the desorbent that can be recycled to the unit	Decrease on the total desorbent consumption of the process	[173, 174]
SMB + Bipolar Electrodialysis	Introduction of an electrodialysis unit after the SMB for separating the raffinate or extract stream from the desorbent that can be recycled to the unit	Decrease on the total desorbent consumption of the process	[175]
SMBR	The reactants are introduced in the unit through the feed stream while the most and least adsorbed products of the reaction are collected in the extract and raffinate ports.	Equipment reduction; Process intensification	[44, 176]

Even though the literature on non-conventional SMB processes is substantial, there are few works regarding Hybrid-SMB. A common approach on the field of hybrid processes is integrating a unit of SMB with modules of crystallization or membranes, usually aiming to purify the desorbent so that it can be recycled back to the unit, which significantly reduces its consumption.

Nonetheless, the most explored technology is the SMBR due to its similar operation when compared with the SMB, needless modifications on the equipment for most applications and high potential of intensifying processes.

2.7.3. The SMBR as a Process Intensification Strategy

Process Intensification (PI) is divided into two main areas: process intensifying equipment and process intensifying methods. The most common PI equipment developed are reactors and intensive heat and mass transfer devices. As for the methods, the most explored are integration of reaction and separation, heat exchange, or phase transition (in multifunctional reactors), hybrid separations, techniques using alternative energy sources, as solar energy and ultrasound, and new process-control methods (intentional unsteady-state operation) [177].

The SMBR overlaps these two PI areas, as it is a new device where new methods are carried. Within the first area, the SMB is already an intensive mass transfer device, the technology was upgraded by adding the chemical reaction process, originating the multifunctional reactor SMBR. In the scope of new methods, it integrates reaction and separation by adsorption to achieve higher conversion yields and diminish or eliminate the need for a second unit for the treatment of the products. The ideal use of the SMBR is to perform reactions limited by chemical equilibrium with two products [176].

The initial step on the application of SMBR was made by Hashimoto et al. in 1983 for producing high fructose syrup in a process where reaction and separation occurred in different

columns [44, 178]. The behaviour of the SMBR is shown in Figure 2.15, for the reaction of the type $A + B \leftrightharpoons C + D$.

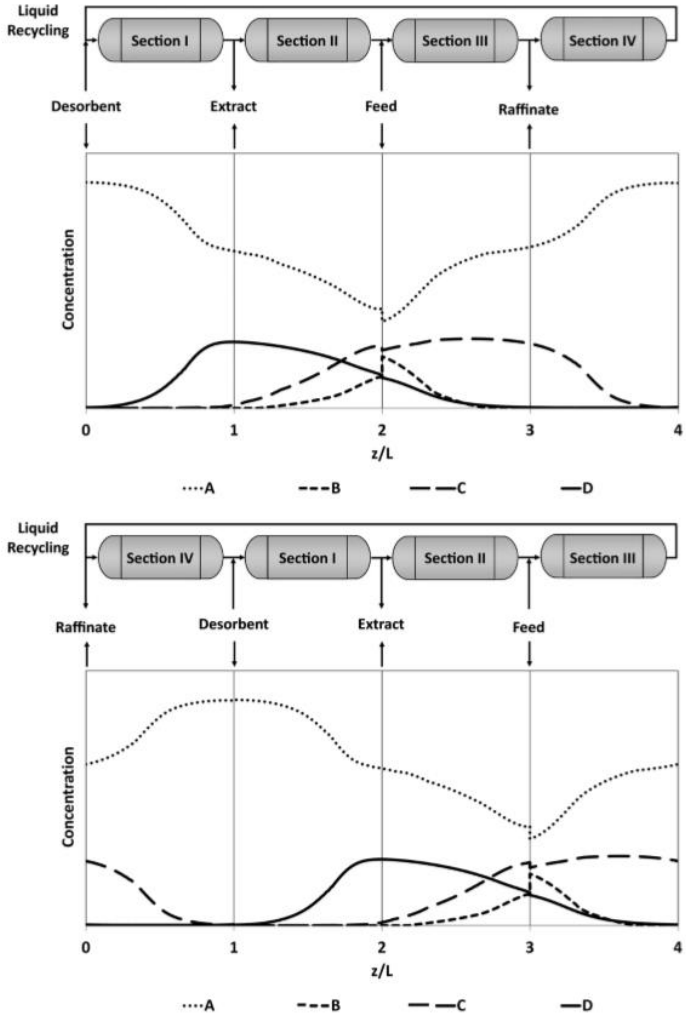

Figure 2.15. Internal concentration profiles in the SMBR for the reaction type $A + B \leftrightharpoons C + D$ [134].

In the scheme, species A and B are the reactants and A is also used as desorbent. Product C is the least retained species and product D the most retained. The operation principle of the SMBR is similar to the SMB, however, there is also the reaction occurring in Sections II and III, near the feed port. In Section I, D must be carried by the liquid phase for the appropriate adsorbent regeneration. In Sections II and III, reactants A and B are converted, and D must travel with the solid to avoid contamination of the raffinate stream and to be collected in the

extract port while C must move in the opposite direction, that is, it has to be carried by the fluid phase so it can be collected in the raffinate port. Finally, in Section IV, neither C nor D should be present in the desorbent for its recovery. In most cases, similarly to the TMB/SMB relation, there can be established a parallel between the TMBR and the SMBR.

As well as with the SMB, numerous alternatives were proposed both for optimizing and changing the Hashimoto original SMBR, broadening the possible application spectrum of this technology. It has been studied for the production of green fuels and solvents, as diethylacetal (DEE), dimethylacetal (DME), dibutylacetal (DBE), ethyl lactate (EL), glycerol ethyl acetal (GEA) [45, 179, 180], in the sugar industry for the sucrose inversion and glucose isomerization, in the petrochemical industry for the isomerization and separation of xylenes [135, 181].

The SMBR is easily adaptable to the non-conventional SMB variations, despite the lack on the literature concerning this topic. The proposed non-conventional SMBR published, as far as the knowledge of the author goes, are summarized in Table 2.7:

Table 2.7. Summary of the non-conventional-SMBR processes.

Process Name	Characteristic	Main Application/Advantage	Ref.
PermSMBR	The fixed-bed columns are replaced by modules of pervaporation membranes packed with a mixture of catalyst and adsorbent or a hybrid solid	Equipment reduction; Process intensification	[44, 182, 183]
FeedCol	A fixed-bed reactor precedes the SMBR so that most of the reactants are consumed in the FBR, reaching equilibrium, and the unreacted substances are completely converted in the SMBR	Slow kinetics reactions; High productivity and purity of the target species	[182]
Multifeed SMBR	The reactants are fed in different positions to promote their countercurrent contact and enhance the performance.	Reactants with very different selectivity. Thermodynamic limited reactions; Processes with high contamination of the outlet streams by the reactants	[184]
VariCol	Asynchronous switch to enlarge or reduce the reactive section	Equipment reduction; High purity of the target species; No additional cost needed	[185]
ModiCon	Feed stream modulation to manipulate the concentration fronts, consequently increasing the net reaction rate in specific locations	High productivity and purity of the target species; No additional cost needed	[181]
Non-isothermal	Temperature modulation to manipulate the concentration fronts by influencing the reaction rate and the adsorption	High productivity; Lower desorbent consumption	[186, 187]

The PermSMBR is an appealing hybrid technology that combines reaction, adsorption and membrane permeation in the same unit. There are two PermSMBR configurations: the integrated PermSMBR, in which the fixed-bed columns are replaced by membrane modules packed with the catalyst and the adsorbent or a hybrid solid; and the coupled PermSMBR, in which each fixed-bed is followed or preceded by an independent membrane module [44]. The first is more interesting under the scope of Process Intensification since a smaller unit is necessary to attain the same productivity, the second is more interesting on the industrial point of view because the maintenance is simpler in separate reaction and separation modules and the lifetime of the membranes is extended since they are not in contact with the catalyst/adsorbent [138].

The other non-conventional SMBR strategies are usually used to increase the number of degrees of freedom of the process to extend the optimization to more variables. Nowadays, the SMB technology is in a new era, with the development of special units and hybrid technologies at a faster pace than the search for alternative operations. The SMBR, however, is still late on the process development rush, and there is plenty of room for investigations on the non-conventional operations for this multifunctional reactor.

2.8. Conclusions and Future Prospects

Like almost all other sectors, the glycerol market was affected by the COVID-19 crisis mainly because many biodiesel plants have diminished production. Despite that, it was attested by the Independent Commodity Intelligence Services that glycerol supply is safe, and the shortcut was caused by logistic problems. Considering that, relying on such chemical as raw material is advantageous due to its low cost, favourable physicochemical properties, and the environmental benefits of valorising it. The main issue of the glycerol side-stream produced by the biodiesel industry is its inability to be absorbed by the traditional markets for

pharmaceuticals and cosmetic applications. Thankfully, new uses for glycerol were discovered and, along with that, new treatment methods and even processes capable of using crude glycerol. Among the many subproducts of glycerol, solketal stands out due to its versatility and promising improvements in fuels when used as additive. Moreover, solketal does not require high-purity reactant, depending on how it is proposed to be produced.

New alternative catalysts have been studied to allow the use of crude or less treated glycerol and to diminish the cost of producing solketal. Additionally, new processes have been proposed to overcome the thermodynamic limitation inherent to this ketalization reaction. Nevertheless, the literature on the use of crude glycerol is still scarce, as well as on alternative technologies that can be applied at large scale to keep up with the glycerol production rate. The Process Intensification strategies proposed in the open literature for the production of solketal present great potential to be applied at industrial scale and an immensurable prospective environmental benefit. Besides enabling the reaction to achieve higher conversion, these strategies can diminish or even eliminate the need for downstream treatment, pointed out by some authors as the most energy demanding step (consequently the costliest) [25,121,122]. Therefore, the most promising strategies are the continuous processes that result in purer product streams, as the Simulated Moving Bed Reactor, thoroughly investigated for the production of other chemicals [180, 182, 188-191], Membrane Reactors [192-195], and other hybrid reaction-separation technologies.

The Conventional SMBR is already known for surpassing the reaction equilibrium by taking advantage of the adsorption. Even better results can be achieved applying the non-conventional SMB strategies to the SMBR. By manipulating the concentration fronts on the ModiCon, the reaction rate can be enhanced in a limited fraction of the reactor and the reaction equilibrium can be surpassed even more when compared to the SMBR. The investigation on the ModiCon, however, is still very limited even for the SMB and most of the studies approach the modulation

by applying pulses, despite the numerous possibilities to manipulate the feed concentration. As for the Multifeed SMBR, the only registry found in the literature is superficial and does not explore the practical implementation of the strategy. This non-conventional operation is particularly beneficial for processes with reactants with large difference in affinity, therefore their contact time may be insufficient to attain good conversion. The counter-current contact promoted by the Multifeed SMBR may increase the conversion. Furthermore, purer products can be obtained because the feeds of the reactants are further apart from the collection ports (technical details will be thoroughly provided in Chapter 6).

Unfortunately, Process Intensification strategies for the production of Solketal are developing at a slow pace, and only few patents propose these strategies at an industrial scale. Additionally, there is a gap in the literature on studies that evaluate the environmental impacts of producing solketal, a common point for all the processes mentioned in this chapter. Considering that this indicator has been gaining strength, it is relevant that the studies perform a Life Cycle Analysis and provide these types of data to evidence if the proposed technologies are competitive from both economic and environmental aspects. This proves the research on solketal still has plenty of room to grow, especially in what concerns the use of non-conventional SMBR.

2.9. Notation

Abbreviations

CSTR	Continuously Stirred Tank Reactor
DBE	Dibutylacetal
DBSA	p-Dodecylbenzenesulfonic Acid
DEE	Diethylacetal
DME	Dimethylacetal
EL	Ethyl Lactate
ER	Eley-Rideal
GEA	Glycerol Ethyl Acetal
IEA	International Energy Agency
ILs	Ionic Liquids
LHHW	Langmuir-Hinshelwood-Hougen-Watson
LD50	Median Lethal Dose
meso-OBRs	Mesoscale Oscillatory Baffled Reactors
MOF	Metal Organic Framework
NFPA	National Fire Protection Association
P	Pressure
PH	Pseudo-Homogeneous
PI	Process Intensification
Prod	Productivity
pTSA	p-toluenesulfonic Acid
RDWC	Reactive Dividing-Wall Column
Sel	Selectivity
SMB	Simulated Moving Bed
SMBR	Simulated Moving Bed Reactor
T	Temperature
TMB	True Moving Bed
TMBR	True Moving Bed Reactor
TPTT	tributyl (tetradecyl)phosphonium p-toluenesulfonate

WHSV	Weight Hourly Space Velocity

Symbols

C	Liquid phase concentration
E_A	Reaction activation energy
$\overleftarrow{E_A}$	Reverse reaction activation energy
ΔG	Gibbs free energy change
ΔH	Enthalpy change
k	Reaction kinetic constant
K	Adsorption equilibrium constant
K_{eq}	Thermodynamic equilibrium constant
q	Adsorbed concentration in the solid phase
$\Re$	Reaction Rate
u	Liquid interstitial velocity
u_s	Solid interstitial velocity
X_{gly}	Conversion
Y_{solk}	Yield

Greek Letters

ε_b	Bulk porosity
γ	Ratio between the liquid and the solid interstitial velocities

Subscripts

i	Chemical species
j	SMBR Section

2.10. References

1. Anastas, P.T. and E.S. Beach, *Changing the Course of Chemistry*, in *Green Chemistry Education*. 2009, American Chemical Society. p. 1-18.
2. Anastas, P. and N. Eghbali, *Green Chemistry: Principles and Practice.* Chem. Soc. Rev., 2010. **39**(1): p. 301-312.
3. Anastas, P.T. and J.C. Warner, *Green chemistry: theory and practice*. 1998, Oxford [England]; New York: Oxford University Press.
4. *Glycerine Market Size, Share & COVID-19 Impact Analysis, By Grade (USP Grade, and Technical Grade), By Application (Personal Care, Food & Beverages, Pharmaceuticals, Polyether Polyols, Chemical Intermediate, Tobacco, and Others), and Regional Forecast 2020-2027*. 2020, Fortune Business Insights.
5. Pousa, G.P.A.G., A.L.F. Santos, and P.A.Z. Suarez, *History and policy of biodiesel in Brazil.* Energy Policy, 2007. **35**(11): p. 5393-5398.
6. Rouhany, M. and H. Montgomery, *Global Biodiesel Production: The State of the Art and Impact on Climate Change*, in *Biodiesel: From Production to Combustion*, M. Tabatabaei and M. Aghbashlo, Editors. 2019, Springer International Publishing: Cham. p. 1-14.
7. Trifoi, A.R., P.Ș. Agachi, and T. Pap, *Glycerol acetals and ketals as possible diesel additives. A review of their synthesis protocols.* Renewable and Sustainable Energy Reviews, 2016. **62**: p. 804-814.
8. Sheldon, R.A., *The E factor 25 years on: the rise of green chemistry and sustainability.* Green Chem., 2017. **19**(1): p. 18-43.
9. Moreira, M.N., R.P.V. Faria, A.M. Ribeiro, and A.E. Rodrigues, *Solketal Production from Glycerol Ketalization with Acetone: Catalyst Selection and Thermodynamic and Kinetic Reaction Study.* Ind. Eng. Chem. Res., 2019. **58**(38): p. 17746-17759.
10. Moreira, M.N., I. Corrêa, A.M. Ribeiro, A.E. Rodrigues, and R.P.V. Faria, *Solketal Production in a Fixed Bed Adsorptive Reactor through the Ketalization of Glycerol.* Ind. Eng. Chem. Res., 2020. **59**(7): p. 2805-2816.
11. *INSIGHT: Spot glycerine soars on biodiesel cut fears*, ICIS, Editor. 2020, Independent Commodity Intelligence Services.
12. Pagliaro, M., *Properties, Applications, History, and Market*, in *Glycerol*. 2017, Elsevier. p. 1-21.
13. Nda-Umar, U.I., I. Ramli, Y.H. Taufiq-Yap, and E.N. Muhamad, *An Overview of Recent Research in the Conversion of Glycerol into Biofuels, Fuel Additives and other Bio-Based Chemicals.* Catalysts, 2018. **9**(1): p. 15.
14. Browning, N. *Factbox: Pandemic brings forward predictions for peak oil demand*. 2020 January 15, 2020]; Available from: https://www.reuters.com/article/oil-demand/factbox-pandemic-brings-forward-predictions-for-peak-oil-demand-idUSL8N2IB5EG.
15. Ciriminna, R., C.D. Pina, M. Rossi, and M. Pagliaro, *Understanding the glycerol market.* Eur. J. Lipid Sci. Technol., 2014. **116**(10): p. 1432-1439.
16. Mushrush, G.W., W.M. Stalick, E.J. Beal, S.C. Basu, J.E. Slone, and J. Cummings, *The synthesis of acetals and ketals of the reduced sugar mannose as fuel system icing inhibitors.* Pet. Sci. Technol., 1997. **15**(3-4): p. 237-244.
17. *Aviation: Benefits Beyond Borders*. 2018, Air Transport Action Group
18. Mushrush, G., *Fuel system icing inhibitor and deicing composition* U.S. Patent, Editor. 1998, The United States of America represented by the Secretary of the Navy: Unites States of America.
19. Cornejo, A., I. Barrio, M. Campoy, J. Lázaro, and B. Navarrete, *Oxygenated fuel additives from glycerol valorization. Main production pathways and effects on fuel properties and engine performance: A critical review.* Renew. Sust. Energ. Rev., 2017. **79**: p. 1400-1413.
20. Le Quéré, C., R.B. Jackson, M.W. Jones, A.J.P. Smith, S. Abernethy, R.M. Andrew, A.J. De-Gol, D.R. Willis, Y. Shan, J.G. Canadell, P. Friedlingstein, F. Creutzig, and G.P. Peters,

Temporary reduction in daily global CO2 emissions during the COVID-19 forced confinement. Nat. Clim. Change, 2020. **10**(7): p. 647-653.

21. Agency, I.E., *Renewable energy market update.* 2020.
22. *Liquid Biofuels Market Size, Share & Trends Analysis Report By Product (Biodiesel, Bioethanol), By Application (Transportation Fuel, Power Generation, Thermal Heating), And Segment Forecasts, 2020 - 2027*. 2020, Grand View Research.
23. Giraldo, S.Y., L.A. Rios, and N. Suárez, *Comparison of glycerol ketals, glycerol acetates and branched alcohol-derived fatty esters as cold-flow improvers for palm biodiesel.* Fuel, 2013. **108**: p. 709-714.
24. Rasmussen, C. *Emission Reductions From Pandemic Had Unexpected Effects on Atmosphere*. 2021.
25. Iodice, P., A. Senatore, G. Langella, and A. Amoresano, *Advantages of ethanol–gasoline blends as fuel substitute for last generation Si engines.* Environ. Prog. Sustainable Energy, 2017. **36**(4): p. 1173-1179.
26. Shi, E. and S. Hanson. *EIA projects U.S. biofuel production to slowly increase through 2050*. 2020 January 15, 2020]; Available from: https://www.eia.gov/todayinenergy/detail.php?id=43096.
27. Tan, H.W., A.R. Abdul Aziz, and M.K. Aroua, *Glycerol production and its applications as a raw material: A review.* Renew. Sust. Energ. Rev., 2013. **27**: p. 118-127.
28. *Solketal: an EHS friendly and sustainable solvent*, I. Switzerland, Editor. 2017, IMPAG Switzerland.
29. Corrêa, I., R.P.V. Faria, and A.E. Rodrigues, *Continuous Valorization of Glycerol into Solketal: Recent Advances on Catalysts, Processes, and Industrial Perspectives.* Sustain. Chem., 2021. **2**(2): p. 286-324.
30. Esteban, J., F. García-Ochoa, and M. Ladero, *Solventless synthesis of solketal with commercially available sulfonic acid based ion exchange resins and their catalytic performance.* Green Process. Synth., 2017. **6**(1): p. 79-89.
31. Melero, J.A., G. Vicente, G. Morales, M. Paniagua, and J. Bustamante, *Oxygenated compounds derived from glycerol for biodiesel formulation: Influence on EN 14214 quality parameters.* Fuel, 2010. **89**(8): p. 2011-2018.
32. Isac-García, J., J.A. Dobado, F.G. Calvo-Flores, and H. Martínez-García, *Chapter 5 - Determining Physical and Spectroscopic Properties*, in *Experimental Organic Chemistry*, J. Isac-García, et al., Editors. 2016, Academic Press. p. 145-175.
33. Alptekin, E., *Emission, injection and combustion characteristics of biodiesel and oxygenated fuel blends in a common rail diesel engine.* Energy, 2017. **119**: p. 44-52.
34. Mota, C.J.A., C.X.A. da Silva, N. Rosenbach, J. Costa, and F. da Silva, *Glycerin Derivatives as Fuel Additives: The Addition of Glycerol/Acetone Ketal (Solketal) in Gasolines.* Energy Fuels, 2010. **24**(4): p. 2733-2736.
35. Ilgen, O., S. Yerlikaya, and F.O. Akyurek, *Synthesis of Solketal from Glycerol and Acetone over Amberlyst-46 to Produce an Oxygenated Fuel Additive.* Period. Polytech., Chem. Eng., 2016.
36. Nanda, M.R., Y. Zhang, Z. Yuan, W. Qin, H.S. Ghaziaskar, and C. Xu, *Catalytic conversion of glycerol for sustainable production of solketal as a fuel additive: A review.* Renew. Sust. Energ. Rev., 2016. **56**: p. 1022-1031.
37. Fischer, E., *Ueber die Verbindungen der Zucker mit den Alkoholen und Ketonen.* Ber. Dtsch. Chem. Ges., 1895. **28**(1): p. 1145-1167.
38. Newman, M.S. and M. Renoll, *Improved Preparation of Isopropylidene Glycerol.* J. Am. Chem. Soc., 1945. **67**(9): p. 1621-1621.
39. Nanda, M.R., Z. Yuan, W. Qin, H.S. Ghaziaskar, M.-A. Poirier, and C.C. Xu, *Thermodynamic and kinetic studies of a catalytic process to convert glycerol into solketal as an oxygenated fuel additive.* Fuel, 2014. **117**: p. 470-477.

40. Maksimov, A.L., A.I. Nekhaev, D.N. Ramazanov, Y.A. Arinicheva, A.A. Dzyubenko, and S.N. Khadzhiev, *Preparation of high-octane oxygenate fuel components from plant-derived polyols.* Pet. Chem., 2011. **51**(1): p. 61-69.
41. Serafim, H., I.M. Fonseca, A.M. Ramos, J. Vital, and J.E. Castanheiro, *Valorization of glycerol into fuel additives over zeolites as catalysts.* Chem. Eng. J. (Amsterdam, Neth.), 2011. **178**: p. 291-296.
42. Ruiz, V.R., A. Velty, L.L. Santos, A. Leyva-Pérez, M.J. Sabater, S. Iborra, and A. Corma, *Gold catalysts and solid catalysts for biomass transformations: Valorization of glycerol and glycerol–water mixtures through formation of cyclic acetals.* J. Catal., 2010. **271**(2): p. 351-357.
43. da Silva, C.X.A., V.L.C. Gonçalves, and C.J.A. Mota, *Water-tolerant zeolite catalyst for the acetalisation of glycerol.* Green Chem., 2009. **11**(1): p. 38-41.
44. Rodrigues, A.E., Madeira, Luís Miguel, Wu, Yi-Jiang, Faria, Rui, *Sorption Enhanced Reaction Processes*. Sorption Enhanced Reaction Processes. 2017.
45. Faria, R.P.V., C.S.M. Pereira, V.M.T.M. Silva, J.M. Loureiro, and A.E. Rodrigues, *Glycerol valorisation as biofuels: Selection of a suitable solvent for an innovative process for the synthesis of GEA.* Chem. Eng. J. (Amsterdam, Neth.), 2013. **233**: p. 159-167.
46. Bruchmann, B., K. Haberle, H. Gruner, and M. Hirn, *Preparation of cyclic acetals or ketals* 1999, BASF Aktiengesellschaf: Germany.
47. Royon, D., S. Locatelli, and E.E. Gonzo, *Ketalization of glycerol to solketal in supercritical acetone.* J. Supercrit. Fluids, 2011. **58**(1): p. 88-92.
48. Eigenberger, G. and W. Ruppel, *Catalytic Fixed-Bed Reactors*, in *Ullmann's Encyclopedia of Industrial Chemistry*. 2012.
49. Clarkson, J.S., A.J. Walker, and M.A. Wood, *Continuous Reactor Technology for Ketal Formation: An Improved Synthesis of Solketal.* Org. Process Res. Dev., 2001. **5**(6): p. 630-635.
50. Cablewski, T., A.F. Faux, and C.R. Strauss, *Development and Application of a Continuous Microwave Reactor for Organic Synthesis.* The Journal of Organic Chemistry, 1994. **59**(12): p. 3408-3412.
51. Monbaliu, J.-C.M., M. Winter, B. Chevalier, F. Schmidt, Y. Jiang, R. Hoogendoorn, M.A. Kousemaker, and C.V. Stevens, *Effective production of the biodiesel additive STBE by a continuous flow process.* Bioresour. Technol., 2011. **102**(19): p. 9304-9307.
52. Kowalska-Kus, J., A. Held, M. Frankowski, and K. Nowinska, *Solketal formation from glycerol and acetone over hierarchical zeolites of different structure as catalysts.* J. Mol. Catal. A: Chem., 2017. **426**: p. 205-212.
53. Zahid, I., M. Ayoub, B.B. Abdullah, M.H. Nazir, M. Ameen, Zulqarnain, M.H. Mohd Yusoff, A. Inayat, and M. Danish, *Production of Fuel Additive Solketal via Catalytic Conversion of Biodiesel-Derived Glycerol.* Ind. Eng. Chem. Res., 2020. **59**(48): p. 20961-20978.
54. Esposito, R., M.E. Cucciolito, A. D'Amora, R. Di Guida, F. Montagnaro, and F. Ruffo, *Highly efficient iron(III) molecular catalysts for solketal production.* Fuel Process. Technol., 2017. **167**: p. 670-673.
55. da Silva, M.J., A.A. Rodrigues, and P.F. Pinheiro, *Solketal synthesis from glycerol and acetone in the presence of metal salts: A Lewis or Brønsted acid catalyzed reaction?* Fuel, 2020. **276**: p. 118164.
56. Manjunathan, P., S.P. Maradur, A.B. Halgeri, and G.V. Shanbhag, *Room temperature synthesis of solketal from acetalization of glycerol with acetone: Effect of crystallite size and the role of acidity of beta zeolite.* J. Mol. Catal. A: Chem., 2015. **396**: p. 47-54.
57. Rossa, V., Y.d.S.P. Pessanha, G.C. Díaz, L.D.T. Câmara, S.B.C. Pergher, and D.A.G. Aranda, *Reaction Kinetic Study of Solketal Production from Glycerol Ketalization with Acetone.* Ind. Eng. Chem. Res., 2017. **56**(2): p. 479-488.
58. Talebian-Kiakalaieh, A. and S. Tarighi, *Hierarchical faujasite zeolite-supported heteropoly acid catalyst for acetalization of crude-glycerol to fuel additives.* J. Ind. Eng. Chem. (Amsterdam, Neth.), 2019. **79**: p. 452-464.

59. Rahaman, M.S., T.K. Phung, M.A. Hossain, E. Chowdhury, S. Tulaphol, S.B. Lalvani, M. O'Toole, G.A. Willing, J.B. Jasinski, M. Crocker, and N. Sathitsuksanoh, *Hydrophobic functionalization of HY zeolites for efficient conversion of glycerol to solketal.* Applied Catalysis A: General, 2020. **592**: p. 117369.
60. Esteban, J., M. Ladero, and F. García-Ochoa, *Kinetic modelling of the solventless synthesis of solketal with a sulphonic ion exchange resin.* Chem. Eng. J. (Amsterdam, Neth.), 2015. **269**: p. 194-202.
61. Cornejo, A., M. Campoy, I. Barrio, B. Navarrete, and J. Lázaro, *Solketal production in a solvent-free continuous flow process: scaling from laboratory to bench size.* React. Chem. Eng., 2019. **4**(10): p. 1803-1813.
62. Sulistyo, H., D.P. Priadana, Y.W. Fitriandini, T. Ariyanto, and M.M. Azis, *Utilization of Glycerol by Ketalization Reactions with Acetone to Produce Solketal using Indion 225 Na as Catalyst.* International Journal of Technology, 2020. **11**.
63. Timofeeva, M.N., V.N. Panchenko, V.V. Krupskaya, A. Gil, and M.A. Vicente, *Effect of nitric acid modification of montmorillonite clay on synthesis of solketal from glycerol and acetone.* Catal. Commun., 2017. **90**: p. 65-69.
64. Amri, S., J. Gómez, A. Balea, N. Merayo, E. Srasra, N. Besbes, and M. Ladero, *Green Production of Glycerol Ketals with a Clay-Based Heterogeneous Acid Catalyst.* Applied Sciences, 2019. **9**(21): p. 4488.
65. Zhang, S., Z. Zhao, and Y. Ao, *Design of highly efficient Zn-, Cu-, Ni- and Co-promoted M-AlPO4 solid acids: The acetalization of glycerol with acetone.* Appl. Catal., A, 2015. **496**: p. 32-39.
66. Gadamsetti, S., N.P. Rajan, G.S. Rao, and K. V. R. Chary, *Acetalization of glycerol with acetone to bio fuel additives over supported molybdenum phosphate catalysts.* J. Mol. Catal. A: Chem., 2015. **410**: p. 49-57.
67. Rodrigues, R., D. Mandelli, N.S. Gonçalves, P.P. Pescarmona, and W.A. Carvalho, *Acetalization of acetone with glycerol catalyzed by niobium-aluminum mixed oxides synthesized by a sol–gel process.* J. Mol. Catal. A: Chem., 2016. **422**: p. 122-130.
68. Gui, Z., N. Zahrtmann, S. Saravanamurugan, I. Reyero, Z. Qi, M.A. Bañares, A. Riisager, and E.J. Garcia-Suarez, *Brønsted Acid Ionic Liquids (BAILs) as Efficient and Recyclable Catalysts in the Conversion of Glycerol to Solketal at Room Temperature.* ChemistrySelect, 2016. **1**(18): p. 5869-5873.
69. Ji, Y., T. Zhang, X. Gui, H. Shi, and Z. Yun, *Solventless ketalization of glycerol to solketal with acetone over the ionic liquid [P(C4H9)3C14H29][TsO].* Chin. J. Chem. Eng., 2020. **28**(1): p. 158-164.
70. Gonçalves, M., R. Rodrigues, T.S. Galhardo, and W.A. Carvalho, *Highly selective acetalization of glycerol with acetone to solketal over acidic carbon-based catalysts from biodiesel waste.* Fuel, 2016. **181**: p. 46-54.
71. Fernández, Fraile, B. García, and Pires, *Sulfonated Hydrothermal Carbons from Cellulose and Glucose as Catalysts for Glycerol Ketalization.* Catalysts, 2019. **9**(10).
72. Carvalho Ballotin, F., M.J. da Silva, A. Paula de Carvalho Teixeira, and R. Montero Lago, *Amphiphilic acid carbon catalysts produced by bio-oil sulfonation for solvent-free glycerol ketalization.* Fuel, 2020. **274**: p. 117799.
73. Kaur, J., A.K. Sarma, P. Gera, and M.K. Jha, *Process optimization with acid functionalised activated carbon derived from corncob for production of 4-hydroxymethyl-2,2-dimethyl-1,3-dioxolane and 5-hydroxy-2,2-dimethyl-1,3-dioxane.* Scientific Reports, 2021. **11**(1): p. 8567.
74. Saikia, K., K. Rajkumari, N.S. Moyon, S. Basumatary, G. Halder, U. Rashid, and S.L. Rokhum, *Sulphonated biomass-based catalyst for solketal synthesis by acetalization of glycerol – A byproduct of biodiesel production.* Fuel Processing Technology, 2022. **238**: p. 107482.
75. Roncaglia, F., L. Forti, S. D'Anna, and L. Maletti, *An Expedient Catalytic Process to Obtain Solketal from Biobased Glycerol.* Processes, 2021. **9**(1): p. 141.

76. Zhou, R., Y. Jiang, H. Zhao, B. Ye, L. Wang, and Z. Hou, *Synthesis of solketal from glycerol over modified SiO2 supported p-phenolsulfonic acid catalyst.* Fuel, 2021. **291**: p. 120207.
77. Chansorn, N., S. Amnuaypanich, S. Soontaranon, S. Rugmai, and S. Amnuaypanich, *Increasing solketal production from the solventless ketalization of glycerol catalyzed by nanodispersed phosphotungstic acid in poly(N-methyl-4-vinylpyridinium) grafted on silica nanoparticles.* Journal of Industrial and Engineering Chemistry, 2022. **112**: p. 233-243.
78. Sandesh, S., A.B. Halgeri, and G.V. Shanbhag, *Utilization of renewable resources: Condensation of glycerol with acetone at room temperature catalyzed by organic–inorganic hybrid catalyst.* J. Mol. Catal. A: Chem., 2015. **401**: p. 73-80.
79. Li, X., Y. Jiang, R. Zhou, and Z. Hou, *Layered α-zirconium phosphate: An efficient catalyst for the synthesis of solketal from glycerol.* Appl. Clay Sci., 2019. **174**: p. 120-126.
80. Vannucci, J.A., N.N. Nichio, and F. Pompeo, *Solketal synthesis from ketalization of glycerol with acetone: A kinetic study over a sulfated zirconia catalyst.* Catal. Today, 2020.
81. Sulistyo, H., I. Perdana, F.T. Pratiwi, and I. Hartati, *Kinetics and Thermodynamics Studies of Ketalization of Glycerol and Acetone in the Presence of Basolite F300 as Catalyst.* IOP Conf. Ser.: Mater. Sci. Eng., 2020. **742**: p. 012007.
82. Podolean, I., J. Zhang, M. Shamzhy, V.I. Pârvulescu, and J. Čejka, *Solvent-free ketalization of polyols over germanosilicate zeolites: the role of the nature and strength of acid sites.* Catal. Sci. Technol., 2020. **10**(24): p. 8254-8264.
83. Li, X., Y. Jiang, R. Zhou, and Z. Hou, *Acetalization of glycerol with acetone over appropriately-hydrophobic zirconium organophosphonates.* Appl. Clay Sci., 2020. **189**: p. 105555.
84. Hussein, H., A. Vivian, L. Fusaro, M. Devillers, and C. Aprile, *Synthesis of Highly Accessible Gallosilicates via Impregnation Procedure: Enhanced Catalytic Performances in the Conversion of Glycerol into Solketal.* ChemCatChem, 2020. **12**(23): p. 5966-5976.
85. Vivian, A., L. Soumoy, L. Fusaro, S. Fiorilli, D.P. Debecker, and C. Aprile, *Surface-functionalized mesoporous gallosilicate catalysts for the efficient and sustainable upgrading of glycerol to solketal.* Green Chem., 2021. **23**(1): p. 354-366.
86. Santos-Vieira, I.C.M.S., R.F. Mendes, F.A. Almeida Paz, J. Rocha, and M.M.Q. Simões, *Solketal Production via Solvent-Free Acetalization of Glycerol over Triphosphonic-Lanthanide Coordination Polymers.* Catalysts, 2021. **11**(5): p. 598.
87. Rodrigues, R., M.S. Santos, R.S. Nunes, W.A. Carvalho, and G. Labuto, *Solvent-free solketal production from glycerol promoted by yeast activated carbons.* Fuel, 2021. **299**: p. 120923.
88. Dashtipour, B., S. Dehghanpour, and M. Sharbatdaran, *Improvement of the acidic properties of MOF by doped SnO2 quantum dots for the production of solketal.* Journal of Chemical Sciences, 2022. **134**(4): p. 106.
89. Julião, D., F. Mirante, and S.S. Balula, *Easy and Fast Production of Solketal from Glycerol Acetalization via Heteropolyacids.* Molecules, 2022. **27**(19): p. 6573.
90. Esposito, R., U. Raucci, M.E. Cucciolito, R. Di Guida, C. Scamardella, N. Rega, and F. Ruffo, *Iron(III) Complexes for Highly Efficient and Sustainable Ketalization of Glycerol: A Combined Experimental and Theoretical Study.* ACS Omega, 2019. **4**(1): p. 688-698.
91. Lee, D.-W., Y.-M. Park, and K.-Y. Lee, *Heterogeneous Base Catalysts for Transesterification in Biodiesel Synthesis.* Catal. Surv. Asia, 2009. **13**(2): p. 63-77.
92. Gomes, I.S., D.C. de Carvalho, A.C. Oliveira, E. Rodríguez-Castellón, S. Tehuacanero-Cuapa, P.T.C. Freire, J.M. Filho, G.D. Saraiva, F.F. de Sousa, and R. Lang, *On the reasons for deactivation of titanate nanotubes with metals catalysts in the acetalization of glycerol with acetone.* Chem. Eng. J. (Amsterdam, Neth.), 2018. **334**: p. 1927-1942.
93. Pinheiro, A.L.G., J.V.C. do Carmo, D.C. Carvalho, A.C. Oliveira, E. Rodríguez-Castellón, S. Tehuacanero-Cuapa, L. Otubo, and R. Lang, *Bio-additive fuels from glycerol acetalization over metals-containing vanadium oxide nanotubes (MeVOx-NT in which, Me = Ni, Co, or Pt).* Fuel Process. Technol., 2019. **184**: p. 45-56.

94. Dmitriev, G.S., A.V. Terekhov, L.N. Zanaveskin, A.L. Maksimov, and S.N. Khadzhiev, *Kinetics of the Formation of Solketal in the Presence of Sulfuric Acid.* Kinet. Catal., 2018. **59**(4): p. 504-508.
95. Taddeo, F., R. Esposito, V. Russo, and M. Di Serio, *Kinetic Modeling of Solketal Synthesis from Glycerol and Acetone Catalyzed by an Iron(III) Complex.* Catalysts, 2021. **11**(1): p. 83.
96. Li, X., J. Lai, H. Cong, C. Shu, R. Zhao, Y. Wang, H. Li, and X. Gao, *Toward sustainable and eco-efficient novel catalytic distillation process for production of solketal using seepage catalytic packing internal.* Catalysis Today, 2022. **388-389**: p. 92-108.
97. Dmitriev, G.S., A.V. Terekhov, S.N. Khadzhiev, and L.N. Zanaveskin, *Specific features of solketal synthesis on KU-2-8 cation-exchange resin.* Russ. J. Appl. Chem., 2016. **89**(1): p. 45-50.
98. Oliveira, P.A., R.O.M.A. Souza, and C.J.A. Mota, *Atmospheric Pressure Continuous Production of Solketal from the Acid-Catalyzed Reaction of Glycerol with Acetone.* J. Braz. Chem. Soc., 2016. **27**: p. 1832-1837.
99. Guidi, S., M. Noè, P. Riello, A. Perosa, and M. Selva, *Towards a Rational Design of a Continuous-Flow Method for the Acetalization of Crude Glycerol: Scope and Limitations of Commercial Amberlyst 36 and AlF3·3H2O as Model Catalysts.* Molecules, 2016. **21**(5): p. 657.
100. Konwar, L.J., A. Samikannu, P. Mäki-Arvela, D. Boström, and J.-P. Mikkola, *Lignosulfonate-based macro/mesoporous solid protonic acids for acetalization of glycerol to bio-additives.* Appl. Catal., B, 2018. **220**: p. 314-323.
101. Domínguez-Barroso, V., C. Herrera, M.Á. Larrubia, R. González-Gil, M. Cortés-Reyes, and L.J. Alemany, *Continuous-Flow Process for Glycerol Conversion to Solketal Using a Brönsted Acid Functionalized Carbon-Based Catalyst.* Catalysts, 2019. **9**(7): p. 609.
102. Kowalska-Kuś, J., A. Held, and K. Nowińska, *A continuous-flow process for the acetalization of crude glycerol with acetone on zeolite catalysts.* Chem. Eng. J. (Amsterdam, Neth.), 2020. **401**: p. 126143.
103. Huang, X., G. Zhang, L. Zhang, and Q. Zhang, *Continuous Flow Synthesis of a ZSM-5 Film in Capillary Microchannel for Efficient Production of Solketal.* ACS Omega, 2020. **5**(33): p. 20784-20791.
104. Zhang, G., L. Zhang, X. Wang, A. Chen, and Q. Zhang, *Microfluidic processing of HZSM-5 films in a capillary microreactor for the continuous acetalisation reaction of glycerol with acetone.* React. Chem. Eng., 2020. **5**(3): p. 539-546.
105. Zaharia, E., C. Bildea, and O. Muntean, *Design, economic evaluation and plantwide control of glycerol ketalization plant.* UPB Scientific Bulletin, Series B: Chemistry and Materials Science, 2015. **77**(2): p. 41-52.
106. Dmitriev, G.S., A.V. Terekhov, L.N. Zanaveskin, S.N. Khadzhiev, K.L. Zanaveskin, and A.L. Maksimov, *Choice of a catalyst and technological scheme for synthesis of solketal.* Russ. J. Appl. Chem., 2017. **89**(10): p. 1619-1624.
107. da Silva, M.J., F. de Ávila Rodrigues, and A.A. Júlio, *SnF2-catalyzed glycerol ketalization: A friendly environmentally process to synthesize solketal at room temperature over on solid and reusable Lewis acid.* Chem. Eng. J. (Amsterdam, Neth.), 2017. **307**: p. 828-835.
108. Al-Saadi, L.S., V.C. Eze, and A.P. Harvey, *Techno-Economic Analysis of Glycerol Valorization via Catalytic Applications of Sulphonic Acid-Functionalized Copolymer Beads.* Front. Chem., 2020. **7**: p. 882.
109. Chol, C.G., R. Dhabhai, A.K. Dalai, and M. Reaney, *Purification of crude glycerol derived from biodiesel production process: Experimental studies and techno-economic analyses.* Fuel Process. Technol., 2018. **178**: p. 78-87.
110. Al-Saadi, L.S., V.C. Eze, and A.P. Harvey, *A reactive coupling process for co-production of solketal and biodiesel.* Green Process. Synth., 2019. **8**(1): p. 516-524.
111. Bumbac, G. and I. Banu, *Modeling and simulation process for solketal synthesis from glycerol and acetone by catalytic distillation in a modified structure of a divided wall column.* Renew. Energy, 2022. **183**: p. 662-675.

112. Clarke, N.S., *The basics of patent searching.* World Pat. Inf., 2018. **54**: p. S4-S10.
113. Frietsch, R., U. Schmoch, B. Van Looy, J.P. Walsh, R. Devroede, M. Du Plessis, T. Jung, Y. Meng, P. Neuhäusler, and B. Peeters, *The value and indicator function of patents*. 2010, Studien zum deutschen Innovations system.
114. Boesch, V. and J.R. Herguijuela, *Process of manufacturing equipment for preparing acetals and ketals*, U.S.P.a.T. Office, Editor. 2003, Roche Vitamins Inc.: United States.
115. Winkler, H., H.-G. Poll, M. Neumann, G. Koehler, and F. Bauer, *Process for preparing acetals and ketals with the aid of multistage pervaporation or vapor permeation*, U.S.P.a.T. Office, Editor. 2004, Evonik Degussa GmbH: United Stated
116. Dubois, J.L., C.S. Iborra, C.A. Corma, and A. Velty, *Process for the synthesis of cyclic acetals by reactive extraction of a polyol in a concentrated solution* N.I.o.I. Property, Editor. 2008, Arkema France SA France.
117. Haiyu, Y., H. Chunlong, J. Peng, C. Qingyan, and X. Liqing, *Industrial continuous method for preparing solketal by catalyst distillation device*. 2018, Guangzhou Yintian New Material Co.,LTD: China.
118. Yujia, L., W. Yamin, X. Changjiu, Z. Bin, L. Min, L. Yibin, and S. Xingtian, *Method for preparing ketal glycerine and/or acetal glycerine*. 2020, China Petroleum & Chem Corp; Sinopec Corp Res Inst Petroleum Processing: China.
119. Yujia, L., X. Changjiu, P. Xinxin, Z. Bin, L. Min, L. Yibin, and S. Xingtian, *Method for preparing ketal glycerine and/or acetal glycerine*. 2020, China Petroleum & Chem Corp; Sinopec Corp Res Inst Petroleum Processing: China.
120. Yujia, L., X. Changjiu, Y. Yongjia, Z. Bin, P. Xinxin, L. Min, L. Yibin, and S. Xingtian, *Method for preparing ketal glycerine and/or acetal glycerine by catalyzing glycerine*. 2020, China Petroleum & Chem Corp; Sinopec Corp Res Inst Petroleum Processing: China.
121. Abe, T. and N. Kawakami, *Method for producing dioxolane compound*, J.P. Office, Editor. 2004, Osaka Organic Chem Ind: Japan.
122. Wimmer, T., C. Ertl, and R. Kalb, *Process for preparing cyclic glycerol acetals or cyclic glycerol ketals or mixtures thereof* E.P. Office, Editor. 2011, Christof International Management Gmbh.
123. Terrill, D.L., B.D. McMurray, D.R. Billodeaux, J.L. Little, and A.S. Howard, *Production of cyclic acetals or ketals using liquid-phase acid catalysts* 2012, Eastman Chemical Co: United States.
124. Mastroianni, S., *Process for producing dioxolane* 2013, Rhodia Operations SA: United States.
125. Rodrigues, E. and A. Malheiro, *Process for the production of a dioxolane compound from crude glycerol including a liquid-liquid extraction step* W.I.P. Organization, Editor. 2013.
126. Rodrigues, E. and A. Malheiro, *Process for the production of a dioxolane compound from crude glycerol* 2014, Rhodia Poliamida e Especialidades Ltda: United States.
127. Terrill, D.L., B.D. McMurray, D.R. Billodeaux, J.L. Little, and A.S. Howard, *Production of cyclic acetals or ketals using solid acid catalysts* 2014, Eastman Chemical Co United States.
128. Terrill, D.L., B.D. McMurray, D.R. Billodeaux, J.L. Little, and A.S. Howard, *Production of cyclic acetals or ketals using solid acid catalysts* 2016, Eastman Chemical Co: United States.
129. Varfolomeev, S.D., G.G. Makarov, V.B. Volyeva, N.L. Komissarova, A.V. Malkova, M.N. Ovsyannikova, E.V. Koverzanova, S.V. Usachev, T.S. Aynullov, A.I. Shamsullin, D.V. Ksenofontov, and R.S. Tkach, *Method of producing solketal* 2018, Institute of Biochemical Physics, Russian Academy of Sciences, in association with Company Tatneft: Russia.
130. Priya, S.S., P.R. Selvakannan, K.V.R. Chary, M.L. Kantam, and S.K. Bhargava, *Solvent-free microwave-assisted synthesis of solketal from glycerol using transition metal ions promoted mordenite solid acid catalysts.* Mol. Catal., 2017. **434**: p. 184-193.
131. Roldán, L., R. Mallada, J.M. Fraile, J.A. Mayoral, and M. Menéndez, *Glycerol upgrading by ketalization in a zeolite membrane reactor.* Asia-Pac. J. Chem. Eng., 2009. **4**(3): p. 279-284.

132. Eze, V.C. and A.P. Harvey, *Continuous reactive coupling of glycerol and acetone – A strategy for triglyceride transesterification and in-situ valorisation of glycerol by-product.* Chem. Eng. J. (Amsterdam, Neth.), 2018. **347**: p. 41-51.
133. Qing, W., J. Chen, X. Shi, J. Wu, J. Hu, and W. Zhang, *Conversion enhancement for acetalization using a catalytically active membrane in a pervaporation membrane reactor.* Chem. Eng. J. (Amsterdam, Neth.), 2017. **313**: p. 1396-1405.
134. Faria, R., N. Graça, and A. Rodrigues, *Green Fuels and Fuel Additives Production in Simulated Moving Bed Reactors*, in *Intensification of Biobased Processes*, Andrzej Górak and A. Stankiewicz, Editors. 2018, The Royal Society of Chemistry. p. 145-165.
135. Rodrigues, A.E., C.S.M. Pereira, M. Minceva, L.S. Pais, A.M. Ribeiro, A. Ribeiro, M. Silva, N. Graça, and J.C. Santos, *Simulated Moving Bed Technology: Principles, Design and Process Applications*. 2015: Elsevier Science.
136. Guiochon, G., A. Felinger, D.G. Shirazi, and A.M. Katti, *Fundamentals of preparative and nonlinear chromatography*. 2006, Amsterdam, The Nederlands: Academic Press.
137. Nishizawa, H., K. Tahara, S. Miyamori, Y. Motegi, T. Shoji, and Y. Abe, *True moving bed chromatography: solid–liquid multi-stage counter-current extraction.* J. Chromatogr. A, 1999. **849**(1): p. 61-69.
138. Faria, R.P. and A.E. Rodrigues, *Instrumental aspects of Simulated Moving Bed chromatography.* J. Chromatogr. A, 2015. **1421**: p. 82-102.
139. Donald B. Broughton, C.G.G.h., *Continuous Sorption Process Employing Fxed Bed of Sorbent and Moving Inlets and Outlets*, U.S.P. Office, Editor. 1961, Universal Oil Products Company: United States.
140. Sá Gomes, P., M. Minceva, and A.E. Rodrigues, *Simulated moving bed technology: old and new.* Adsorption, 2006. **12**(5-6): p. 375-392.
141. Kim, K.-M., J.W. Lee, S. Kim, F.V. Santos da Silva, A. Seidel-Morgenstern, and C.-H. Lee, *Advanced Operating Strategies to Extend the Applications of Simulated Moving Bed Chromatography.* Chemical Engineering & Technology, 2017. **40**(12): p. 2163-2178.
142. Aniceto, J.P.S. and C.M. Silva, *Simulated Moving Bed Strategies and Designs: From Established Systems to the Latest Developments.* Separation & Purification Reviews, 2015. **44**(1): p. 41-73.
143. Yu, Y., K.R. Wood, and Y.A. Liu, *Simulation and Comparison of Operational Modes in Simulated Moving Bed Chromatography.* Industrial & Engineering Chemistry Research, 2015. **54**(46): p. 11576-11591.
144. Pais, L.S. and A.E. Rodrigues, *Design of simulated moving bed and Varicol processes for preparative separations with a low number of columns.* Journal of Chromatography A, 2003. **1006**(1): p. 33-44.
145. Rodrigues, R.C.R., J.M.M. Araújo, M.F.J. Eusébio, and J.P.B. Mota, *Experimental assessment of simulated moving bed and varicol processes using a single-column setup.* Journal of Chromatography A, 2007. **1142**(1): p. 69-80.
146. Masuda, T., T. Sonobe, and F. Matsuda, *Pocess for Fractional Separation of Multi-component Fluid Mixture* 1993, Japan Organo Co., Ltd., Tokyo, Japan: United States of America.
147. Mata, V.G. and A.E. Rodrigues, *Separation of ternary mixtures by pseudo-simulated moving bed chromatography.* Journal of Chromatography A, 2001. **939**(1): p. 23-40.
148. Kearney, M.M. and K.L. Hieb, *Time variable simulated moving bed process* 1992, The Amalgamated Sugar Company: United States.
149. Zhang, Z., M. Mazzotti, and M. Morbidelli, *PowerFeed operation of simulated moving bed units: changing flow-rates during the switching interval.* Journal of Chromatography A, 2003. **1006**(1): p. 87-99.
150. Jermann, S., S. Katsuo, and M. Mazzotti, *Intermittent Simulated Moving Bed Processes for Chromatographic Three-Fraction Separation.* Organic Process Research & Development, 2012. **16**(2): p. 311-322.

151. Lutin, F., M. Bailly, and D. Bar, *Process improvements with innovative technologies in the starch and sugar industries.* Desalination, 2002. **148**(1): p. 121-124.
152. Zang, Y. and P.C. Wankat, *SMB operation strategy - Partial feed.* Industrial and Engineering Chemistry Research, 2002. **41**(10): p. 2504-2511.
153. Bae, Y.-S. and C.-H. Lee, *Partial-discard strategy for obtaining high purity products using simulated moving bed chromatography.* Journal of Chromatography A, 2006. **1122**(1): p. 161-173.
154. Sá Gomes, P. and A.E. Rodrigues, *Outlet Streams Swing (OSS) and MultiFeed Operation of Simulated Moving Beds.* Separation Science and Technology, 2007. **42**(2): p. 223-252.
155. Song, J.-Y., K.-M. Kim, and C.-H. Lee, *High-performance strategy of a simulated moving bed chromatography by simultaneous control of product and feed streams under maximum allowable pressure drop.* Journal of Chromatography A, 2016. **1471**: p. 102-117.
156. Li, Y., Z. Ding, J. Wang, J. Xu, W. Yu, and A.K. Ray, *A comparison between simulated moving bed and sequential simulated moving bed system based on multi-objective optimization.* Chemical Engineering Science, 2020. **219**: p. 115562.
157. Schramm, H., M. Kaspereit, A. Kienle, and A. Seidel-Morgenstern, *Simulated moving bed process with cyclic modulation of the feed concentration.* Journal of Chromatography A, 2003. **1006**(1-2): p. 77-86.
158. Zhang, Z., M. Mazzotti, and M. Morbidelli, *Continuous chromatographic processes with a small number of columns: Comparison of simulated moving bed with Varicol, PowerFeed, and ModiCon.* Korean Journal of Chemical Engineering, 2004. **21**(2): p. 454-464.
159. Bailly, M., R.-M. Nicoud, P. Adam, and O. Ludemann-Hombourger, *Method and Device for Chromatography Comprising a Concentration Step*. 2006, NOVASEP.
160. Paredes, G., H.-K. Rhee, and M. Mazzotti, *Design of Simulated-Moving-Bed Chromatography with Enriched Extract Operation (EE-SMB): Langmuir Isotherms.* Industrial & Engineering Chemistry Research, 2006. **45**(18): p. 6289-6301.
161. Lee, H.-H., K.-M. Kim, and C.-H. Lee, *Improved performance of simulated moving bed process using column-modified feed.* AIChE Journal, 2011. **57**(8): p. 2036-2053.
162. Kim, K.-M. and C.-H. Lee, *Backfill-simulated moving bed operation for improving the separation performance of simulated moving bed chromatography.* Journal of Chromatography A, 2013. **1311**: p. 79-89.
163. Antos, D. and A. Seidel-Morgenstern, *Application of gradients in the simulated moving bed process.* Chemical Engineering Science, 2001. **56**(23): p. 6667-6682.
164. Abel, S., M. Mazzotti, and M. Morbidelli, *Solvent gradient operation of simulated moving beds: 2. Langmuir isotherms.* Journal of Chromatography A, 2004. **1026**(1): p. 47-55.
165. Migliorini, C., M. Wendlinger, M. Mazzotti, and M. Morbidelli, *Temperature Gradient Operation of a Simulated Moving Bed Unit.* Industrial & Engineering Chemistry Research, 2001. **40**(12): p. 2606-2617.
166. Song, S.-M., M.-B. Park, and I.H. Kim, *Three-zone simulated moving-bed (SMB) for separation of cytosine and guanine.* Korean Journal of Chemical Engineering, 2012. **29**(7): p. 952-958.
167. Shen, B., M. Chen, H. Jiang, Y. Zhao, and F. Wei, *Modeling Study on a Three-Zone Simulated Moving Bed without Zone I.* Separation Science and Technology, 2011. **46**(5): p. 695-701.
168. Lee, K., *Two-section simulated moving-bed process.* Separation Science and Technology, 2000. **35**(4): p. 519-534.
169. Xie, Y., C.Y. Chin, D.S.C. Phelps, C.-H. Lee, K.B. Lee, S. Mun, and N.-H.L. Wang, *A Five-Zone Simulated Moving Bed for the Isolation of Six Sugars from Biomass Hydrolyzate.* Industrial & Engineering Chemistry Research, 2005. **44**(26): p. 9904-9920.
170. Nicolaos, A., L. Muhr, P. Gotteland, R.-M. Nicoud, and M. Bailly, *Application of the equilibrium theory to ternary moving bed configurations (4+4, 5+4, 8 and 9 zones): II. Langmuir case.* Journal of Chromatography A, 2001. **908**(1): p. 87-109.

171. Clavier, J.Y., R.M. Nicoud, and M. Perrut, *A new efficient fractionation process: The simulated moving bed with supercritical eluent*, in *Process Technology Proceedings*, P.R. von Rohr and C. Trepp, Editors. 1996, Elsevier. p. 429-434.
172. Rajendran, A., S. Peper, M. Johannsen, M. Mazzotti, M. Morbidelli, and G. Brunner, *Enantioseparation of 1-phenyl-1-propanol by supercritical fluid-simulated moving bed chromatography.* Journal of Chromatography A, 2005. **1092**(1): p. 55-64.
173. Jin, W. and P.C. Wankat, *Hybrid Simulated Moving Bed Processes for the Purification of p-Xylene.* Separation Science and Technology, 2007. **42**(4): p. 669-700.
174. Rodrigues, A.E., C.S.M. Pereira, and J.C. Santos, *Chromatographic Reactors.* Chemical Engineering & Technology, 2012. **35**(7): p. 1171-1183.
175. Kochendoerfer, K., P. Sa Gomes, D.N. Rütze, T. Pathapati, P. de Wit, and M. Zaalberg, *Hybridizing Simulated Moving Bed and Electrodialysis: Product Purification and Eluent Regeneration.* Chemical Engineering & Technology, 2018. **41**(12): p. 2418-2426.
176. Mazzotti, M., A. Kruglov, B. Neri, D. Gelosa, and M. Morbidelli, *A continuous chromatographic reactor: SMBR.* Chemical Engineering Science, 1996. **51**(10): p. 1827-1836.
177. Stankiewicz, A. and J.A. Moulijn, *Process Intensification: Transforming Chemical Engineering.* Chem. Eng. Prog., 2000. **96**: p. 22-33.
178. Hashimoto, K., S. Adachi, H. Noujima, and Y. Ueda, *A new process combining adsorption and enzyme reaction for producing higher-fructose syrup.* Biotechnology and Bioengineering, 1983. **25**(10): p. 2371-2393.
179. Pereira, C.S.M., V.M.T.M. Silva, and A.E. Rodrigues, *Fixed Bed Adsorptive Reactor for Ethyl Lactate Synthesis: Experiments, Modelling, and Simulation.* Separation Science and Technology, 2009. **44**(12): p. 2721-2749.
180. Pereira, C.S.M., P.S. Gomes, G.K. Gandi, V.M.T.M. Silva, and A.E. Rodrigues, *Multifunctional Reactor for the Synthesis of Dimethylacetal.* Industrial & Engineering Chemistry Research, 2008. **47**(10): p. 3515-3524.
181. Agrawal, G., J. Oh, B. Sreedhar, S. Tie, M.E. Donaldson, T.C. Frank, A.K. Schultz, A.S. Bommarius, and Y. Kawajiri, *Optimization of reactive simulated moving bed systems with modulation of feed concentration for production of glycol ether ester.* Journal of Chromatography A, 2014. **1360**: p. 196-208.
182. Constantino, D.S.M., R.P.V. Faria, C.S.M. Pereira, J.M. Loureiro, and A.E. Rodrigues, *Enhanced Simulated Moving Bed Reactor Process for Butyl Acrylate Synthesis: Process Analysis and Optimization.* Industrial & Engineering Chemistry Research, 2016. **55**(40): p. 10735-10743.
183. Constantino, D.S.M., C.S.M. Pereira, R.P.V. Faria, J.M. Loureiro, and A.E. Rodrigues, *Simulated moving bed reactor for butyl acrylate synthesis: From pilot to industrial scale.* Chemical Engineering and Processing: Process Intensification, 2015. **97**: p. 153-168.
184. Faria, R.P.V., J.C. Gonçalves, I. Corrêa, A.M. Ribeiro, and A.E. Rodrigues, *Improving the Performance of a Simulated Moving Bed Reactor for the Synthesis of Solketal by Implementing Multifeed Strategy.* Industrial & Engineering Chemistry Research, 2022. **61**(39): p. 14531-14545.
185. Subramani, H.J., K. Hidajat, and A.K. Ray, *Optimization of reactive SMB and Varicol systems.* Computers & Chemical Engineering, 2003. **27**(12): p. 1883-1901.
186. Wang, J., Y. Tian, Y. Li, J. Xu, W. Yu, and A.K. Ray, *Multi-objective optimization of non-isothermal simulated moving bed reactor: Methyl acetate synthesis.* Chemical Engineering Journal, 2020. **395**: p. 125041.
187. Graça, N.S., L.S. Pais, V.M.T.M. Silva, and A.E. Rodrigues, *Thermal effects on the synthesis of acetals in a simulated moving bed adsorptive reactor.* Chemical Engineering Journal, 2012. **207-208**: p. 504-513.
188. Faria, R.P.V., C.S.M. Pereira, V.M.T.M. Silva, J.M. Loureiro, and A.E. Rodrigues, *Sorption enhanced reactive process for the synthesis of glycerol ethyl acetal.* Chem. Eng. J. (Amsterdam, Neth.), 2014. **258**(0): p. 229-239.

189. Minceva, M., P.S. Gomes, V. Meshko, and A.E. Rodrigues, *Simulated moving bed reactor for isomerization and separation of p-xylene.* Chem. Eng. J. (Amsterdam, Neth.), 2008. **140**(1-3): p. 305-323.
190. Ströhlein, G., M. Mazzotti, and M. Morbidelli, *Optimal operation of simulated-moving-bed reactors for nonlinear adsorption isotherms and equilibrium reactions.* Chem. Eng. Sci., 2005. **60**(6): p. 1525-1533.
191. Kawase, M., T.B. Suzuki, K. Inoue, K. Yoshimoto, and K. Hashimoto, *Increased esterification conversion by application of the simulated moving-bed reactor.* Chem. Eng. Sci., 1996. **51**(11): p. 2971-2976.
192. Dubé, M.A., A.Y. Tremblay, and J. Liu, *Biodiesel production using a membrane reactor.* Bioresour. Technol., 2007. **98**(3): p. 639-647.
193. Itoh, N., *A membrane reactor using palladium.* AIChE J., 1987. **33**(9): p. 1576-1578.
194. De Falco, M., M. Capocelli, and A. Giannattasio, *Membrane Reactor for one-step DME synthesis process: Industrial plant simulation and optimization.* J. CO2 Util., 2017. **22**: p. 33-43.
195. Deshayes, A.L., E.E. Miró, and G.I. Horowitz, *Xylene isomerization in a membrane reactor: Part II. Simulation of an industrial reactor.* Chem. Eng. J. (Amsterdam, Neth.), 2006. **122**(3): p. 149-157.

Chapter 3

Fixed-bed Adsorptive Reactor

ADAPTED FROM: Corrêa, I.; Faria, R. P. V.; Rodrigues, A. E., Continuous Valorization of Glycerol into Solketal: From the Fixed-Bed Adsorptive Reactor to the Simulated Moving-Bed Reactor. *Industrial & Engineering Chemistry Research* **2022**, 61 (11), 4017-4030.

3.1. Introduction

The development of multifunctional reactors has been gaining more importance since Process Intensification techniques are demanded to solve industrial challenges (e.g., low efficiency reactions and separations). The fixed-bed reactor is a multifunctional equipment that allies separation and reaction, therefore promotes sorption enhanced operations. Solketal production via glycerol ketalization is a kinetically limited reaction that takes especial advantage of such process, as the direct reaction can be fostered because of the removal of water from the reaction medium by adsorption.

A factor of major importance for sorption enhanced processes is the choice of the stationary phase. In previous research, the optimal combination of stationary phase (among Amberlyst-35, Amberlyst-15 and zeolite H-BEA) and eluent (among ethanol, dimethyl sulfoxide and methanol) was assessed by performing pulse injections of solketal and water in a fixed-bed packed with each of the solids and each of the solvents, also used as desorbent. Because of the miscibility challenge of the reactants and the mass transfer limitation due to the high viscosity of glycerol, it is advisable to rely on a solvent to aid the mass transfer mechanism. Combining Amberlyst-35 and ethanol resulted in the highest retention of solketal and water, as well as the greatest separation between them. Furthermore, using ethanol as the solvent has many advantages: it does not strongly compete with water in terms of being adsorbed, it does not react with the reagents and products, it is abundant and renewable [1, 2].

Solketal production by SMBR is mostly limited by temperature-dependent phenomena: reaction rate, adsorption selectivity between solketal and acetone, and mass transfer. The equilibrium conversion and the reaction rate dependence has already been addressed [2]; however, the thermodynamic parameters must be estimated to select the optimal operating conditions. The temperature must be high enough to assure glycerol's adequate flow through the SMBR columns and the complete miscibility of the reaction compounds, yet not too high

to prevent acetone evaporation, or the reaction to be affected. In Chapter 3, fundamental adsorption data was collected to develop mathematical models that allow the estimation of optimum conditions for the operation of the SMBR, the main goal of the present Thesis.

3.2. Experimental Description

3.2.1. Materials and Chemicals

The chemicals selected to perform the adsorption and sorption enhanced reaction experiments in the fixed-bed reactor were glycerol (>99% - Sigma-Aldrich), acetone (>99% Fisher Chemicals), solketal (>97% VWR International) and ethanol (>99% Panreac-AppliChem). The water used in this work was purified in the LSRE-LCM laboratories. Methanol (>99% VWR International) was used as washing solvent for the analytical method and blue dextran (molecular weight of 2,000,000 - Sigma-Aldrich) was used as tracer.

Amberlyst-35 is a highly acid macroreticular ion exchange resin composed by a styrene divinylbenzene polymeric matrix functionalized with sulfonic groups. It can perform catalysis and adsorption, simultaneously. It was selected as stationary phase in the fixed-bed adsorptive reactor based on previous know-how from the LSRE-LCM research group [2]. The main characteristics of the resin are presented in Table 3.1.

Table 3.1. Amberlyst-35 physicochemical properties [3].

Property	Value
Acidity ($eq \cdot kg^{-1}$)	5.2
Particle Diameter (μm)	780
Average pore diameter (nm)	30
Particle porosity	0.396
Tortuosity	4.1
Surface area ($m^2 \cdot g^{-1}$)	50
Solid density ($kg \cdot m^{-3}$)	800

3.2.2. Analytical Methods

The samples collected were analysed by Gas Chromatography (DANI Master GC) equipped with flame ionization (FID) and thermal conductivity detector (TCD) at least in duplicate. The column used to separate the compounds was the silica capillary column Stabilwax (60 m, 0.25 mm i.d., film thickness of 0.25 μm) in which Helium N50 was used as the carrier gas at a flowrate of 8 $ml.min^{-1}$. The linear velocity was set to 30 $cm.s^{-1}$ and the sample injection volume was 1.0 μL, with a split ratio of 60. The temperature of the injector and of the detectors was set to 573 K. The proper column temperature program is set for each binary. Methanol is used as the washing solvent.

3.2.3. Experimental Set-up and Procedure

The fixed-bed experiments were performed in a laboratory-scale jacketed column (length, 11.5 cm; diameter, 2.6 cm) packed with Amberlyst-35. Different mixtures were fed to the fixed column using a high-pressure liquid chromatographic pump at a flowrate of 5.0 $mL \cdot min^{-1}$. For all the experiments, the temperature of the system was kept constant by a thermostatic bath. The set-up also comprised a three-port injection valve at the inlet of the fixed-bed column and a backpressure valve at its outlet. The experimental scheme for the adsorption and reaction experiments is exhibited in Figure 3.1.

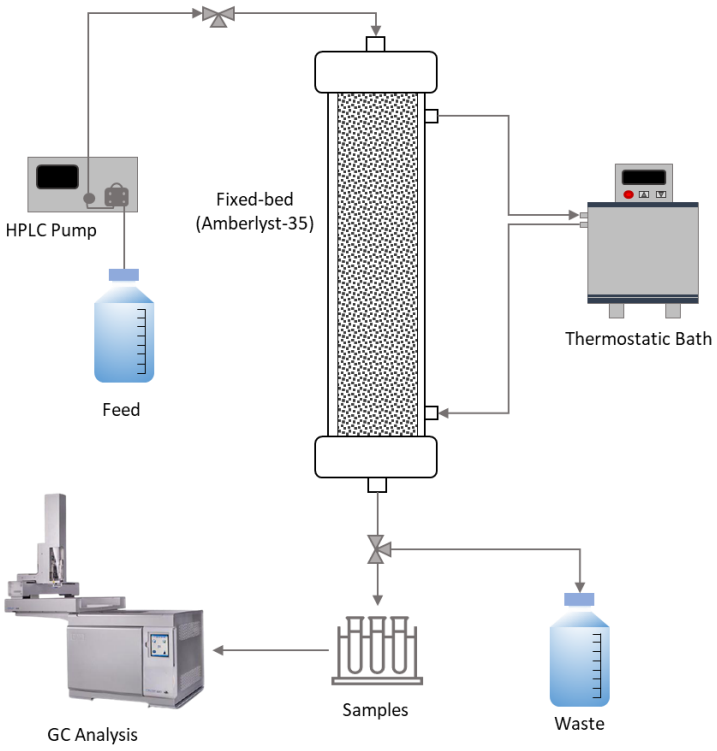

Figure 3.1. Experimental set-up used for the breakthrough and fixed-bed adsorptive reactor experiments.

Hydrodynamic Study

In the hydrodynamics study, 200 µL of a Blue Dextran solution (approximately 5 $g \cdot L^{-1}$) were injected in the fixed-bed column for its characterization through tracer experiments. In previous works within the same conditions, it has been proven that there is no dependence between the bed porosity or the Peclet number and the flowrate, therefore only injections at 5.0 $mL \cdot min^{-1}$ were performed [3]. Water was used as eluent and the outlet concentration history was recorded with a UV-Vis detector (Gilson, model 115) at 300 nm.

Adsorption Isotherms

After concluding the bed characterization, the estimation of fundamental adsorption data could be initiated. Studies in the open literature reveal that a reliable method to obtain adsorption equilibrium isotherms is the Frontal Analysis Methodology [4-6]. The procedure

consists in sequentially feeding binary mixtures containing ethanol and one of the reactants or one of the products into the column until it gets saturated with the feed mixture. The experimental set-up described in Section 3.2.3. was used to perform the experiments summarized in Table 3.2:

Table 3.2. Summary of the breakthrough experiments performed.

Binary Mixture	Flow ($mL.min^{-1}$)	Compound 1		Compound 2	
		C_0 ($mol.L^{-1}$)	C_{feed} ($mol.L^{-1}$)	C_0 ($mol.L^{-}$	C_{feed} ($mol.L^{-1}$)
		303 K			
Acetone (1) + Ethanol (2)	5.27	0.00	0.72	16.99	16.08
	5.34	0.72	2.37	16.08	13.99
	5.33	2.37	6.20	13.99	9.15
	5.49	6.20	10.11	9.15	4.21
	5.31	10.11	13.44	4.21	0.00
	5.12	13.44	11.35	0.00	2.64
	5.31	11.35	7.64	2.64	7.33
	5.24	7.64	4.74	7.33	10.99
	5.30	4.74	1.57	10.99	15.01
	5.22	1.57	0.00	15..01	16.99
Water (1) + Ethanol (2)	5.27	0.00	0.88	16.99	16.72
	5.34	0.88	2.98	16.72	16.09
	5.33	2.98	9.12	16.09	14.22
	5.49	9.12	23.97	14.22	9.72
	5.31	23.97	56.02	9.72	0.00
	5.12	56.02	31.76	0.00	7.36
	5.31	31.76	13.38	7.36	12.93
	5.24	13.38	6.56	12.93	14.99
	5.30	6.56	2.05	14.99	16.37
	5.22	2.05	0.17	16.37	16.94
Solketal (1) + Ethanol (2)	5.18	0.00	0.77	16.99	15.49
	5.25	0.77	2.22	15.49	12.70
	5.26	2.22	4.85	12.70	7.63
	5.09	4.85	7.09	7.63	3.31
	5.35	7.09	8.63	3.31	0.35
	5.12	8.63	7.71	0.35	2.11
	5.43	7.71	5.45	2.11	6.47

	5.29	5.45	3.89	6.47	9.48
	5.22	3.89	1.43	9.48	14.23
	5.19	1.43	0.00	14.23	16.99
	5.20	0.00	0.87	16.99	15.90
	5.25	0.87	2.38	15.90	14.01
Glycerol (1)	5.29	2.38	4.59	14.01	11.26
+ Ethanol (2)	5.17	4.59	3.24	11.26	12.94
	5.30	3.24	1.97	12.94	14.53
	5.27	1.97	0.00	14.53	16.99
			323 K		
	5.28	0.00	0.78	16.58	16.35
	5.34	0.78	2.98	16.35	15.69
	5.33	2.98	9.34	15.69	13.78
	5.31	9.34	23.40	13.78	9.55
Acetone (1)	5.28	23.40	55.16	9.55	0.00
+ Ethanol (2)	5.20	55.16	29.63	0.00	7.68
	5.36	29.63	13.52	7.68	12.52
	5.34	13.52	6.14	12.52	14.74
	5.38	6.14	1.82	14.74	16.04
	5.38	1.82	0.31	16.04	16.57
	5.28	0.00	0.78	16.58	16.35
	5.34	0.78	2.98	16.35	15.69
	5.33	2.98	9.34	15.69	13.78
	5.31	9.34	23.40	13.78	9.55
Water (1) +	5.28	23.40	55.16	9.55	0.00
Ethanol (2)	5.20	55.16	29.63	0.00	7.68
	5.36	29.63	13.52	7.68	12.52
	5.34	13.52	6.14	12.52	14.74
	5.38	6.14	1.82	14.74	16.04
	5.38	1.82	0.31	16.04	16.57
	5.34	0.00	0.79	16.59	15.06
	5.31	0.79	2.53	15.06	11.69
	5.16	2.53	4.50	11.69	7.88
Solketal (1)	4.97	4.50	7.06	7.88	2.93
+ Ethanol (2)	5.19	7.06	8.57	2.93	0.02
	5.35	8.57	7.68	0.02	1.73
	5.24	7.68	5.87	1.73	5.23
	5.32	5.87	3.57	5.23	9.68

	5.28	3.57	1.71	9.68	13.27
	5.33	1.71	0.00	13.27	16.59
Glycerol (1) + Ethanol (2)	5.35	0.00	0.95	16.58	15.42
	5.33	0.95	1.78	15.42	14.39
	5.38	1.78	2.56	14.39	13.43
	5.36	2.56	3.18	13.43	12.68
	5.11	3.18	4.64	12.68	10.87
	5.35	4.64	0.00	10.87	16.6

Fixed-bed adsorptive reactions

The synthesis of solketal in the fixed-bed adsorptive reactor was performed by feeding ternary mixtures with the two reactants (acetone and glycerol) and the eluent (ethanol) to the column pre-saturated with the eluent, and monitoring the outlet concentration of the reactor throughout the entire experiment until the steady-state is achieved. The feed was constituted of acetone-to-glycerol molar ratio of 1.0 diluted in 50% of ethanol, on a molar basis, to overcome the miscibility issues between acetone and glycerol. After the reaction, the reactor bed was regenerated by feeding pure ethanol, also monitoring the outlet concentration. In the same experimental set-up of the adsorption isotherms determination, the following injections were performed with the outlet concentration history carefully monitored:

Table 3.3. Summary of the fixed-bed adsorptive reactor experiments performed.

Ternary Mixture	Flow ($mL.min^{-1}$)	Compound 1		Compound 2		Compound 3	
		C_0 ($mol.L^{-1}$)	C_{feed} ($mol.L^{-1}$)	C_0 ($mol.L^{-1}$)	C_{feed} ($mol.L^{-1}$)	C_0 ($mol.L^{-1}$)	C_{feed} ($mol.L^{-1}$)
303 K							
Acetone (1) + Glycerol (2) + Ethanol (3)	5.27	0.00	3.77	0.00	3.542	16.98	7.542
	5.29	1.94	0.00	1.87	0.00	8.56	16.98

				323 K			
Acetone (1) + Glycerol (2) + Ethanol (3)	5.30	0.00	3.77	0.00	3.54	16.98	7.54
	5.29	3.77	0.00	3.54	0.00	7.54	16.98

3.3. Modelling studies

As previously stated, solketal synthesis in a fixed-bed is a complex combination of several phenomena: hydrodynamics, chemical reaction, adsorption, and mass transfer between phases. The independent studies of the adsorption and of the reaction are essential to assess the behaviour of the process and allow better design, modelling, and optimization. The design variables can be estimated either by performing numerous experiments or by building mathematical models that can predict the dynamic behaviour of the unit. The second option is more practical and economically viable. Besides it enables the study of more complex multicolumn units [7].

The model for the fixed-bed column packed with a hybrid solid admits the following assumptions: (1) plug-flow with axial dispersion and negligible radial dispersion, (2) velocity variations due to changes in the bulk composition, (3) internal and external mass transfer resistances lumped and estimated by the linear driving force model, (4) constant flow, temperature, length and porosity, and (5) the reaction occurs exclusively at the active sites inside the catalyst pores and (6) multicomponent adsorption equilibrium described by the competitive Langmuir adsorption isotherm model [8].

Molar Balance – Bulk:

$$\frac{\partial C_i}{\partial t} + \frac{\partial (uC_i)}{\partial z} + \frac{1-\varepsilon_b}{\varepsilon_b}\frac{3}{r_p}k_{L,i}\left(C_i - \bar{C}_{p,i}\right) = D_{ax}\frac{\partial^2 C_i}{\partial z^2} \tag{3.1}$$

C_i represents the bulk concentration, u the interstitial fluid velocity, ε_b the bed porosity, r_p the particle radius, $k_{L,i}$ the global mass-transfer coefficient, $\bar{C}_{p,i}$ the average concentration in the particle pores, D_{ax} the axial dispersion coefficient, t is time, and z is the axial coordinate.

Interstitial fluid velocity variation (obtained from the global mass balance to the system):

$$\frac{du}{dz} = -\frac{1-\varepsilon_b}{\varepsilon_b}\frac{3}{r_p}\sum_{i=1}^{NC} k_{L,i}V_{M,i}\left(C_i - \bar{C}_{p,i}\right) \tag{3.2}$$

$V_{M,i}$ is the molar volume of component i.

Molar Balance – Particle:

$$\frac{3}{r_p}k_{L,i}\left(C_i - \bar{C}_{p,i}\right) = \varepsilon_p\frac{\partial \bar{C}_{p,i}}{\partial t} + \left(1-\varepsilon_p\right)\frac{\partial \bar{q}_i}{\partial t} - \nu_i\frac{\rho_b}{(1-\varepsilon_b)}\Re\left(\bar{C}_{p,i}\right) \tag{3.3}$$

where ε_p is the particle porosity, $\bar{q}_i$ represents the adsorbed concentration for component i, and ρ_b is the bulk density. The variables ν_i and $\Re$ are related to the chemical reaction and represent component's i stoichiometric coefficient and the reaction rate based on the local intraparticle composition, respectively. Previous studies on the glycerol ketalization in batch demonstrate the reaction rate can be described by the Langmuir-Hinshelwood-Hougen-Watson expressed in terms of the activities (calculated using the UNIFAC model) [3, 9]. More details are presented in Appendix A.

$$\Re = k_c\frac{a_{acetone}a_{glycerol} - \frac{a_{solk}a_{water}}{K_{eq}}}{\left(1 + K_{S,W}a_{water}\right)^2} \tag{3.4}$$

Initial and Danckwerts boundary conditions:

$$t = 0 \qquad C_i = \bar{C}_{p,i} = C_{i,0} \tag{3.5}$$

$$z = 0 \qquad uC_{in,i} = uC_i|_{z=0} - D_{ax}\left.\frac{\partial C_i}{\partial z}\right|_{z=0} \tag{3.6}$$

$$z = 0 \qquad u = u|_{z=0} \tag{3.7}$$

$$z = L \qquad \left.\frac{\partial x_i}{\partial z}\right|_{z=L} = 0 \tag{3.8}$$

where x_i is the molar fraction of component i and L is the column length. The initial conditions state that at the beginning of the process the concentration in the bulk and in the particle pores are equal and that the liquid and adsorbed concentrations are in equilibrium. As for the Danckwerts boundary conditions, they admit that the axial dispersion occurs as soon as the feed enters the fixed bed column and that there is no change in concentration in the final limit of the reactor.

Global mass-transfer coefficient:

$$\frac{1}{k_{L,i}} = \frac{1}{k_{ext,i}} + \frac{1}{\varepsilon_p k_{int,i}} \tag{3.9}$$

k_{ext} and k_{int} are the external and internal mass-transfer coefficients, respectively. The internal mass-transfer coefficient was estimated by Equation 3.10 [10], while the external mass-transfer coefficient was estimated by the Wilson and Geankopolis correlation [11] (Equation 3.11).

$$k_{int,i} = \frac{5D_{i,m}/\tau_p}{r_p} \tag{3.10}$$

$$Sh_p = \frac{1.09}{\varepsilon_p}\left(Re_p Sc\right)^{0.33};\ 0.0015 < Re_p < 55 \tag{3.11}$$

$D_{i,m}$ is the molecular diffusivity coefficient of a compound in a mixture, τ_p is the particle tortuosity, Sh_p and Re_p are the Sherwood and Reynolds numbers relative to the particle, respectively, described by Equations 3.12 and 3.13, and Sc is the Schmidt number (Equation 3.14).

$$Sh_p = \frac{k_{ext,i} 2r_p}{D_{i,m}} \tag{3.12}$$

$$Re_p = \frac{\rho 2r_p u}{\eta_m} \tag{3.13}$$

$$Sc = \frac{\eta_m}{\rho D_{i,m}} \tag{3.14}$$

where ρ is the fluid phase density and η_m is the mixture viscosity.

To compute the molecular diffusivity, $D_{i,m}$, the infinite dilution diffusivities must be first estimated through the Scheibel correlation [12]:

$$D_{i,j}^0 = \frac{8.2 \times 10^{-8} T}{\eta_j V_{M,i}^{\frac{1}{3}}} \left[1 + \left(\frac{3V_{M,j}}{V_{M,i}} \right)^{\frac{2}{3}} \right] \tag{3.15}$$

$D_{i,j}^0$ is the diffusion coefficient for a dilute solute i in a solvent j, T is the temperature, η_j is the viscosity of solvent j. Then, for multicomponent systems, the Perkins and Geankoplis correlation [13] can be used to predict $D_{i,m}$:

$$D_{i,m} \eta_m^{0.8} = \sum_{\substack{j=1 \\ j \neq i}}^{NC} x_j \, D_{i,j}^0 \eta_j^{0.8} \tag{3.16}$$

Finally, the effective diffusion coefficient ($D_{eff,i}$) is estimated as follows.

$$D_{eff,i} = \frac{\varepsilon_p D_{i,m}}{\tau} \tag{3.17}$$

The numerical solution for the model equations were performed using the software General PROcess Modelling System (gPROMS) version 7.0.7. The partial differential and algebraic equations were solved using a method of Orthogonal Collocation in Finite Elements (OCFEM) and discretizing the axial dimension of the fixed-bed column in 30 finite elements with two interior collocation points in each finite element. An integrated differential-algebraic equation solver (DASOLV) was used to solve the system of ordinary differential equations in time.

3.4. Hydrodynamics Study

The hydrodynamics study intends to estimate the values of Peclet and bed porosity through tracer experiments. Injecting a solution of blue dextran in the column, with a molecule larger than the particle pores, one can obtain the residence time distribution curve ($E(t)$) and then estimate the mean residence time ($\bar{t_r}$). The bed porosity is calculated by dividing the mean residence time by the reactor space time. Since the Peclet number correlates convective and dispersive effects, it is related to the variance of the residence time distribution curve. The equations that describe these variables are given:

$$\bar{t_r} = \varepsilon_b \frac{\mathrm{V}}{Q} = \int_0^\infty tE(t)dt \tag{3.18}$$

$$\sigma^2 = \int_0^\infty (t - \bar{t_r})^2 E(t)dt = \frac{2}{Pe}\bar{t_r}^2 \tag{3.19}$$

The variable V is the fixed-bed column volume and Q represents the experimental flow rate.

The hydrodynamic study is also helpful to validate the model designed to describe the fixed-bed flow pattern since there is no reaction, no mass transfer between the fluid phase and the solid phase, and no adsorption. Hence, Equation 3.20 that represent the mass balance on the bed is simplified to the following equation:

$$\frac{\partial C_i}{\partial t} + \frac{\partial (uC_i)}{\partial z} = D_{ax}\frac{\partial^2 C_i}{\partial z^2} \tag{3.20}$$

Figure 3.2 shows a good agreement between the experimental and modelled residence time distribution curves obtained through tracer experiments.

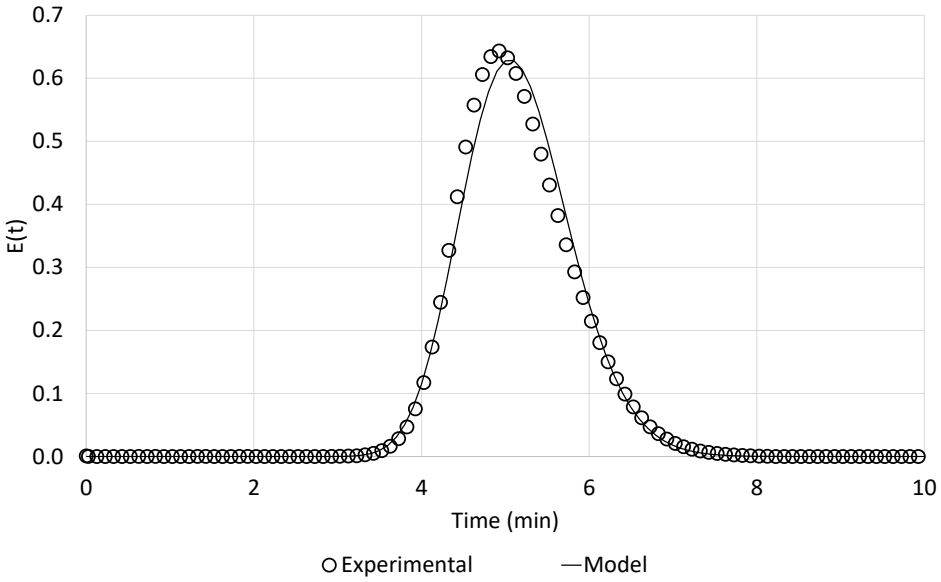

Figure 3.2. Residence time distribution determined with tracer experiments at 5.0 mL·min^{-1}.

Three injections were performed to test the data reproducibility and the results are presented in Table 3.4.

Table 3.4. Tracer experimental results at 5.0 ml.min^{-1}.

Run	$\bar{t_r}$ **(min)**	ε_b	Pe
1	5.14	0.413	127.8
2	5.11	0.411	127.0
3	5.16	0.415	128.4

The average bed porosity is 0.413 ± 0.002 and the average Peclet number is 127.7 ± 0.7, considering all the experimental results.

3.5. Adsorption Isotherms

The Frontal Analysis experiments provide breakthrough curves from where it is possible to obtain the plateau concentrations, and, by the global mass balance (Equations 3.21 and 3.22), one can estimate the concentration adsorbed in or desorbed from the solid phase. This methodology requires relatively low sample amounts to provide enough experimental data

points to describe the entire isotherm. The data from the complete isotherm is a necessary condition to perform the correct parameter estimation, as it was concluded in previous studies where it was proven that parameters estimated from partial isotherms carry large deviations [14].

$$n_{ads/des,i} = Q \int_0^t \alpha_i \left(C_{in,i} - C_i|_{z=L}\right) dt \tag{3.21}$$

$$\frac{n_{ads/des,i}\alpha_i}{V} = \left(\varepsilon_b + (1-\varepsilon_b)\varepsilon_p\right)\left(C_{in,i} - C_{i,0}\right) + (1-\varepsilon_b)\left(1-\varepsilon_p\right)\left(q_{in,i} - q_{i,0}\right) \tag{3.22}$$

α_i is a coefficient that takes a value of 1 or -1 depending on if the species is being adsorbed or desorbed, respectively, and the variables $C_{i,0}$, $C_{in,i}$ represent the initial and the inlet concentration of compound i in the liquid phase, and $q_{i,0}$ and $q_{in,i}$ represent the initial adsorbed concentration and the concentration of compound i in the solid phase in equilibrium with the two previous liquid phase concentrations. The mixtures fed must be non-reactive to enable the determination of the adsorption parameters for each of the species involved.

Experimentally, binary mixtures of know composition containing the eluent and one of the other species were fed stepwise into the column pre-saturated with ethanol until a new concentration plateau is reached. The flow rate adopted for the experiments was 5.0 mL·min^{-1}, fed to the column by a high-pressure liquid chromatographic (HPLC) pump. Knowing by previous studies that the steady stated is reached at about 30 to 40 minutes [3], the experiments lasted at least 60 minutes. Each experiment provides one point of the adsorption equilibrium isotherm. Since the experiments are carried with multicomponent mixtures and all the compounds adsorb in the solid phase, the isotherms measured are competitive rather than of each compound isolated. With studies at two temperatures, 303 K and 323 K, it is aimed to complement the previous study conducted at 313 K to assess the optimum condition to promote the sorption enhanced reaction [3].

Several models can describe adsorption equilibrium and one of the most used is the multicomponent Langmuir adsorption equilibrium isotherm (Equation 3.23) because it is simple to apply and describes well the adsorbed concentration as a function of the liquid concentration in multicomponent systems [15-18].

$$\bar{q}_i = \frac{Q_i K_i \bar{C}_{p,i}}{1 + \sum_{j=1}^{NC} K_j \bar{C}_{p,j}} \tag{3.23}$$

Q_i represents the monolayer capacity and K_i the equilibrium constant for component i. The model assumes that each adsorption site can hold only one molecule, there is no interaction between adsorbate molecules, and the energy of adsorption is equal for all sites, hence it does not phenomenologically describe the adsorption. The limitation of the model is verified for highly concentrated systems with widely different molecular sizes, where the assumption of a maximum monolayer adsorption capacity usually fails [3, 15]. This, however, can be bypassed by estimating the monolayer adsorption capacity for each species (Q_i) as the capacity of the adsorbent (Q_v) divided by the respective molar volume of the species ($V_{M,i}$). This strategy has already been validated in similar experiments [3, 19].

The thermodynamic parameters of adsorption can be determined by the integration of the Van't Hoff equation, described as follows:

$$K_i = K_{i,0} \exp\left[-\frac{\Delta H_{ads,i}}{U}\left(\frac{1}{T} - \frac{1}{T_{ref}}\right)\right] \tag{3.24}$$

where $K_{i,0}$ is the pre-exponential adsorption equilibrium constant for component i at the reference temperature T_{ref} (313 K). The enthalpy, $\Delta H_{ads,i}$, assumes negative values for physisorption, indicating the exothermic nature of the process. U is the universal gas constant.

In possession of all the results from the breakthrough experiments performed at 303 K and 323 K and the results at 313 K gathered in a previous step of the research by our research group [3], the data fitting on the Langmuir adsorption equilibrium isotherm was performed using

Matlab's integrated solver (*fmincon*) to minimize the sum of the relative errors between the experimental adsorbed concentration ($q_{i,j,k}^{ads,exp}$) and the theoretical values predicted by the model ($q_{i,j,k}^{ads,model}$) for experiment j,compound i in data point k, setting a convergence tolerance of 10^{-5}. The objective function described above assumes the following mathematical expression:

$$fob = \min\left(\sum_{j}^{NE}\sum_{i}^{NC}\sum_{k}^{NP}\left(\frac{\left|\left(q_{i,j,k}^{ads,model} - q_{i,j,k}^{ads,exp}\right)\right|}{q_{i,j,k}^{ads,exp}}\right)\right) \quad (3.25)$$

NE, NC and NP represent the number of experiments, compounds, and experimental data points. The methodology resulted in eleven parameters (the adsorbent capacity, Q_v, the adsorption equilibrium constant for each component at 313 K, $K_{i,0}$, and the enthalpy for each component, $\Delta H_{ads,i}$). With these parameters, one can obtain the compounds equilibrium constants at all the temperatures.

According to the literature, this parameter estimation methodology is regarded as more reliable due to larger set of experimental data employed compared to estimating parameters for each temperature separately, resulting in parameters with higher confidence [20]. Furthermore, since less parameters are estimated, the errors associated are reduced. The errors of the parameter estimation were determined through the Bootstrap methodology (B = 2000, resampling residuals) [3, 21] and quantitatively measured by the standard deviation – SD.

$$SD = \sqrt{\frac{\sum_{b}^{B}(y_b - \bar{y})^2}{B-1}} \quad (3.26)$$

where y_b is the parameter value for sample b and $\bar{y}$ is the mean parameter value. The estimated parameters are exhibited in Table 3.5 and the experimental adsorption isotherms are exhibited from Figure 3.3 to Figure 3.6 for 303 K and from Figure 3.7 to Figure 3.10 for 323 K. The fob value is 33.22.

Table 3.5. Langmuir competitive adsorption parameters obtained from the data fitting.

Compound	$Q_v\left(L \cdot L_{Ads}^{-1}\right)$	$K_{i,0}(L_{ads} \cdot mol^{-1})$	$\Delta H_{ads,i}\ (kJ.mol^{-1}K^{-1})$
Acetone	0.397 ± 0.006	4.7 ± 1.1	-37.0 ± 15.9
Glycerol		20.1 ± 4.3	-45.3 ± 13.1
Solketal		3.4 ± 0.6	-75.8 ± 10.9
Water		49.3 ± 6.3	-56.2 ± 9.3
Ethanol		13.4 ± 1.7	-58.1 ± 7.8

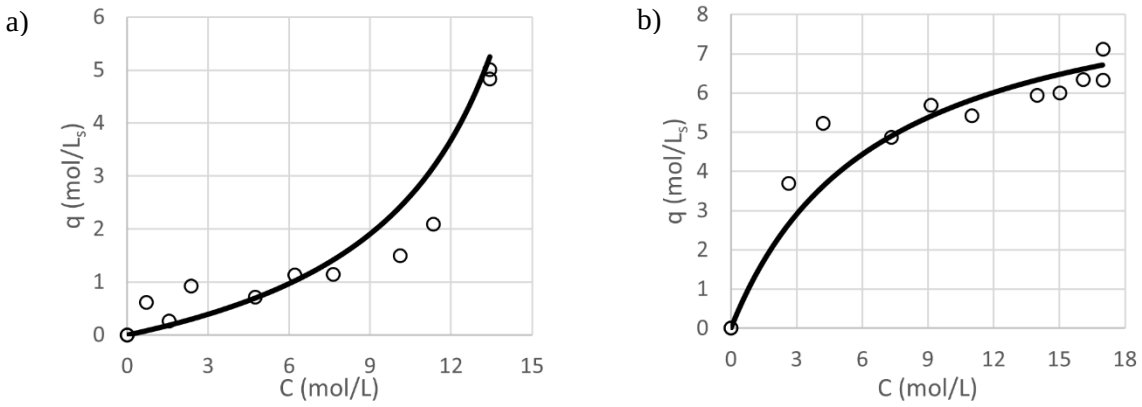

Figure 3.3. Experimental results for the adsorption isotherm of binary mixtures of (a) acetone and (b) ethanol over Amberlyst-35 at 303 K (○ experimental results; ─ mathematical model).

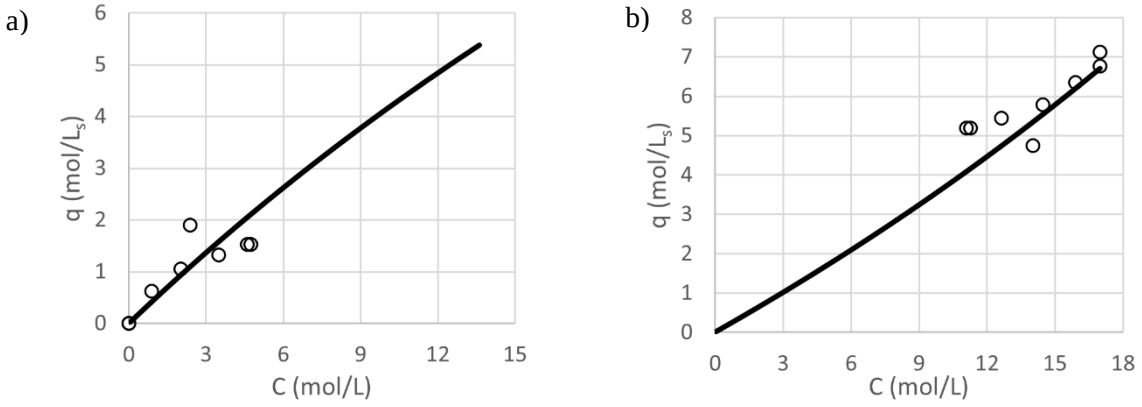

Figure 3.4. Experimental results for the adsorption isotherm of binary mixtures of (a) glycerol and (b) ethanol over Amberlyst-35 at 303 K (○ experimental results; ─ mathematical model).

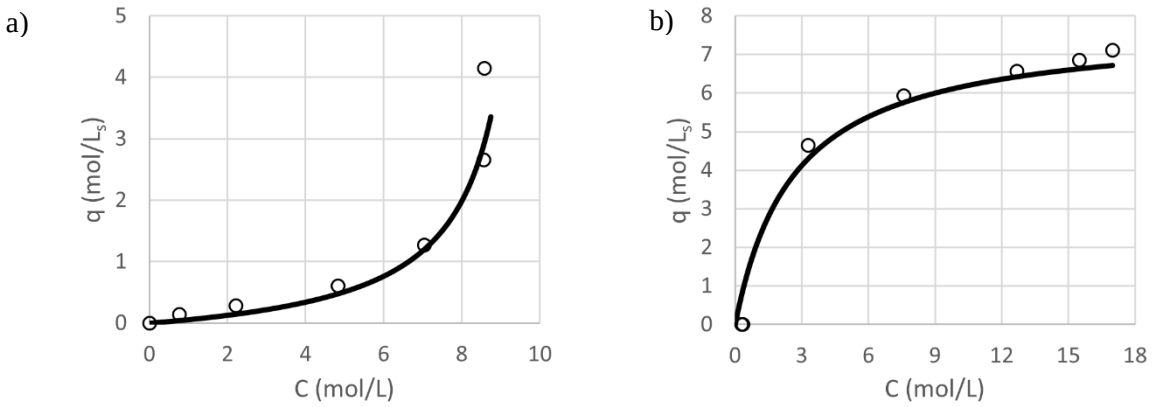

Figure 3.5. Experimental results for the adsorption isotherm of binary mixtures of (a) solketal and (b) ethanol over Amberlyst-35 at 303 K (○ experimental results; ─ mathematical model).

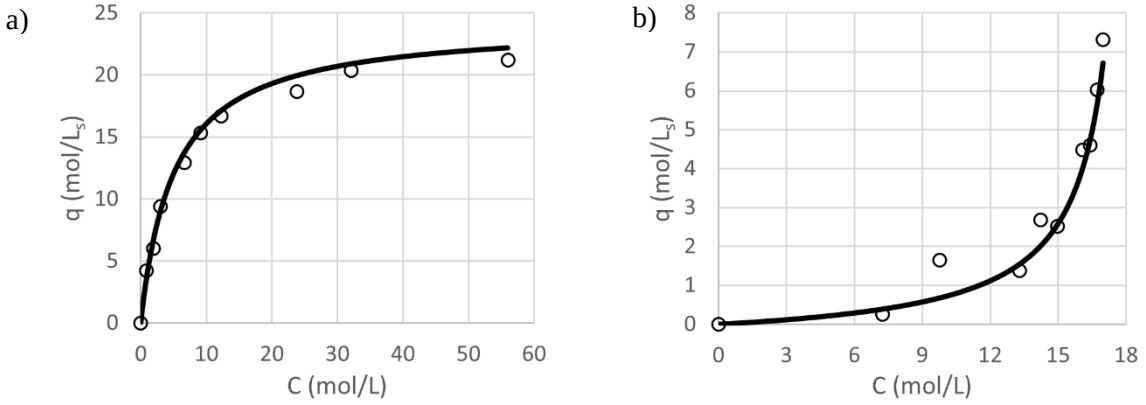

Figure 3.6. Experimental results for the adsorption isotherm of binary mixtures of (a) water and (b) ethanol over Amberlyst-35 at 303 K (○ experimental results; ─ mathematical model).

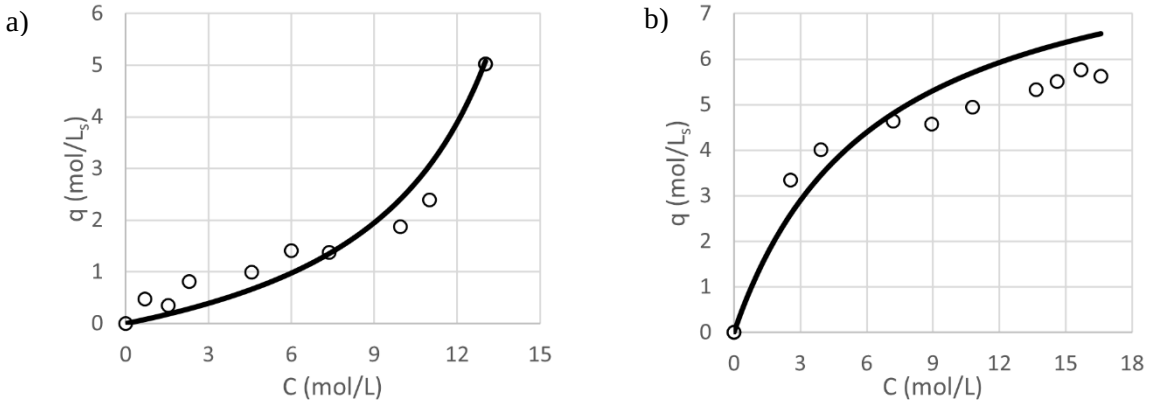

Figure 3.7. Experimental results for the adsorption isotherm of binary mixtures of (a) acetone and (b) ethanol over Amberlyst-35 at 323 K (○ experimental results; ─ mathematical model).

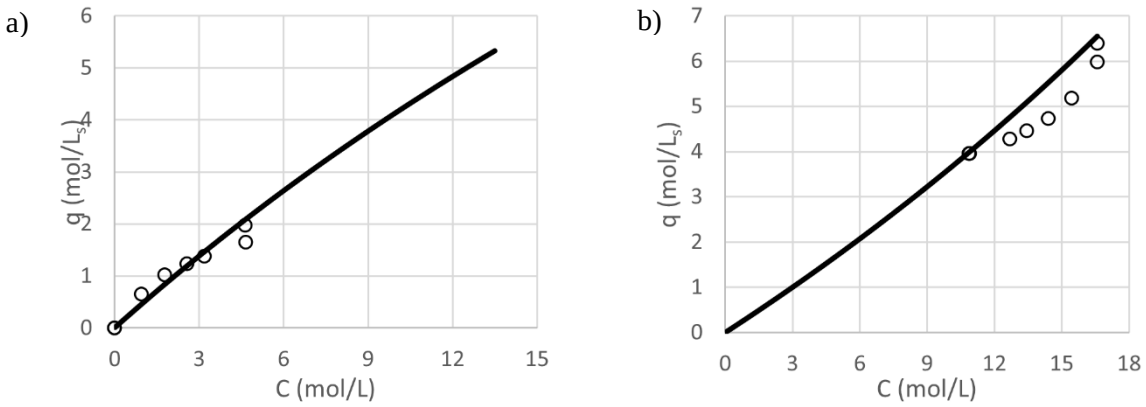

Figure 3.8. Experimental results for the adsorption isotherm of binary mixtures of (a) glycerol and (b) ethanol over Amberlyst-35 at 323 K (○ experimental results; ─ mathematical model).

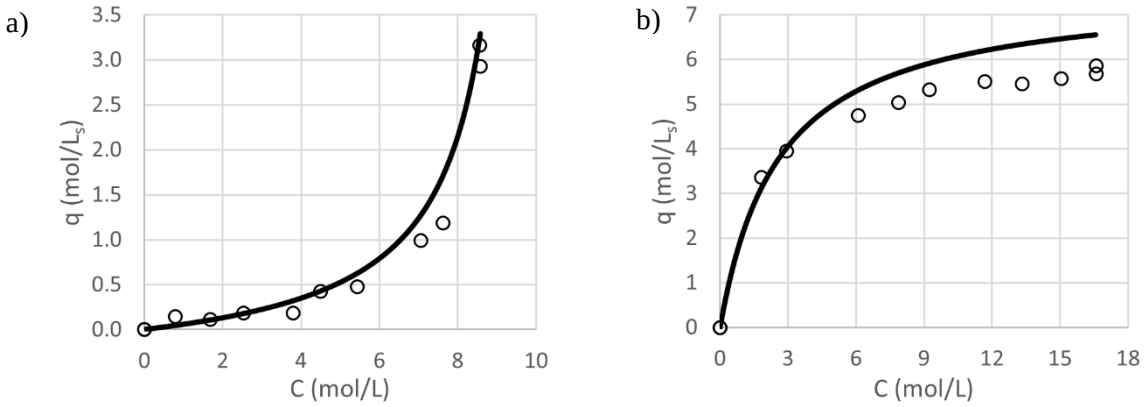

Figure 3.9. Experimental results for the adsorption isotherm of binary mixtures of (a) solketal and (b) ethanol over Amberlyst-35 at 323 K (○ experimental results; ─ mathematical model).

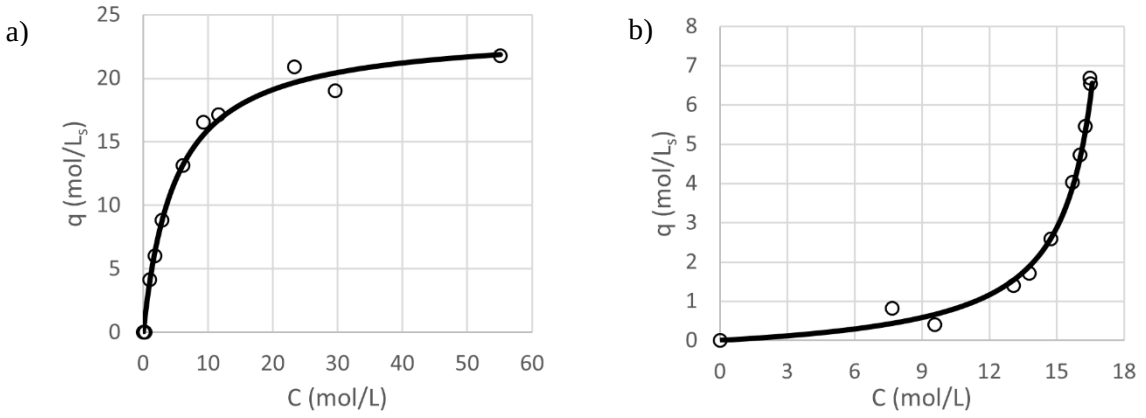

Figure 3.10. Experimental results for the adsorption isotherm of binary mixtures of (a) water and (b) ethanol over Amberlyst-35 at 323 K (○ experimental results; ─ mathematical model).

As previously stated, physisorption is an exothermic process, therefore it is negatively influenced by a raise in temperature. The parameters estimated agree with this statement, as lower values of the Langmuir Isotherm equilibrium constant were obtained at 323 K, indicating a loss in the adsorption capacity when compared to the process at 303 K. Also, the adsorption enthalpies confirm the exothermic nature of the adsorption for all the compounds.

The estimated parameters were validated through the comparison of the experimental adsorbed concentration (q_{exp}^{ads}) with the correspondent theoretical data (q_{model}^{ads}), resulting in the parity plot exhibited in Figure 3.11. The regression of the experimental and the model predicted data resulted in a linear fitting with a slope equal to 1.00 and a coefficient of determination of 0.990. From these results, it is possible to conclude that the parameters can predict the adsorbed concentrations with high accuracy.

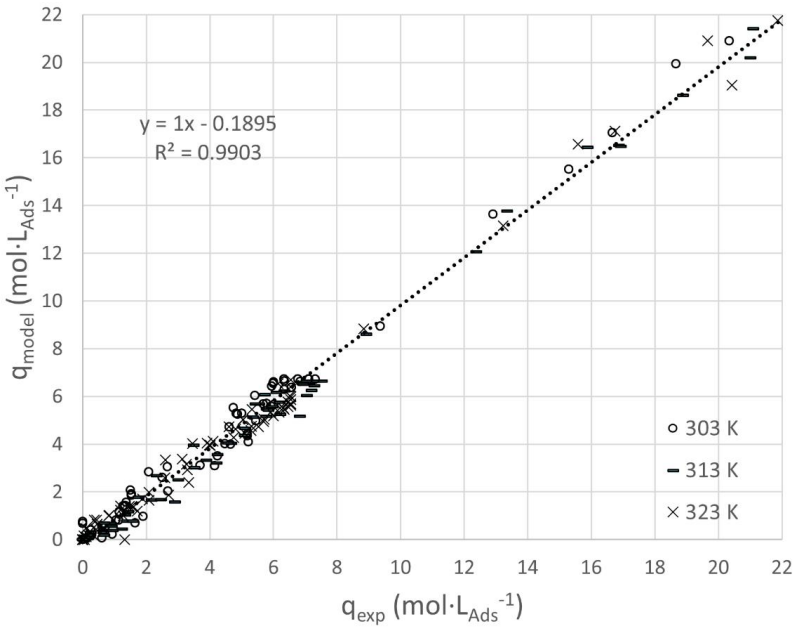

Figure 3.11. Comparison of the experimental adsorbed concentration and theoretical values obtained from the estimated parameters.

The mathematical model developed with the estimated parameters was validated through simulations of the breakthrough experiments performed with non-reactive pairs. The

comparison between the experimental data and simulation results for each binary is presented in Figure 3.12 to Figure 3.19. The quantitative analysis of the quality of the fitting was estimated by the coefficient of determination (R^2) specified by the following equation:

$$R^2 = 1 - \frac{\sum_j^{NE}\sum_i^{NC}\sum_k^{NP}(C_{i,j,k}^{exp} - C_{i,j,k}^{model})^2}{\sum_j^{NE}\sum_i^{NC}\sum_k^{NP}(C_{i,j,k}^{exp} - \overline{C_\iota})^2} \tag{3.27}$$

$C_{i,j,k}^{exp}$ and $C_{i,j,k}^{model}$ are the experimental and predicted outlet concentration for experiment j,compound i in data point k, and $\overline{C_\iota}$ is the average concentration value of compound i in all data points. The values of the coefficient of determination for the acetone-ethanol, glycerol-ethanol, solketal-ethanol and water-ethanol breakthrough experiments were 0.994, 0.987, 0.992 and 0.994 for 303 K and 0.998, 0.989, 0.997 and 0.991 for 323 K, respectively, which satisfactorily validates the mathematical model designed.

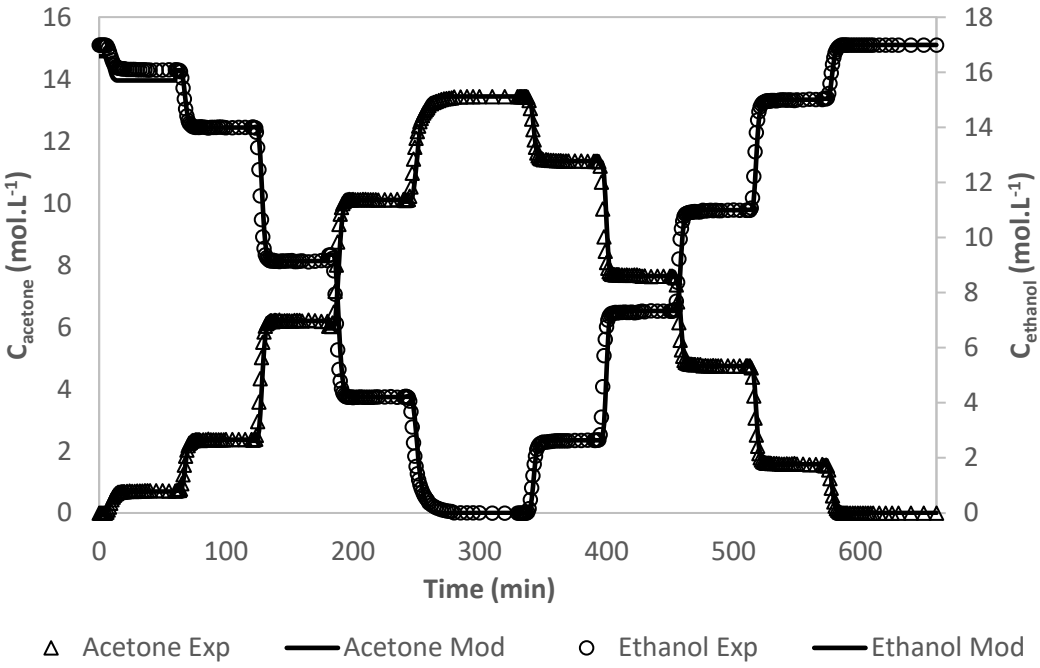

Figure 3.12. Experimental and predicted outlet concentration histories for the breakthrough curves performed with binary mixtures of acetone and ethanol at 303 K and 5.0 mL·min^{-1} on Amberlyst-35 (R^2 = 0.994).

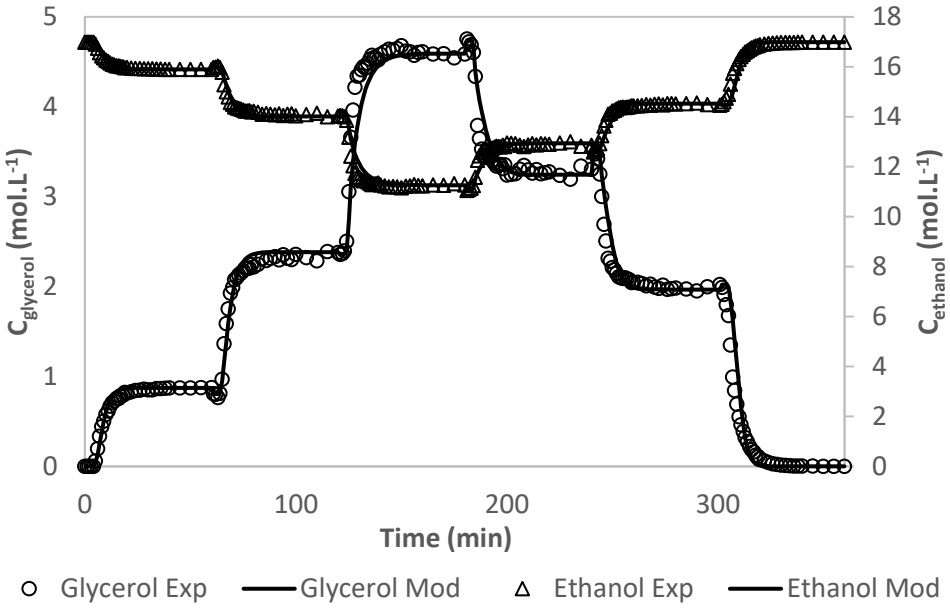

Figure 3.13. Experimental and predicted outlet concentration histories for the breakthrough curves performed with binary mixtures of glycerol and ethanol at 303 K and 5.0 mL·min^{-1} on Amberlyst-35 (R^2 = 0.987).

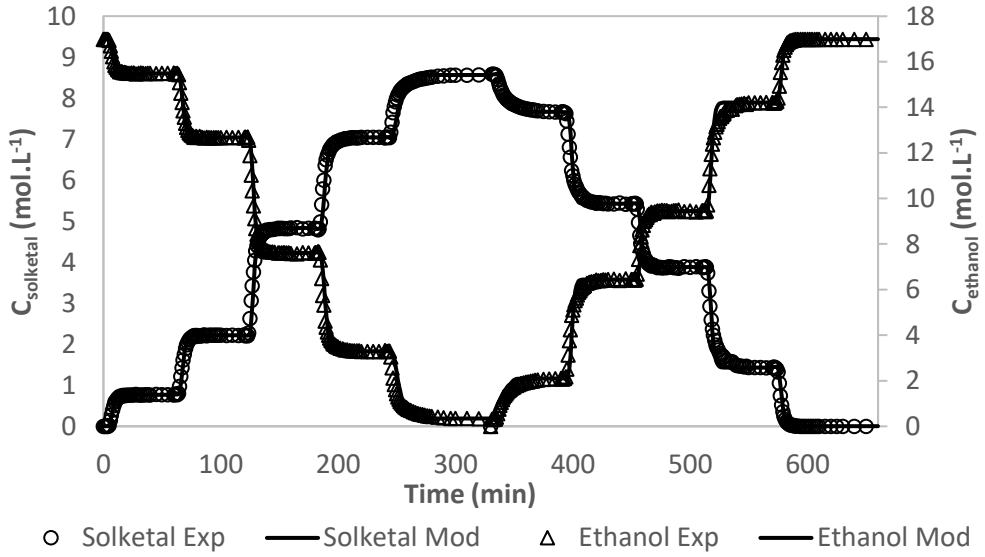

Figure 3.14. Experimental and predicted outlet concentration histories for the breakthrough curves performed with binary mixtures of solketal and ethanol at 303 K and 5.0 mL·min^{-1} on Amberlyst-35 (R^2 = 0.992).

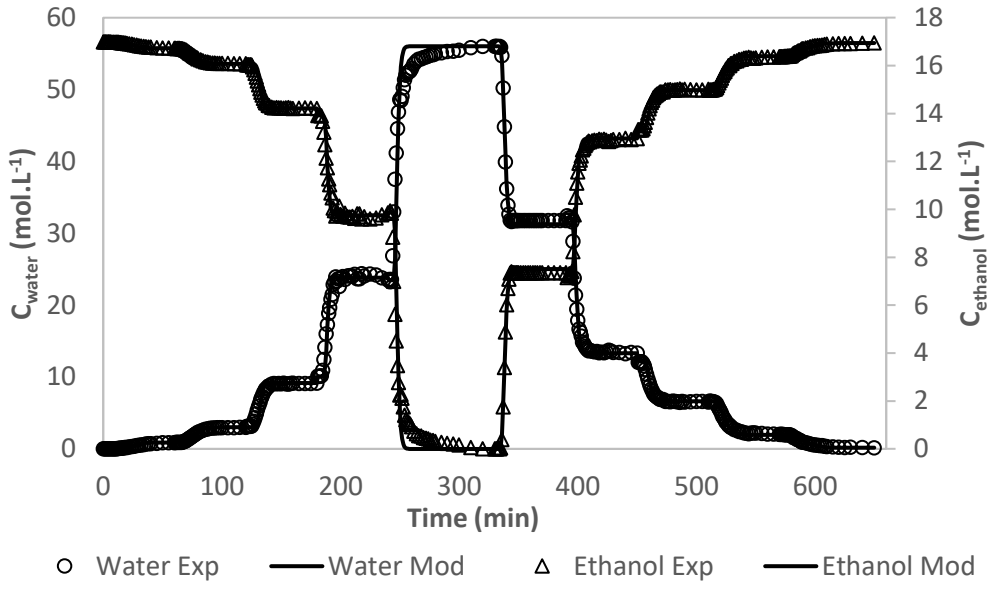

Figure 3.15. Experimental and predicted outlet concentration histories for the breakthrough curves performed with binary mixtures of water and ethanol at 303 K and 5.0 mL·min^{-1} on Amberlyst-35 (R^2 = 0.994).

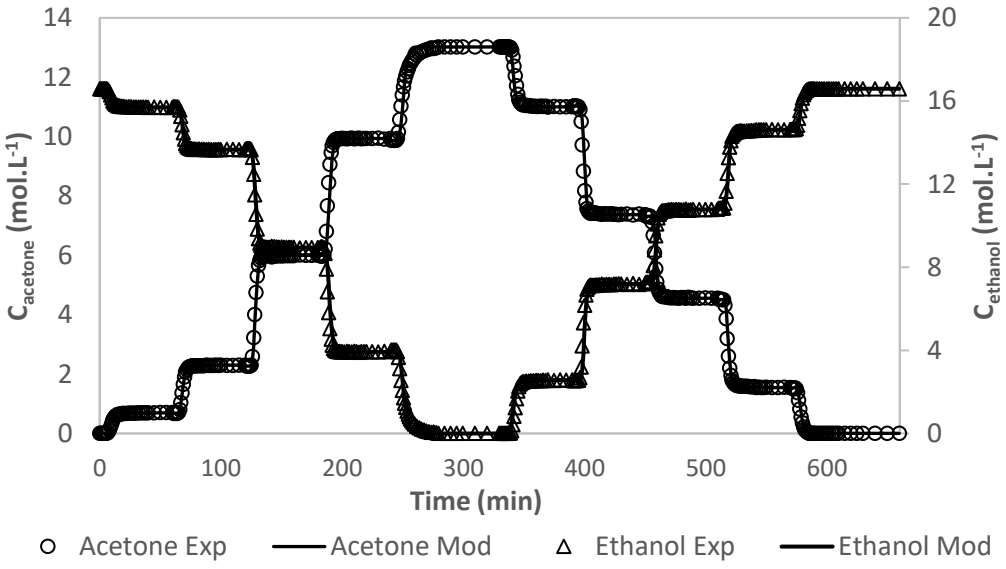

Figure 3.16. Experimental and predicted outlet concentration histories for the breakthrough curves performed with binary mixtures of acetone and ethanol at 323 K and 5.0 mL·min^{-1} on Amberlyst-35 (R^2 = 0.998).

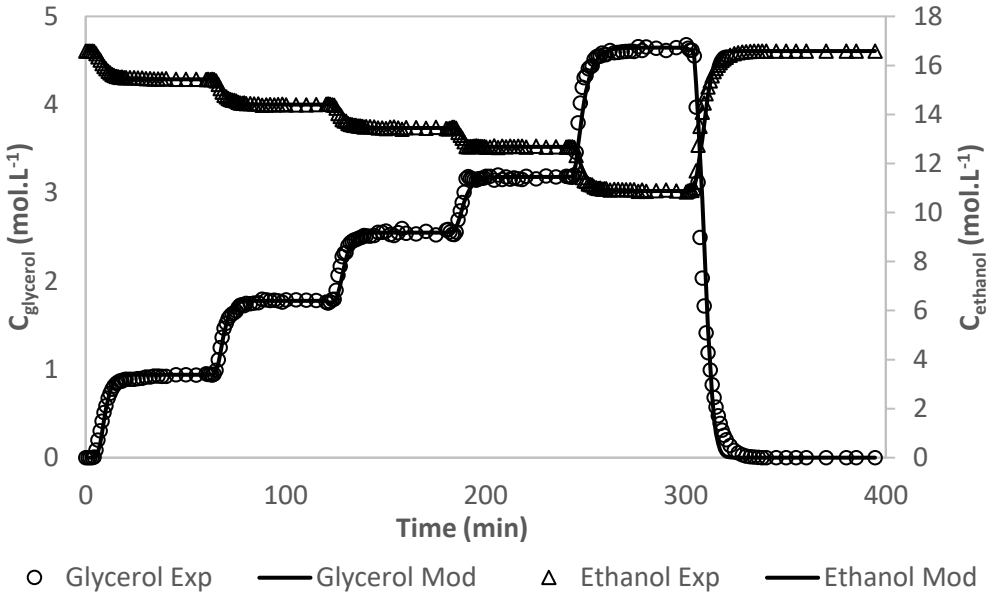

Figure 3.17. Experimental and predicted outlet concentration histories for the breakthrough curves performed with binary mixtures of glycerol and ethanol at 323 K and 5.0 mL·min^{-1} on Amberlyst-35 (R^2 = 0.989).

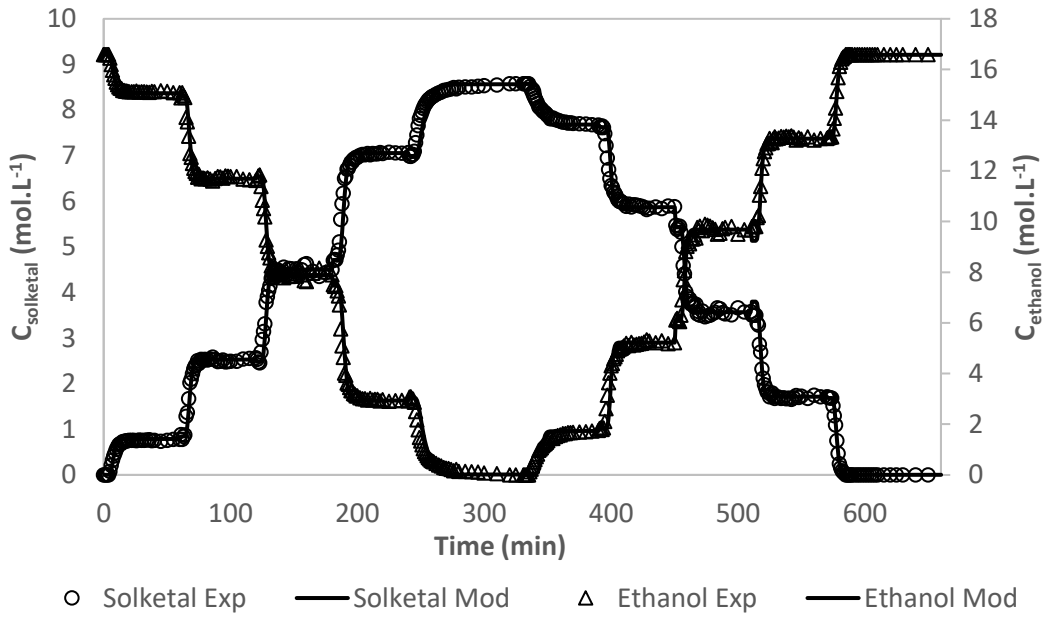

Figure 3.18. Experimental and predicted outlet concentration histories for the breakthrough curves performed with binary mixtures of solketal and ethanol at 323 K and 5.0 mL·min^{-1} on Amberlyst-35 (R^2 = 0.997).

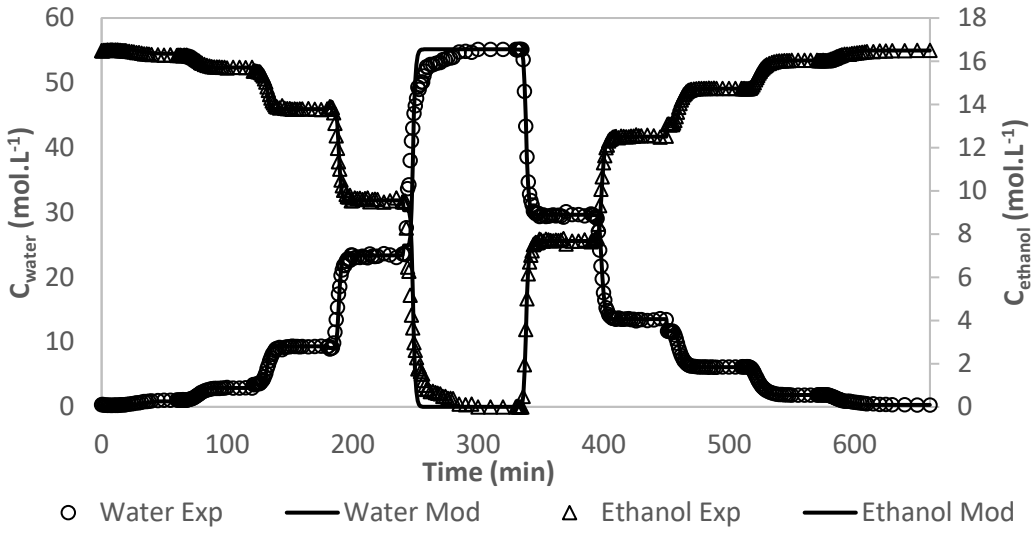

Figure 3.19. Experimental and predicted outlet concentration histories for the breakthrough curves performed with binary mixtures of water and ethanol at 323 K and 5.0 mL·min^{-1} on Amberlyst-35 (R^2 = 0.991).

The results reported from Figure 3.12 to Figure 3.19 and the quantitative analysis of the fittings presented in the caption of each figure evidence the good agreement between the model and the experimental data. This confirms that the model can accurately predict the dynamic behaviour of the adsorptive bed, including the dispersive effects that result from the mass transfer phenomena, as well as from the adsorption equilibrium.

3.6. Solketal Synthesis in the Fixed-bed Adsorptive Reactor

To assess the operating temperature that leads to the highest solketal productivity in the fixed-bed adsorptive reactor and to evaluate the influence of the temperature on the dynamic behaviour of the process, ternary mixtures composed by acetone and glycerol in a 1:1 molar ratio were diluted in 50% of ethanol (molar basis) and fed at 5.0 mL·min-1 to a reactor initially saturated with the eluent at 303 K and 323 K. The resulting outlet concentration histories are presented in Figure 3.20 and Figure 3.21.

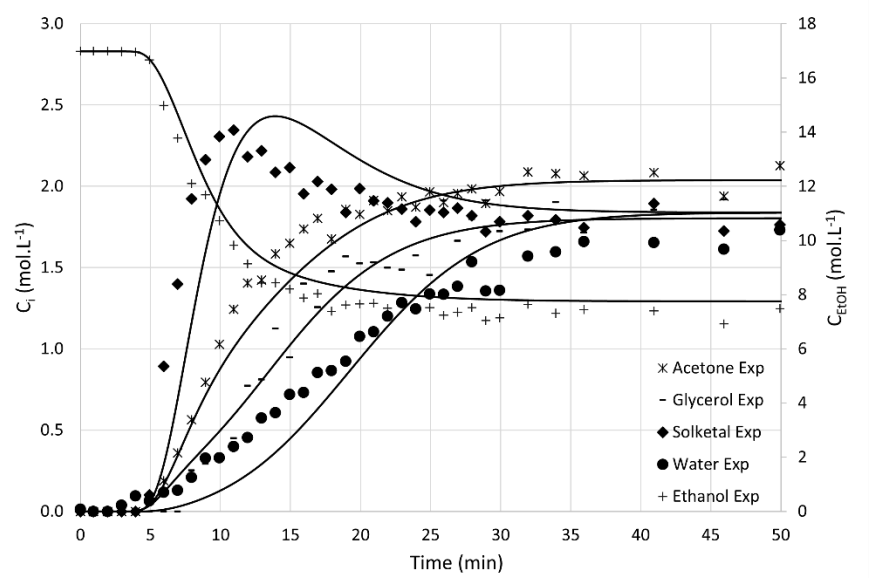

Figure 3.20. Experimental and predicted outlet concentration histories for the solketal synthesis in the fixed-bed reactor at 303 K, x_{gly}: x_{acet} ≈ 1:1 and 5.0 mL·min^{-1} with Amberlyst-35 as the catalyst/adsorbent (the lines represent the mathematical model).

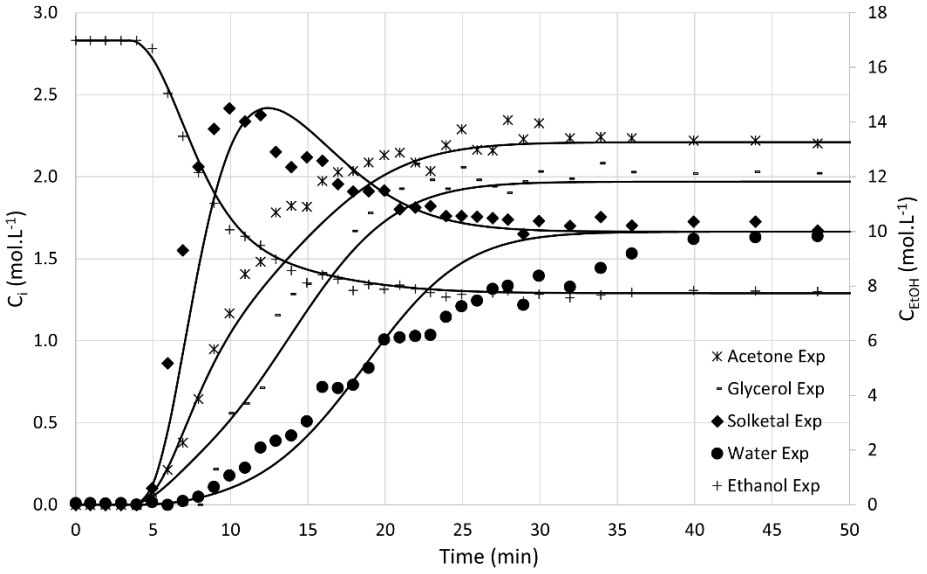

Figure 3.21. Experimental and predicted outlet concentration histories for the solketal synthesis in the fixed-bed reactor at 323 K, x_{gly}: x_{acet} ≈1:1 and 5.0 mL·min^{-1} with Amberlyst-35 as the catalyst/adsorbent (the lines represent the mathematical model).

The conversion (X) is one of the key indicators of the sorption enhancement promoted by the retention of water. Therefore, this parameter was monitored throughout the entire experiment

by Equation 3.28 to assess its evolution and detect the maximum conversion transitorily achieved.

$$X = \left[\frac{F_{Solketal}^{out}}{F_{glycerol}^{in}}\right] \times 100\% \tag{3.28}$$

where $F_{Solketal}^{out}$ is solketal's outlet molar flow and $F_{glycerol}^{in}$ is glycerol's inlet molar flow.

The reactive fixed-bed experiments demonstrate the potential for implementing sorption-enhanced reactive processes for the synthesis of solketal on ethanol and Amberlyst-35, once the thermodynamic equilibrium conversion is transitorily surpassed by approximately 21% at 303 K and 40% at 323 K. This enhancement is due to water adsorption, which fosters the direct reaction. In a previous study at 313 K, the equilibrium was overcame by approximately 30% [3]. The steady state conversion is lower for the reaction at 323 K, 46%, while it reaches 55% at 303 K, as expected for exothermic reactions such as glycerol ketalization. These values correspond to the equilibrium conversion at the experimental conditions for both temperatures. The maximum conversions were 66% also for both temperatures. No additional peaks were detected in the GC analysis, indicating that only solketal and water were formed in the reactive experiments.

The coefficient of determination (R^2) for the experiment at 303 K was 0.91 and for 323 K, 0.96, which satisfactorily validates the fixed-bed adsorptive reactor mathematical model. This is a relevant output of the present work, as it qualifies the model to be used in the scale-up of the process and on the transition to the continuous SMBR operation. In terms of sorption enhancement, the most significative effect was observed when operating at 323 K, as the maximum conversion transitorily surpassed the equilibrium conversion by almost 40%, while at 303 K it surpasses only by nearly half of it. Nevertheless, the maximum solketal concentration is fundamentally equal for both temperatures.

A simulation study to evaluate the adsorption impact on the reaction as a function of the reactor space-time ($\tau = V/Q$) was summarized in Figure 3.22, where equimolar amounts of glycerol and ethanol diluted in 50% (molar basis) of ethanol were fed to the fixed-bed adsorptive reactor.

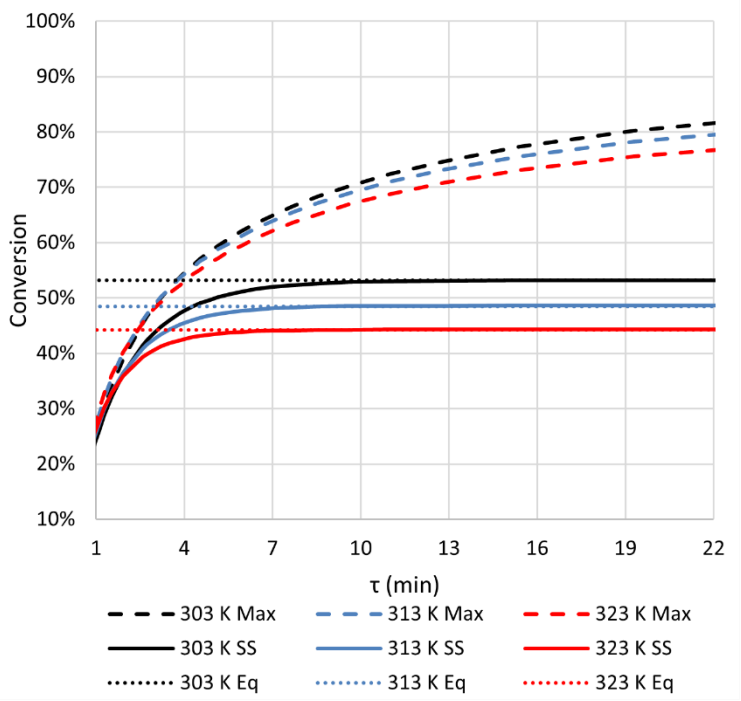

Figure 3.22. Effect of the space time on the conversion of the fixed-bed adsorptive reactor (x_{gly}: x_{acet} = 1:1).

It is well known that the maximum conversion in a conventional isothermal fixed-bed reactor is the equilibrium conversion, therefore the steady state conversion must not surpass the equilibrium conversion. Indeed, this was verified for this process. However, there is a significative enhancement on the maximum conversion achieved transitorily due to the combination of reaction and adsorption. To verify the impact of the temperature on the overall process, the influence of this variable on the adsorption and on the mass transfer was carefully studied.

The mass transfer can substantially impair the reactants conversion under diffusion-controlled regime, as solketal synthesis in Amberlyst-35 [2]. The effective diffusivity ($D_{eff,i}$) indicates how easily a compound is transported inside the catalyst, being the transport easier for higher $D_{eff,i}$ values. The temperature influence on the mass transfer was assessed by estimating the effective diffusivity ($D_{eff,i}$) by Equation 3.17. Although glycerol viscosity is at least two orders of magnitude higher than the other compounds, due to solketal's larger molecular mass and molecular volume, it presents the lowest $D_{eff,i}$. Furthermore, at 323 K, the values of $D_{eff,i}$ are approximately 37% higher than at 303 K, confirming the easier transport inside the catalyst at higher temperatures. The results support the conclusion that higher temperatures lead to a greater sorption enhancement, as the compounds would take less time to reach the adsorption/reaction active sites, therefore these phenomena become facilitated, and it becomes easier to enhance the conversion by adsorption.

To estimate the influence of temperature on the adsorption equilibrium, the selectivity of the stationary phase towards the reactants and products was assessed resorting to Equation 3.29. The estimated values are presented in Table 3.6.

$$S = \frac{q_i / q_{Ethanol}}{C_i / C_{Ethanol}} \tag{3.29}$$

Table 3.6. Selectivity of the reaction compounds over Amberlyst-35 (x_{EtOH} = 0.95 and x_i = 0.05).

Temperature (K)	**303 K**	**313 K**	**323 K**
Acetone	0.42	0.53	0.70
Glycerol	1.80	2.08	2.38
Solketal	0.32	0.26	0.21
Water	16.40	16.75	17.08

By comparing the differences in the selectivity of the reactants (acetone and glycerol) and of the products (solketal and water), it is possible to conclude that a raise in temperature leads the reactants to move closer together inside the column, in opposition to what happens to the products, that travel slightly further apart. As with the mass transfer, there is a more significant effect on the sorption enhancement for reactions at 323 K.

Despite the above-mentioned, considering the maximum solketal productivity as the goal to select the best operating temperature, there is no advantage in adopting 323 K, given that the maximum conversion is roughly the same as at 303 K. The steady state conversion, however, is considerably higher for 303 K, as expected for an exothermic reaction, which can be seen as a major advantage of operating under this temperature. Consequently, the productivity would be higher at this temperature. Finally, it is usually cheaper to operate industrially under milder conditions.

3.7. Conclusion

The investigation presented in the chapter aimed to assess the solketal synthesis on a fixed-bed adsorptive reactor packed with Amberlyst-35, a preliminary step needed to transition the process to the SMBR.

To study the hydrodynamics of the fixed-bed adsorptive reactor, tracer experiments were performed and the conclusion is that the plug flow model with axial dispersion and negligible radial dispersion could satisfactorily describe the flow throughout the bed. Also, this procedure was necessary to determine the bed porosity and the Peclet number, 0.413 ± 0.002 and 127.7 ± 0.7, respectively.

Adsorption equilibrium curves were assessed through the Frontal Analysis Methodology and mathematically fitted to the Langmuir competitive adsorption model. The equilibrium constants and the maximum monolayer capacities for all the compounds at 303 K and 323 K

confirm that water has the stronger affinity to the resin and solketal the weaker, a promising conclusion when considered the target of producing solketal by a sorption enhanced technology. The estimated adsorption constant values for acetone, glycerol, solketal, water and ethanol at 303 K were 5.33 $L \cdot mol^{-1}$, 5.40 $L \cdot mol^{-1}$, 3.47 $L \cdot mol^{-1}$, 22.21 $L \cdot mol^{-1}$, and 6.74 $L \cdot mol^{-1}$, respectively, while their maximum capacities were 7.56 $mol \cdot L_{ads}^{-1}$, 35.83 $mol \cdot L_{ads}^{-1}$, 8.91 $mol \cdot L_{ads}^{-1}$, 100.18 $mol \cdot L_{ads}^{-1}$, and 27.97 $mol \cdot L_{ads}^{-1}$ (in the same order). At 323 K the adsorption constant values were 5.17 $L \cdot mol^{-1}$, 5.35 $L \cdot mol^{-1}$, 3.40 $L \cdot mol^{-1}$, 21.87 $L \cdot mol^{-1}$, and 6.58 $L \cdot mol^{-1}$ and the maximum capacities 3.02 $mol \cdot L_{ads}^{-1}$, 11.78 $mol \cdot L_{ads}^{-1}$, 1.38 $mol \cdot L_{ads}^{-1}$, 25.26 $mol \cdot L_{ads}^{-1}$, and 6.71 $mol \cdot L_{ads}^{-1}$ (also in the same order). Along with the adsorption enthalpies estimated through the model, it is also possible to confirm the exothermic nature of the process. The large data set used for estimating the adsorption parameters produced a reliable mathematical model to describe the adsorption at different temperatures.

Reactive experiments on the adsorptive fixed-bed at 303 K and 323 K led to conclude that at higher temperatures, the sorption enhancement is higher due to the better mass transfer and favoured selectivity. Nonetheless, there was only a marginal difference on the maximum conversion for both temperatures and the steady state conversion is higher for 303 K, as expected for exothermic reactions. Another important output of the study is the validity of the mathematical models developed for the adsorption and for the sorption enhanced reaction. Being the fixed-bed the elementary unit of the SMBR, the comparison between the experimental data and the models developed suggests that they can be reliably used for the elaboration of more complex models that describe the solketal synthesis in the Conventional and non-conventional SMBR.

3.8. Notation

Abbreviations

gPROMS	General PROcess Modelling System
OCFEM	Orthogonal Collocation in Finite Elements
DASOLV	Differential-algebraic equation solver

Symbols

a_i	Activity coefficient of compound i	–
B	Total number of bootstrap samples	–
b	Bootstrap sample	–
C_i	Concentration of component i in the liquid phase	mol L^{-1}
$\bar{C}_{p,i}$	Average concentration of component i in the particle pores	mol L^{-1}
$C_{i,0}$	Initial concentration of compound i in the liquid phase	mol L^{-1}
$C_{in,\mathrm{i}}$	Inlet concentration of compound i	mol L^{-1}
D_{ax}	Axial dispersion coefficient	cm^2 s^{-1}
$D_{eff,i}$	Effective diffusion coefficient	cm^2 s^{-1}
$D_{i,m}$	Diffusion coefficient of component i in a mixture	cm^2 s^{-1}
$D_{i,j}^0$	Diffusion coefficient for a dilute solute i in a solvent	cm^2 s^{-1}
$\Delta H_{ads,i}$	Adsorption enthalpy for compound i	$kJ.mol^{-1}K^{-1}$
E	Residence time distribution	s^{-1}
F	Molar flow	mol s^{-1}
fob	Objective function	–
k_c	Reaction kinetic constant	mol kg^{-1} s^{-1}
K_{eq}	Reaction thermodynamic equilibrium constant	–
$k_{ext,i}$	External mass transfer coefficient of compound i	$cm{\cdot}s^{-1}$
K_i	Langmuir adsorption equilibrium constant for compound i	$L{\cdot}mol^{-1}$
$K_{i,0}$	Pre-exponential adsorption equilibrium constant for compound i	$L{\cdot}mol^{-1}$
$k_{int,i}$	Internal mass transfer coefficient of compound i	$cm{\cdot}s^{-1}$
$k_{L,i}$	Global mass transfer coefficient of compound i	$cm{\cdot}s^{-1}$
$K_{S,W}$	Adsorption equilibrium constant for water (rate law)	–

L	Fixed bed length	cm
$n_{ads/des,i}$	Adsorbed/desorbed amount of compound i	mol
NE	Number of experiments	–
NC	Number of compounds	–
NP	Number of experimental data points	–
Pe	Peclet number	–
Q	Flow rate	L min^{-1}
Q_i	Langmuir maximum capacity for compound i	mol L_{Ads}^{-1}
$q_{i,0}$	Initial adsorbed concentration of compound i	mol L_{Ads}^{-1}
$q_{in,\mathrm{i}}$	Adsorbed concentration of compound i in equilibrium with the feed concentration	mol L_{Ads}^{-1}
$\overline{q_i}$	Average adsorbed concentration of compound i	mol L_{Ads}^{-1}
Q_v	Langmuir capacity normalized by the molar volume	L L_{Ads}^{-1}
R	Coefficient of determination	–
$\Re$	Reaction rate	mol kg^{-1} s^{-1}
Re_p	Reynolds number (particle)	–
r_p	Particle radius	cm
S	Selectivity	–
Sc	Schmidt number	–
SD	Standard deviation	–
Sh_p	Sherwood number (particle)	–
T	Temperature	K
T_{ref}	Reference temperature	K
t	Time	s
$\overline{t_r}$	Mean residence time	min
U	Universal Gas Constant	J mol^{-1} K^{-1}
u	Interstitial velocity	cm·s^{-1}
V	Fixed-bed volume	L
$V_{M,i}$	Molar volume of compound i	L mol^{-1}
x_i	Molar fraction of compound i	–
X	Conversion	%

y_b	Parameter value for bootstrap sample b	–
$\bar{y}$	Mean parameter value	–
z	Axial coordinate	–

Greek Letters

α_i	Adsorption/desorption coefficient
ε_b	Bulk porosity
ε_p	Particle porosity
η	Viscosity
η_j	Viscosity of solvent
v	Stoichiometric coefficient
ρ	Fluid phase density
ρ_b	Bulk density
σ^2	Variance of the residence time distribution curve
τ	Reactor space-time
τ_p	Particle tortuosity

Subscripts/Superscripts

0	Initial
ads	Adsorbed
des	Desorbed
exp	Experimental
ext	External
i	Chemical species
in	Inlet
int	Internal
m	Mixture
mod	Model
out	Outlet

3.9. References

1. Faria, R.P.V., C.S.M. Pereira, V.M.T.M. Silva, J.M. Loureiro, and A.E. Rodrigues, *Glycerol valorisation as biofuels: Selection of a suitable solvent for an innovative process for the synthesis of GEA.* Chemical Engineering Journal, 2013. **233**: p. 159-167.
2. Moreira, M.N., R.P.V. Faria, A.M. Ribeiro, and A.E. Rodrigues, *Solketal Production from Glycerol Ketalization with Acetone: Catalyst Selection and Thermodynamic and Kinetic Reaction Study.* Ind. Eng. Chem. Res., 2019. **58**(38): p. 17746-17759.
3. Moreira, M.N., I. Corrêa, A.M. Ribeiro, A.E. Rodrigues, and R.P.V. Faria, *Solketal Production in a Fixed Bed Adsorptive Reactor through the Ketalization of Glycerol.* Ind. Eng. Chem. Res., 2020. **59**(7): p. 2805-2816.
4. Serafim, H., I.M. Fonseca, A.M. Ramos, J. Vital, and J.E. Castanheiro, *Valorization of glycerol into fuel additives over zeolites as catalysts.* Chemical Engineering Journal, 2011. **178**: p. 291-296.
5. Ruiz, V.R., A. Velty, L.L. Santos, A. Leyva-Pérez, M.J. Sabater, S. Iborra, and A. Corma, *Gold catalysts and solid catalysts for biomass transformations: Valorization of glycerol and glycerol–water mixtures through formation of cyclic acetals.* Journal of Catalysis, 2010. **271**(2): p. 351-357.
6. Deutsch, J., A. Martin, and H. Lieske, *Investigations on heterogeneously catalysed condensations of glycerol to cyclic acetals.* J. Catal., 2007. **245**(2): p. 428-435.
7. Faria, R., N. Graça, and A. Rodrigues, *Green Fuels and Fuel Additives Production in Simulated Moving Bed Reactors*, in *Intensification of Biobased Processes*, Andrzej Górak and A. Stankiewicz, Editors. 2018, The Royal Society of Chemistry. p. 145-165.
8. Rodrigues, A.E., Madeira, Luís Miguel, Wu, Yi-Jiang, Faria, Rui, *Sorption Enhanced Reaction Processes*. Sorption Enhanced Reaction Processes. 2017.
9. Corrêa, I., R.P.V. Faria, and A.E. Rodrigues, *Continuous Valorization of Glycerol into Solketal: Recent Advances on Catalysts, Processes, and Industrial Perspectives.* Sustain. Chem., 2021. **2**(2): p. 286-324.
10. Glueckauf, E., *Theory of chromatography. Part 10. Formulae for diffusion into spheres and their application to chromatography.* Trans. Faraday Soc., 1955. **51**(0): p. 1540-1551.
11. Wilson, E.J. and C.J. Geankoplis, *Liquid Mass Transfer at Very Low Reynolds Numbers in Packed Beds.* Ind. Eng. Chem., 1966. **5**(1): p. 9-14.
12. Scheibel, E.G., *Correspondence. Liquid Diffusivities. Viscosity of Gases.* Ind. Eng. Chem., 1954. **46**(9): p. 2007-2008.
13. Perkins, L.R. and C.J. Geankoplis, *Molecular diffusion in a ternary liquid system with the diffusing component dilute.* Chem. Eng. Sci., 1969. **24**(7): p. 1035-1042.
14. Vasanth Kumar, K. and S. Sivanesan, *Equilibrium data, isotherm parameters and process design for partial and complete isotherm of methylene blue onto activated carbon.* J. Hazard. Mater, 2006. **134**(1-3): p. 237-44.
15. Silva, V.M.T.M. and A.E. Rodrigues, *Dynamics of a fixed-bed adsorptive reactor for synthesis of diethylacetal.* AlChE J., 2002. **48**(3): p. 625-634.
16. Graça, N.S., L.S. Pais, V.M.T.M. Silva, and A.E. Rodrigues, *Thermal effects on the synthesis of 1,1-dibutoxyethane in a fixed-bed adsorptive reactor.* Chem. Eng. Technol., 2012. **35**(11): p. 1989-1997.
17. Regufe, M.J., R.P.V. Faria, A.M. Ribeiro, J.M. Loureiro, and A.E. Rodrigues, *Synthesis of the Biofuel Additive 1,1-Diethoxybutane in a Fixed-Bed Column with Amberlyst-15 Wet.* Chem. Eng. Technol., 2016. **39**: p. 1509-1518.
18. Faria, R.P.V., C.S.M. Pereira, V.M.T.M. Silva, J.M. Loureiro, and A.E. Rodrigues, *Sorption enhanced reactive process for the synthesis of glycerol ethyl acetal.* Chem. Eng. J. , 2014. **258**(0): p. 229-239.

19. Pereira, C.S.M., V.M.T.M. Silva, and A.E. Rodrigues, *Fixed Bed Adsorptive Reactor for Ethyl Lactate Synthesis: Experiments, Modelling, and Simulation.* Separation Science and Technology, 2009. **44**(12): p. 2721-2749.
20. Osmari, T.A., R. Gallon, M. Schwaab, E. Barbosa-Coutinho, J.B. Severo, and J.C. Pinto, *Statistical Analysis of Linear and Non-Linear Regression for the Estimation of Adsorption Isotherm Parameters.* Adsorp. Sci. Technol., 2013. **31**(5): p. 433-458.
21. Joshi, M., A. Kremling, and A. Seidel-Morgenstern, *Model based statistical analysis of adsorption equilibrium data*. Chem. Eng. Sci., 2006. **61**(23): p. 7805-7818.

Chapter 4

Process Intensification on a Conventional Simulated Moving Bed Reactor

ADAPTED FROM: Corrêa, I.; Faria, R. P. V.; Rodrigues, A. E., Continuous Valorization of Glycerol into Solketal: From the Fixed-Bed Adsorptive Reactor to the Simulated Moving-Bed Reactor. *Industrial & Engineering Chemistry Research* **2022**, 61 (11), 4017-4030.

4.1. Introduction

The Simulated Moving Bed (SMB) was developed as a energetically advantageous process that benefits from the continuous counter-current operation to overcome the obstacles of the traditional batch chromatographic processes, namely interruption of the feed to regenerate the catalyst/adsorbent, which is associated with the high desorbent consumption of this process. The technology simulates the movement of the stationary and mobile phases by periodically shifting the two inlet (feed and desorbent) and the two outlet (raffinate and extract) ports in the direction of the fluid flow, in a series of columns packed with the catalyst/adsorbent, in a close loop configuration [1]. The operation enhances the productivity maximizing the separation driving forces and the usage of the stationary phase and minimizing the desorbent consumption [2]. Moreover, it enables difficult separations that could not be accomplished with traditional chromatographic methods [3]. The positions of the four streams set the borders between the unit's sections, each of them operating at specific flowrates.

Solketal production by continuous sorption-enhanced reactive process is still rather unexplored. As explained in Chapter 3, the process is mostly limited by temperature-dependent phenomena (reaction rate, adsorption selectivity, mass transfer), thus it is necessary to assess this parameter influence on the process performance to determine the optimal temperature for the production on the Simulated Moving Bed Reactor (SMBR). This was the first objective of Chapter 4.

After selecting the best operational temperature, optimizations were performed by manipulating the design and operational variables (time switch, flowrates, and unit's configuration) with the objective function of maximizing the productivity. A novel optimization procedure was followed and validated by comparing the optimum points with the ones obtained by delimiting the Reactive Separation Region. The definition of the best set of operational parameters for solketal synthesis in the SMBR with Amberlyst-35 and the

validations of the optimization methodology were the main objectives of Chapter 4. The validation of the new optimization procedure is a ground-breaking strategy for optimizing the operation on the SMBR.

4.2. Modelling Studies

The fixed-bed column is the elementary unit of the SMBR, therefore, to determine the behaviour of this complex system, the process variables for all columns must be simultaneously estimated. The assumptions made for the modelling a single column are still valid for these more complex configuration: (1) plug-flow with axial dispersion and negligible radial dispersion, (2) velocity variations due to changes in the bulk composition, (3) internal and external mass transfer resistances lumped and estimated by the linear driving force model, (4) all the beds equally packed with constant flow, temperature, length and porosity, and (5) the reaction occurs exclusively at the active sites inside the catalyst pores and (6) multicomponent adsorption equilibrium described by the competitive Langmuir adsorption isotherm model [1].

Since there are numerous variables involved in the SMBR modelling, high computational effort is required, especially for optimizing systems with many columns. The strategy to simplify the SMBR modelling is developing an analogous TMBR model, since the steady-state equations can be directly used in the model, rather than solving the system dynamically until it reaches the cyclic steady state as it would be necessary for modelling the actual SMBR. Therefore, the TMBR assumes an actual flow of the solid phase in the opposite direction to the liquid phase and steady inlet and outlet streams positions.

The actual SMBR model is more precise, once it simulates the real system, nonetheless this simplification strategy can lead to satisfactory similarity between the models, which will be higher for units with a larger number of columns and/or smaller time switches (higher solid velocity in the TMBR). This modelling strategy is often used for thermodynamic limited

processes, as glycerol ketalization, due to the large number of columns necessary to achieve worthwhile conversion and purity.

The modelling of the moving bed is described by Equation 3.1 to Equation 3.17, however, for the TMBR it is necessary to account the solid velocity (u_s) into the mass balance in the particle. Thus, Equation. 3.3 is rewritten as follows:

$$\varepsilon_p \frac{\partial \bar{C}_{p,i}}{\partial t} + (1-\varepsilon_p)\frac{\partial \bar{q}_i}{\partial t} = u_s\left(\varepsilon_p \frac{\partial \bar{C}_{p,i}}{\partial z} + (1-\varepsilon_p)\frac{\partial \bar{q}_i}{\partial z}\right) + \frac{3}{r_p}k_{L,i}(C_i - \bar{C}_{p,i}) + \nu_i \frac{\rho_b}{(1-\varepsilon_b)}\Re(\bar{C}_{p,i}) \tag{4.1}$$

Besides, it is necessary to estimate the inlet and outlet stream concentrations, which is accomplished by the mass balance to the nodes of the SMBR, represented by the following equations:

Desorbent node

$$Q_I C_{i,n_D}\big|_{z=0} = Q_{Rec} C_{i,n_D-1}\big|_{z=L} + Q_D C_{D,i} \tag{4.2}$$

$$Q_I = Q_{Rec} + Q_D \tag{4.3}$$

Extract Node

$$C_{i,n_X}\big|_{z=0} = C_{i,n_X-1}\big|_{z=L} \tag{4.4}$$

$$Q_{II} = Q_{Rec} + Q_D - Q_X \tag{4.5}$$

Feed node

$$Q_{III} C_{i,n_F}\big|_{z=0} = Q_{II} C_{i,n_F-1}\big|_{z=L} + Q_F C_{F,i} \tag{4.6}$$

$$Q_{III} = Q_{Rec} + Q_D - Q_X + Q_F \tag{4.7}$$

Raffinate Node

$$C_{i,n_R}\big|_{z=0} = C_{i,n_R-1}\big|_{z=L} \tag{4.8}$$

$$Q_{IV} = Q_{Rec} \tag{4.9}$$

where Q represents the fluid flowrate and the indexes I, II, III and IV the sections of the SMBR. C_b is the fluid concentration in the bulk and the indexes Rec, D, X, R and F refer to the recycle, desorbent, extract, raffinate and feed streams. The variables n_D, n_X, n_F and n_R mean the number of the column immediately after the desorbent, extract, feed and raffinate nodes, which are incremented by the number of positions each stream moves in the direction

of the fluid flow at the end of the time switch (t^*). The equivalence between the TMBR and the SMBR is made by keeping the liquid velocity constant relative to the solid velocity in each section j, as described by Equation. 4.10.

$$u_j^{SMBR} = u_j^{TMBR} + u_s \tag{4.10}$$

Since γ_j represents the ratio between the liquid and the solid interstitial velocities in each section j ($\gamma_j = u_j / u_s$), in terms of this variable, the equivalence between the TMBR and the SMBR (Equation 4.10) can be rewritten as Equation 4.11[4]:

$$\gamma_j^{SMBR} = \gamma_j^{TMBR} + 1 \tag{4.11}$$

The SMBR solid velocity is defined according to Equation 4.12.

$$u_s = \frac{L}{t^*} \tag{4.12}$$

To completely describe the system, the performance of the SMBR is quantitatively assessed through the Raffinate and Extract Purity (PuR and PuX), limiting reactant conversion (X_{lim}), raffinate productivity (PR), and desorbent consumption (DC).

$$PuR = \frac{C_{Solketal,R}}{C_{Gly,R} + C_{Ac,R} + C_{Water,R} + C_{Solketal,R}} \tag{4.13}$$

$$PuX = \frac{C_{Water,X}}{C_{Gly,X} + C_{Ac,X} + C_{Water,X} + C_{Solketal,X}} \tag{4.14}$$

$$X_{lim} = \left[1 - \frac{Q_X . C_{lim,X} + Q_R . C_{lim,R}}{Q_F . C_{lim,F}}\right] \times 100\% \tag{4.15}$$

$$PR = \frac{Q_R . M_{Solketal} . C_{Solketal,R}}{(1 - \varepsilon_b) . V} \tag{4.16}$$

$$DC = \frac{(Q_D . C_{D,Ethanol} + Q_F . C_{F,Ethanol}) . V_{M,Ethanol}}{Q_R . M_{Solketal} . C_{Solketal,R}} \tag{4.17}$$

For the correct operation of the SMBR the following steps must simultaneously occur: in Section I, desorption of water (the most-retained reaction product) for the solid regeneration,

in Section II, chemical reaction and desorption of solketal (the less-retained product) to avoid contaminating the extract, in Section III, chemical reaction and adsorption of water to avoid contaminating the raffinate and, in Section IV, desorption of solketal for the eluent regeneration [1]. Therefore, the unit must be designed through careful consideration of the ratio between the liquid and the solid phases interstitial velocities (γ_j), and the species' affinities towards the adsorbent material.

The Equilibrium Theory is a robust design methodology that considers γ_j a key parameter. This methodology takes into account the nonlinearity of the adsorption equilibrium isotherm, whereas it neglects chemical reaction and the effect of axial dispersion and mass transfer resistances associated with the chromatographic separation [5]. To account for the effect of the mass transfer resistances not considered in the triangle theory, a safety factor (SF) is added to the sectional flow rate ratios [1]. The Equilibrium Theory is an useful model to easily estimate the boundaries of the separation and regeneration regions; however, since it is a simplified design methodology, it was used as a starting point for the optimization procedure, which relied on the detailed model to optimize the process variables [4]. The following equations mathematically describe the constraints that limit the velocity ratio between the liquid and solid phases in each section of the TMBR [1, 6]:

$$\gamma_I^{TMBR} > \frac{1-\varepsilon_b}{\varepsilon_b}\left[\varepsilon_p + (1-\varepsilon_p)\frac{q(C_{Water})}{C_{Water}}\right] \tag{4.18}$$

$$\begin{aligned}\frac{1-\varepsilon_b}{\varepsilon_b}\left[\varepsilon_p + (1-\varepsilon_p)\frac{q(C_{Solketal})}{C_{Solketal}}\right] < \gamma_{II}^{TMBR} < \gamma_{III}^{TMBR} \\ < \frac{1-\varepsilon_b}{\varepsilon_b}\left[\varepsilon_p + (1-\varepsilon_p)\frac{q(C_{Water})}{C_{Water}}\right]\end{aligned} \tag{4.19}$$

$$\gamma_{IV}^{TMBR} < \frac{1-\varepsilon_b}{\varepsilon_b}\left[\varepsilon_p + (1-\varepsilon_p)\frac{q(C_{Solketal})}{C_{Solketal}}\right] \tag{4.20}$$

$$\gamma_1^{SF} = (1+SF)\cdot\gamma_1 \tag{4.21}$$

$$\gamma_4^{SF} = \frac{1}{(1+SF)} \cdot \gamma_4 \tag{4.22}$$

In terms of the ratio between fluid and solid interstitial velocities, the Reactive Separation Region (RSR) is represented in the $\gamma_{II} \times \gamma_{III}$ plane contemplating the constrain $\gamma_{III} > \gamma_{II}$. Inside this region, any point would lead to the products separation, but the highest productivity is achieved on the vertex – $(\gamma_{III} - \gamma_{II})_{max}$. The regeneration region follows the same principles, being represented in the $\gamma_I \times \gamma_{IV}$ plane, where the vertex is the operation point in which least desorbent is needed – $(\gamma_I - \gamma_{IV})_{min}$. The optimum point is the one with the highest productivity considering the lowest desorbent consumption.

The numerical solution of the model was obtained using gPROMS version 7.0.7. The partial differential and algebraic equations were solved using the Orthogonal Collocation in Finite Elements Method (OCFEM), while the ordinary differential equations in time were solved by an integrated differential-algebraic equation solver (DASOLV).

4.3. Assessment of the Optimal Operational Temperature

The selection of the best operational temperature to perform the SMBR experiments was the starting point of the modelling studies, also with the purpose of confirming that the behaviour of the reaction and adsorption in this more complex unit would be similar to the single column (Section 3.6). The SMBR is an equipment with several design and operational variables that can be manipulated to help overcoming the reaction and separation limitations of processes that would be hardly feasible otherwise.

The process was modelled considering a pilot-scale SMBR with 12 columns with the same characteristics of the one where the fixed-bed experiments were performed (namely length, 23 cm; diameter, 2.6 cm). A key variable for thermodynamic limited reactions is the unit configuration, that means, the length/number of columns of each section. For this system, the

2-4-4-2 configuration was selected, providing to the unit a larger reaction and product separation area.

Closely related to this is the solid velocity, that must be low enough to ensure the reactants have enough contact time with the catalyst and that the resin is satisfactorily regenerated. From Figure 3.22 it can be confirmed that it is necessary a relatively long space time to achieve higher conversion values. Therefore, the solid velocity was set to 1.4 cm/min, corresponding to a time switch of 16.4 min in the equivalent SMBR. This is considered a long time for the operation on a moving bed reactor, however, for similar systems, the range of time switch studied was between 8 and 17 minutes [7].

To assure full regeneration of both the solid and the liquid phase, γ_I and γ_{IV} are multiplied by a safety factor. For this system, it was selected a value of 30%, considered robust, due to the high affinity of water to the solid phase and to the mass transfer issues mainly caused by glycerol's high viscosity.

There are many algorithms to determine the RSR. The methodology usually aims to scan the entire region of the Triangle Theory and delimit the area in which the extract and raffinate purity limits are satisfied. The initial γ_I and γ_{IV} are calculated by the Equilibrium Theory (Equation 4.18 and Equation 4.20), therefore Q_{Rec} and Q_D are also known. The simulation must start with a high value of γ_{II} and γ_{III} (low Q_F and Q_X) to guarantee that the operational point is outside the RSR. Then, for the same Q_F, the value of Q_X is incremented and a new operational point is estimated. This procedure follows forming a line parallel to the diagonal $\gamma_{II} = \gamma_{III}$. At some point, the extract and raffinate limits are satisfied, marking the point entry in the region. Q_X keeps incrementing until the purity limitations are no longer satisfied, marking the boundary of the region. Q_F is then incremented, and the procedure follows, this time decreasing Q_X and forming another line parallel to the diagonal $\gamma_{II} = \gamma_{III}$, but one feed increment further away in the perpendicular direction. The point gets inside the region, Q_X keeps decreasing, and, when

the point gets outside, Q_F is again incremented. The procedure follows until the purity requirements are not satisfied, indicating that the maximum Q_F was found (the vertex of the RSR). The region was delimited by setting a purity requirement of 96% for both raffinate and extract.

The RSR attained for the studied system at 303 K, 313 K and 323 K are presented in Figure 4.1.

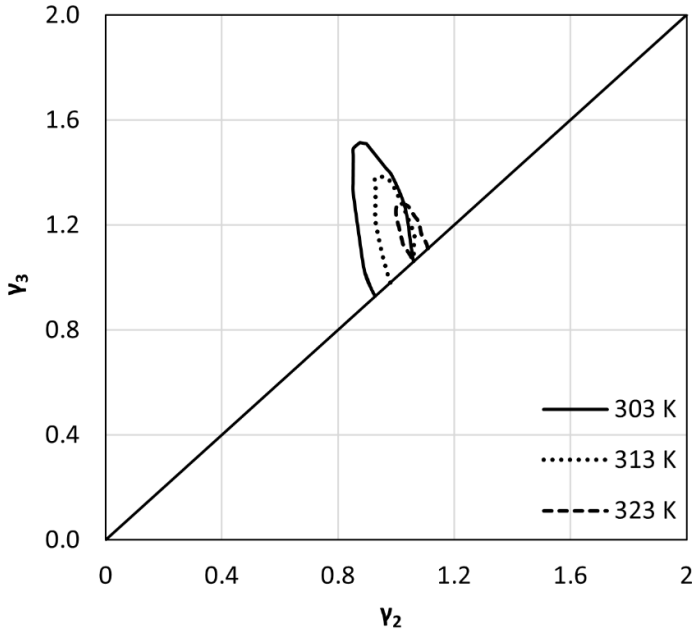

Figure 4.1. Reactive separation regions for 303 K, 313 K and 323 K (column configuration: 2-4-4-2; u_s = 1.4 cm/min; β = 30%).

The largest RSR corresponds to 303 K, besides being the region with the operating point further away from the diagonal. This point consists of the condition under which the maximum productivity and lowest desorbent consumption are achieved, 1.52 $kg_{Solk.}L_{Ads}^{-1}day^{-1}$ and 21.3 $L_{Des}.kg_{Prod}$, respectively. The maximum productivity and minimum desorbent consumption for 313 K are 1.07 $kg_{Solk.}L_{Ads}^{-1}day^{-1}$ and 30.6 $L_{Des}.kg_{Prod}$, and for 323 K, 0.63 $kg_{Solk.}L_{Ads}^{-1}day^{-1}$and 46.6 $L_{Des}.kg_{Prod}$.

To evaluate the effect of temperature in the performance of the SMBR the internal concentration profiles at 303 K and 323 K were compared (Figure 4.2).

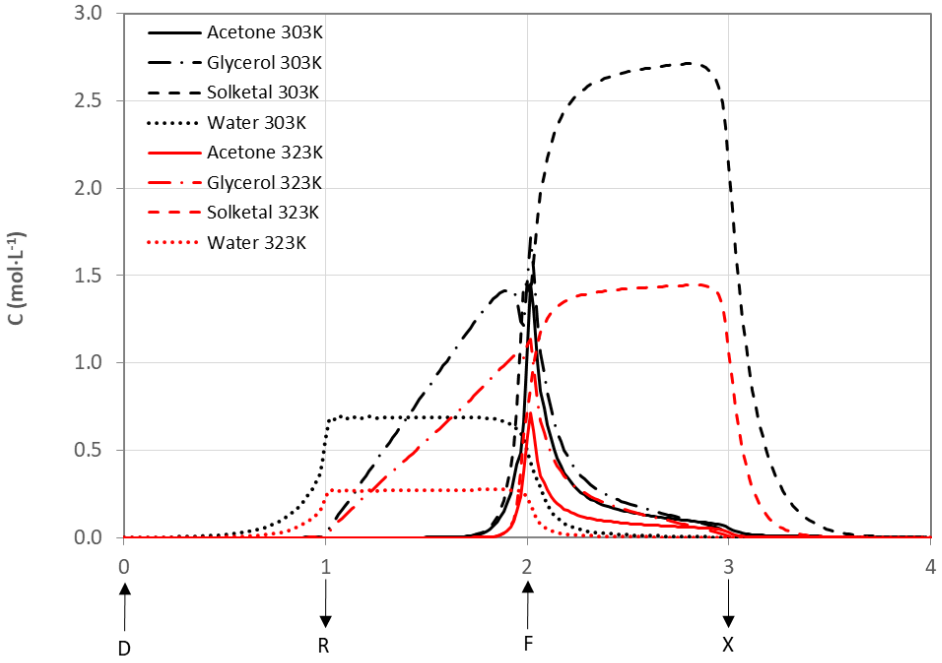

Figure 4.2. Internal concentration profiles for the synthesis of solketal by SMBR at: (a) 303 K (γ_I = 6.10; γ_{II} = 0.88; γ_{III} = 1.52; γ_{IV} = 0.48); (b) 323 K (γ_I = 6.24; γ_{II} = 1.01; γ_{III} = 1.28; γ_{IV} = 0.47). (D: desorbent, R: Raffinate, F: Feed and X: Extract; column configuration: 2-4-4-2; u_s = 1.4 cm/min; β = 30%). Ethanol's profile is not shown to ease the visualization of the other compounds.

The detailed analysis of the internal concentration profiles provided a preliminary insight regarding the main factors affecting the performance of the SMBR. Comparing the distribution of the reactant's concentration bands between Sections II and III of the SMBR, it is possible to conclude that glycerol has a much higher affinity towards the solid stationary phase than acetone (as it was already expected considering the adsorption isotherms previously determined). Such an uneven reactants distribution throughout the unit reduces the contact time between the species, which consequently decreases their conversion. Moreover, focusing exclusively on Section III, two main issues arise. First, it is possible to observe that solketal and acetone concentration fronts percolate the beds at similar velocities, as already expected given the low adsorption selectivity calculated from the adsorption isotherm parameters

presented in Table 3.5. This represents a challenge to the process since the separation between this reactant and the target product might not be easily accomplished if the reactant cannot be fully converted. Second, and most importantly, considering the relative compositions of reactants and products in the surroundings of the raffinate port (axial position z = 3), it is possible to conclude that the reverse reaction and the unfavourable thermodynamic equilibrium might present one of the major obstacles to the improvement of the performance of the SMBR. If the extension of the reverse reaction near the raffinate port is significant, as it seems to be the case for this system, a certain amount of products might always be present at this location, limiting the unit's performance. This issue becomes more relevant at higher temperatures (323 K) since this is an exothermic reaction, suggesting that this might be a key aspect for the selection of the optimal operating temperature.

To further clarify the effect of temperature in the performance of the SMBR, new reactive separation regions were determined for two additional feed stream compositions: first, the feed composition was changed to match the equilibrium composition attained at each temperature for a stoichiometric mixture of reactants diluted in 50% of ethanol (molar basis); then, an equimolar mixture of the products (solketal and water) diluted in 50% of ethanol (molar basis) was used as feed. The resulting reactive separation regions are compared with the previous ones (for acetone:glycerol:ethanol mixtures of 1:1:2) in Figure 4.3.

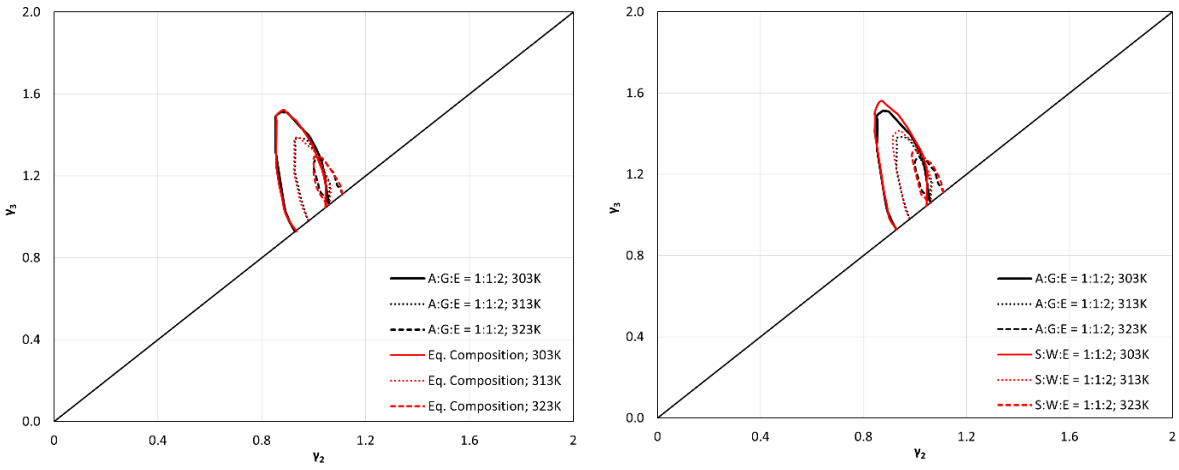

(a) (b)

Figure 4.3. SMBR performance for different feed streams from 303 K to 323 K: (a) acetone:glycerol:ethanol mixtures of 1:1:2 vs equilibrium compositions; (b) acetone:glycerol:ethanol mixtures of 1:1:2 vs solketal:water:ethanol mixtures of 1:1:2.

The use of pre-reactors associated with SMBR units has been suggested for systems that are strongly limited by the reaction kinetics [8]. This strategy allows the reactants to be converted, typically up to the equilibrium conversion, before entering the SMBR. Hence, products separation may start to occur immediately at the vicinity of the feed port, which enhances the unit's ability to displace the thermodynamic equilibrium, overcoming the inevitable loss in productivity that occurs if a large volume of the stationary phase in the reactive sections of the SMBR (Sections II and III) is dedicated to convert reactants at a slow rate. According to the simulation results obtained for the present case-study, the synthesis of solketal, the reactive separation regions determined for feed streams composed of acetone:glycerol:ethanol mixtures of 1:1:2 and composed of equilibrium mixtures were almost overlapping (Figure 4.3a). This suggests that the performance of the SMBR for this system is not controlled by the reaction kinetics.

To complement these results, reactive separation regions were determined for a hypothetical feed stream exclusively composed of solketal and water, the two reaction products.

Surprisingly, these regions were extremely similar to those obtained for 1:1:2 acetone:glycerol:ethanol mixtures, which means that the performance of the SMBR basically remained unaffected by this change. The analysis of the internal concentration profiles obtained for the reactive separation regions associated with the new feed stream provide a deeper insight on this issue and demonstrated that the extension of the reverse reaction was noteworthy, which led to the contamination of the outlet streams with the reactants formed in its surroundings.

Considering the above-mentioned, the results suggest that the thermodynamic equilibrium is one of the main factors limiting the overall SMBR performance for the synthesis of solketal. This fact also helps to explain why larger separation regions are attained at lower temperatures. Since this is an exothermic reaction, the equilibrium conversion is higher at lower temperatures and, therefore, the extent of the reverse reaction has a lower impact on the performance of the unit at 303 K than at 313 K or 323 K. Other factors include the low selectivity of the stationary-phase between solketal and acetone and the high difference in the reactant's adsorption capacity, which makes them travel in opposite directions inside the unit and reduces the contact time required to its conversion. Nevertheless, the SMBR technology was still able to overcome the equilibrium limitations up to some extent, since the limiting reactant conversions were typically above 97% (far higher than the equilibrium conversion, which is approximately 50% within the range of studied temperatures) and was also able to collect purified fractions of the products in the raffinate and extract streams, reaching a solketal purity of 97%, as required for most industrial applications.

Aiming the large scale solketal production, the fact that the best performance was attained at 303 K is an auspicious result, as one of the highest costs for industrial implementation of a process concerns heating. Hence, working under milder temperatures is an appealing economic advantage.

The SMBR is regarded as a more energetically efficient technology due to operating under mild conditions. The comparison with other Process Intensification technologies is usually performed in terms of energy necessary to produce a certain amount of product. Considering the novelty of the present work, there is still no literature reporting the techno-economical evaluation of solketal synthesis on the SMBR However, for similar systems, it is registered a energy consumption of 1800 kJ/kg_{Prod} [9]. Comparing to the Reactive-distillation, one of the most studied PI strategies for solketal synthesis, the energy demand is substantially reduced, as this process usually requires around 2500 kJ/ kg_{Prod} [10, 11]. This is also a promising result when considering the scale-up of the process to the industrial level.

Comparing the unit's performance for solketal production with other SMBR processes with similar systems, such as production of 2-ethylhexyl acetate, butyl acrylate, glycerol ethyl acetal and inversion of sucrose, it is possible to conclude that there is still room for improvement, as the productivity is between 5 to 10 times lower than for these chemicals [1, 9, 12]. Therefore, before the experiments on a lab-scale SMBR, an optimization study to maximize the unit's productivity and minimize the desorbent consumption is recommended by performing sensitivity analysis to the main process variables.

4.4. Optimization studies for solketal synthesis in the Conventional SMBR

Considering the numerous variables that can be manipulated in the SMBR operation, there are multiple optimal points that can lead to appropriate productivity and purity. To determine the best operating conditions, the first step was performing independent optimizations for different column configuration with the safety factor of 30%, high enough to assure the solid and the desorbent proper regeneration. By specifying the safety factor, one defines the limit flowrate ratios between the liquid and the solid phases in the desorbent and adsorbent regenerations sections (Sections I and IV, respectively), estimated by the well-known

Equilibrium Theory (numerically described by Equations 4.18 to 4.20). The feed concentration was fixed in 1:1 glycerol:acetone diluted in 50% of ethanol.

By setting the column configuration and the safety factors for the regeneration sections, the decision variables to be optimized were reduced to solid velocity, extract flowrate and feed flowrate. Afterwards, in the second step of the study, independent optimizations were performed by changing the safety factors (and consequently the optimal feed and extract flowrates and the solid velocity) targeting maximum productivity (objective function), subjected to a minimum solketal purity in the raffinate and water purity in the extract of 97% (optimization constraints). The algorithms of the optimization are presented in Figure 4.4:

a)

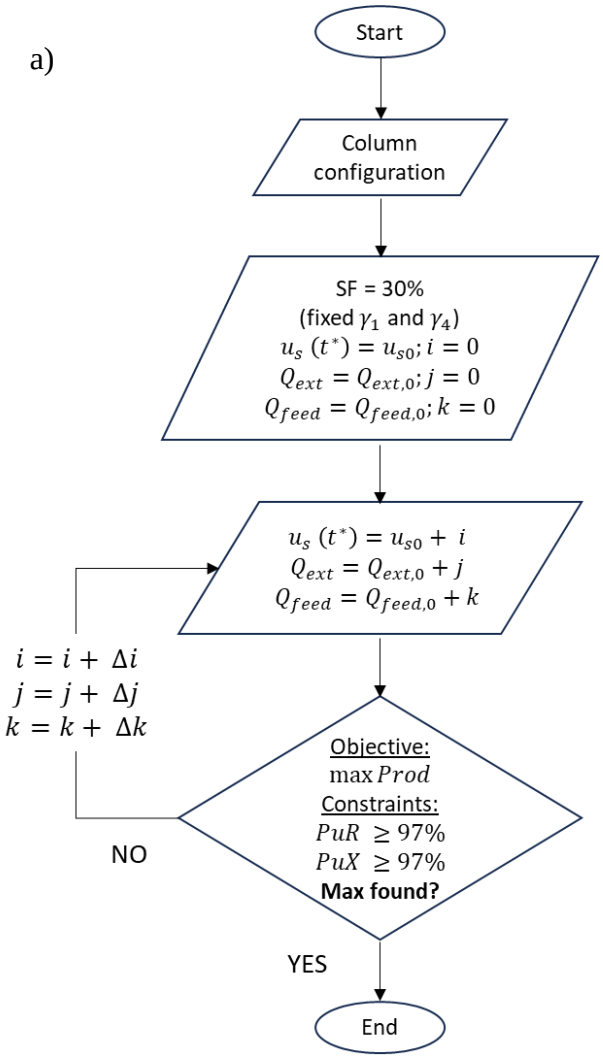

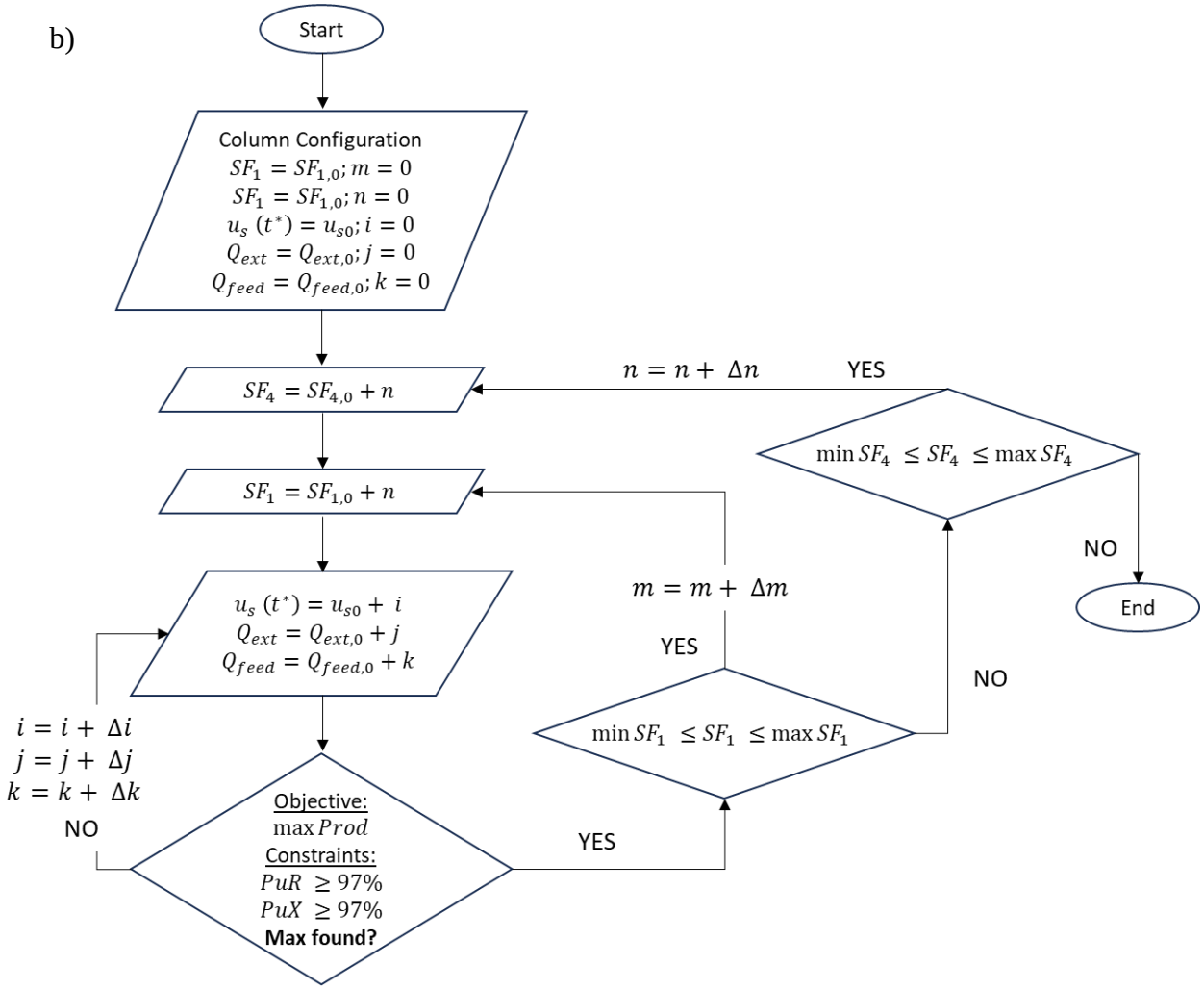

Figure 4.4. Optimization algorithms. (a) First step (b) Second step.

Finally, to assess the robustness of the operation and to confirm the reliability of the novel optimization strategy, the RSR for the best configuration with a safety factor of 30% was determined. For that, an algorithm was developed to scan the entire region of the Triangle Theory, delimiting the region that encompassing the operational points that lead to the specified extract and raffinate streams purity.

Since this is a decisive step for defining the optimal operation conditions that would be used for solketal synthesis in the SF-SMB(R), the process was modelled considering a SMBR with 8 columns with length and diameter of 15 cm and 2.12 cm, respectively.

The optimization of the SMBR was performed with gPROMS, using the NLPSQP (Non-Linear Problem Sequential Quadratic Programming) solver, included in the software, which

solves nonlinear optimization problems by applying a sequential quadratic programming method. The convergence tolerance was set to 10^{-5}. The application where the optimization parameters (objective function, constrains, initial conditions, and manipulated variables) were defined was gOPT (global OPTimization). This tool is integrated in gPROMS and it is designed to find global optima of complex nonlinear problems. The type of optimization was set to "Steady state via time relaxation", which consists of using variables from the steady state to initialize the first interaction, but allowing the system to dynamically solve the problem with the new set of parameters of the manipulated variables until reaching a new steady state. Then, the following interaction use the steady state of the previous interaction, and the optimization continues until finding the optimal point of the objective function.

4.4.1. Sensitivity Analysis to the unit's configuration

The column configuration is particularly relevant for SMBR processes with thermodynamic limited reactions once an increase in the reactive area can substantially enhance the reactants conversion and, consequently, the productivity and purity. The most relevant performance parameters obtained for the configurations that attained the best results are presented in Table 4.1.

Table 4.1. Effect of the configuration on the Conventional SMBR performance for a safety factor of 30% (ranked in terms of productivity).

Config.	γ_1	γ_2	γ_3	γ_4	u_s $(\text{cm}\cdot\text{min}^{-1})$	PR $(\text{kg}\cdot\text{L}^{-1}\cdot\text{day}^{-1})$	DC $(\text{L}\cdot\text{kg}^{-1})$	PuR	PuX	X
1-2-4-1	6.06	0.88	1.38	0.48	0.47	0.936	22.68	0.97	0.99	0.97
2-2-3-1	6.06	0.89	1.32	0.48	0.55	0.927	26.36	0.97	0.98	0.97
1-3-3-1	6.06	0.88	1.36	0.48	0.47	0.884	23.46	0.97	0.99	0.97
1-2-3-2	6.06	0.89	1.36	0.48	0.44	0.825	23.51	0.97	0.99	0.97
2-1-4-1	6.06	0.90	1.35	0.48	0.46	0.813	24.70	0.97	0.98	0.97
1-1-5-1	6.06	0.90	1.39	0.48	0.42	0.810	22.68	0.97	0.98	0.97

1-1-4-2	6.06	0.90	1.38	0.48	0.40	0.757	23.03	0.97	0.98	0.97
2-3-2-1	6.06	0.89	1.29	0.48	0.46	0.732	27.08	0.97	0.99	0.97
1-4-2-1	6.06	0.88	1.32	0.48	0.41	0.715	24.99	0.97	0.98	0.97
2-1-3-2	6.06	0.90	1.34	0.48	0.41	0.708	24.97	0.97	0.98	0.97
1-3-2-2	6.06	0.88	1.32	0.48	0.40	0.691	24.92	0.97	0.99	0.97
3-2-2-1	6.06	0.89	1.30	0.48	0.42	0.679	26.58	0.97	0.99	0.97
2-2-2-2	6.06	0.89	1.30	0.48	0.42	0.679	26.50	0.97	0.99	0.97
1-2-2-3	6.06	0.89	1.33	0.48	0.37	0.651	24.85	0.97	0.99	0.97
2-1-2-3	6.06	0.90	1.33	0.48	0.33	0.555	25.11	0.97	0.98	0.97
3-1-2-2	6.06	0.90	1.33	0.48	0.33	0.555	25.14	0.97	0.98	0.97
2-3-1-2	6.06	0.88	1.28	0.48	0.25	0.390	26.00	0.97	0.98	0.97
2-2-1-3	6.06	0.89	1.29	0.48	0.23	0.390	26.00	0.97	0.98	0.97
3-2-1-2	6.06	0.89	1.29	0.48	0.23	0.372	25.58	0.97	0.99	0.97

A common conclusion taken from the analysis of the configurations is that the best productivities were achieved when there were at least 5 columns in Sections II and III, or, in other words, when at least 63% of the unit was dedicated to reaction and separation of the products. Going even further, better productivities were attained when there were more columns in Section III, where most of the reaction takes place and where the separation of the less retained species occurs. The reasons for this are the low reaction extent and the low selectivity between acetone and solketal.

Concerning the reaction, it is affected by the low equilibrium conversion, by the different affinities of the reactants (acetone and glycerol), which start getting separated as soon as they are fed to the unit, and by the high characteristic diffusion times of glycerol and solketal (between 1 and 2 minutes), since the mass transfer resistance is considerable for highly viscous species, as glycerol, and for species with high molar volume, as solketal. Due to the mass transfer obstacle, low flowrates must be adopted to assure the reactants have enough time to

diffuse into the catalyst active sites and be converted into products, and for the products to diffuse into the liquid back again.

As for the similar adsorption affinity of acetone and solketal, their concentration bands percolate Section III columns at similar velocities. This imposes constraints on the maximum feed flow rate that can be processed in the unit because the unreacted acetone might contaminate the raffinate stream. A common strategy to foster thermodynamically limited reactions in the SMBR is using one of the reactants as desorbent, consequently it is in excess in the reaction medium. For solketal synthesis, however, this is not viable due to the reactant's low miscibility [13].

From the analysis of the internal concentration profiles of the configuration that performed better in terms of productivity, the 1-2-4-1 achieved higher values due to the larger number of columns in Section III, where most of the reaction occurs, and due to acetone being fed further apart from the raffinate collection port.

Comparing the performance of the first entries of Table 4.1, one can confirm that since acetone is carried in the direction of the fluid flow, most of the reaction take place in Section III, and this reactant is present in significative amounts only in the column immediately before the feed port, therefore there was no need for more than two columns in Section II. The reaction thermodynamics limitation seems to be what hinders the performance of the Conventional SMBR, since it is necessary an excess of columns in the sections assigned for this purpose. As for the regeneration sections, in most of the cases there is no need for more than one column in each section to satisfactorily perform this task.

Finally, regardless being possible to produce solketal in a SMBR, it performs poorly, as very low productivity was achieved for all configurations. By Figure 3.22, it is confirmed that a large space time is necessary to achieve reasonable conversion. Furthermore, acetone and glycerol have significantly different selectivity towards the stationary phase, meaning the

process must operate with low flowrates and solid velocity to minimize the reactants separation; acetone and solketal have similar velocities, which makes the system prone to contamination of the raffinate stream; and the strong affinity of water with Amberlyst-35 requires a considerable desorbent flowrate to regenerate the solid material in Section I.

One of the main attention points in optimization problems is assuring that the global optimum is found, rather than a local optimum. To confirm that the novel optimization strategy provides the global optimum, the RSR for the 1-2-4-1 configuration with a safety factor of 30% for γ_1 and γ_4 and the solid velocity determined was delimited and exhibited in Figure 4.5. By running the RSR algorithm, one allows to identify all the combinations of extract and feed flowrates under the purity constraint of 97%. The point that leads to the highest productivity, and, therefore, the optimum point, is in the vertex of the RSR. Since all the combinations of extract and feed flowrates under the purity constraints are identified, it is guaranteed that the optimal point in the vertex of the region is indeed the global optimum.

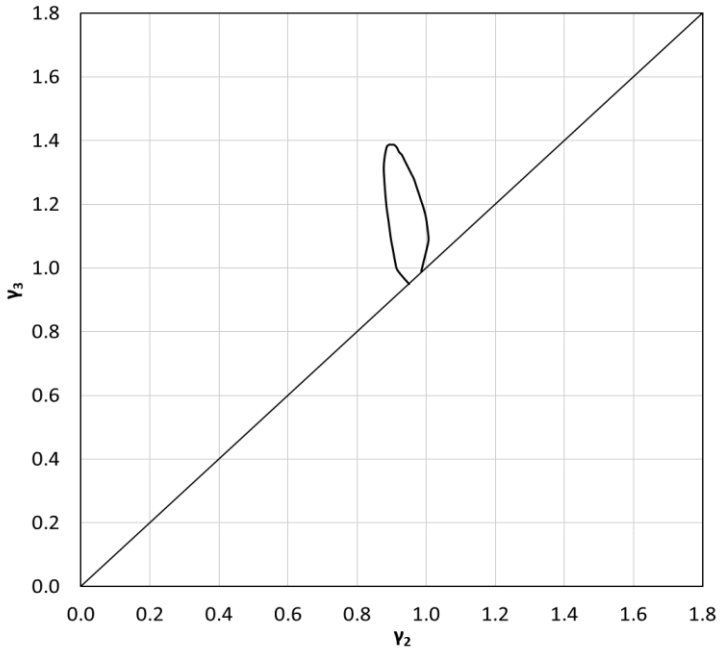

Figure 4.5. Reactive separation regions for the SMBR with a column configuration 1-2-4-1 at the optimal point for a safety factor of 30% applied to Sections I and IV (u_s = 0.47 cm·min^{-1}).

Table 4.2. Comparison of the operational and performance parameters resultant from the RSR and the novel optimization strategy for a 1-2-4-1 configuration, SF of 30% applied to Sections I and IV and a solid velocity of 0.47 cm·min^{-1}. Productivity (PR) in kg·L^{-1}·day^{-1} and Desorbent Consumption (DC) in L·kg^{-1}.

	γ_1	γ_2	γ_3	γ_4	PR	DC	PuR	PuX	X
RSR	6.06	0.88	1.38	0.48	0.936	22.68	0.97	0.99	0.97
New optimization	6.06	0.89	1.39	0.48	0.924	22.96	0.97	0.98	0.97

It was possible to confirm the reliability of the optimization methodology, once the optimal point of the RSR corresponds to the same optimal point found by the novel optimization methodology, as shown in Table 4.2. The deviations are negligible and are due to using different numerical methods.

4.4.2. Optimization of the Conventional SMBR

As previously stated, the safety factors limit the flowrate ratios of Sections I and IV where the regeneration occurs. Nonetheless, the influence of this parameter goes much further than only in the desorbent consumption, since the solid velocity, extract flowrate and feed flowrate are manipulated altogether in the proposed optimization.

Therefore, to assess the influence of the safety factor on the process for the 1-2-4-1 configuration, the sensitivity analysis was performed by varying this variable (consequently, the flowrate ratios of Sections I and IV) from 5% to 40% to find the point of maximum productivity (objective function) subjected to the constrains of 97% of purity for both raffinate and extract streams. A detailed analysis of the influence of this parameter on the SMBR performance and operation is provided in the following subsections.

Effect on the productivity

The safety factors are used in Sections I and IV to assure the solid and liquid phases are properly regenerated before being recycled into the unit. Therefore, the regeneration will be more effective as higher the safety factors (higher γ_1 and lower γ_4), and consequently the productivity will also be enhanced, until a maximum value when there is no more improvement because the solid and liquid phases are completely regenerated. The resultant plot from the influence of the safety factor on the productivity is exhibited in Figure 4.6.

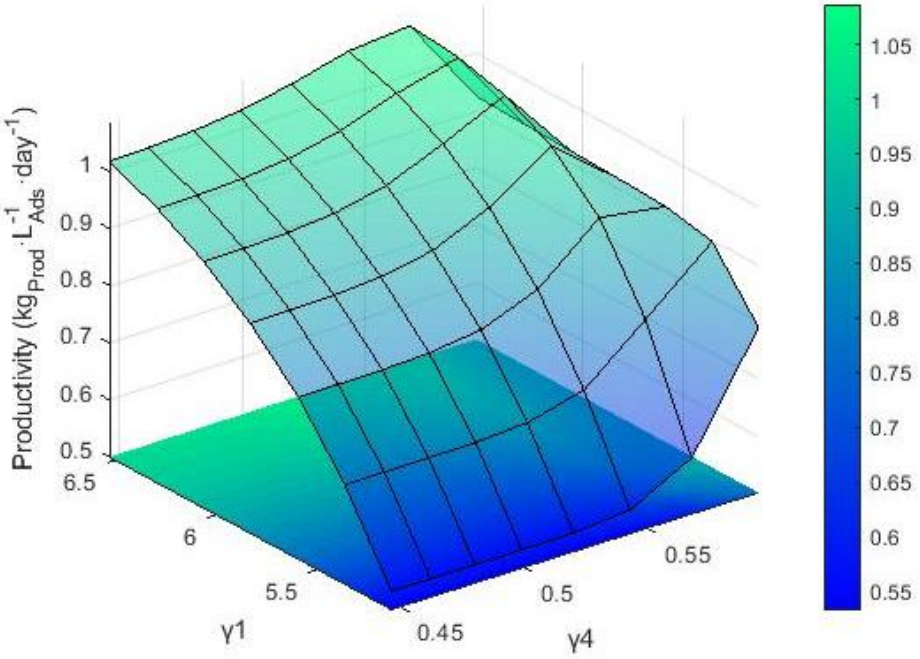

Figure 4.6. Effect of the flow rate ratio in Sections I (γ_1) and IV (γ_4) on the productivity of a SMBR, with a 1-2-4-1 configuration, at 303 K.

The relation between flowrate ratios and the maximum productivity that should be reached for high safety factors is valid for constant solid velocities. In the present study, the solid velocity and the feed and desorbent flow rates were optimized at the same time. Therefore, the productivity kept increasing with the increase of γ_1 and γ_4 as a direct consequence of the simultaneous increase of the solid velocity and the inlet and outlet flowrates. Despite such increase in the operational parameters, it would still have been expected that the productivity

reached a plateau because the unit would have exhausted the capacity of the stationary phase. Since the Conventional SMBR performance is mediocre, within the range of safety factors studied, the plateau has not been reached. The same behaviour was observed in previous studies [4].

Also, the insufficient regeneration of Sections I and IV restrains the productivity, as verified for low γ_1 and high γ_4. It is noteworthy that for an inadequate regeneration of the liquid phase, the productivity had not improved even if γ_1 enhanced, or, in practice, even if more fresh desorbent was fed to the unit. This is due to the contamination of the outlet streams by the remaining solketal in the column after switching the inlet and outlet positions.

Effect on the desorbent consumption

From the analysis of Equations (4.16) and (4.17) it is possible to conclude that the desorbent consumption (DC) is a function of the Productivity. Also, one of the most straightforward conclusions of the analysis of the influence of the flowrate ratios in the regeneration section is related with the DC. Figure 4.7 summarizes the sensitivity analysis for the safety factor on this performance parameter:

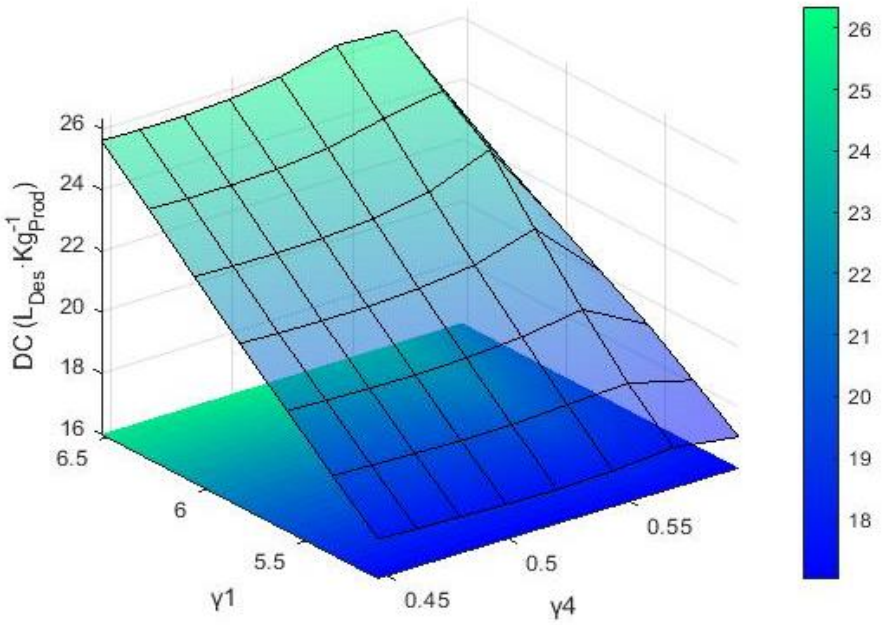

Figure 4.7. Effect of the flow rate ratio in Sections I (γ_1) and IV (γ_4) on the desorbent consumption (DC) of a SMBR, with a 1-2-4-1 configuration, at 303 K.

Based on Equations (4.3) and (4.9), two conclusions are easily withdrawn. First, for a constant γ_1, increasing γ_4 results in a decrease in the DC. Second, for a constant γ_4, the increase in γ_1 is accompanied by an increase in the DC. The latter trend was indeed confirmed in Figure 4.7, which shows a direct relationship between γ_1 and the DC; however, the inverse relationship between γ_4 and the DC was not verified, as this parameter increases with the increase of γ_4. The main reason for this is that these relations are valid for a constant solid velocity. In the optimization procedure followed in the present work, for higher γ_4 values, the optimum solid velocity was also higher, therefore, by diminishing the safety factor applied to Section IV, the SMBR was able to operate with higher inlet and outlet flowrates and consequently the unit reached higher productivities. For very low SF applied to γ_4 (below 10%), however, the performance was severely affected by the improper regeneration of the liquid phase.

Finally, in the range of SF explored in the present study, the maximum productivity was attained for a SF of 40% in Section I and 10% in Section IV. At this point, the productivity was 1.082 $kg_{Solk} \cdot L_{Ads}^{-1} \cdot day^{-1}$ with a DC of 26.24 $L_{Desorbent} \cdot kg_{Prod}^{-1}$. Following the trend of the graph in Figure 4.6, increasing even more the SF applied to γ_1 would generate higher productivity at a cost, of course, of higher DC. Since the viability of every industrial process is evaluated in terms of the economical balance, it is unreasonable to consider solely the productivity maximization as the decision parameter to elect the optimum operational parameters. Therefore, to avoid increasing the DC indefinitely and consequently the costs with ethanol and its treatment, the upper limit of 40% for the SF was established.

Effect on the solid velocity

The sensitivity analysis to the solid velocity is exhibited in Figure 4.8:

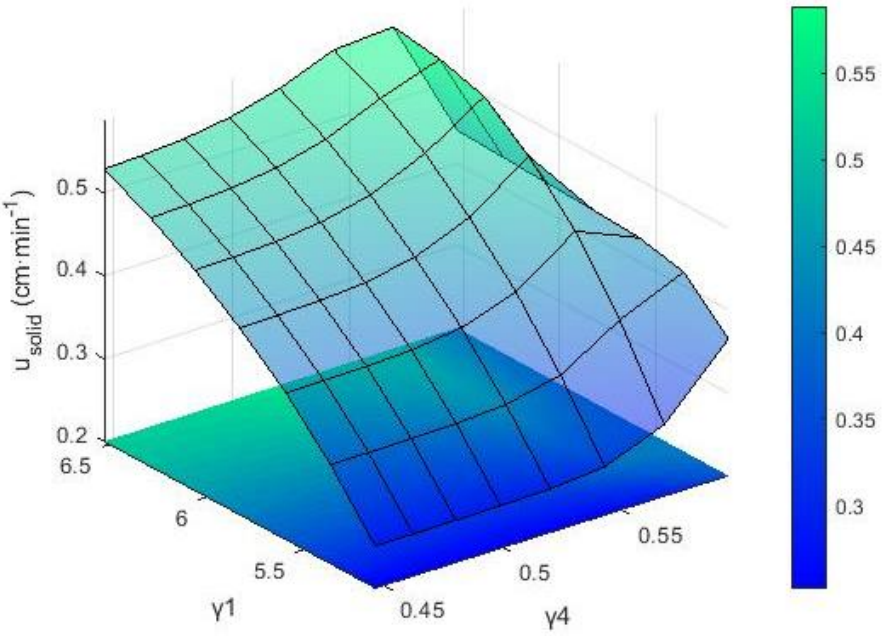

Figure 4.8. Effect of the flow rate ratio in Sections I (γ_1) and IV (γ_4) on the optimum solid velocity of a SMBR, with a 1-2-4-1 configuration, at 303 K.

By comparing the solid velocity and the productivity behaviour (Figure 4.6), the dependency between this performance parameter and this operational parameter becomes clear. This evidences, once again, that the unit performance is driven by the interaction of the reaction compounds with the stationary phase.

Also, the insufficient regeneration of the liquid phase (high γ_4) limited the solid phase velocity. This occurs because setting a lower safety factor on the flow rate ratio of Section IV allows solketal's concentration front to travel deeper in this section, as verified in Figure 4.9, that exhibits the internal concentration profiles comparison for SMBR units operating with a fixed γ_1 of 30% and γ_4 values of 5% and 40%. This fact increased the concentration of the target compound in the vicinity of the raffinate collection port, however, since Section IV was not properly regenerated, the remaining solketal present in the columns of this section contaminates the extract stream, limiting the unit's flow rates and solid velocity and, consequently, the SMBR performance.

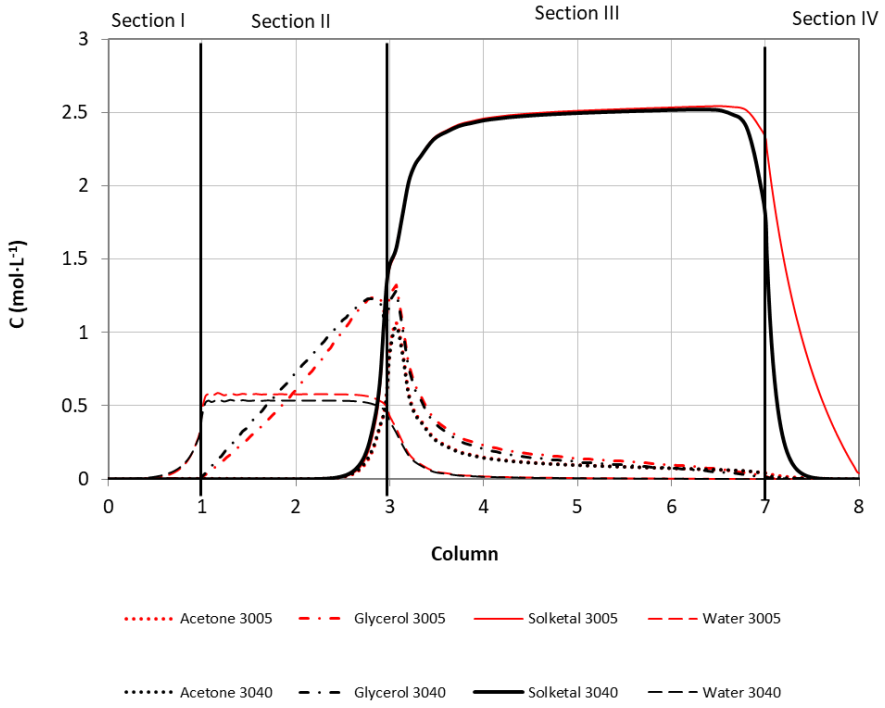

Figure 4.9. Effect of the flow rate ratio in Section IV (γ_4) on the internal concentration profile for a fixed flow rate ratio in Section I (γ_1) of a SMBR, with a 1-2-4-1 configuration, at 303 K feeding equimolar amounts of glycerol and acetone diluted in 50% of ethanol.

Effect on the solketal concentration

The influence of the safety factors in the concentration of solketal in the vicinity of the raffinate port is summarized as follows:

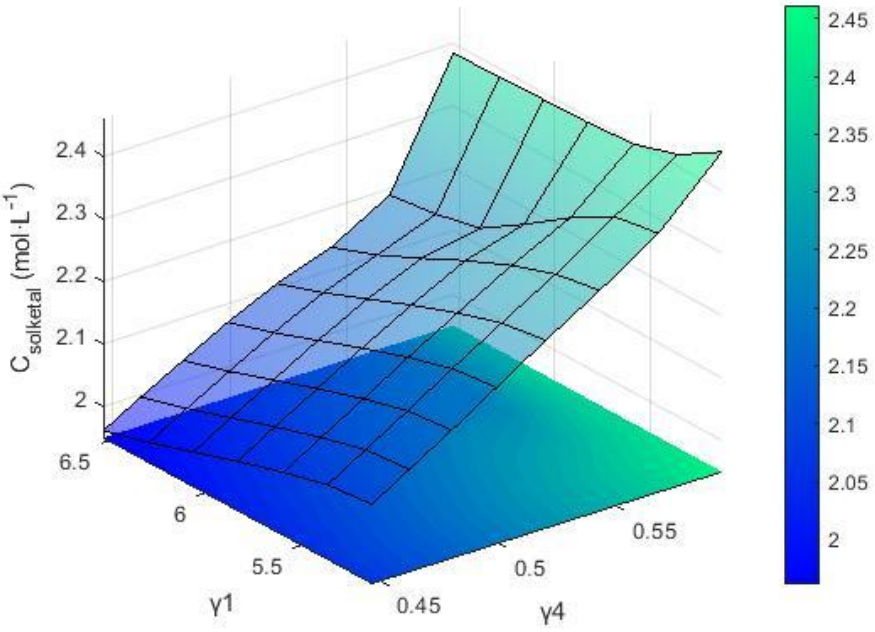

Figure 4.10. Effect of the flow rate ratio in Sections I (γ_1) and IV (γ_4) on the solketal concentration in the vicinity of the raffinate port of a SMBR, with a 1-2-4-1 configuration, at 303 K.

As previously discussed, since solketal is allowed to travel deeper in Section IV for lower safety factors, its concentration near the raffinate port is higher. Nonetheless, high flow rate ratios in this section limits the feed flow rate that can be processed in the unit due to contamination of the extract stream because solketal is recycled from Section IV to Section I. Therefore, despite having lower solketal concentration, because higher feed, raffinate and extract flow rates could be used for higher safety factors, the productivity was also higher.

Effect on the conversion

The effect of the sensitivity analysis on the conversion is exhibited in Figure 4.11:

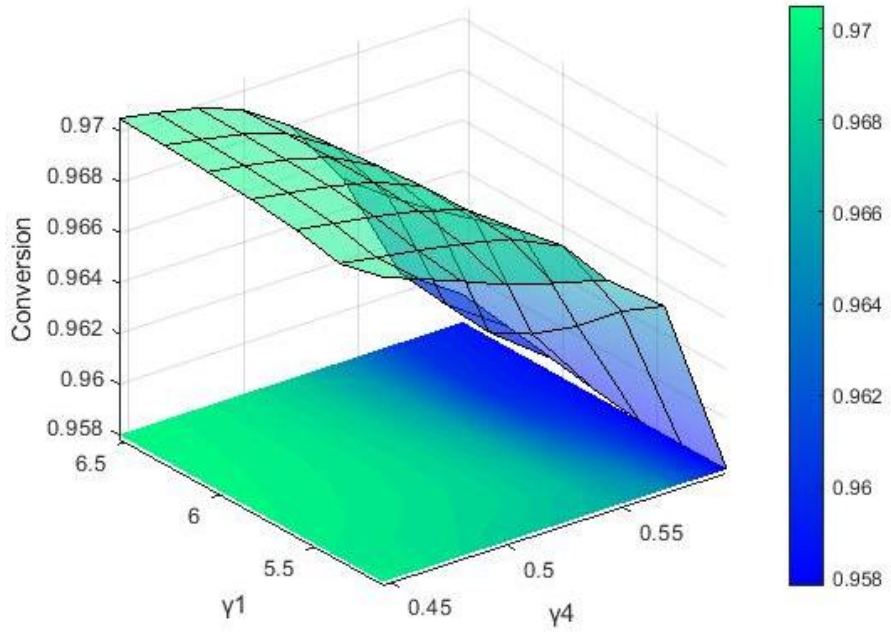

Figure 4.11. Effect of the flow rate ratio in Sections I (γ_1) and IV (γ_4) on the conversion of a SMBR, with a 1-2-4-1 configuration, at 303 K.

One of the most straightforward conclusions from the analysis of Figure 4.11 is the strong dependence of the conversion with the SF applied to γ_4, while it remains virtually unchanged with variations in γ_1. As already mentioned, one of the obstacles of the reaction of glycerol and acetone to produce solketal is the thermodynamic limitation, therefore, the conversion relies, in a great extent, on the contact time of the reactants with the stationary phase. By increasing the SF applied to Section I and keeping a constant γ_4, the flowrates and the solid velocity increase. The addition of more reactant into the unit, which foster the direct reaction, is somewhat compensated by the increase in the solid velocity and the final conversion ends up almost not varying.

As for the effect of a higher γ_4, there is, of course, the directly proportional increase in the recycle flowrate (Equation (4.9)) and, for a constant γ_1, the increase in the solid velocity (Figure 4.8). Different from the variations in γ_1, the increase in the solid velocity is not compensated by the increment in the other operational flowrates (except for the recycle flowrate) and the final effect is a decrease in the conversion due to the reduced contact times of the reactants with Amberlyst-35 and the hastier separation of the reactants. This excludes points with very low SF applied to γ_4, in which the conversion is impaired even though the solid velocity is also low, because of the insufficient regeneration of the stationary phase. However, the impact of increasing the SF applied to γ_4 (lower γ_4) in the operational parameters is much less significative than varying γ_1 due to the large difference in the absolute values of these variables.

4.5. Equivalence between the TMBR and the SMBR

As previously mentioned (Section 4.2), it is a common strategy to use the TMBR model to simulate the real SMBR due to the high computational effort the later requires. The equivalence between these models is made through Equations (4.10) to (4.11), being as accurate as larger the number of columns and shorter the time switch. These equations, however, were conceived and proposed, for the equivalence between the TMB and the SMB, which only involves the adsorption and mass transfer phenomena. In fact, even for these systems, the equivalence is limited when operating with a high concentration range, nonlinear adsorption equilibrium and high mass transfer resistances [14]. Therefore, the equivalence equations are not necessarily suitable for the reactive separation systems because the target products are being separated as they form inside the unit [15, 16].

Despite the inaccuracy in the equivalence of the models, the gains in terms of computational effort and simulation time encourage the use of the TMBR for non-rigorous modelling [17,

18]. This strategy can be especially useful to describe thermodynamic limited processes, due to the large number of columns required to reach good productivity under the purity requirements. However, in practice, the cost of a SMBR unit with many columns is high and the most common range of columns in pilot scale units is between six and twelve [19-22]. Also, the mass transfer limitation often leads to high time switch to assure the reactants have enough contact time to reach the active sites of the catalyst.

For solketal synthesis in the SF-SMB(R), the equivalence between the TMBR and the SMBR is particularly challenging because the number of columns is limited to eight, and the time switch is high due to the reaction and separation limitations. This affects the similarity of the models. For instance, at the optimal point, namely safety factors of 40% applied to γ_1 and 10% to γ_4, by using the corresponding flow rates and time switch in the SMBR, there is not enough regeneration of the desorbent, and solketal is recycled from Section IV to Section I, contaminating the extract stream. The presence of this compound together with water in the vicinity of the extract port leads to the reverse reaction and the consequent contamination of this stream. This reveals how strongly driven by the thermodynamic equilibrium the system is.

The second-best optimum point is obtained with a SF of 40% in Section I and 15% in Section IV; nevertheless, at this point, the problem of solketal recycling persisted. Since the time switch is one of the main process variables, its value was gradually increased, keeping all the flow rate ratios constant, until a RSR was obtained [23]. With this strategy, however, the equivalence may be attained at the cost of reducing the productivity. Figure 4.12 summarizes the results of this study:

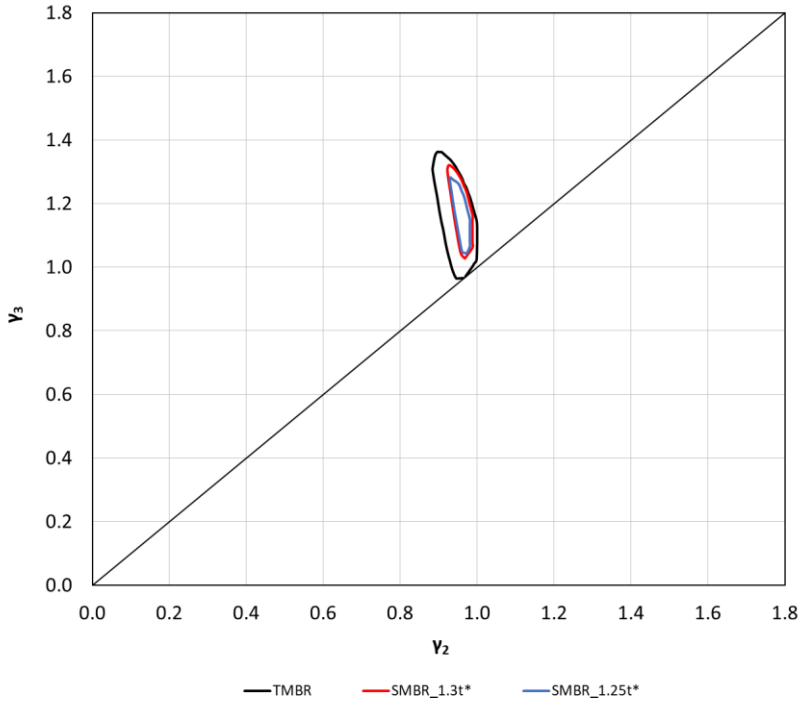

Figure 4.12. RSR of the TMBR and SMBR, with a 1-2-4-1 configuration and a SF of 40% applied to Section I and 15% to Section IV, at 303 K, and feeding equimolar amounts of glycerol and acetone diluted in 50% of ethanol (u_s = 0.56 cm·min^{-1} and t^* = 25.70 min). SMBR relative velocities exhibited as $\gamma_j^{SMBR,graph} = \gamma_j^{SMBR} - 1$ for comparison with the TMBR.

It is possible to confirm that a comparable RSR is obtained only when a correction factor is applied to the time switch. The raffinate purity limit of the SMBR for a correction factor of 30% coincides with the TMBR, demonstrating the similarity of the models in the vicinity of the raffinate port. As for the extract, it was discussed that the improper regeneration in Section IV and the consequent solketal recycle from Section IV to Section I impairs the extract purity. This may be the reason that justifies the extract purity limit keeping unchanged in the SMBR despite increasing the time switch. The comparison of the performance parameters at the point of maximum productivity is exhibited in Table 4.3.

Table 4.3. Comparison of the operational and performance parameters resultant from the RSR of the TMBR and SMBR for a 1-2-4-1 configuration, SF of 40% applied to Section I and 15% to Section IV and a solid velocity of 0.56 cm·min^{-1} and t^* = 25.70 min. Productivity (PR) in kg·L^{-1}·day^{-1} and Desorbent Consumption (DC) in L·kg^{-1}.

	PR	DC	PuR	PuX	X
TMBR	1.07	26.41	0.97	0.98	0.97
SMBR_1.25t*	0.69	34.53	0.97	0.97	0.97
SMBR_1.30t*	0.75	30.98	0.97	0.97	0.97

It is expected that the productivity may be negatively affected by the increase in the time switch. This was not harshly felt in the case of solketal synthesis because the longer time switch increased the contact time of the reactants with the stationary phase.

4.6. Conclusion

Solketal synthesis on the SMBR was studied through the fixed-bed model extension to this unit. The influence of the temperature in the SMBR was studied by delimiting RSR for 303, 313 and 323K, supporting the conclusion that 303K is the best operational temperature for the industrial production of solketal through sorption enhanced processes with Amberlyst-35, as a larger reactive separation region is obtained, with the additional benefit of operating under milder conditions.

With this operational parameter defined, the next step was to optimize the SMBR by manipulating its main design and operation variables, as column configuration, flowrates, and solid velocity (time switch). By comparing the performance of several column configurations, 1-2-4-1 attained the highest productivity, 0.936 $kg_{Solk}·L^{-1}_{Ads}·day^{-1}$, with a DC of 22.68 $L_{Desorbent}·kg^{-1}_{Prod}$. From the sensitivity analysis to the SF, the combination that achieves the

highest productivity in the studied range is 40% in Section I and 10% in Section IV. At this point, the productivity is 1.086 $kg_{Solk} \cdot L_{Ads}^{-1} \cdot day^{-1}$ and the DC is 26.24 $L_{Desorbent} \cdot kg_{Prod}^{-1}$.

Compared to other design/optimization techniques, as the determination of RSR, the novel optimization methodology thoroughly studied in the present work reduces substantially the computational effort and the time required to obtain the optimal operational parameters. For the optimization of the Conventional SMBR in units with a limited number of columns and high time switch, as in the present study, one of the main challenges is the equivalence between the TMBR and the SMBR. Due to the small number of columns of the SF-SMB(R) and the high time switch of solketal synthesis in the SMBR, the equivalence is compromised. By delimiting the RSR for the SMBR with the optimum set of SF's (40% and 10%), it was confirmed that this SF in Section IV is insufficient for the proper regeneration of the liquid phase and the extract stream does not reach the required purity (97%). For the second-best optimum point among the range of SF explored (40% and 15%), there is a considerable RSR only if a minimum correction factor of 30% is applied to the time switch, one of the main SMBR design parameters.

Finally, solketal synthesis in the SMBR with Amberlyst-35 performs poorly due to the reaction thermodynamic limitation, the high diffusion time of the species in the solid phase, the high difference in the selectivity of acetone and glycerol with the solid, which makes them get separated shortly after being fed, and the similar affinity of acetone and solketal, which makes the raffinate stream prone to contamination. The results reported allowed a better understanding of solketal synthesis in the Conventional SMBR and are fundamental to open the way to investigate and understand non-conventional SMBR strategies.

4.7. Notation

Abbreviations

DASOLV	Differential-algebraic equation solver
gPROMS	General PROcess Modelling System
NLPSQP	Non-Linear Problem Sequential Quadratic Programming
OCFEM	Orthogonal Collocation in Finite Elements
RSR	Reactive Separation Region
SF-SMB(R)	Supercritical Fluid Simulated Moving Bed Reactor
SMB	Simulated Moving Bed
SMBR	Simulated Moving Bed Reactor
TMBR	True Moving Bed Reactor

Symbols

C_i	Concentration of component i in the liquid phase	mol L^{-1}
$\bar{C}_{p,i}$	Average concentration of component i in the particle pores	mol L^{-1}
DC	Desorbent consumption	$L_{des.}\ kg^{-1}_{solk}$
$k_{L,i}$	Global mass transfer coefficient of compound i	$cm \cdot s^{-1}$
L	Fixed bed length	cm
M	Molar mass	$g \cdot mol^{-1}$
PR	Productivity	$kg_{solk}\ L_{Ads}^{-1} s^{-}$
PuR	Raffinate purity	
PuX	Extract purity	
Q	Flowrate	L min^{-1}
$\overline{q_i}$	Average adsorbed concentration of compound i	mol L_{Ads}^{-1}
$\Re$	Reaction rate	mol kg^{-1} s^{-1}
r_p	Particle radius	cm
SF	Safety factor	
t	Time	s
t^*	Time switch	s
u	Interstitial velocity	$cm \cdot s^{-1}$

u_s	Solid velocity	cm·s^{-1}
V	Fixed-bed volume	L
$V_{M,i}$	Molar volume of compound i	L mol^{-1}
X_{lim}	Limiting reactant conversion	%
z	Axial coordinate	–

Greek Letters

α_i	Adsorption/desorption coefficient
ε_b	Bulk porosity
ε_p	Particle porosity
γ	Ratio between the liquid and the solid interstitial velocities
v	Stoichiometric coefficient
ρ_b	Bulk density

Subscripts/Superscripts

i	Chemical species
j	S/TMBR section
D	Desorbent
Rec	Recycle
X	Extract
F	Feed
R	Raffinate
min	Minimum
max	Maximum
lim	Limiting
n	Number of columns

4.8. References

1. Rodrigues, A.E., Madeira, Luís Miguel, Wu, Yi-Jiang, Faria, Rui, *Sorption Enhanced Reaction Processes*. Sorption Enhanced Reaction Processes. 2017.
2. Nishizawa, H., K. Tahara, S. Miyamori, Y. Motegi, T. Shoji, and Y. Abe, *True moving bed chromatography: solid–liquid multi-stage counter-current extraction.* J. Chromatogr. A, 1999. **849**(1): p. 61-69.
3. Faria, R.P. and A.E. Rodrigues, *Instrumental aspects of Simulated Moving Bed chromatography.* J. Chromatogr. A, 2015. **1421**: p. 82-102.
4. Rodrigues, A.E., C.S.M. Pereira, M. Minceva, L.S. Pais, A.M. Ribeiro, A. Ribeiro, M. Silva, N. Graça, and J.C. Santos, *Simulated Moving Bed Technology: Principles, Design and Process Applications*. 2015: Elsevier Science.
5. Storti, G., M. Mazzotti, M. Morbidelli, and S. Carrà, *Robust design of binary countercurrent adsorption separation processes.* AIChE Journal, 1993. **39**(3): p. 471-492.
6. Rodrigues, A.E. and M. Minceva, *Modelling and simulation in chemical engineering: Tools for process innovation.* Comput. Chem. Eng., 2005. **29**(6): p. 1167-1183.
7. Mitra Ray, N. and A.K. Ray, *Modelling, simulation, and experimental study of a simulated moving bed reactor for the synthesis of biodiesel.* Can. J. Chem. Eng., 2016. **94**(5): p. 913-923.
8. Constantino, D.S.M., R.P.V. Faria, C.S.M. Pereira, J.M. Loureiro, and A.E. Rodrigues, *Enhanced Simulated Moving Bed Reactor Process for Butyl Acrylate Synthesis: Process Analysis and Optimization.* Ind. Eng. Chem. Res., 2016. **55**(40): p. 10735-10743.
9. Constantino, D.S.M., C.S.M. Pereira, R.P.V. Faria, J.M. Loureiro, and A.E. Rodrigues, *Simulated moving bed reactor for butyl acrylate synthesis: From pilot to industrial scale.* Chem. Eng. Process., 2015. **97**: p. 153-168.
10. Bumbac, G. and I. Banu, *Modeling and simulation process for solketal synthesis from glycerol and acetone by catalytic distillation in a modified structure of a divided wall column.* Renew. Energy, 2022. **183**: p. 662-675.
11. Liu, Y., X. Li, H. Cong, H. Li, and X. Gao, *Experimental Investigation, Process Design, and Optimization Analysis on the Production of Solketal in the Reactive Dividing Wall Column.* Ind. Eng. Chem. Res., 2021. **60**(15): p. 5612-5626.
12. Graça, N.S., L.S. Pais, V.M.T.M. Silva, and A.E. Rodrigues, *Analysis of the synthesis of 1,1-dibutoxyethane in a simulated moving-bed adsorptive reactor.* Chem. Eng. Process. , 2011. **50**(11): p. 1214-1225.
13. Esteban, J., A.J. Vorholt, A. Behr, M. Ladero, and F. Garcia-Ochoa, *Liquid–Liquid Equilibria for the System Acetone+ Solketal+ Glycerol at (303.2, 313.2, and 323.2) K.* Journal of Chemical & Engineering Data, 2014. **59**(9): p. 2850-2855.
14. Dünnebier, G., J. Fricke, and K.-U. Klatt, *Optimal Design and Operation of Simulated Moving Bed Chromatographic Reactors.* Industrial & Engineering Chemistry Research, 2000. **39**(7): p. 2290-2304.
15. Pereira, C.S.M., M. Zabka, V.M.T.M. Silva, and A.E. Rodrigues, *A novel process for the ethyl lactate synthesis in a simulated moving bed reactor (SMBR).* Chemical Engineering Science, 2009. **64**(14): p. 3301-3310.
16. Lode, F., M. Mazzotti, and M. Morbidelli, *Comparing true countercurrent and simulated moving-bed chromatographic reactors.* AIChE Journal, 2003. **49**(4): p. 977-990.
17. Azevedo, D.C.S. and A.r.E. Rodrigues, *Design methodology and operation of a simulated moving bed reactor for the inversion of sucrose and glucose–fructose separation.* Chemical Engineering Journal, 2001. **82**(1): p. 95-107.
18. Pereira, C.S.M., P.S. Gomes, G.K. Gandi, V.M.T.M. Silva, and A.E. Rodrigues, *Multifunctional Reactor for the Synthesis of Dimethylacetal.* Industrial & Engineering Chemistry Research, 2008. **47**(10): p. 3515-3524.

19. Subramani, H.J., K. Hidajat, and A.K. Ray, *Optimization of Simulated Moving Bed and Varicol Processes for Glucose–Fructose Separation.* Chemical Engineering Research and Design, 2003. **81**(5): p. 549-567.
20. Harada, H., K. Suzuki, K. Sato, K. Okada, M. Tsuruta, T. Yajima, and Y. Kawajiri, *Process development for advanced simulated moving bed (ASMB) chromatography by parameter refinement using pilot plant experimental data.* Separation and Purification Technology, 2022. **281**: p. 119932.
21. Juza, M., M. Mazzotti, and M. Morbidelli, *Simulated moving-bed chromatography and its application to chirotechnology*. Trends in Biotechnology, 2000. **18**(3): p. 108-118.
22. Graça, N.S., L.S. Pais, V.M.T.M. Silva, and A.E. Rodrigues, *Analysis of the synthesis of 1,1-dibutoxyethane in a simulated moving-bed adsorptive reactor*. Chemical Engineering and Processing: Process Intensification, 2011. **50**(11–12): p. 1214-1225.
23. Faria, R.P.V., *Glycerol valorisation as biofuels: Glycerol acetals production by Simulated Moving Bed Reactor*, in *Department of Chemical Engineering* 2014, University of Porto. p. 236.

Chapter 5

Non-conventional Simulated Moving Bed Reactor: Multifeed SMBR

ADAPTED FROM: Faria, R.P.V., Gonçalves, J. C., Corrêa, I., Ribeiro, A. M., Rodrigues, A. E., Improving the Performance of a Simulated Moving Bed Reactor for the Synthesis of Solketal by Implementing Multifeed Strategy. *Industrial & Engineering Chemistry Research*, **2022**. 61(39): p. 14531-14545.

5.1. Introduction

One of the major advantages of the SMBR technology is its versatility, since the number of degrees of freedom of the Conventional SMBR can be manipulated to extend the range of potential applications for the SMBR and reach even better performance parameters. These alternative operating strategies are generally called non-conventional operation modes. The number of sections, the number of inlet and outlet ports, the feed composition and other dynamic configurations can be modified with relatively simple adaptations on the physical equipment [1-4].

The Multifeed SMBR is a multi-feed strategy, where the reactants are fed in different positions, providing to the unit a behaviour of "distributed feed". Section III of the SMBR is divided in Sections IIIA and IIIB and acetone and glycerol are fed by different ports, as exhibited in Figure 5.1. This is a noteworthy non-conventional strategy because it requires small changes in the equipment, namely the addition of only one pump and a set of valves.

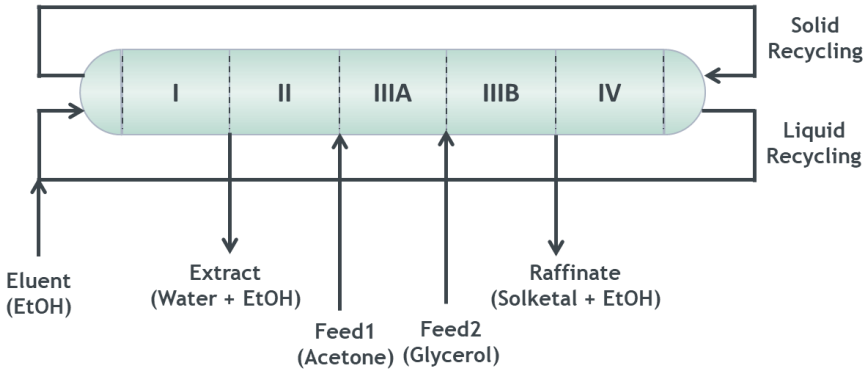

Figure 5.1. Multifeed SMBR.

In Chapter 3, it has been thoroughly described the plight involved in the solketal synthesis, namely reaction limitations, adsorption selectivity issues and process hurdle due to the reactants' miscibility and the viscosity of glycerol. In Chapter 4, these issues were proved to affect the Conventional SMBR performance so severely that this sorption-enhanced strategy

can hardly be seen as the solution for the continuous industrial production of solketal via reaction of glycerol and acetone.

In Chapter 5, the Multifeed SMBR is proposed as a non-conventional strategy to produce solketal because by feeding acetone and glycerol through different nodes, the first next to the extract port and the second next to the raffinate port, the reactants' counter-current contact is promoted, and the unit reaches higher performance. The reaction predominantly occurs in Section IIIB and, in comparison with the Conventional SMBR, acetone inlet is further apart from the raffinate port, for this reason, solketal contamination is less likely to occur. Hence, the major advantage of using the Multifeed SMBR for the solketal synthesis is the possibility of operating with higher flowrates and, consequently, obtaining better performance parameters.

5.2. Modelling Studies

The modelling of the Multifeed SMBR, as for the Conventional SMBR, begins with its elementary unit, the fixed-bed column. The assumptions valid for both the fixed-bed and the multicolumn unit are (1) plug-flow with axial dispersion and negligible radial dispersion, (2) velocity variations due to changes in the bulk composition, (3) internal and external mass transfer resistances lumped and estimated by the linear driving force model, (4) all the beds equally packed with constant temperature, length and porosity, and (5) the reaction occurs exclusively at the active sites inside the catalyst pores and (6) multicomponent adsorption equilibrium described by the competitive Langmuir adsorption isotherm model [5]. The mathematical model developed for the study of the Conventional SMBR in Chapter 4 (Section 4.2.) is valid for the Multifeed SMBR. For reference, the main model equations are summarized in Table 5.1.

Table 5.1. Mathematical model equations for the Multifeed SMBR.

Bulk molar balance	$\frac{\partial C_i}{\partial t} + \frac{\partial (uC_i)}{\partial z} + \frac{1-\varepsilon_b}{\varepsilon_b}\frac{3}{r_p}k_{L,i}\left(C_i - \bar{C}_{p,i}\right) = D_{ax}\frac{\partial^2 C_i}{\partial z^2}$	(5.1)
Particle molar balance	$\frac{3}{r_p}k_{L,i}\left(C_i - \bar{C}_{p,i}\right) = \varepsilon_p\frac{\partial \bar{C}_{p,i}}{\partial t} + \left(1-\varepsilon_p\right)\frac{\partial \bar{q}_i}{\partial t} - \nu_i\frac{\rho_b}{(1-\varepsilon_b)}\Re\left(\bar{C}_{p,i}\right)$	(5.2)
Interstitial fluid velocity	$\frac{du}{dz} = -\frac{1-\varepsilon_b}{\varepsilon_b}\frac{3}{r_p}\sum_{i=1}^{NC}k_{L,i}V_{M,i}\left(C_i - \bar{C}_{p,i}\right)$	(5.3)
Initial condition	$t = 0 \rightarrow C_i = \bar{C}_{p,i} = C_{i,0}$	(5.4)
Boundary conditions	$z = 0 \rightarrow uC_{in,i} = uC_i\vert_{z=0} - D_{ax}\frac{\partial C_i}{\partial z}\Big\vert_{z=0}$	(5.5)
	$z = 0 \rightarrow u = u\vert_{z=0}$	(5.6)
	$z = L \rightarrow \frac{\partial x_i}{\partial z}\Big\vert_{z=L} = 0$	(5.7)

The main difference in the models of the Conventional SMBR and the Multifeed SMBR is that Section III of the Conventional is divided into two independent sections. Therefore, Equations (4.6) and (4.7) that describe the global mass balance of Section III are modified to Equations 5.12 to 5.15. The mass balances of the other nodes are the same:

Desorbent node	$Q_I C_{i,n_D}\vert_{z=0} = Q_{Rec}C_{i,n_D-1}\vert_{z=L} + Q_D C_{D,i}$	(5.8)
	$Q_I = Q_{Rec} + Q_D$	(5.9)
Extract node	$C_{i,n_X}\vert_{z=0} = C_{i,n_X-1}\vert_{z=L}$	(5.10)
	$Q_{II} = Q_{Rec} + Q_D - Q_X$	(5.11)
Feed I node		(5.12)

$$Q_{IIIA}C_{i,n_{F1}}\big|_{z=0} = Q_{II}C_{i,n_{F1}-1}\big|_{z=L} + Q_{F1}C_{F1,i}$$

$$Q_{IIIA} = Q_{Rec} + Q_D - Q_X + Q_{F1} \tag{5.13}$$

$$Q_{IIIB}C_{i,n_{F2}}\big|_{z=0} = Q_{IIIA}C_{i,n_{F2}-1}\big|_{z=L} + Q_{F2}C_{F2,i} \tag{5.14}$$

Feed II node

$$Q_{IIIB} = Q_{Rec} + Q_D - Q_X + Q_{F1} + Q_{F2} \tag{5.15}$$

$$C_{i,n_R}\big|_{z=0} = C_{i,n_R-1}\big|_{z=L} \tag{5.16}$$

Raffinate node

$$Q_{IV} = Q_{Rec} \tag{5.17}$$

The performance of the SMBR is quantitatively assessed through Equations (4.13) to (4.17).

The numerical solution of the model was performed using gPROMS version 7.0.7, similar to the procedures of the Conventional SMBR modelling. The partial differential and algebraic equations were solved using a method of Orthogonal Collocation in Finite Elements (OCFEM), discretizing the axial domain in 30 finite elements and two interior collocation points in each element, while the ordinary differential equations in time were solved by an integrated differential-algebraic equation solver (DASOLV), with a 10^{-5} convergence tolerance.

The optimization procedure was also similar to the one previously reported for the Conventional SMBR, having as objective function the productivity maximization, limited by the minimum commercially required solketal purity in the raffinate and a water purity in the extract of 97% (optimization algorithm exhibited in Figure 4.4). The optimization of the SMBR design variables were conducted with gPROMS, using the NLPSQP (Non-Linear Problem Sequential Quadratic Programming) solver included in the software, which solves nonlinear optimization problems by applying a sequential quadratic programming method. The convergence tolerance was set to 10^{-5}. The global OPTimization (gOPT) tool described in Chapter 3 was also used for the optimization of the Multifeed SMBR.

5.3. Optimization studies for solketal synthesis in the Multifeed SMBR

The additional feed stream of the Multifeed SMBR increases the number of degrees of freedom of the process and consequently increases the complexity of the optimization from the numerical perspective. This highlights the relevance of developing an equivalent Multifeed TMBR model. The benefits are the same from modelling the Conventional SMBR, namely enabling the direct use of steady-state equations in the model, which significantly decreases computational effort and the required time to complete this procedure. The equivalence between the models for this non-conventional SMBR is further explained in Section 5.2.

The same procedure used for the Conventional SMBR was applied to the sensitivity analysis and optimization of the non-conventional SMBR: the first step was to perform independent optimizations for different column configuration applying a safety factor of 30% to the regeneration sections flow rate ratios predicted by the equilibrium theory, in order to ensure the solid and the desorbent regeneration. The optimized variables were extract, feed 1 and feed 2 flowrates and solid velocity. To confirm that the novel optimization strategy provides the global optimum, and not a local optimum, the RSR for the best configuration with a safety factor (SF) of 30% for γ_1 and γ_4 and the optimal solid velocity determined was delimited.

The second step consisted of performing a sensitivity analysis to the safety factors with independent optimizations targeting the productivity maximization (objective function) and subjected to the restriction of solketal purity in the raffinate and water purity in the extract of 97% (optimization constraints). Finally, in the third step of the optimization, a careful study on the equivalence between the TMBR and the SMBR was performed to assure the first can describe with sufficient accuracy the real unit. This procedure was performed considering the dimensions of the SF-SMB(R), namely 8 columns with length and diameter of 15 cm and 2.12 cm, respectively.

5.3.1. Sensitivity Analysis of the unit's configuration

As mentioned, the introduction of an additional feed stream increases the complexity of the unit and the number of degrees of freedom, since a larger number of combinations of columns per section can be assumed.

Similarly to the verified for the four-section SMBR, the configuration is expected to have a considerable impact on the Multifeed SMBR performance and, therefore, it was the first variable analysed. Table 5.2 presents the optimal operating conditions and the main performance parameters of SMBR units with different configurations assuming a safety factor of 30% for the regeneration sections flow rate ratios.

Table 5.2. Effect of the configuration on the Multifeed SMBR performance considering a safety factor of 30% for Sections I and IV (ranked in terms of productivity). Solid velocity (u_s) in cm·min^{-1}, Productivity (PR) in kg·L^{-1}·day^{-1} and Desorbent Consumption (DC) in L·kg^{-1}.

Config.	$\gamma_1{}^{in}$	$\gamma_2{}^{in}$	$\gamma_{3A}{}^{in}$	$\gamma_{3B}{}^{in}$	$\gamma_4{}^{out}$	u_s	PR	DC	PuR	PuX	X
1-1-1-4-1	6.00	0.71	1.53	2.32	0.48	0.61	7.154	3.88	0.97	0.99	0.99
2-1-1-3-1	6.00	0.76	1.32	1.85	0.48	0.70	5.506	5.78	0.97	0.97	0.99
1-1-2-3-1	6.00	0.72	1.49	2.24	0.48	0.49	5.436	4.10	0.97	0.99	0.99
1-2-1-3-1	6.00	0.73	1.49	2.24	0.48	0.49	5.419	4.11	0.97	1.00	0.99
1-1-1-3-2	6.00	0.72	1.50	2.26	0.48	0.48	5.414	4.04	0.97	0.99	0.99
2-1-2-2-1	6.00	0.77	1.30	1.81	0.48	0.48	3.662	5.97	0.97	0.97	0.99
2-1-1-2-2	6.00	0.76	1.31	1.83	0.48	0.47	3.654	5.88	0.97	0.97	0.99
3-1-1-2-1	6.00	0.76	1.31	1.82	0.48	0.48	3.653	5.92	0.97	0.97	0.99
2-2-1-2-1	6.00	0.76	1.31	1.82	0.48	0.47	3.653	5.91	0.97	0.97	0.99
1-1-3-2-1	6.00	0.76	1.36	1.96	0.48	0.41	3.640	5.15	0.97	1.00	0.99
1-2-2-2-1	6.00	0.77	1.37	1.96	0.48	0.41	3.639	5.15	0.97	1.00	0.99
1-1-2-2-2	6.00	0.76	1.37	1.98	0.48	0.41	3.639	5.08	0.97	1.00	0.99
1-1-1-2-3	6.00	0.76	1.38	1.98	0.48	0.41	3.632	5.08	0.97	1.00	0.99
1-3-1-2-1	6.00	0.77	1.37	1.96	0.48	0.41	3.631	5.15	0.97	1.00	0.99
1-1-2-1-3	6.00	0.78	1.29	1.80	0.48	0.24	1.803	5.93	0.97	1.00	0.99

2-1-1-1-3	6.00	0.77	1.30	1.81	0.48	0.24	1.802	5.91	0.97	0.97	0.99
1-1-1-1-4	6.00	0.77	1.30	1.81	0.48	0.24	1.802	5.87	0.97	0.97	0.99
2-2-1-1-2	6.00	0.77	1.30	1.81	0.48	0.24	1.802	5.90	0.97	0.97	0.99
3-1-1-1-2	6.00	0.77	1.30	1.81	0.48	0.24	1.802	5.90	0.97	0.97	0.99
3-1-2-1-1	6.00	0.78	1.29	1.80	0.48	0.24	1.802	5.97	0.97	1.00	0.99
2-2-2-1-1	6.00	0.76	1.29	1.80	0.48	0.24	1.802	5.94	0.97	0.97	0.99
1-3-2-1-1	6.00	0.78	1.29	1.81	0.48	0.24	1.801	5.89	0.97	1.00	0.99
2-3-1-1-1	6.00	0.77	1.30	1.81	0.48	0.24	1.801	5.90	0.97	0.97	0.99
3-2-1-1-1	6.00	0.77	1.30	1.81	0.48	0.24	1.801	5.90	0.97	0.97	0.99
4-1-1-1-1	6.00	0.77	1.30	1.81	0.48	0.24	1.801	5.90	0.97	0.97	0.99
1-4-1-1-1	6.00	0.78	1.30	1.82	0.48	0.24	1.801	5.86	0.97	0.99	0.99
2-1-3-1-1	6.00	0.78	1.28	1.79	0.48	0.24	1.800	6.00	0.97	1.00	0.99
1-1-3-1-2	6.00	0.78	1.29	1.81	0.48	0.24	1.800	5.90	0.97	1.00	0.99
1-2-3-1-1	6.00	0.78	1.29	1.80	0.48	0.24	1.800	5.95	0.97	1.00	0.99
1-1-4-1-1	6.00	0.78	1.28	1.80	0.48	0.24	1.798	5.97	0.97	1.00	0.99

The results presented in Table 5.2 demonstrate the viability of producing solketal in a continuous chromatographic reactor using the non-conventional strategy. The productivities of the configurations that performed better are in line with the range of values reported in the open literature for similar systems [6-9]. The results are even more remarkable when compared to the Conventional SMBR. The productivity increases more than 7.5 times and the solid velocity increases by almost 30%, which combined with the increase in the feed flowrates contributes to an increment of almost 6 times in the amount of the reactants fed to the unit. The Multifeed SMBR is a clear example of Process Intensification once the performance of the unit is exceedingly increased by the much more extensive use of the unit and of the stationary phase.

The considerable increase in the reactor operational parameters and consequent improvement in the reactor performance was made possible by the counter-current movement of the reactants

inside the unit promoted by the strategy of feeding the reactants by different ports. This way, one of the main impairments of the Conventional SMBR, the different affinities of the reactants, was overcome because their contact time was appreciably extended. This can be confirmed by the analysis of the internal concentration profiles attained under the optimal operating conditions for an SMBR with a 1-1-1-4-1 configuration, as shown in Figure 5.2.

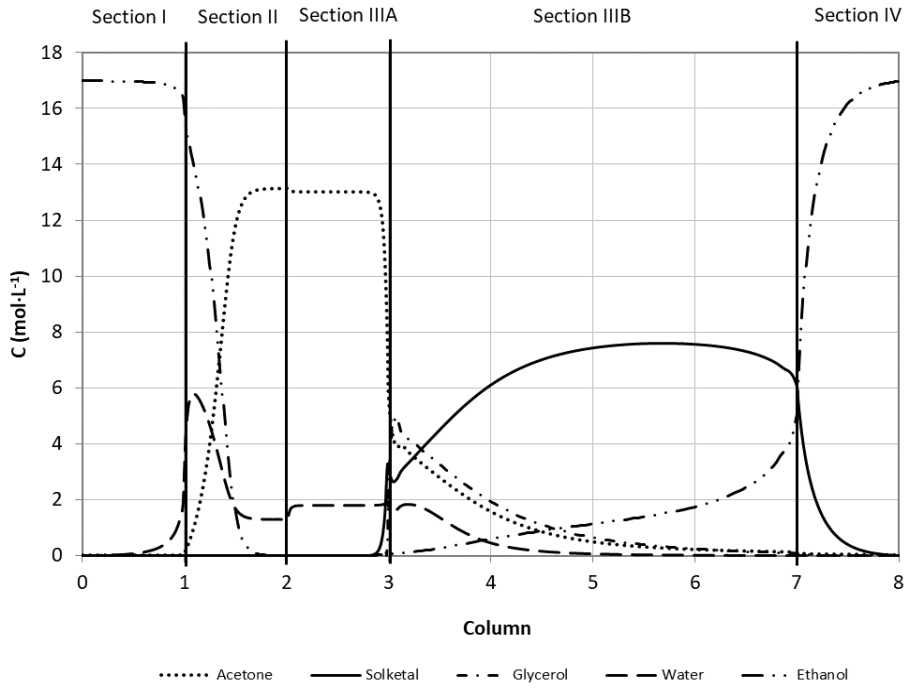

Figure 5.2. Internal concentration profiles within the Multifeed SMBR, with a 1-1-1-4-1 configuration, at 303 K, feeding pure glycerol and acetone through two independent feed streams. ($\gamma_1{}^{in} = 6.00, \gamma_2{}^{in} = 0.30, \gamma_{3A}{}^{in} = 1.53, \gamma_{3B}{}^{in} = 2.32, \gamma_4{}^{out} = 0.44, u_s = 0.61$ cm·min^{-1}).

Another noteworthy conclusion is the linear relation between the productivity and the number of columns in Section IIIB, as shown in Figure 5.3.

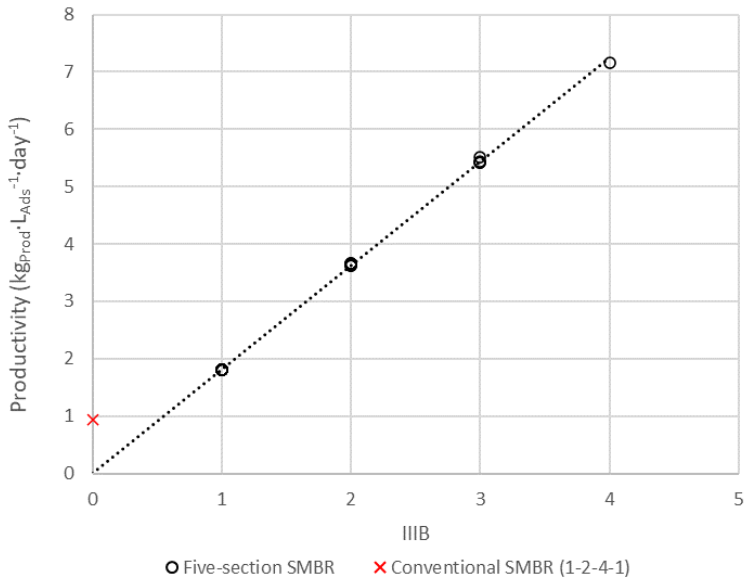

Figure 5.3. Relation between the number of columns in Section IIIB and the productivity for a safety factor of 30%. The × corresponds to the best configuration of the Conventional SMBR (1-2-4-1) with a safety factor of 30%.

This reveals the productivity limitation by the length of this section, which is explained by the fact that most of the reaction occurs between the second feed port and the raffinate collection port (Figure 5.2). Also, there is not significative difference in the unit productivity for configurations with the same number of columns in Section IIIB, revealing that the unit performance is driven by this parameter. Since the maximum number of columns in Section IV is four, the only possible configuration is 1-1-1-4-1. Compared to the best configuration of the Conventional SMBR, even the configurations that performed worse surpass the productivity of this unit.

Following the same principle of the Conventional SMBR, when using a new optimization methodology, it is wise to confirm the reliability of the optimum point found as a global, and not a local optimum. In the present work, this was performed by delimiting the RSR for the 1-1-1-4-1 configuration with SF of 30% applied to γ_1 and γ_4 and the solid velocity determined by the methodology (Figure 5.4). The RSR algorithm provides all the combinations of feed and

extract flowrates that can be used to produce solketal subjected to the purity constraint of 97% for the raffinate and extract streams, being the optimal point the one in the vertex of the RSR. Figure 5.4 presents a comparison of the Conventional TMBR and the Multifeed TMBR RSRs.

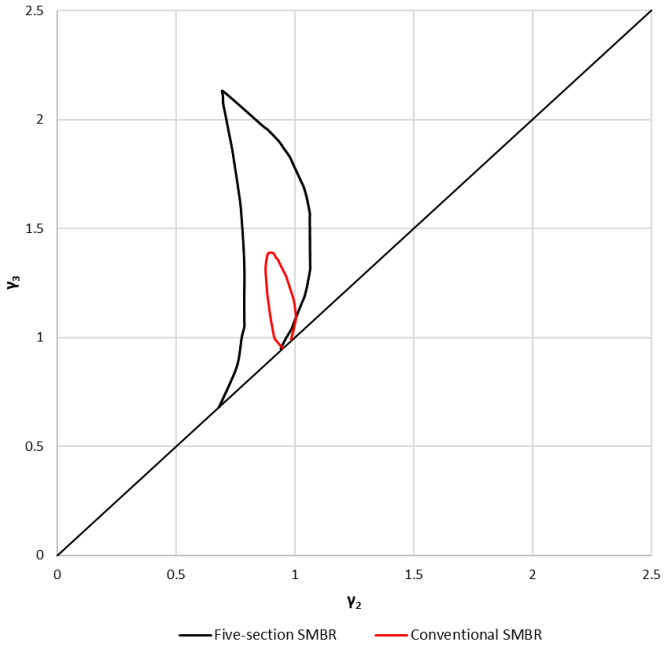

Figure 5.4. Reactive separation regions for the Multifeed SMBR with a column configuration 1-1-1-4-1 at the optimal point for a safety factor of 30% applied to Sections I and IV (u_s = 0.61 cm·min^{-1}) and for the Conventional SMBR with a column configuration 1-2-4-1 at the optimal point for a safety factor of 30% applied to Sections I and IV (u_s = 0.47 cm·min^{-1}).

Table 5.3. Comparison of the operational and performance parameters resultant from the RSR and the novel optimization strategy for a 1-1-1-4-1 configuration, SF of 30% applied to Sections I and IV and a solid velocity of 0.61 cm·min^{-1}. Productivity (PR) in kg·L^{-1}·day^{-1} and Desorbent Consumption (DC) in L·kg^{-1}.

	${\gamma_1}^{in}$	${\gamma_2}^{in}$	${\gamma_{3A}}^{in}$	${\gamma_{3B}}^{in}$	${\gamma_4}^{out}$	PR	DC	PuR	PuX	X
RSR	6.00	0.71	1.53	2.32	0.48	7.15	3.88	0.97	0.99	0.99
New optimization	6.00	0.70	1.53	2.34	0.48	7.14	3.82	0.97	0.99	0.99

The reliability of the optimization methodology was confirmed once the optimal point of the RSR corresponds to the same optimal point for the first entry of Table 5.2. The deviations are

negligible and are mainly related with the different step sizes used in each approach. Compared to the Conventional SMBR, the operation subjected to the predefined purity constraints is much more robust, once the RSR area is bigger, and the vertex of the RSR is further away from the diagonal, indicating that a much superior productivity can be reached.

5.3.2. Optimization of the Multifeed SMBR

Besides the increased complexity of the optimization of the Multifeed SMBR as a result of the larger number of possible combinations of columns per section, there is also the possibility of operating it under different feed flowrates, which results in the potential of manipulating the reactants ratio fed to the unit. Therefore, compared to the Conventional SMBR, there is one more decision variable to be optimized, the second feed flowrate.

The sensitivity analysis procedure was similar to the reported for the Conventional SMBR: independent optimizations were performed by varying the safety factor from 5% to 40% with the objective function of maximizing the productivity subjected to the constrains of 97% of purity for both raffinate and extract. The effect on the performance parameters were then thoroughly discussed.

Effect on the productivity

The sensitivity analysis of the productivity with variations in the flowrate ratios are presented in Figure 5.5.

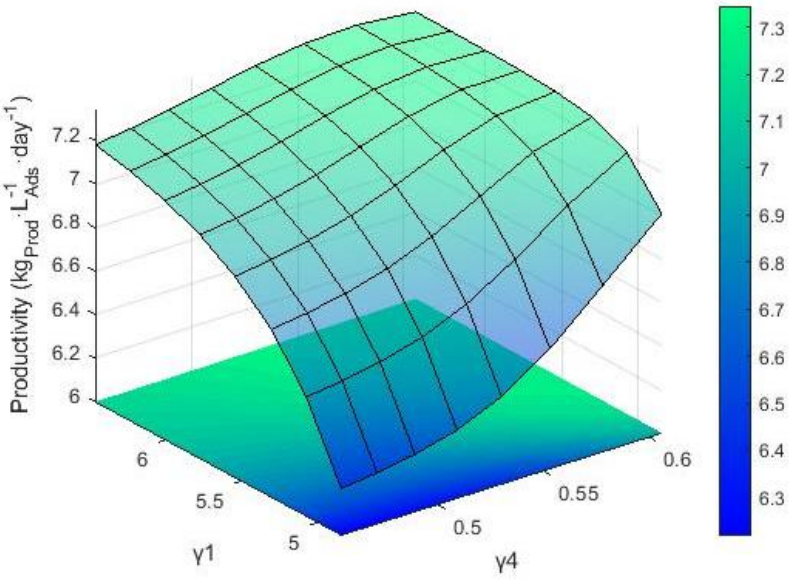

Figure 5.5. Effect of the flow rate ratio in Sections I (γ_1) and IV (γ_4) on the productivity of a SMBR, with a 1-1-1-4-1 configuration, at 303 K.

As mentioned in Section 5.3.2, it is expected that the productivity enhances with a more effective regeneration, or, in practice, for higher safety factors (higher γ_1 and lower γ_4 absolute values), until reaching a plateau when the solid and liquid phases are properly regenerated and do not improve this performance parameter. This was not observed in the Conventional SMBR because the performance is so reduced that, for the range of safety factors studied, the unit has not been able to reach the maximum productivity due to exhaust Amberlyst-35 capacity. Therefore, the increase in the operational parameters (solid velocity and inlet/outlet flowrates) ended up positively influencing the productivity. For the Multifeed SMBR, the mentioned plateau is reached because the unit reaches a maximum productivity limited by the catalysts activity and the adsorbent capacity. Yet, the higher productivity expected for a lower γ_4 is not observed due to the simultaneous increase in the solid velocity and consequent ability of the unit of processing higher flowrates when a higher γ_4 is used.

Effect on the desorbent consumption

The effect of the SF on the desorbent consumption (DC) is summarized in Figure 5.6:

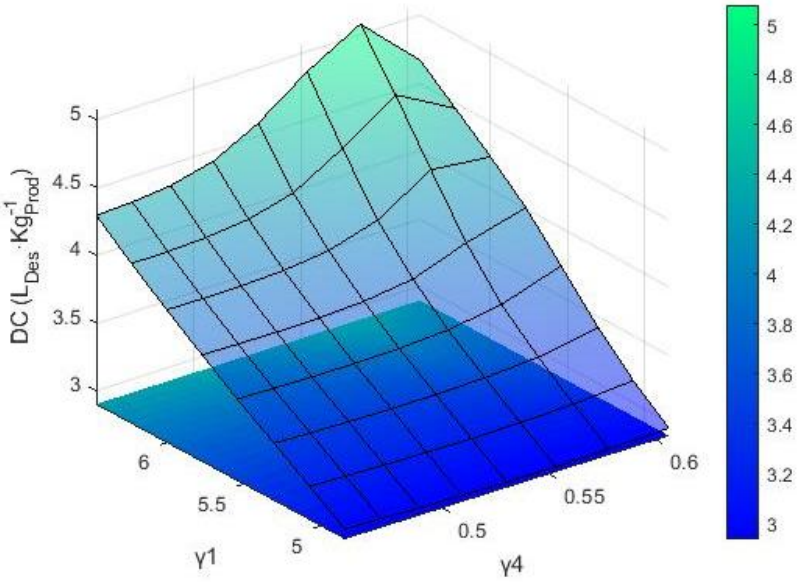

Figure 5.6. Effect of the flow rate ratio in Sections I (γ_1) and IV (γ_4) on the desorbent consumption (DC) of a SMBR, with a 1-1-1-4-1 configuration, at 303 K.

As it happens in the Conventional SMBR, for lower SF applied to Section IV (higher γ_4) the optimum solid velocity and the operational flowrates are higher, and the unit reaches higher productivities. It would be expected, then, a decrease in the DC, once this performance parameter is inversely proportional to the productivity. However, the DC is directly proportional to the difference between γ_1 and γ_4, so to keep γ_1 constant, the desorbent flowrate must also increase. This also justifies the increase in the DC by increasing the SF applied to Section I (consequently γ_1), considering a constant γ_4. Besides, when the liquid phase is not properly regenerated, the unit runs with lower operational parameters and the performance is severely affected.

In the range of SF studied, the maximum productivity was attained for a SF of 40% in Section I and 10% in Section IV. It is 7.345 kg_{Solk}·L^{-1}_{Ads}·day^{-1}, with a DC of 5.08 $L_{Desorbent}$·kg^{-1}_{Prod}. This combination of SF is the same of the Conventional SMBR, confirming that a SF of at least 10%

is necessary for the proper regeneration of the liquid phase when there is only one column in Section IV. As for the SF applied to Section I, since the productivity plateau is reached, there is no gain in increasing the amount of fresh desorbent fed to the unit.

Effect on the solid velocity

The effect of the sensitivity analysis on the solid velocity is exhibited in Figure 5.7:

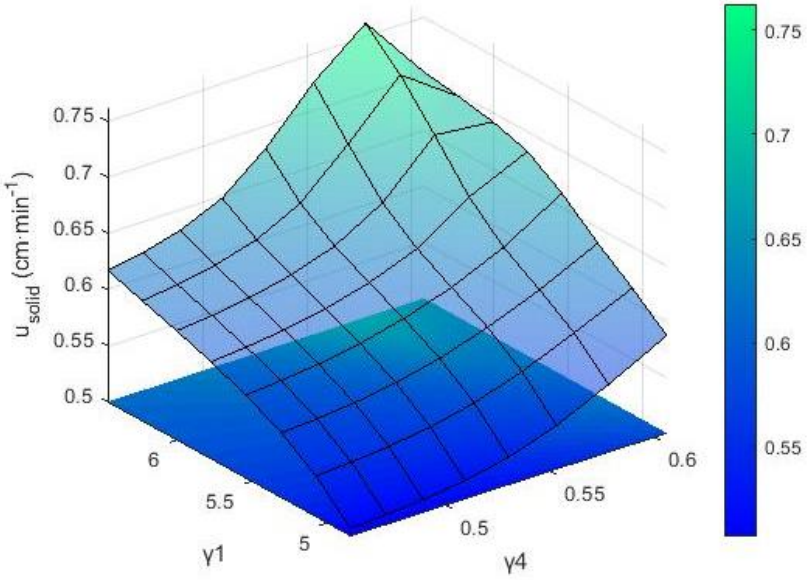

Figure 5.7. Effect of the flow rate ratio in Sections I (γ_1) and IV (γ_4) on the solid velocity of a SMBR, with a 1-1-1-4-1 configuration, at 303 K.

As it happens for the DC, the behaviour of the solid velocity is alike the Conventional SMBR. The main difference between the two units is that in the Multifeed SMBR, for small variations in the productivity, the solid velocity varied more drastically than in the Conventional SMBR. Therefore, the maximum productivity capacity could be reached with relatively lower solid phase velocities (compared to the maximum solid velocity attained in the unit).

Since the Multifeed SMBR is able to process higher absolute flowrate values, to compensate de displacement of the concentration bands inside the unit, the solid phase velocity must also

increase. As it was observed in Figure 5.5 and Figure 5.6 this is accompanied by an increase in the productivity, at the cost of an increase in the DC.

Effect on the solketal concentration

The effect of the variation on the safety factors in the concentration of solketal in the vicinity of the raffinate port is presented in Figure 5.8:

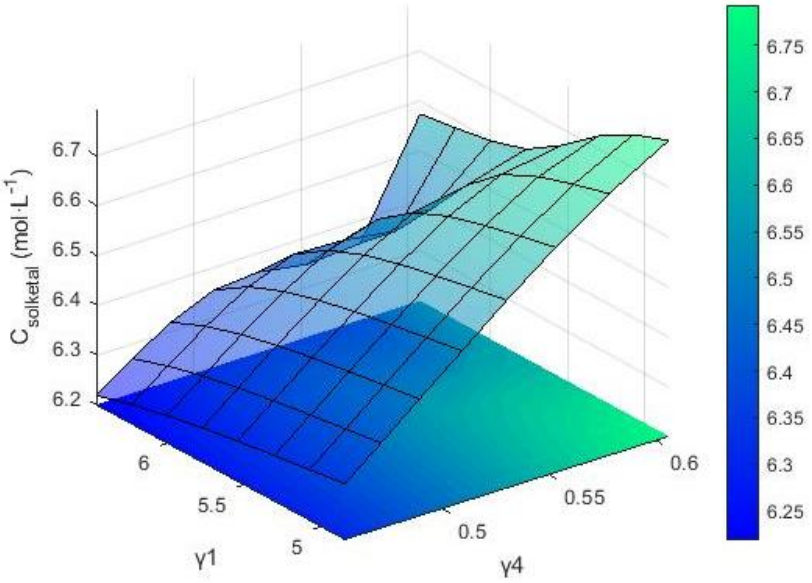

Figure 5.8. Effect of the flow rate ratio in Sections I (γ_1) and IV (γ_4) on the solketal concentration in the vicinity of the raffinate port of a SMBR, with a 1-1-1-4-1 configuration, at 303 K.

Solketal's concentration behaviour is very similar for the Conventional and the Multifeed SMBR and the explanation for this is the same. Solketal is allowed to travel deeper in Section IV if lower safety factors are applied to this section flow rate ratio, and thus its concentration near the raffinate port is higher. The productivity, however, is affected when using lower safety factors due to the improper regeneration of the liquid phase and consequent presence of this compound in Section I after the switch. Therefore, the lower solketal concentration near the

raffinate port when operating with higher SF is compensated by the higher flowrates that can be processed in the unit and the productivity is higher.

Effect on the conversion

Figure 5.9 summarizes the influence of the safety factor in the conversion:

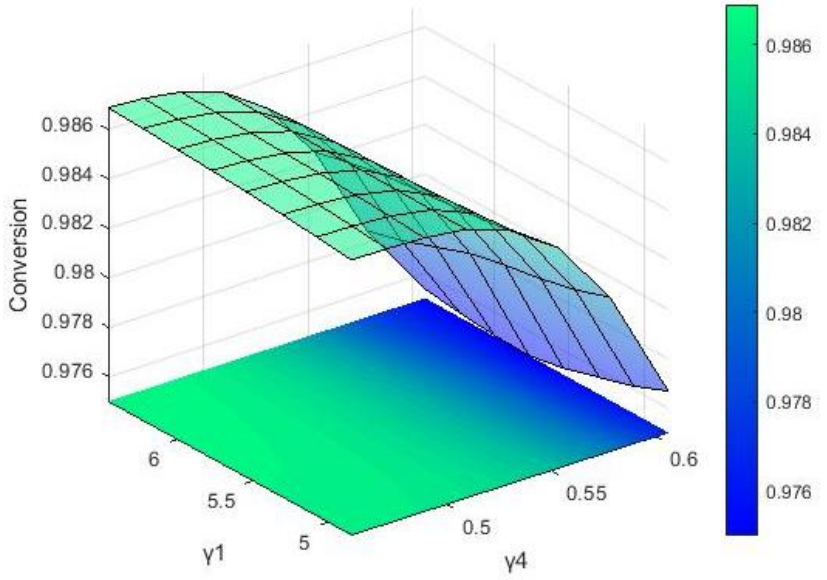

Figure 5.9. Effect of the flow rate ratio in Sections I (γ_1) and IV (γ_4) on the conversion of a SMBR, with a 1-1-1-4-1 configuration, at 303 K.

The behaviour of the conversion is strongly driven by the SF applied to γ_4, while it remains almost unchanged with γ_1, similarly to what was observed for the Conventional SMBR. By relying on a higher γ_4, the recycle flowrate, which is directly related to the flowrate ratio in Section IV, increased, together with the solid phase velocity. The flowrates in all the other sections only experience minor changes. The increment in these two variables, recycle flowrate and solid velocity, was enough to hinder the conversion by reducing the contact time of the reactants with the stationary phase. Due to the strong thermodynamic limitation of glycerol reaction with acetone to produce solketal, assuring the sufficient contact time of the reactants with the catalyst is a crucial aspect to reach good conversion.

The increase in γ_1 drives the increase in the solid velocity and in all the operational flowrates. The reduced contact time by the increase in the solid velocity was compensated by the higher amount of reactants fed to the unit, which fostered the direct reaction. This justifies the unchanged behaviour of the conversion with variations in γ_1.

Effect on the feed flowrate ratio

A noteworthy conclusion of the sensitivity analysis to the safety factor is the approximately constant ratio between the reactants regardless of the γ_1 and γ_4 values considered. The ratio between the feed streams flowrates is 1.03, which results in a molar excess of acetone fed to the unit of approximately 5%. This small excess assures that enough acetone reaches glycerol to form solketal and water. The excess of acetone was removed together with water by the extract stream and, due to the distance between acetone and the raffinate port, it was avoided one of the main issues of the Conventional SMBR, the contamination of the raffinate stream with this reactant.

The fact that the feed flowrates can be independently optimized demonstrates another major advantage of the Multifeed SMBR, that is to control the amount of each reactant fed to the unit.

5.4. Equivalence between the TMBR and the SMBR

The TMBR modelling is used to simulate the real SMBR due to the savings in terms of computational effort and time. The equivalence is made by keeping the liquid velocity constant relative to the solid velocity in each section *j*, as described by Equations (4.10) and (4.11), and thoroughly explained in Section 4.5. The main issues in the equivalence for reactive systems and for systems with nonlinear adsorption equilibrium have been discussed once the equations were derived for purely separative systems. The conditions that make the equivalence more suitable have also been indicated, namely larger number of columns and shorter time switches.

The equivalence between the TMBR and the SMBR for the synthesis of solketal in the SF-SMB(R) was already rather challenging for the conventional operation because of the limited number of columns and due to the mass transfer and thermodynamic limitations, that require relatively long time switches to assure the reactants have enough time to reach the active sites of the catalyst. Besides all these issues, for the Multifeed SMBR there was another degree of difficulty. Since the feed streams were independently optimized, it was necessary to assure the reactant ratio was kept unchanged relatively to the TMBR. This is an especially sensitive aspect for glycerol and acetone reaction, once the system requires, at the same time, a certain excess of the latter compound to foster the direct reaction and compensate glycerol higher concentration in the solid phase, but not as much so it affects the raffinate purity, by contaminating this stream.

Therefore, as a way of assuring the reactants have a more similar residence time distribution for the TMBR and the SMBR, a more rigorous modelling was proposed considering the changes in velocity due to changes in bulk composition. The volumetric flow rates were calculated in the nodes of the unit's section, that means, between the end of the last column of section j and the beginning of the first column of section $j+1$. The inlet and outlet volumetric flow rates resultant from these considerations are:

$$Q_D = \left(\gamma_1^{inlet} - \gamma_4^{outlet}\right) \varepsilon_b \, A \, \frac{L}{t^*} \tag{5.18}$$

$$Q_X = \left(\gamma_1^{outlet} - \gamma_2^{inlet}\right) \varepsilon_b \, A \, \frac{L}{t^*} \tag{5.19}$$

$$Q_{F1} = \left(\gamma_{3A}^{inlet} - \gamma_2^{outlet}\right) \varepsilon_b \, A \, \frac{L}{t^*} \tag{5.20}$$

$$Q_{F2} = \left(\gamma_{3B}^{inlet} - \gamma_{3A}^{outlet}\right) \varepsilon_b \, A \, \frac{L}{t^*} \tag{5.21}$$

$$Q_R = \left(\gamma_{3B}^{outlet} - \gamma_4^{inlet}\right) \varepsilon_b \, A \, \frac{L}{t^*} \tag{5.22}$$

$$Q_{Rec} = \gamma_4^{outlet} \, \varepsilon_b \, A \, \frac{L}{t^*} \tag{5.23}$$

where ε_b is the bulk porosity, A is the fixed bed cross sectional area, L is the length of the column, and t^* the SMBR time switch.

Similarly to the Conventional SMBR, the maximum productivity from the optimization is achieved for SF's of 40% in Section I and 10% in Section IV; however, when using the rigorous SMBR model, the desorbent is not sufficiently regenerated and solketal ends up being recycled from Section IV to Section I and contaminating the extract stream. Therefore, for this combination of SF's, there is not an operational condition under the extract and raffinate purity constraints. Increasing the SF applied to Section IV to 25% provides comparable performance parameters, as exhibited in Table 5.4. It is noteworthy that there is no need of applying a correction factor to the optimal time switch, as required for the Conventional SMBR.

Table 5.4. Comparison of the performance parameters obtained by equivalent TMBR and SMBR for a 1-1-1-4-1 configuration, SF of 40% applied to Section I and 25% to Section IV. Productivity (PR) in kg·L^{-1}·day^{-1} and Desorbent Consumption (DC) in L·kg^{-1}.

		PR	DC	PuR	PuX	X
TMBR	u_s(cm·min^{-1}) = 0.65	7.27	4.41	0.97	0.98	0.99
SMBR	t^*(min) = 23.14	7.03	5.02	0.97	0.97	0.98

As a final note, the Multifeed SMBR is a Process Intensification strategy that enhances even more the efficiency of an already intensified equipment. As stated in Section 5.3, using the same unit and the same amount of catalyst, it was possible to process higher feed flowrates due to the enhanced contact of the reactants and the better separation of acetone from solketal. In terms of performance parameters, clearly it is much more advantageous to operate the SMBR

using the multi-feed strategy than the conventional operation. When taking into consideration the scale-up of the process to the industrial level, however, one must be conscious of the balance between the increase in the OpEx (operating expenses) and the reduction in the CapEx (capital expenditures).

The increase in the process profits due to producing more solketal is directly related to an increase in the productive cost due to consuming more reactants. At the point of maximum productivity for both systems, namely a SF of 40% applied to Section I and 10% to Section IV, the Conventional SMBR attains 1.086 $kg_{Solk} \cdot L_{Ads}^{-1} \cdot day^{-1}$ and the Multifeed SMBR 7.345 $kg_{Solk} \cdot L_{Ads}^{-1} \cdot day^{-1}$. This results in an increase of almost 7 times in the productivity; however, this may not reflect on a profit growth of the same magnitude because the increase in the molar flux of the reactants is also around 7 times. It is noteworthy that the absolute amount of eluent required for both processes remains almost unchanged because the DC decreases substantially and there is no ethanol on neither feed streams of the Multifeed SMBR.

5.5. Conclusion

The Multifeed SMBR is a non-conventional operation strategy proposed to overcome the main challenges of glycerol reaction with acetone in the Conventional SMBR, namely the high characteristic diffusion times of the species involved in this system, the low reactants conversion and the low adsorption selectivity between acetone and solketal, which dramatically limits the performance of the process. Indeed, the practical implementation of solketal production in the Conventional SMBR is unfeasible. By introducing one more feed stream, the countercurrent contact between the reactants is promoted and the separation of solketal and acetone is improved.

The study on the column configurations reveals that the performance of units with the same number of columns in Section IIIB is similar and that the productivity grows linearly with the

increase of the number of columns in this section. Since the reaction and the separation of acetone and solketal take place almost exclusively in this section, this shows the system is strongly driven by the available reactive region. The only possible configuration to maximize the number of columns in Section IIIB is 1-1-1-4-1. With a safety factor of 30% applied to Sections I and IV, the unit reaches a productivity of 7.15 $kg_{Solk} \cdot L_{Ads}^{-1} \cdot day^{-1}$ with a DC of 3.88 $L_{Desorbent} \cdot kg_{Prod}^{-1}$. This is in the range of productivities reported for similar processes and proves that solketal can be produced by a continuous chromatographic reactor.

From the sensitivity analysis to the SF, the combination that achieves the highest productivity in the range studied is 40% in Section I and 10% in Section IV. At this point, the productivity is 7.35 $kg_{Solk} \cdot L_{Ads}^{-1} \cdot day^{-1}$, with a DC of 5.08 $L_{Desorbent} \cdot kg_{Prod}^{-1}$. The equivalence between the TMBR and the SMBR faces the same issues as the conventional operation. A novel and more rigorous equivalence was proposed considering the changes in velocity due to changes in the bulk composition to assure that the same ratio of reactants is fed to the unit.

Finally, the comparison of the simplified economic potential of the Conventional and the Multifeed SMBR also supports the latter as the best option to produce solketal using the reactive-separation technology.

5.6. Notation

Abbreviations

gPROMS	General PROcess Modelling System
OCFEM	Orthogonal Collocation in Finite Elements
DASOLV	Differential-algebraic equation solver
NLPSQP	Non-Linear Problem Sequential Quadratic Programming

Symbols

A	Fixed-bed cross sectional area	
C_i	Concentration of component i in the liquid phase	mol L^{-1}
$\bar{C}_{p,i}$	Average concentration of component i in the particle pores	mol L^{-1}
$C_{i,0}$	Initial concentration of compound i in the liquid phase	mol L^{-1}
D_{ax}	Axial dispersion coefficient	cm^2 s^{-1}
DC	Desorbent consumption	$L_{des.}$ $kg^{-1}{}_{solk}$
$k_{L,i}$	Global mass transfer coefficient of compound i	cm·s^{-1}
L	Fixed bed length	cm
NC	Number of components	
PR	Productivity	kg_{solk} $L_{Ads}^{-1}s^{-}$
PuR	Raffinate purity	
PuX	Extract purity	
Q	Flowrate	L min^{-1}
$\overline{q_i}$	Average adsorbed concentration of compound i	mol L_{Ads}^{-1}
$\Re$	Reaction rate	mol kg^{-1} s^{-1}
r_p	Particle radius	cm
SF	Safety factor	
t	Time	s
t^*	Time switch	s
u	Interstitial velocity	cm·s^{-1}
u_s	Solid velocity	cm·s^{-1}
$V_{M,i}$	Molar volume of compound i	L mol^{-1}

x_i	Molar fraction of compound i	−
X	Limiting reactant conversion	%
z	Axial coordinate	−

Greek Letters

ε_b	Bulk porosity
ε_p	Particle porosity
γ	Ratio between the liquid and the solid interstitial velocities
v	Stoichiometric coefficient
ρ_b	Bulk density

Subscripts/Superscripts

i	Chemical species
D	Desorbent
Rec	Recycle
X	Extract
F	Feed
R	Raffinate
in	Inlet
n	Number of columns

5.7. References

1. Faria, R.P. and A.E. Rodrigues, *Instrumental aspects of Simulated Moving Bed chromatography.* J. Chromatogr. A, 2015. **1421**: p. 82-102.
2. Kim, K.-M., J.W. Lee, S. Kim, F.V. Santos da Silva, A. Seidel-Morgenstern, and C.-H. Lee, *Advanced Operating Strategies to Extend the Applications of Simulated Moving Bed Chromatography.* Chemical Engineering & Technology, 2017. **40**(12): p. 2163-2178.
3. Aniceto, J.P.S. and C.M. Silva, *Simulated Moving Bed Strategies and Designs: From Established Systems to the Latest Developments.* Separation & Purification Reviews, 2015. **44**(1): p. 41-73.
4. Yu, Y., K.R. Wood, and Y.A. Liu, *Simulation and Comparison of Operational Modes in Simulated Moving Bed Chromatography.* Industrial & Engineering Chemistry Research, 2015. **54**(46): p. 11576-11591.
5. Rodrigues, A.E., Madeira, Luís Miguel, Wu, Yi-Jiang, Faria, Rui, *Sorption Enhanced Reaction Processes*. Sorption Enhanced Reaction Processes. 2017.
6. Silva, V.M.T.M. and A.E. Rodrigues, *Novel process for diethylacetal synthesis.* AIChE Journal, 2005. **51**(10): p. 2752-2768.
7. Pereira, C.S.M., P.S. Gomes, G.K. Gandi, V.M.T.M. Silva, and A.E. Rodrigues, *Multifunctional reactor for the synthesis of dimethylacetal.* Industrial and Engineering Chemistry Research, 2008. **47**(10): p. 3515-3524.
8. Graça, N.S., L.S. Pais, V.M.T.M. Silva, and A.E. Rodrigues, *Analysis of the synthesis of 1,1-dibutoxyethane in a simulated moving-bed adsorptive reactor.* Chemical Engineering and Processing: Process Intensification, 2011. **50**(11–12): p. 1214-1225.
9. Faria, R.P.V., J.C. Gonçalves, I. Corrêa, A.M. Ribeiro, and A.E. Rodrigues, *Improving the Performance of a Simulated Moving Bed Reactor for the Synthesis of Solketal by Implementing Multifeed Strategy.* Industrial & Engineering Chemistry Research, 2022. **61**(39): p. 14531-14545.

Chapter 6

Non-conventional Simulated Moving Bed Reactor: ModiCon SMBR

ADAPTED FROM: Corrêa, I, Faria, R.P.V., Rodrigues, A. E., Enhanced simulated moving bed reactor performance for the synthesis of solketal by implementing the ModiCon strategy. *Adsorption* (2023). https://doi.org/10.1007/s10450-023-00427-6.

6.1. Introduction

The flexibility of the SMBR to non-conventional operations is one of the main advantages of this technology compared to other multifunctional reactors. The number of degrees of freedom of the SMBR can be manipulated to extend the range of potential applications and reach even better performance parameters. Since the performance of this equipment is dependent on physical chemical phenomena as reaction and mass transfer, it can be enhanced by manipulating variables that improve the interaction of the reactants with each other and with the stationary phase. In practice, the number of sections, the number of inlet and outlet ports, the feed composition and other dynamic configurations can be modified with relatively simple adaptations on the physical equipment [1-4].

The periodically Modulated Feed strategy (ModiCon) is a dynamic operating strategy of modulating the feed stream concentration throughout the switching time (Figure 6.2), this way the unit benefits from having at least two more degrees of freedom: the length of the subintervals of the time switch, and the feed concentration in each of these subintervals. The precursor of the ModiCon strategy was modulating the feed flowrate, which was not thoroughly explored due to the disadvantages of decreasing the productivity, difficulty on the valves control algorithms, reducing pump lifetime because of alternating loads, and higher fault probability. These issues entailed the concentration modulation development, that may be simply performed by a valve with small adaptations on the automation algorithm [5, 6].

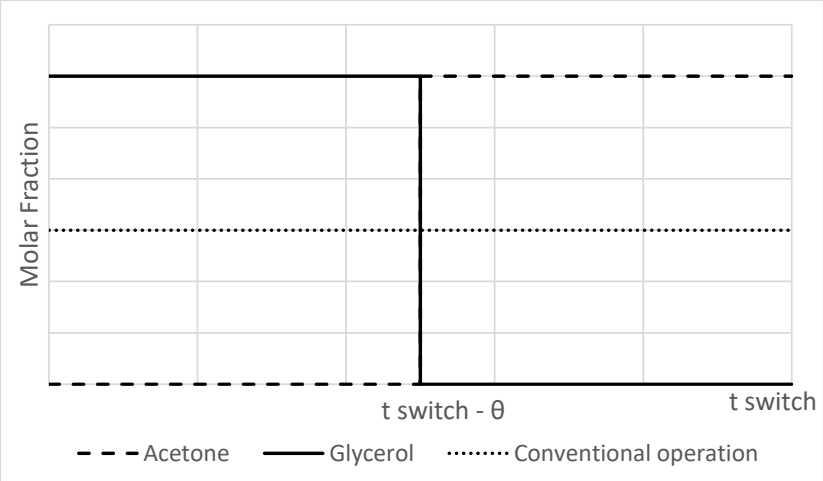

Figure 6.1. Concentration profile of the feed stream for the ModiCon strategy.

The ModiCon has been well accepted by the scientific community, reaching the status of one of the most thoroughly studied SMB operating strategies (purely separative). Nonetheless, the literature on the use of the ModiCon strategy for sorption enhanced reactive processes is still rather scarce. Agrawal et al. produced one of the few works on the ModiCon SMBR, where the esterification of propylene glycol methyl ether acetate (PMA) from 1-methoxy-2-propanol (PM) and acetic acid was studied using a hybrid stationary phase. In this process, PM is used as reactant and desorbent, therefore in the first fraction of the time switch, this compound is fed alone and in the second a reactive mixture with acetic acid is fed [7].

The ModiCon SMBR may be even more advantageous for systems where none of the reactants can be used as desorbent (as solketal synthesis) due to enhancing their contact. For producing solketal using this operating strategy, glycerol (the most retained reactant) is fed in the first fraction of the time switch, followed then by acetone. This way, similarly to the effect in the Multifeed SMBR, the countercurrent contact of the reactants improves their interaction and, consequently, solketal output. Furthermore, as the acetone concentration front is further apart from the raffinate port because it is inserted later, it is possible to reduce the raffinate stream contamination.

In Chapter 5, the Multifeed SMBR was proposed as a non-conventional strategy to produce solketal. In this strategy, the reactants are fed in different positions, acetone near the extract port and glycerol near the raffinate, to take advantage of the different affinities of the species with the stationary phase and promote their counter current contact. This way, the contact time of the reactants was enhanced and the raffinate contamination was avoided due to the larger distance between the acetone feed port and solketal withdrawn port. Consequently, the unit's capacity increased due to the possibility operating with higher flowrates and ultimately, the goal of increasing the unit productivity was achieved by only changing the mode of operation [8].

The Multifeed SMBR strategy requires implementation of some modification in the unit, namely adding an additional pump and a set of valves. The major advantage of the ModiCon is requiring even less modifications in the physical equipment. To implement this strategy, it is necessary only an additional valve between the HPLC pump and the feed containers.

In Chapter 6, the ModiCon is proposed as a dynamic non-conventional operation that takes advantage of similar effects as the Multifeed SMBR, namely increased contact of the reactants and acetone concentration front being further away from the raffinate collection port. The main goal of this chapter is developing and optimizing solketal synthesis in the ModiCon SMBR. To evaluate the improvement of implementing such strategy, the process is compared with the Multifeed SMBR proposed in Chapter 5.

6.2. Modelling Studies

The ModiCon SMBR modelling assumptions are the same of the other SMBR units, namely (1) plug-flow with axial dispersion and negligible radial dispersion, (2) velocity variations due to changes in the bulk composition, (3) internal and external mass transfer resistances lumped and estimated by the linear driving force model, (4) all the beds equally packed with constant

flow, temperature, length and porosity, and (5) the reaction occurs exclusively at the active sites inside the catalyst pores and (6) multicomponent adsorption equilibrium described by the competitive Langmuir adsorption isotherm model [9].

The mathematical model developed for the study of the Conventional SMBR in Chapter 4 (Section 4.2) was simplified by developing an analogous TMBR model. This strategy reduces the computational effort by directly using the steady-state equations to solve the model, rather than solving the system dynamically until reaching the cyclic steady state. The ModiCon is a dynamic non-conventional operational strategy, thus it is not possible to numerically solve the model by using steady-state equations. The mathematical model of the fixed-bed adsorptive reactor developed in Chapter 3 (Equations (3.1) to 3.17) is valid for each of the columns of the ModiCon SMBR. The molar balances in the nodes of the SMBR described in Chapter 4 (Equations (4.2) to (4.9)) are also valid for the ModiCon SMBR. For reference on the main model equations, Table 6.1 summarizes the molar balances in each of the columns and in the nodes of the SMBR.

Table 6.1. Mathematical model equations for the ModiCon SMBR.

Bulk molar balance	$$\frac{\partial C_i}{\partial t}+\frac{\partial (uC_i)}{\partial z}+\frac{1-\varepsilon_b}{\varepsilon_b}\frac{3}{r_p}k_{L,i}\left(C_i-\bar{C}_{p,i}\right)=D_{ax}\frac{\partial^2 C_i}{\partial z^2}$$	(6.1)
Particle molar balance	$$\frac{3}{r_p}k_{L,i}\left(C_i-\bar{C}_{p,i}\right)=\varepsilon_p\frac{\partial \bar{C}_{p,i}}{\partial t}+\left(1-\varepsilon_p\right)\frac{\partial \bar{q}_i}{\partial t}-\nu_i\frac{\rho_b}{(1-\varepsilon_b)}\Re\left(\bar{C}_{p,i}\right)$$	(6.2)
Interstitial fluid velocity	$$\frac{du}{dz}=-\frac{1-\varepsilon_b}{\varepsilon_b}\frac{3}{r_p}\sum_{i=1}^{NC}k_{L,i}V_{M,i}\left(C_i-\bar{C}_{p,i}\right)$$	(6.3)
Initial condition	$$t=0\rightarrow C_i=\bar{C}_{p,i}=C_{i,0}$$	(6.4)
	$$z=0\rightarrow uC_{in,i}=uC_i\vert_{z=0}-D_{ax}\frac{\partial C_i}{\partial z}\Big\vert_{z=0}$$	(6.5)

Boundary conditions	$z = 0 \rightarrow u = u\|_{z=0}$	(6.6)
	$z = L \rightarrow \frac{\partial x_i}{\partial z}\Big\|_{z=L} = 0$	(6.7)
Desorbent node	$Q_I C_{i,n_D}\Big\|_{z=0} = Q_{Rec} C_{i,n_D-1}\Big\|_{z=L} + Q_D C_{D,i}$	(6.8)
	$Q_I = Q_{Rec} + Q_D$	(6.9)
Extract Node	$C_{i,n_X}\Big\|_{z=0} = C_{i,n_X-1}\Big\|_{z=L}$	(6.10)
	$Q_{II} = Q_{Rec} + Q_D - Q_X$	(6.11)
Feed node	$Q_{III} C_{i,n_F}\Big\|_{z=0} = Q_{II} C_{i,n_F-1}\Big\|_{z=L} + Q_F C_{F,i}$	(6.12)
	$Q_{III} = Q_{Rec} + Q_D - Q_X + Q_F$	(6.13)
Raffinate Node	$C_{i,n_R}\Big\|_{z=0} = C_{i,n_R-1}\Big\|_{z=L}$	(6.14)
	$Q_{IV} = Q_{Rec}$	(6.15)

The time switch (t^*) in the ModiCon strategy may be divided in as many subintervals as desired, with the feed concentration ($C_{F,i}$) pattern admitting as many configurations as possible [10]. Equations 6.16 and 6.17 represent these variables:

$$t^* = [t_1^*, t_2^*, t_3^*, \dots, t_{nt}^*] \tag{6.16}$$

$$C_{F,i} = [C_{F,i,1}, C_{F,i,2}, C_{F,i,3}, \dots, C_{F,i,nt}] \tag{6.17}$$

The performance of the SMBR is quantitatively assessed through Equations (4.13) to (4.17).

The numerical solution of the model was performed using gPROMS version 7.0.7, similar to the procedures of the Conventional SMBR and Multifeed SMBR modelling. The partial differential and algebraic equations were solved using a method of Orthogonal Collocation in Finite Elements (OCFEM), discretizing the axial domain in 30 finite elements and two interior collocation points in each element, while the ordinary differential equations in time were solved

by an integrated differential-algebraic equation solver (DASOLV), with a 10^{-5} convergence tolerance.

6.3. Simulation studies for the Solketal Synthesis in the ModiCon SMBR

The advantage of implementing the ModiCon, that is the flexibility provided by adding at least two more degrees of freedom, is precisely what increases the complexity of the optimization from the numerical perspective. Due to being a dynamic non-conventional operating strategy, the model equations must be dynamically solved, starting from the initial conditions given by Equation 6.4 and successively simulating each cycle, with the bed conditions from the previous cycle being the initial conditions for the next, until CSS is reached [11].

The computational effort to solve CSS problems is extensive, which makes unfeasible to reproduce the optimization procedure proposed by Faria et al. and followed in Chapters 4 and 5 for the Conventional and the Multifeed SMBR, respectively [8]. Indeed, most of the literature on the ModiCon strategy concerns the separation of non-reactive mixtures under the optimal conditions of the Conventional SMBR and the comparison of the performance of these units, rather than the rigorous optimization in a wide range of conditions [12].

Besides the high computational effort required to simulate CSS problems, implementing the ModiCon strategy requires the definition of two new parameters: the duration of the subintervals of the time switch and the correspondent feed concentration of each subinterval. The concentration of the feed stream for the Conventional and the Multifeed SMBR was addressed by Faria et al., based on the fundamental study of Moreira et al. [8, 13]. In the second work, the authors concluded that reducing the amount of reactants fed to the unit, or, in other words, diluting the feed stream in ethanol, negatively affected not only the reaction kinetics, but the equilibrium conversion [13]. It is inevitable to feed a diluted stream in the Conventional

SMBR due to the miscibility issues of the reactants. For the Multifeed SMBR, on the other hand, feeding pure acetone and pure glycerol does not engender the separation of the reaction compounds in two phases [8]. The same behavior occurs in the ModiCon, therefore the feed stream was constituted of 100% glycerol in the first fraction of the time switch and 100% acetone in the second fraction. This reduces the number of decision variables in simulation studies.

The unit considered is the SF-SMB(R) constituted of 8 columns (length: 15 cm; diameter: 2.12 cm) divided into four sections, with two inlet and two outlet streams and synchronous shift of these streams. Since the Multifeed and the ModiCon SMBR improvement is based on the same principles of maximizing the contact of the reactants and keeping acetone concentration front further apart from the raffinate collection port, the Multifeed optimization was seen as an exploration step of the ModiCon optimization. The ModiCon optimization, in turn, was seen as the exploitation step, and followed the approach of defining the Reactive Separation Region. In practice, the optimal points of the Multifeed SMBR were used as inputs to define the main SMBR design variables of the ModiCon SMBR, namely configuration, sectional flow rates, and time switch [8].

The 1-2-4-1 configuration of the ModiCon SMBR is the closest equivalent to the 1-1-1-4-1 configuration of the Multifeed. Most of the reaction takes place in Section III of the ModiCon and in Section IIIB of the Multifeed, therefore assigning more columns to these sections leads to better performance. Besides, it is where the most difficult separation occurs, between solketal and acetone.

By defining the safety factors applied to Sections I and IV, one defines the flowrates of the desorbent and the recycle streams. Also, knowing the ratio of the reactants fed to the unit, it is possible to estimate the duration of each subinterval of the time switch. Since the time switch is one of the main decision variables of the process due to the reaction and mass transfer

kinetics, it was also a decision variable to be optimized. Thus, the decision variables optimized were time switch, feed and extract flowrates, and duration of the subintervals of the time switch.

The optimization procedure followed in this work is based on the separation volume optimization. This procedure proposes finding the operation point in the ($\gamma_2 \times \gamma_3$) plane that is further away from the diagonal within the required purity constraints [14, 15]. The inputs for these studies are the combination of SF's in Sections I and IV (γ_1 and γ_4) and optimal time switch resultant from the independent optimizations on the Multifeed SMBR. Then, the algorithm scans the ($\gamma_2 \times \gamma_3$) plane searching for the (γ_2, γ_3) combination that maximizes the productivity subjected to the purity constraints of 97% in the raffinate and extract streams. This value is stored, and the procedure is repeated for the same value of γ_1 and a lower value of γ_4 (and the optimal time switch from the Multifeed optimization) until there is no more operational point under the purity constraints. Then the procedure is repeated for a lower γ_1 until the purity constrains are no longer satisfied, demonstrating that the separation of the reaction products is unfeasible.

In the second step of the optimization, for the combination of SFs that perform better, a sensitivity analysis to the time switch is carried out. Similarly to the procedure followed in the previous step, the feed and extract flow rates are optimized, with the objective function of maximizing the productivity. Finally, following the same procedure, a sensitivity analysis to the duration of the subintervals of the time switch is performed.

6.3.1. Optimization of the ModiCon SMBR

The effect of SFs variations on the productivity (a) and the desorbent consumption (b) for the ModiCon SMBR are exhibited in Figure 6.2. It is noteworthy that no RSR was identified for a SF lower than 30% in Section I. Also, the unit performance is severely affected when a SF of 15% in Section IV is used, therefore this was set as the minimum SF for this section. To

assure a sufficiently large optimization area, the maximum SF applied to Section I is 70% and to Section IV, 35%.

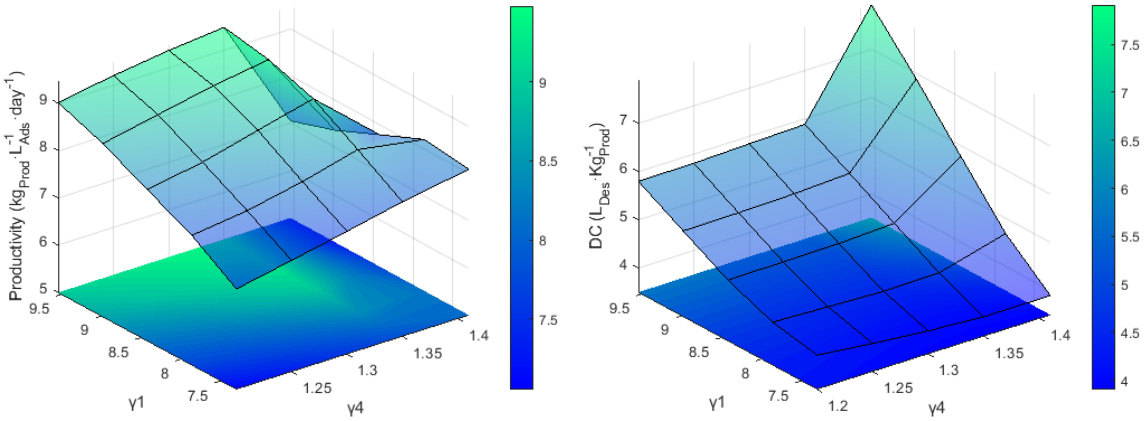

Figure 6.2. Effect of the flow rate ratio in Sections I (γ_1) and IV (γ_4) on the productivity (a) and desorbent consumption (b) of a SMBR, with a 1-2-4-1 configuration, at 303 K.

As mentioned, a relatively large SF in Section I (30%) is necessary to find a set of operational parameters under the purity constraints. From the analysis of the compound's concentration profiles, it is verified that water concentration is high in Section I when lower SFs are used, therefore a minimum of 30% is necessary to assure the sufficient regeneration of the solid.

As mentioned in the optimization of the Multifeed SMBR, higher safety factors typically lead to better performances due to the better regeneration of the solid phase and eluent. Indeed, this behavior is observed in the ModiCon SMBR when a sufficient SF is applied to γ_4 to assure the regeneration of the liquid phase. When γ_4 is close to the value of the equilibrium theory, however, the productivity does not improve even if γ_1 enhances (more fresh desorbent fed to the unit). In fact, the productivity decreases due to the higher solid velocities imposed. As mentioned previously, such increase in the solid velocity is to compensate the displacement of the concentration bands caused by the higher velocity of Section I. Consequently, the overall flowrates in the entire unit increase. For the ModiCon SMBR the reduced contact time of the species with the stationary phase limits the unit capacity, and the feed flowrate reduces, which affects the productivity. Consequently, the DC increases significantly, once it is inversely

proportional to the productivity. It was also observed that the displacement of acetone concentration band leads to the contamination of the raffinate stream.

It was also mentioned in the Multifeed SMBR optimization that the maximum productivity reaches a plateau after which there is no point in adding more eluent or reducing the recycle flow rate because both eluent and solid are properly regenerated. In the ModiCon SMBR, such plateau was not reached within the range of SFs explored. This is related to the simultaneous decrease in the time switch, which, as mentioned, is linked with the higher flowrates processed in the unit. This indicates that the maximum capacity of the unit was not reached for SFs of 70% applied to Section I and 35% to Section IV.

As it was observed for the Multifeed SMBR, the productivity behavior with variations in γ_4 is counterintuitive once it increases for higher flow rates in Section IV, while it would be expected a decrease due to the worse regeneration of the eluent. The reason is the simultaneous decrease in time switch, which increases the overall flowrates and consequently the SMBR processing capacity.

The effect of variations in the SFs on the desorbent consumption must be carefully analysed once this variable is inversely proportional to the productivity and directly proportional to the difference between γ_1 and γ_4. For a constant γ_1, DC is kept almost unchanged with an increase in γ_4 because it compensates the reduction that would be consequence of the increased productivity. For high flow rates in Section IV, the insufficient regeneration of the liquid phase affects the productivity and consequently the DC. The effect of γ_1 in this performance parameter is much more significative than γ_4 due to the larger absolute value of the first variable compared to the second, even considering the increased productivity for higher flow rates in Section I.

Considering the objective function of maximizing the productivity, the optimum combination of SFs is 70% in Section I and 20% in Section IV, resulting in a productivity of

9.48 $kg_{Solk} \cdot L_{Ads}^{-1} \cdot day^{-1}$ with a DC of 5.88 $L_{Desorbent} \cdot kg_{Prod}^{-1}$. It is noteworthy that at this point a higher feed flowrate is processed compared to the optimal point of the Multifeed SMBR. The following steps of the optimization were performed considering this combination of SFs.

6.3.2. Sensitivity Analysis to the time switch

The first step of the optimization aims to find the combination of γ_2 and γ_3 of each time switch within the studied range that leads to the maximum productivity. Thus, the optimal point is the vertex of the RSR for a given time switch and desorbent and recycle flowrates. When the vertex is found, this value is stored, the time switch is incremented, and the procedure is repeated until finding a new optimum.

The impact of the time switch in the unit performance, namely on the productivity and on the desorbent consumption, is evaluated by varying it between 80% and 105% of the optimal from the Multifeed SMBR. For that, the separation region was determined for constant SFs in Sections I and IV (70% and 20%, respectively) to find the (γ_2, γ_3) pair that reaches the highest productivity. Figure 6.3 represents the results of this study.

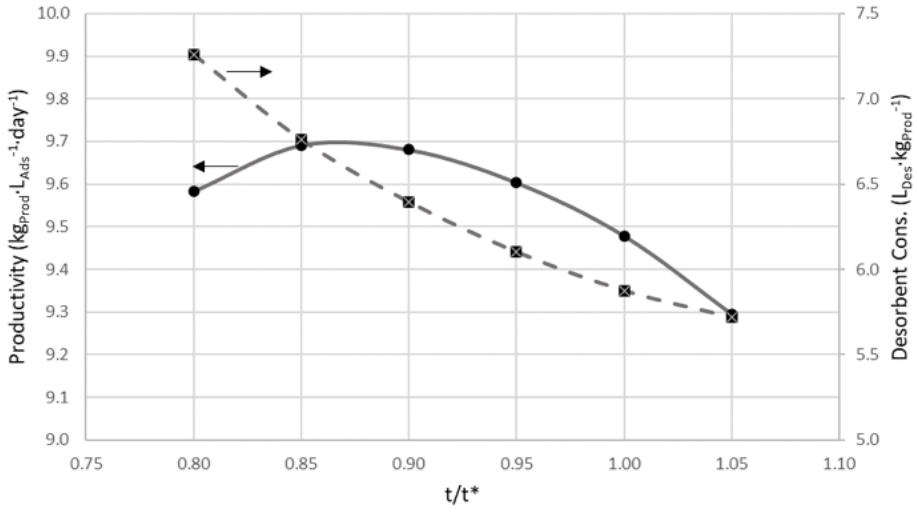

Figure 6.3. Effect of the time switch on the productivity (solid line) and desorbent consumption (dashed line) of a SMBR, with a 1-2-4-1 configuration, at 303 K.

The highest productivity is attained for a time switch of 85% of the Multifeed SMBR optimal. It is 15.42 min and results in a productivity of 9.69 $kg_{Solk} \cdot L^{-1} \cdot day^{-1}$ with a DC of 6.76 $L \cdot kg_{Solk}^{-1}$. The increase in the DC is consequence of the need for a higher desorbent flowrate to regenerate the solid phase when higher time switches are used. Also, from the analysis of the internal concentration profiles, when using the time switch from the Multifeed SMBR, the compounds concentration fronts are displaced in the direction of the fluid flow. This is due to the increased capacity of the unit of operating with higher flow rates. The SMBR performance improves by using a lower time switch (higher solid velocity) because it compensates for the displacement caused by operating with higher flow rates.

Comparing with the internal concentration profile of the Multifeed SMBR at its optimal (SFs of 40% and 25%), it is verified that the extract stream in the Multifeed is highly susceptible to contamination with acetone, since there is only one column between acetone feed port and the extract collection port. Indeed, acetone is the main contaminant of the extract stream on the Multifeed SMBR, and such contamination may limit the amount of reactants fed to the unit and, consequently, the productivity.

The following steps of the ModiCon SMBR simulation studies were performed using time switches of 85% of the Multifeed SMBR optimal.

6.3.3. Sensitivity Analysis to the subdivision of the time switch

Also considering the Multifeed SMBR, in the optimum point, the acetone to glycerol ratio is 1.03, which results in an excess of acetone fed to the unit of around 5%. Since the feed concentration is fixed, the strategy to control the reactants ratio is to manipulate the duration of the subintervals of the time switch. The subdivision of the time switch that promotes the same excess of acetone is feeding glycerol during 49% of the time switch and acetone in the remaining time. Since glycerol reaction with acetone is a one equivalent reaction, the sensitivity

analysis was performed to a range of subdivisions of time switch that did not promote a large excess of one of the reactants.

The sensitivity analysis to the duration of each subinterval of the time switch reveals that the operation is highly limited by the reaction equilibrium since there is no RSR when varying this variable even slightly. When operating with the same combination of safety factors from the Multifeed optimal (70% and 20%) and 90% of the optimal time switch, but feeding glycerol during 48% of the time switch, the raffinate stream purity is impaired by the acetone contamination. As for feeding each reactant during half of the time switch, glycerol is present in high enough amount near the raffinate port to hinder this stream purity.

6.4. Conclusion

In the present chapter, the ModiCon SMBR was developed as an alternative to improve the performance of the SMBR to produce solketal from the reaction between glycerol and acetone. The ModiCon SMBR improvements is based on the principle of promoting the countercurrent contact between the reactants to improve the separation and keeping acetone concentration front further apart from the raffinate collection port. From previous studies, 303K was selected as the best operational temperature and Amberlyst-35 and ethanol are used as stationary phase and eluent, respectively. The process was modelled considering the SF-SMB(R), available at the LSRE-LCM. The optimization was based on the "Reactive-Separation Volumes" methodology due to being a well-established procedure.

Since the optimization of the ModiCon SMBR is more limited due to the much higher computational effort needed, in the first step the time switch values used were prevenient from the Multifeed optimization. It was verified that a larger SF in Section I is needed to achieve the productivity plateau due to the capacity of the unit of processing higher flowrates. The sensitivity analysis to the time switch indicates that higher productivities are achieved when

using a slightly lower time switch. As for the sensitivity to the amount of reactants fed, it was revealed that the process is highly limited by the reaction equilibrium, once no RSR was found when the reactants ration deviates from an excess of acetone of 5%.

The optimal combination of SFs is 70% in Section I and 20% to Section IV with a time switch of 15.42 min (85% from the optimum of the Multifeed SMBR). At this optimal point, the productivity is 9.69 $kg_{Solk} \cdot L_{Ads}^{-1} \cdot day^{-1}$ with a DC of 6.76 $L_{Desorbent} \cdot kg_{Prod}^{-1}$. This indicates an increase in the productivity of 38% compared to the Multifeed, with a cost of an increase of 35% in the desorbent consumption. The most promising result is that the reactants consumption decreases by 12%. These results demonstrate it is more advantageous to operate using the ModiCon than the Multifeed, once the first strategy intensifies even more an equipment that by itself is an example of Process Intensification.

6.5. Notation

Abbreviations

gPROMS	General PROcess Modelling System
OCFEM	Orthogonal Collocation in Finite Elements
DASOLV	Differential-algebraic equation solver
NLPSQP	Non-Linear Problem Sequential Quadratic Programming

Symbols

A	Column cross section area	cm^2
C_i	concentration of component i in the liquid phase	mol L^{-1}
DC	desorbent consumption	$L_{des.}\ kg^{-1}{}_{solk}$
L	fixed bed length	cm
PR	raffinate productivity	$kg_{solk}\ L_{Ads}^{-1} s^{-1}$
PuR	raffinate purity	%
PuX	extract purity	%
Q	flowrate	L min^{-1}
t^*	time switch	s
u	interstitial velocity	$cm.s^{-1}$
u_s	solid velocity	$cm.s^{-1}$

Greek Letters

ε_b	Bulk porosity
γ	Ratio between the liquid and the solid interstitial velocities

Subscripts/Superscript

i	Chemical species
in	inlet
D	Desorbent
Rec	Recycle
X	Extract

$F1$	Feed 1
$F2$	Feed 2
R	Raffinate
lim	Limiting
out	outlet
n	number of columns

6.6. References

1. Faria, R.P. and A.E. Rodrigues, *Instrumental aspects of Simulated Moving Bed chromatography.* J. Chromatogr. A, 2015. **1421**: p. 82-102.
2. Kim, K.-M., J.W. Lee, S. Kim, F.V. Santos da Silva, A. Seidel-Morgenstern, and C.-H. Lee, *Advanced Operating Strategies to Extend the Applications of Simulated Moving Bed Chromatography.* Chemical Engineering & Technology, 2017. **40**(12): p. 2163-2178.
3. Aniceto, J.P.S. and C.M. Silva, *Simulated Moving Bed Strategies and Designs: From Established Systems to the Latest Developments.* Separation & Purification Reviews, 2015. **44**(1): p. 41-73.
4. Yu, Y., K.R. Wood, and Y.A. Liu, *Simulation and Comparison of Operational Modes in Simulated Moving Bed Chromatography.* Industrial & Engineering Chemistry Research, 2015. **54**(46): p. 11576-11591.
5. Schramm, H., M. Kaspereit, A. Kienle, and A. Seidel-Morgenstern, *Simulated moving bed process with cyclic modulation of the feed concentration.* Journal of Chromatography A, 2003. **1006**(1-2): p. 77-86.
6. Schramm, H., A. Kienle, M. Kaspereit, and A. Seidel-Morgenstern, *Improved operation of simulated moving bed processes through cyclic modulation of feed flow and feed concentration.* Chemical Engineering Science, 2003. **58**(23): p. 5217-5227.
7. Agrawal, G., J. Oh, B. Sreedhar, S. Tie, M.E. Donaldson, T.C. Frank, A.K. Schultz, A.S. Bommarius, and Y. Kawajiri, *Optimization of reactive simulated moving bed systems with modulation of feed concentration for production of glycol ether ester.* Journal of Chromatography A, 2014. **1360**: p. 196-208.
8. Faria, R.P.V., J.C. Gonçalves, I. Corrêa, A.M. Ribeiro, and A.E. Rodrigues, *Improving the Performance of a Simulated Moving Bed Reactor for the Synthesis of Solketal by Implementing Multifeed Strategy.* Industrial & Engineering Chemistry Research, 2022. **61**(39): p. 14531-14545.
9. Rodrigues, A.E., Madeira, Luís Miguel, Wu, Yi-Jiang, Faria, Rui, *Sorption Enhanced Reaction Processes*. Sorption Enhanced Reaction Processes. 2017.
10. Calderón Supelano, R., A.G. Barreto, and A.R. Secchi, *Optimal performance comparison of the simulated moving bed process variants based on the modulation of the length of zones and the feed concentration.* Journal of Chromatography A, 2021. **1651**: p. 462280.
11. Minceva, M., L.S. Pais, and A.E. Rodrigues, *Cyclic steady state of simulated moving bed processes for enantiomers separation.* Chemical Engineering and Processing: Process Intensification, 2003. **42**(2): p. 93-104.
12. Schramm, H., M. Kaspereit, A. Kienle, and A. Seidel-Morgenstern, *Improving Simulated Moving Bed Processes by Cyclic Modulation of the Feed Concentration.* Chemical Engineering & Technology, 2002. **25**(12): p. 1151-1155.
13. Moreira, M.N., R.P.V. Faria, A.M. Ribeiro, and A.E. Rodrigues, *Solketal Production from Glycerol Ketalization with Acetone: Catalyst Selection and Thermodynamic and Kinetic Reaction Study.* Ind. Eng. Chem. Res., 2019. **58**(38): p. 17746-17759.
14. Minceva, M. and A.E. Rodrigues, *Two-level optimization of an existing SMB for p-xylene separation.* Computers & Chemical Engineering, 2005. **29**(10): p. 2215-2228.
15. Mazzotti, M., G. Storti, and M. Morbidelli, *Optimal operation of simulated moving bed units for nonlinear chromatographic separations.* Journal of Chromatography A, 1997. **769**(1): p. 3-24.

Chapter 7

Assembly of the Supercritical Fluid Simulated Moving Bed Reactor – SF-SMB(R)

7.1. Introduction

The present chapter was developed in form of the operating manual of the Supercritical Fluid Simulated Moving Bed Reactor – SF -SMB(R). Therefore, it describes the construction, control and data acquisition system implemented in this equipment. Detailed information on each equipment used in the installation is provided to guarantee the correct operation and maintenance.

In Section 7.2, the experimental set-up is presented, through the description of all the elements responsible for performing the reactive-separation experiments. The automation components are also introduced in this section.

The software for the control and automation of the unit was developed in LabVIEW (Laboratory Virtual Instrument Engineering Workbench). In Section 7.2 it is provided an instruction manual of the software with detailed information on the program design and all its features.

7.2. SF-SMB(R) Unit Design

As mentioned in Chapter 2 (Section 2.7.2.), there are several modes of operation besides the Conventional SMBR, therefore, it is of best interest to build a unit as versatile and flexible as possible. With that in mind, the valve system strategy is a key factor when planning the assembly of a new unit.

The SMB unit comprises eight chromatographic columns, the minimum number of columns necessary to operate with more than one column per section. The distributed valve strategy was selected. It consists of a two-position valve-to-column design, with an additional two-position valve per column and an independent recycling line. The additional degrees of freedom provide the unit with the ability of operating with diverse number of columns, zones, and streams, zone bypass operation and independent ports switching.

The pressure and temperature of each column are individually monitored and registered by pressure sensors and thermocouples. The feed, desorbent and recycle flowrates are promoted by HPLC pumps and the extract and raffinate flowrates are regulated by Coriolis mass flow controllers.

The automation of the unit is performed by a LabVIEW program developed for this purpose. The user can define the operating parameters (inlet, outlet and recycling streams flowrates, pressure, temperature, unit configuration, and time switch) directly in the interface, as well as monitoring the process variables (flowrates, pressure, and temperatures).

7.2.1. The SMBR

The design of the unit in Figure 7.1 exhibits the configuration of the transfer lines within the unit.

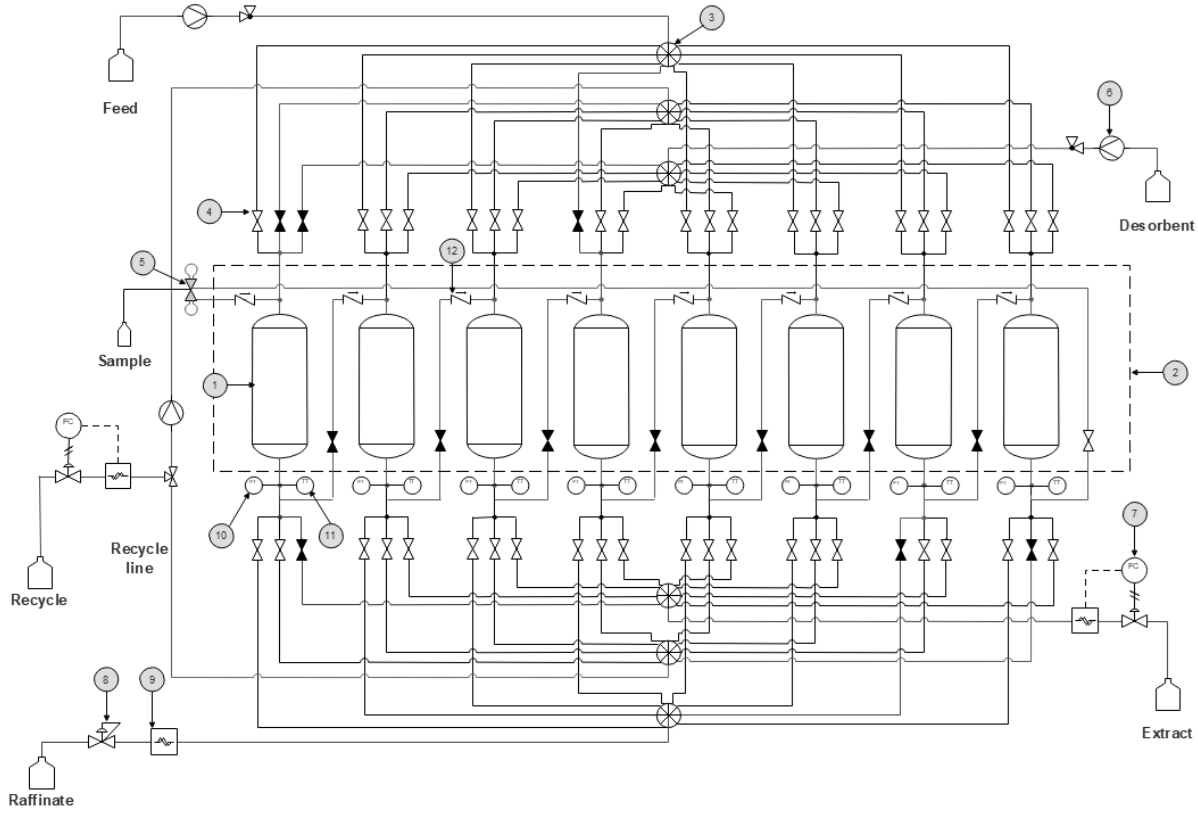

Figure 7.1. PFD of the SF-SMB(R). The image represents the first step of a closed loop operation (the filled valves represent closed valves).

As mentioned, the SMB unit comprises eight chromatographic columns (1) with a length of 15.0 cm and a diameter of 2.12 cm. A sintered stainless-steel filter (0.2 µm) was installed at the inlet and at the outlet of each column to avoid the eventual release of fines resulting from the solid phase material attrition, that could severely damage the remaining components of the unit or lead to the clogging of the transfer lines. The SF-SMB(R) was assembled in a custom-designed structure in which the columns are stowed in a polycarbonate casing (2) with a set of three resistances and air recirculating pump to assure the temperature control (Figure 7.2). The temperature set-point is controlled manually. The feed and the desorbent streams transfer lines cross the heat recirculation chamber of the unit providing a sufficiently large residence time to increase its temperature up to the operating setpoint value before being distributed in the manifolds.

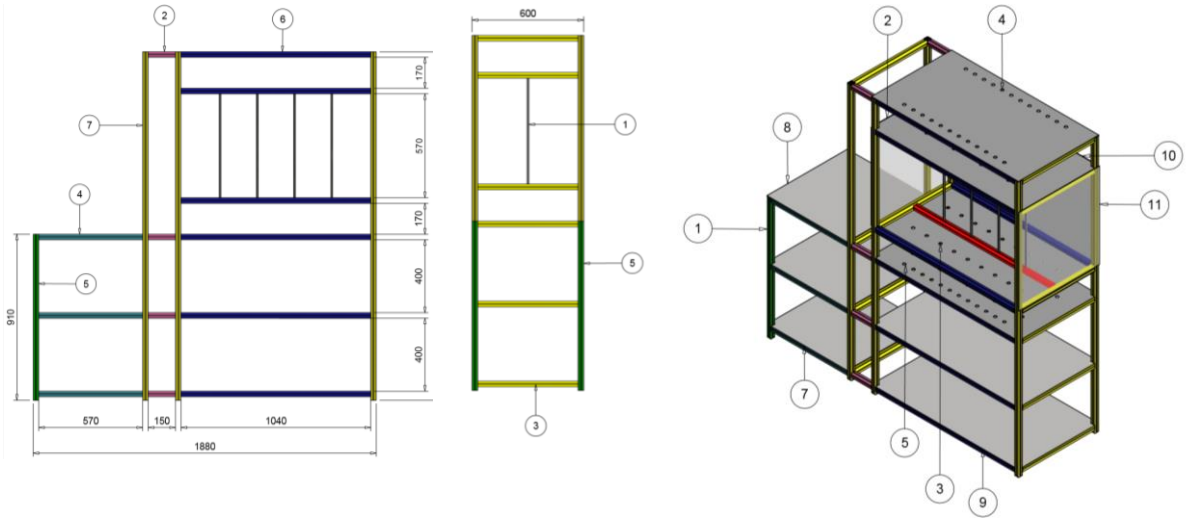

Figure 7.2. Structure of the SMBR.

Each external stream (feed - F, desorbent/eluent - E, raffinate - R and extract - X) is connected to an individual manifold (3) that distributes the said stream by a number of valves (4) equal to the number of chromatographic columns in the unit. These valves are then connected to the transfer lines between every two adjacent columns. A multiloop valve (5) installed between the eight and the first column enables the samples' collection.

The valve's setup in the top and bottom plates of the custom-designed structure follows the layout exhibited in Figure 7.3:

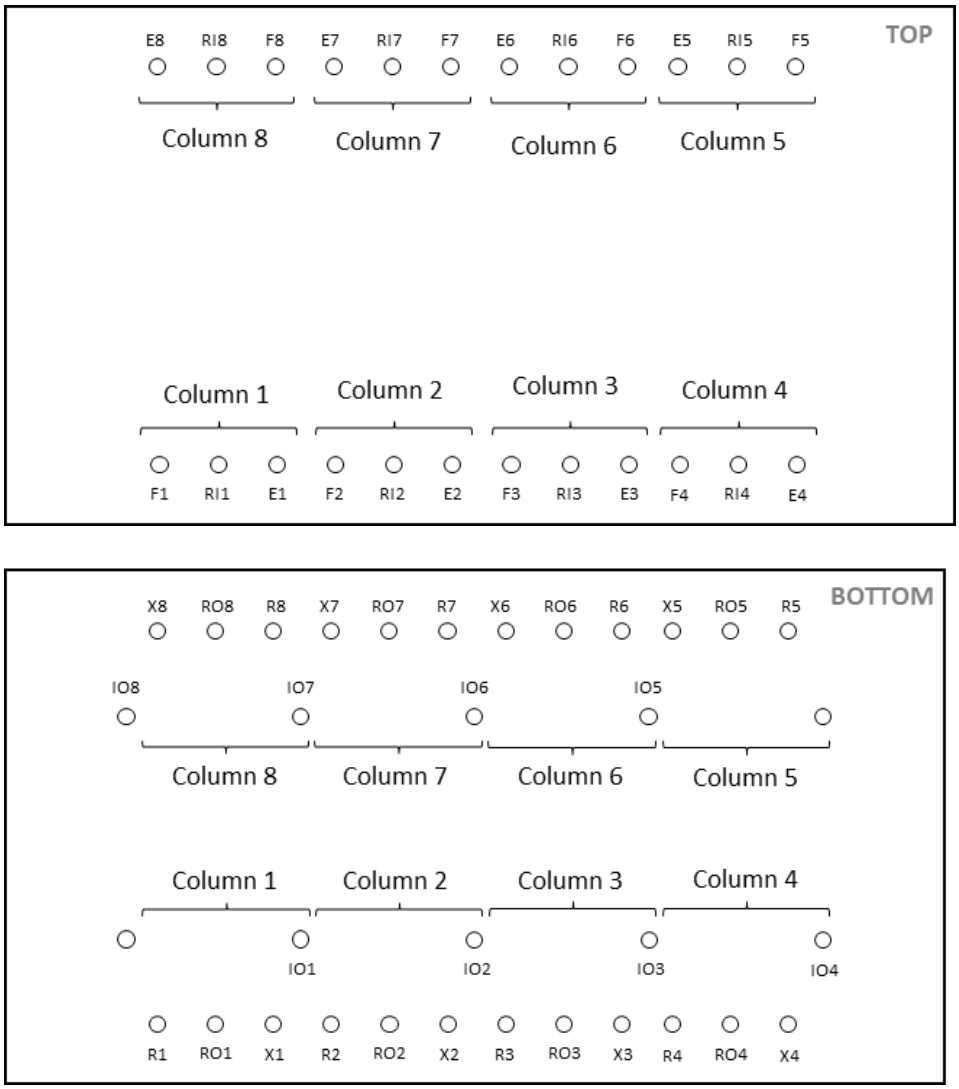

Figure 7.3. Valve setup on the top and bottom plates of the structure (F: feed, RI: recycle inlet, E: eluent, R: raffinate, RO: recycle outlet, X: extract, IO: intercolumn valve)

HPLC pumps (Knauer, BlueShadow 40P) (6) are used to set the feed and the desorbent streams flow rate. Two mass flow controllers (Bronkhorst, mini-CORI FLOW M14-AGD-11-0-S with RC200) (7) are used to regulate the flow of the outlet streams and a back-pressure regulator (Bronkhorst, EL-PRESS P-522C) (8) is used to define the operating pressure. To avoid variable flow rate recycling pumps that could generate undesirable disturbances in all the

sectional flow rates and compromise the separation, an independent recycling line is installed. Two mass flow meters (Bronkhorst, mini-CORI FLOW M14-AGD-11-0-S) (9) are positioned in the raffinate and in the recycle lines.

The temperature and pressure profiles within the unit are monitored by thermocouples (10) and pressure transducers (11) placed at the outlet of each column. To avoid backmixing, a problem likely to occur when using compressible fluids, lift check valves (12) were added to the lines between two adjacent columns near to the intersection between the outlet stream of one of the columns, the inlet stream of the following one and the feed/desorbent/recycling node. For safety reasons, two relief valves (13) were added after the HPLC pumps of the feed and desorbent streams.

All the transfer lines within the unit were made of 1/16'' stainless steel tubing (0.75mm i.d.) to control the dead volumes' dimension and distribution throughout the SMBR. Efforts were made to minimize the dead volumes inside the unit by resorting to technical dimensional drawings to analyse several hypothetical configurations. To manage he distribution of the dead volume through the unit, it is necessary to assure that all the fluid transfer lines associated with each column have equivalent lengths. For that purpose, the different transfer lines segments were cut in batches of eight similar elements. Figure 7.4 and Figure 7.5 show the transfer lines conceptualized through the dimensional drawings and the actual transfer lines installed in the unit near the inlet streams manifolds and near the outlet streams manifolds, respectively.

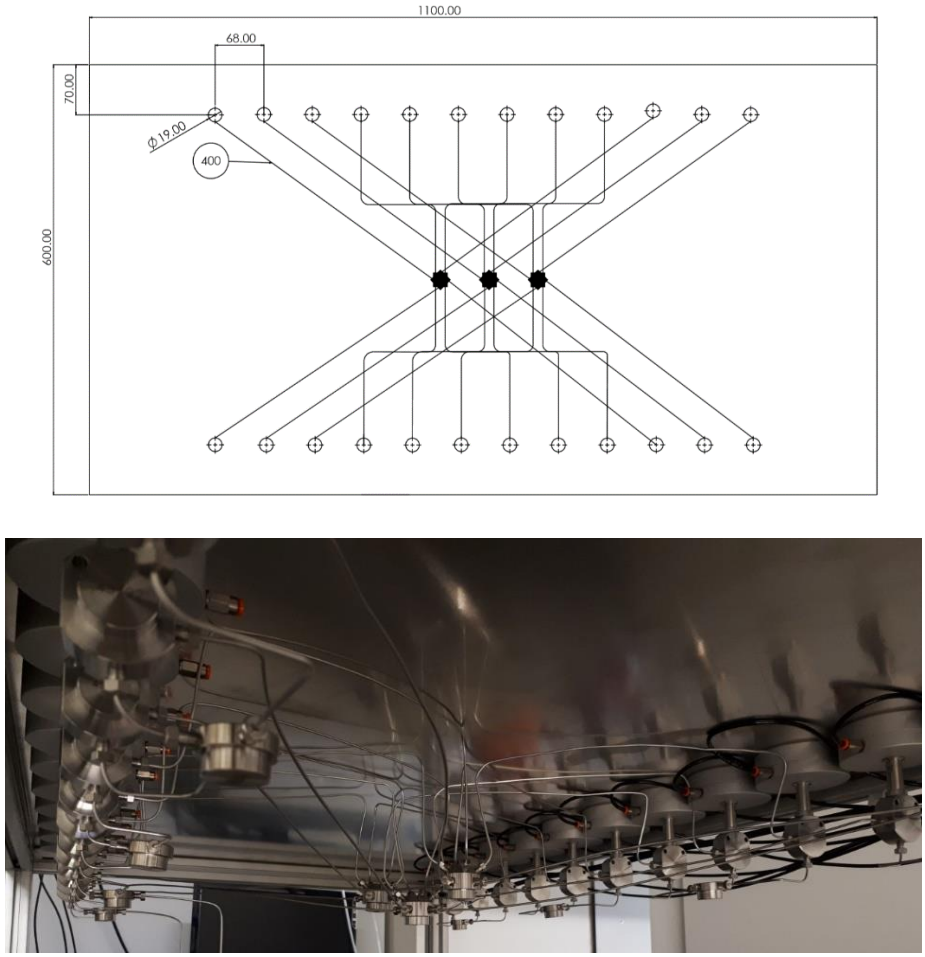

Figure 7.4. Technical drawing and actual transfer lines of the top of the SMBR.

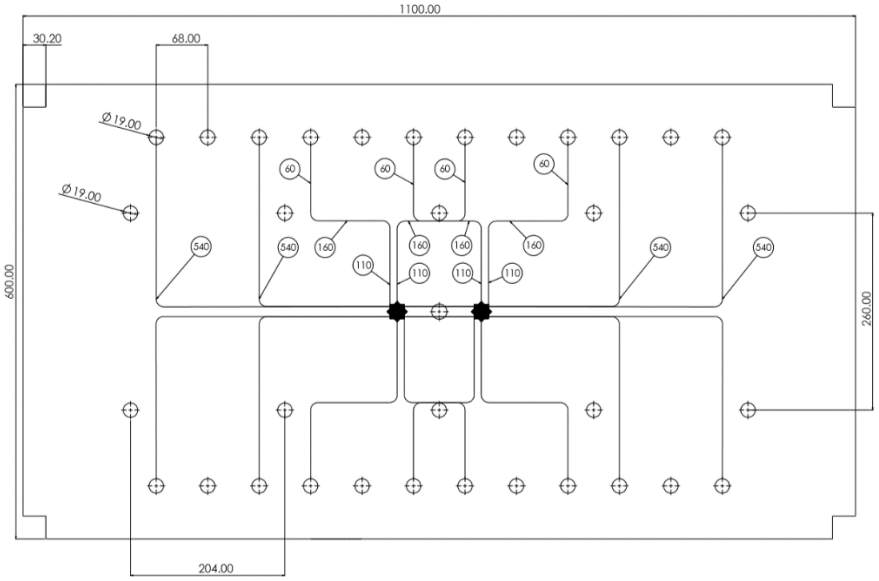

Figure 7.5. Technical drawing and actual transfer lines of the bottom of the SMBR.

The maximum operating temperature and pressure of the unit are 333 K and 200 bar, respectively. The feed, desorbent and recycling flow rates are limited to 50 $mL \cdot min^{-1}$. The list of all equipment installed is presented in Table 7.1, and the most relevant technical specifications of each of them is presented in Annex A. Nonetheless, it is recommended that the users read carefully the manuals provided by the manufacturers prior to performing any experiments.

Finally, the complete SF -SMB(R) is exhibited in Figure 7.6, along with the electrical assembly.

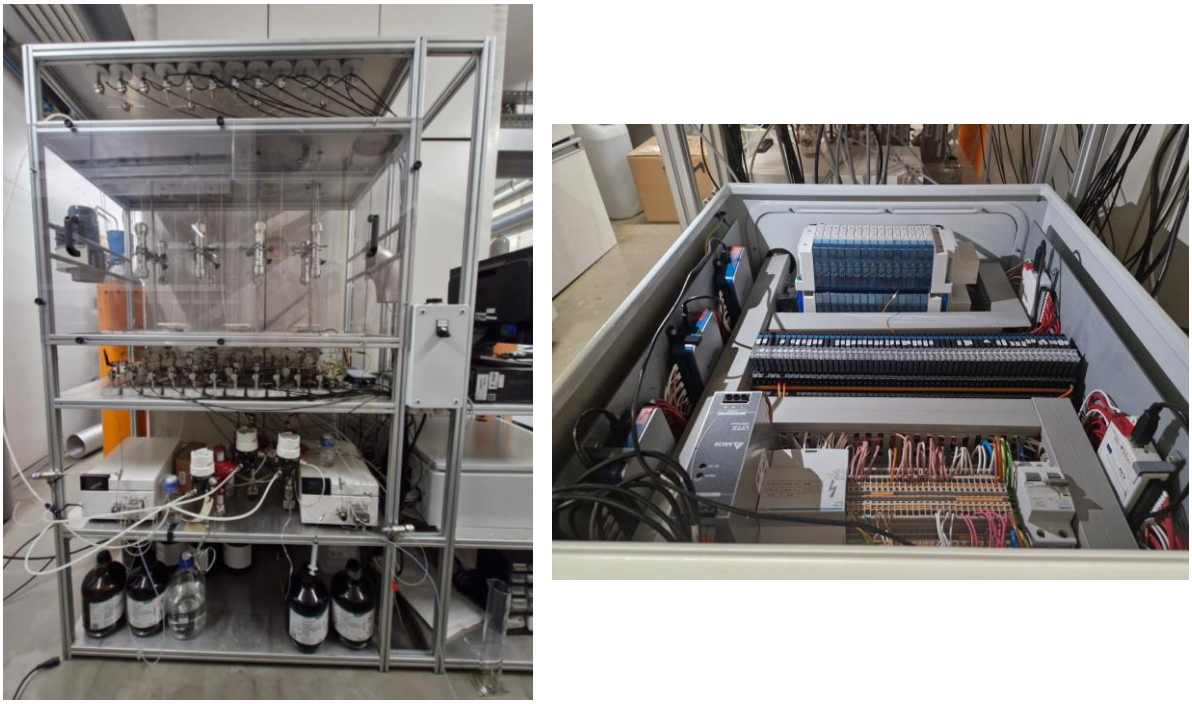

Figure 7.6. The SF -SMB(R) and its electrical case.

Table 7.1. Equipment installed in the SF-SMB(R) unit.

Equipment	Model	Un.	Manufacturer
Column	96520	8	Alltech
Two-way valve	EMT6CSD12UW	56	Vici-valco, Switzerland
Check valve	SS-53S4	8	Swagelok Company
Relief Valve	SS-4R3A		Swagelok Company
Multiloop valve	2C8UW	1	Vici-valco, Switzerland
Manifold	Z8M1	5	Vici-valco, Switzerland
HPLC pump	BlueShadow Pump 40P	3	KNAUER
Pressure transducer	M5200	8	TE Connectivity
Thermocouple	Type K - 397-1264	8	RS Components Ltd.
Coriolis flow meter	M14-AGD-11-0-S	3	Bronkhorst High-Tech BV
Control Valve	RC200	3	Badger Meter
Signal converter	TEIP11-PS	3	ABB
Back pressure regulator	EL-PRESS P-522C	1	Bronkhorst High-Tech BV
Acquisition Board NI 6501	USB-6501	1	National Instruments Corp.
Acquisition Board NI 6008	USB-6008	1	National Instruments Corp.
Acquisition Board NI 6001	USB-6001	3	National Instruments Corp.
Chassis cDAQ-9171	cDAQ-9171	1	National Instruments Corp.
Acquisition Board NI 9212	NI-9212	1	National Instruments Corp.
USB to RS232 converter	ICUSB2324		STARTECH
Five port solenoid valve	SMC – SY 3A00-5U1	60	SMC Pneumatics
DIN rail power supply 24VDC	DRL-24V120W1AA	1	Delta Electronics
Fittings, tubing, accessories			Vici-valco, Switzerland/ Swagelok

Finally, two additional advantages of the developed SMBR unit must be highlighted. First, all the equipment and materials used in its construction are also suitable for the implementation of supercritical SMB(R) processes. Furthermore, several unconventional operating modes can be implemented in this unit, as the Multifeed SMBR (accomplished through the addition of Section IIIB) and the ModiCon, two strategies studied in the Thesis. Depending on the operating strategy, it may be necessary to implement minor adjustments to the system.

7.2.2. Dead Volumes

The dead volume is something to be considered since the design of the unit. It is detrimental to the process, but it is inevitable and should be minimized. One of the strategies to reduce it is to use zero dead volume fittings and connectors (i.e., tees, crosses, and manifolds), as the ones used in the SF-SMB(R). This way, considering the lines are assembled correctly, one may account only for the dead volume of tubes, valves, and pumps. The overall dead volumes of the SF-SMB(R) are presented in Table 7.2.

Table 7.2. SF-SMB(R) dead volumes.

Component	Units	Unitary Dead Volume (mL)	Total Dead Volume (mL)
External tubing	-	-	5.29
Internal tubing	-	-	6.09
On/Off Valves	48	0.002	0.96
Cross	8	0.058	0.46
Sampler	1	1.00	1.00
Recycle Pump	1	1.28	1.28
Control valves (RC200)	2	3.61	7.22
Check Valves	8	0.32	2.58
Coriolis flow meter (M14-AGD-11-0-S)	3	7.91	23.73
Back pressure regulator (EL-PRESS P-522C)	1	6.54	6.54
Column Volume (mL) *	8	52.95	423.58
Dead Volume (mL - %)			57.90 -13.6%

* Considering a column of 15 cm of height and 2.12 cm of i.d.

The major disadvantage of units with distributed valve design strategy, as the SF-SMB(R), is the large dead volume due to the need of so many lines and valves. This effect is reduced by using pneumatic on/off valves with very small internal volume (2 μL). Nonetheless, the unit still has 13.6% of dead volume. This value is within the range for lab-scale units, as the FlexSMB-LSRE ®, which has 11% of dead volume [1]. For pilot and industrial-scale units, this value is reduced to around 3% [2].

At this point, it is relevant to mention that there are two main types of dead volume in an SMB(R) unit depending on their location: internal dead volume, and external streams dead volume. The compensating strategies depend on the type of dead volume. The main consequence of external streams dead volume is cross-contamination of the outlet streams. This

affects more harshly systems where the streams share lines or manifolds, as units with central valves, for instance. Contamination of the inlet and outlet streams is greatly avoided in units with distributed valve strategy, as the SF-SMB(R).

The inline dead volumes include tubing between columns, check valves, recycling pump and bed voids [2-4]. To minimize the dead volume in the unit, especially inline dead volume, tubes with small diameter were used (1/16”). This led to a high pressure drop in the SF-SMB(R). All the components and equipment were designed to handle high pressures aiming to avoid that the pressure drop imposed limitations on the operation and, of course, to allow experiments to be carried in supercritical conditions. The control valves, for instance, can undertake a maximum pressure of 340 bar.

High pressures, however, may compact the packing bed, which generates an extra bed void in the columns. This is aggravated by the fact the columns are packed with water because of the hydrodynamic studies, and the resin is at its maximum swelling when in water. Therefore, the shrinking of Amberlyst-35 when in contact with the reactional mixtures also leads to an extra bed void volume. Furthermore, it is essential to use filters in units with tubes of such a small diameter to avoid clogging of the lines.

Still regarding the system pressure, the robustness, speed, and reliability of a control system improve when the set point is closer to the midpoint between the Upper and Lower Control Limits.

The dead volume issue is aggravated if severe mixing occurs, as consequence of using check valves and pumps, for instance, that create large local dead volumes where axial dispersion is likely to occur [2, 3]. The most straightforward approach is to simply not include these types of equipment in between columns [3]. This, however, was not possible for the SF-SMB(R) due to the necessity of including a recycling pump between the last and the first columns to guarantee the operation in closed-loop. Besides, since this unit was built to operate with

supercritical fluids, which are sensitive to pressure variations and present liquid and gas properties, it is imperative to include check valves that prevent the backwards flow to guarantee the correct operation and the integrity of the unit.

7.2.3. Automation

The automation and control of the unit was performed by a LabVIEW (National Instruments, USA) program, because it is a robust and flexible software, and provides a user-friendly interface. Indeed, the conceptualization of a flexible program that can be adapted to diverse operating strategies is as relevant as the assembly of the unit. In the building of the SF-SMB(R), the automation software and the physical equipment were planned concurrently.

The communication with the valves, pressure transducers and thermocouples was performed by three multifunctional boards NI USB-6001 (8 analog inputs, 2 analog outputs, and 13 I/O digital channels), one NI USB-6008 (8 analog inputs, 2 analog outputs, and 12 I/O digital channels), one NI USB-6501 (24 I/O digital channels) and one cDAQ-9171 CompactDAQ Chassis with a NI 9212 module installed (8 thermocouples input channels). cDAQ9171 and NI9212 are exclusively dedicated to the acquisition of the thermocouples data. The communication with the mass flow meter, the mass flow controllers, and the back pressure regulator is performed by RS-232. The detailed electrical scheme is available in Appendix C.

Two-way valves

As mentioned at the beginning of the Chapter, the distributed valve design was selected for the SF-SMB(R) due to the flexibility of operating with diverse non-conventional SMB(R) strategies. Therefore, the unit adopted a two-position valve-to-column design, with an additional valve located between every two adjacent columns and an independent recycling circuit. Hence, the unit contains a total of 56 valves, actuated pneumatically, for safety reasons, as it may operate with flammable liquids. The valves actuation time is below 1s and the air

supply to the valves (between 3 to 6 bar) is controlled by a module of 56 five port solenoid valves (SMC – SY 3A00-5U1). The digital signal required to actuate the solenoid valves is provided by the NI USB-6501, the NI USB-6008 and two NI USB-6001 multifunctional boards, accordingly to Table 7.3. The power supply is provided by a DIN rail power supply of 24VDC (DRL-24V120W1AA).

Table 7.3. Two-way valve connections, physical correspondence, and codes to LabView program.

Channel	Valve Code	Solenoid Valve		LabView Code	Valve Nº
		Wire Colour	Wire Mark		
6501.01.P01.0	F01	Orange	- Red	I2	Valve1
6501.01.P01.1	RI01		- Black	I3	Valve2
6501.01.P01.2	E01	Light Gray	- Red	I1	Valve3
6501.01.P01.3	R01		- Black	O2	Valve4
6501.01.P01.4	RO01	White	- Red	O3	Valve5
6501.01.P01.5	X01		- Black	O1	Valve6
6501.01.P01.6	IO01	Yellow	- Red	R0	Valve7
6501.01.P01.7	F02		- Black	I2	Valve8
6501.01.P02.0	RI02	Pink	- Red	I3	Valve9
6501.01.P02.1	E02		- Black	I1	Valve10
6501.01.P02.2	R02	Orange	-- Red	O2	Valve11
6501.01.P02.3	RO02		-- Black	O3	Valve12
6501.01.P02.4	X02	Light Gray	-- Red	O1	Valve13
6501.01.P02.5	IO02		-- Black	R0	Valve14
6501.01.P02.6	F03	White	-- Red	I2	Valve15
6501.01.P02.7	RI03		-- Black	I3	Valve16
6501.01.P03.0	E03	Yellow	-- Red	I1	Valve17
6501.01.P03.1	R03		-- Black	O2	Valve18
6501.01.P03.2	RO03	Pink	-- Red	O3	Valve19
6501.01.P03.3	X03		-- Black	O1	Valve20
6501.01.P03.4	IO03	Orange	--- Red	R0	Valve21
6501.01.P03.5	F04		--- Black	I2	Valve22
6501.01.P03.6	RI04	Light Gray	--- Red	I3	Valve23
6501.01.P03.7	E04		--- Black	I1	Valve24

6008.01.P0.0	R04	White	--- Red	O2	Valve25
6008.01.P0.1	RO04		--- Black	O3	Valve26
6008.01.P0.2	X04	Yellow	--- Red	O1	Valve27
6008.01.P0.3	IO04		--- Black	R0	Valve28
6008.01.P0.4	F05	Pink	--- Red	I2	Valve29
6008.01.P0.5	RI05		--- Black	I3	Valve30
6008.01.P0.6	E05	Orange	- Red	I1	Valve31
6008.01.P0.7	R05		- Black	O2	Valve32
6008.01.P1.0	RO05	Light Gray	- Red	O3	Valve33
6008.01.P1.1	X05		- Black	O1	Valve34
6008.01.P1.2	IO05	White	- Red	R0	Valve35
6008.01.P1.3	F06		- Black	I2	Valve36
6001.01.P0.0	RI06	Yellow	- Red	I3	Valve37
6001.01.P0.1	E06		- Black	I1	Valve38
6001.01.P0.2	R06	Pink	- Red	O2	Valve39
6001.01.P0.3	RO06		- Black	O3	Valve40
6001.01.P0.4	X06	Orange	-- Red	O1	Valve41
6001.01.P0.5	IO06		-- Black	R0	Valve42
6001.01.P0.6	F07	Light Gray	-- Red	I2	Valve43
6001.01.P0.7	RI07		-- Black	I3	Valve44
6001.01.P1.0	E07	White	-- Red	I1	Valve45
6001.01.P1.1	R07		-- Black	O2	Valve46
6001.01.P1.2	RO07	Yellow	-- Red	O3	Valve47
6001.01.P1.3	X07		-- Black	O1	Valve48
6001.02.P0.0	IO07	Pink	-- Red	R0	Valve49
6001.02.P0.1	F08		-- Black	I2	Valve50
6001.02.P0.2	RI08	Orange	--- Red	I3	Valve51
6001.02.P0.3	E08		--- Black	I1	Valve52
6001.02.P0.4	R08	Light Gray	--- Red	O2	Valve53
6001.02.P0.5	RO08		--- Black	O3	Valve54
6001.02.P0.6	X08	White	--- Red	O1	Valve55
6001.02.P0.7	IO08		--- Black	R0	Valve56

HPLC Pumps

The feed, desorbent and recycling streams are delivered by a conventional HPLC pump. The recycling pump (from 0 to 50 $mL \cdot min^{-1}$) was installed in the middle of the recycling loop.

Flow meters and controllers

Coriolis mass flow meters/controllers (Brockhorst mini-CORI FLOW M14-AGD-11-0-S) were used in this unit to register and control the flow rate of the SMBR outlet streams, in a range comprised between 1 $mL \cdot min^{-1}$ and 50 $mL \cdot min^{-1}$, and with an accuracy of 0.2%.

The data acquisition from the Coriolis Mass Flow Meters & Controllers (mini-CORI FLOW M14-AGD-11-0-S) is via RS232 because Bronkhorst High-Tech BV delivers a free and user-friendly driver that allows a thorough configuration of the equipment. Besides, the connection is more stable, and it is easier to identify and correct errors in case any maintenance is needed.

To communicate with this equipment, it is necessary to supply power directly from the DIN rail power supply and send/receive information directly from the computer via RS232. Since the supply of power and information comes from different sources, it is necessary to use the M12 8p A-coded T-adapter (serial number 7.03.773) from Bronkhorst High-Tech BV to connect cable RS232 M12-A 8p sub D9 female (serial number 7.03.778) to the computer and cable PiPS-IN-8DIN to the power supply. Only pins 2 and 3 from the RS232 are used to transmit and receive information from the flow meters, respectively.

An RC200 valve from Badger Meter was coupled to the mass flow controllers to regulate the flow. Since the RC200 is pneumatically actuated, the signal converter TEIP11-PS is required to convert the standard electrical signals into pneumatic signal.

To control the pressure inside the unit a Bronkhorst back pressure regulator (EL-PRESS P-522C), which was also coupled to an RC200 Badger Meter valve (and a TEIP11-PS signal converter), was installed at the end of the raffinate line.

Pressure and temperature measurement

A pressure transducer (TE Connectivity, U5272) and a thermocouple (Type K) were placed at the outlet of each chromatographic column to monitor the internal pressure and temperature profiles of the SMBR. As previously indicated, NI USB-6001 boards are used to record and convert the analog output of the pressure transducers (0-5V) while the NI USB-9212 module is exclusively used to register the system temperature. The pressure transducer measurement range is comprised between 1 and 350 bar, presenting an accuracy of 0.1%.

Table 7.4. Pressure transducers and thermocouples connections.

Pressure Transducers		**Thermocouples**	
Channel	**Equipment**	**Channel**	**Equipment**
6001.01.AI0	PT1	**9212.01.TC0**	TC1
6001.01.AI1	PT2	**9212.01.TC1**	TC2
6001.01.AI2	PT3	**9212.01.TC2**	TC3
6001.01.AI3	PT4	**9212.01.TC3**	TC4
6001.02.AI0	PT5	**9212.01.TC4**	TC5
6001.02.AI1	PT6	**9212.01.TC5**	TC6
6001.02.AI2	PT7	**9212.01.TC6**	TC7
6001.02.AI3	PT8	**9212.01.TC7**	TC8

7.3. The SF-SMB(R) Software

A LabVIEW program was built for the automation and control of the unit. As mentioned, it provides a user-friendly interface for the user. Four pages were conceived and developed for the complete configuration and further operation of the SF-SMB(R). Each of them will be thoroughly explained in the following sections.

7.3.1. System configuration

In this page (Figure 7.7), the user sets the number of columns installed and the inlet and outlet streams that will be used in the experiment. The inlet streams may be Eluent, Feed, Recycle and Additional Stream (for the case of Multifeed operation). The outlet streams may be Extract,

Raffinate and Recycle. It is noteworthy that the system cannot operate in closed loop when the Multifeed strategy is used, once one of the inlet streams must be dedicated to the second feed stream.

In the second subsection of this page, the user sets the calibration parameters for all the pressure transducers and for the Coriolis mass flow meters/controllers.

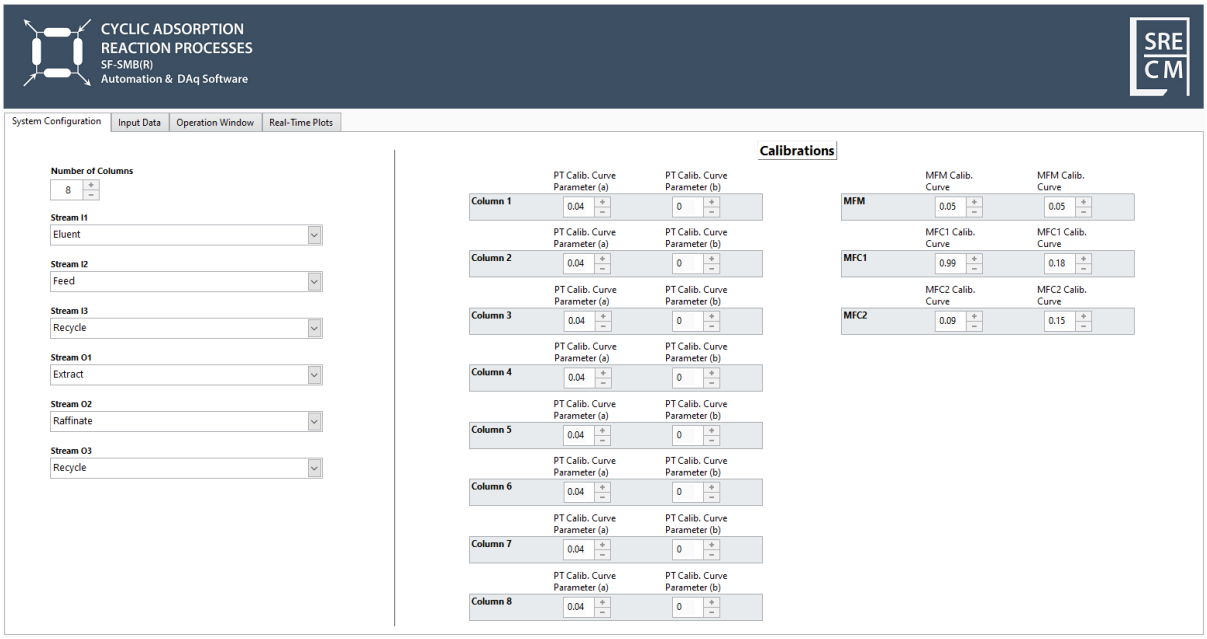

Figure 7.7. System Configuration interface of the SF-SMB(R).

7.3.2. Input data

This a page dedicated to setting up the experiment parameters (Figure 7.8). Most of the conditions necessary to run the SF-SMB(R) are set in this interface, as operation mode, switching time, column configuration, initial and final flow rates and unit's operational pressure. The operation modes available are SMB(R) Conventional, SMB(R) Open Loop, Multifeed Open Loop SMB(R), Varicol SMB(R), Flow rate Modulation SMB(R) and the combination between Multifeed and Flow rate Modulation SMB(R). More modes of operation can be added in the LabVIEW program. The fields that the user must fill before starting the experiment are clearly indicated after selecting the operating mode. It is also possible to operate with a custom-made sequence created in other software (Microsoft Excel, for instance) by

importing it in the File Selection field and pressing the Create Sequence button. After filling all the necessary fields, the user must press the "Locked" button to avoid that the sequence is modified by accident during the experiment (the user will be required to do so in case he/she has forgotten before starting in an experiment).

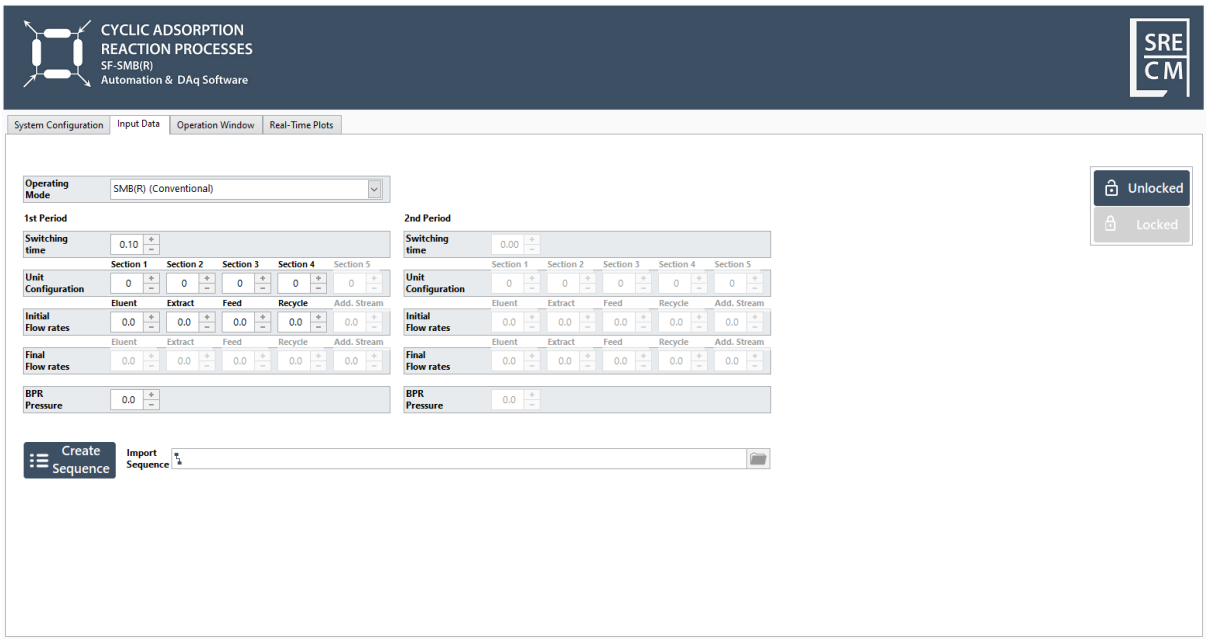

Figure 7.8. Input Data interface of the SF-SMB(R).

7.3.3. Operation Window

This is the main page of the program (Figure 7.9), as it summarizes all the information acquired from the Coriolis mass flow meters/controllers and from the NI Data acquisition boards. It is also where the user can perform modifications to the set-points of the mass flow controllers and back pressure regulator.

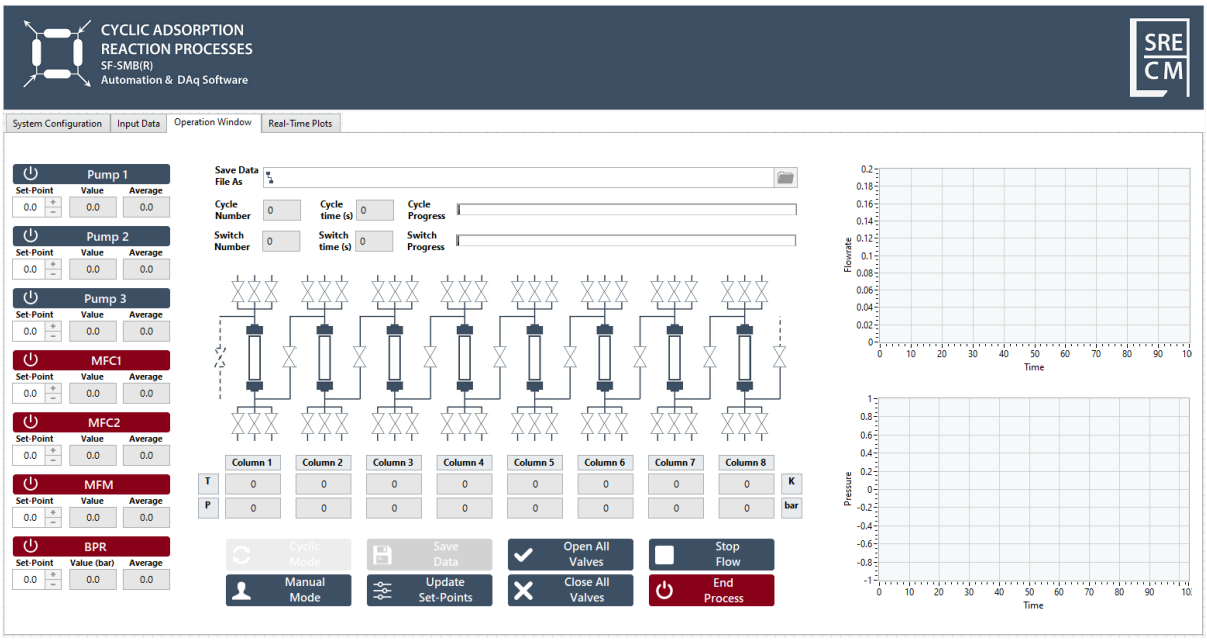

Figure 7.9. Operation Window interface of the SF-SMB(R).

There are two operation modes: Manual Mode and Cyclic Mode. The first mode was conceived for performing tests to individual components of the unit once it is possible to manipulate the state of each of them individually. It is useful for testing all two-way valves individually and performing calibrations, for instance.

The Cyclic Mode button is only available for the user when the Locked button from the Input Data (Figure 7.8) interface is selected. By doing this, the user is also required to select a file where the experimental data will be saved. After completing this step, the input from the previous interface is automatically set and the experiment effectively begins. The user can assess the cycle and switch number and the development of these variables by the progress bars. There were also included graphs for the user to follow the flow rate measurements from the mass flow meters and pressure variations from the pressure transducers. During the Cyclic Mode, the user cannot modify the state of the two-way valves or turn off the mass flow meter/controller, but he/she can update the set-points. The Stop Flow button was added for safety reasons in case of emergencies that require the immediate interruption of the process, as

overpressure, for instance. When the experiment finishes, the user may press the End Process button to stop the LabVIEW program. It is noteworthy that the user is never asked to inform the number of cycles he/she wants to perform, therefore the end of the process is not automated and the user must perform all the steps to finalize an experiment (as described in Section 7.5.2.).

7.3.4. Real-Time Plots

This interface summarizes the main process variables that the user must consider for confirming the process in running safely. The flow rates from the HPLC pumps and the ones measured by the Coriolis mass flow meters/controllers are shown in the External and Internal Flowrates graphs respectively. The program also gives information on the pressure and temperature from the pressure transducers and thermocouples. This interface was mainly conceived for the user to have a comprehensive sight of the process, once it will expose any pressure loss due to leakage, overpressure due to obstructions, overtemperature due to an uncontrolled adsorption or reaction and unexpected flowrate variation that could severely impact the process and even damage the SF-SMB(R).

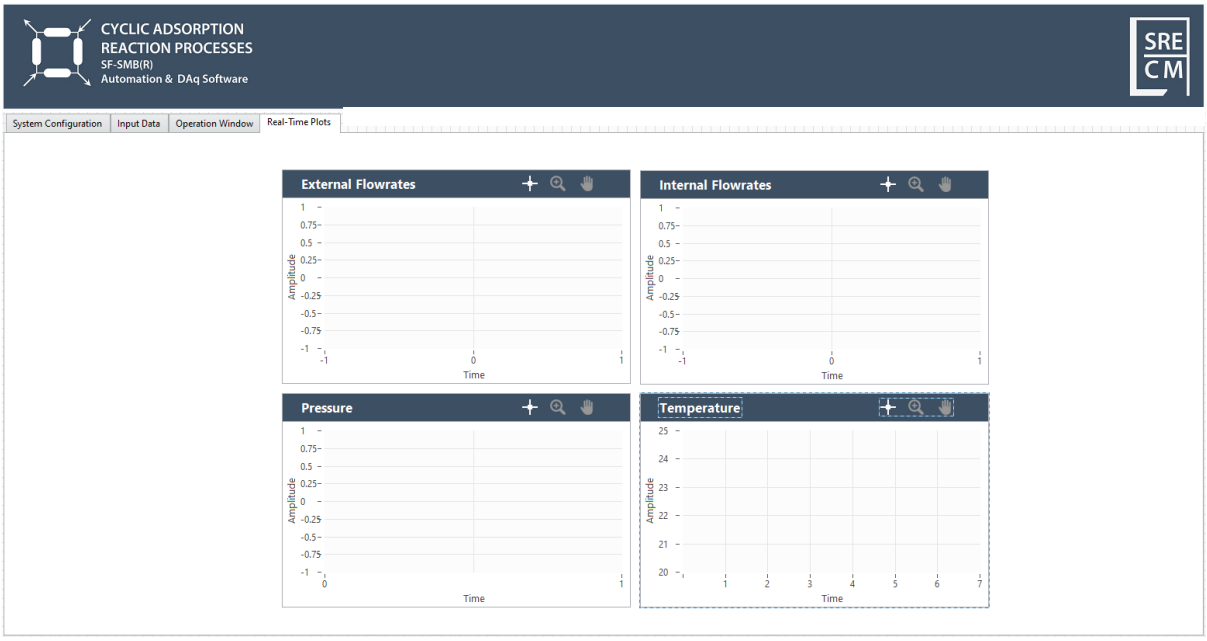

Figure 7.10. Real-Time Plots Window interface of the SF-SMB(R).

7.4. Adaptations to operate under supercritical conditions

As mentioned, one of the greatest features of the SF-SMB(R) is its ability to operate under supercritical conditions. This type of unit requires a much more precise control system and reliable equipment that responds quickly and well to commands of the control system. Besides, all elements must handle high pressures. Indeed, the additional care required by supercritical equipment is usually related to preventing sudden depressurization spots and handling depressurization appropriately when it is inevitable, as in the outlets of the SMBR. The consequences of faults of the control system are usually irremediable for the experiment, which leads to material and immaterial losses, and may be of great risk for the integrity of the equipment and of the user. Therefore, operating the SF-SMB(R) under supercritical conditions required some adaptation on both, physical equipment and automation and control software.

The modification required in the automation and control software is to prevent the abrupt response of the control valves. This would lead to disturbances in all the concentration front that most probably would ruin any experiment. A new Driver Virtual Instrument (DVI) was developed with the purpose of limiting the opening of the control valve. This way, the user can input a value up to 100% (which is the default and means the valve can be completely opened) that would change the range of aperture of the control valve, similarly to what is done manually when using a needle valve. By limiting the opening of the control valve, one prevents sudden depressurization when the software sends a signal to open the outlet valves. The determination of the appropriate aperture limit must be accompanied by a careful examination of the response of the system in terms of pressure, once limiting it too much could lead to an overpressurization.

To reduce the effects of abrupt depressurization and to improve the response of the MFC and BPR, needle valves (Swagelok SS-SS1-VH) (1) were installed on the outlet streams, after the control valves, and on the outlet of the multiloop valve (for sample collection). This promotes the stepwise depressurization of these streams. A ball valve (Swagelok SS-2P4T) was installed

at the inlet of the multiloop valve to prevent the sample from escaping by this way when changing the position of the multiloop. All needle valves are heated by heating resistance strips (2) controlled by a thermostat, to prevent ice clogging, caused by the Joule–Thomson effect. This control system is independent from the main automation and control software.

The CO_2 pump head (3) and the CO_2 tube from the bottle are cooled to ensure this compound enters the pump in liquid state, and that it continues liquid during the pumping, avoiding cavitation. Just after the CO_2 pump, there is a relief valve regulated to release the pressure if it exceeds 180 bar. The SF-SMB(R) is only able to operate in open loop, once the depressurized CO_2 from the outlet streams is released to the atmosphere.

Finally, it is essential to select a proper outlet collection strategy, once the samples leave the system with high velocity due to depressurization, even after going through the first depressurization step. Collecting the samples in a liquid trap is one of the simplest and most straightforward strategies, besides the advantage of not requiring investment in any additional equipment, as sample collection vessels and cyclones. This strategy consists in submerging the end of the outlet tube in a recipient containing a solvent that has low volatility, as dimethyl sulfoxide and ethyl acetate. The system will bubble due to the release of CO_2 and the liquid species will be entrapped by the solvent. For selecting the appropriate solvent, one must have in mind the solubility of the sample within the solvent and the analysis method.

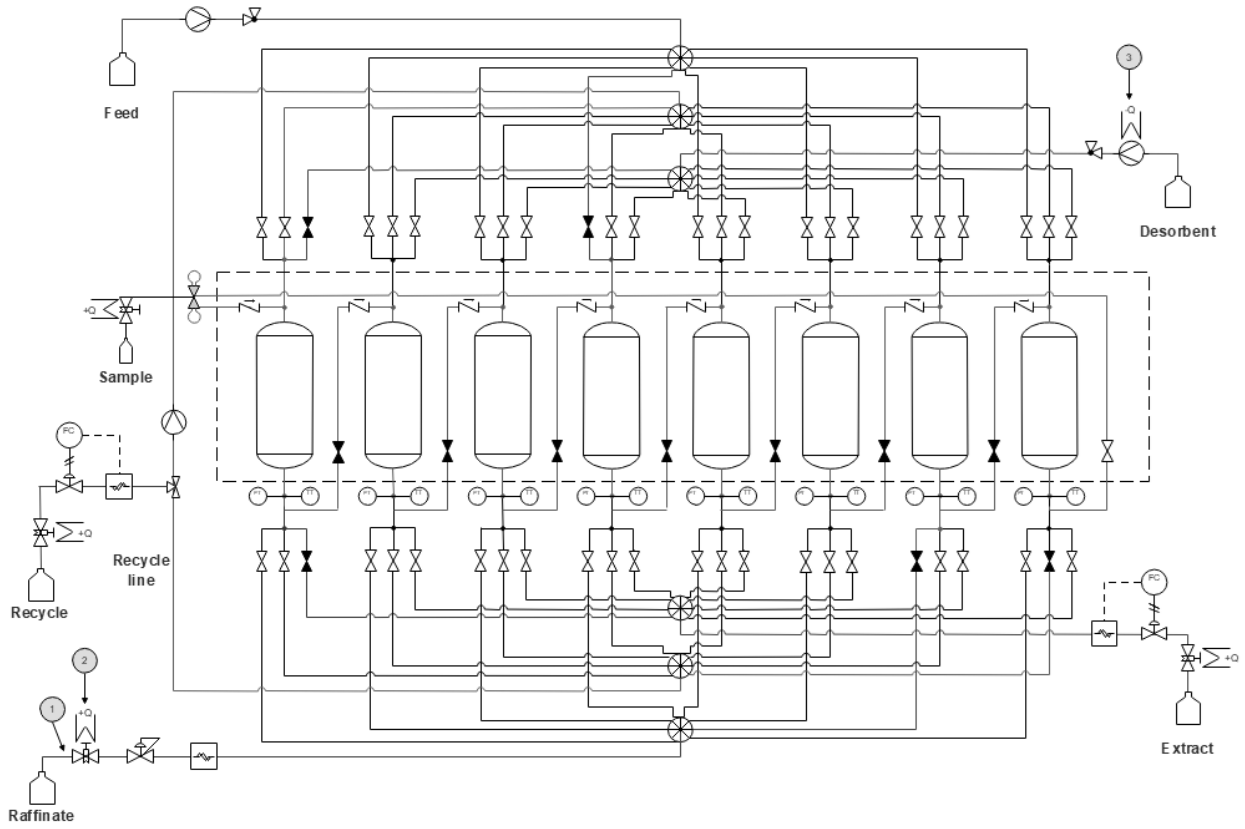

Figure 7.11. PFD of the SF-SMB(R) with the adaptations to operate under supercritical conditions.

7.5. Operating the SF-SMB(R)

Before starting an experiment, the user must guarantee that all pressure transducers and mass flow meters are correctly calibrated, at least one outlet is unobstructed, the system is stabilized with the solvent and compressed air is supplied to the unit. Then, the experiment may be initiated.

7.5.1. Starting an Experiment

1. Switch on the SF-SMB(R) by turning the key on the electrical case.
2. Switch on the HPLC pumps.
3. Switch on the temperature controller on the structure where the columns are located and set the desired temperature.
4. Switch on the PC and the LabVIEW interface.

5. Start the software pushing the start routine button on the top of the LabVIEW window.
6. Correct the calibration parameters in the System Configuration interface, if necessary.
7. Select the mode of operation in the Input Data interface, fill the boxes that become available (switching tome, column configuration, flow rates) and press the Locked button.
8. Purge the Feed and Eluent pumps.
9. In the Operation Window interface, create a file or select a pre-existent file where the experimental data will be saved.
10. Update the pump set-points, the mass flow meters/controllers and the back pressure regulator and press the Update Set Points button.
11. When ready, press the Cyclic Mode button to effectively start the experiment. Automatically the two-way valves will be opened/closed.

7.5.2. Finishing an experiment

1. When the experiment is finished, change the mode of operation to Manual by pressing the button. Make sure at least one outlet valve remains open.
2. Switch off the temperature controller.
3. Diminish the flow rate of the HPLC pumps.
4. Change the state of the two-way valves to closed to isolate the system and immediately stop the pumps. Then switch off the pumps.
5. Stop the software pushing the stop routine button on the top of the LabVIEW window.
6. Switch off the PC.
7. Switch off the SF-SMB(R) by turning the key on the electrical case.

7.6. Conclusion

Assembly of such complex equipment as the SF-SMB(R) is a task that demands much more than technical skills. Heuristics, problem-solving, communication, time management and patience are some examples of abilities that must be developed to succeed and produce a useful, reliable and robust plant. Nonetheless, technical skills are still the most important part of the process, both because of the assembly of the physical equipment requires a deep know-how on the fundamental processes that will take place inside the unit, and because the development of completely novel automation and control software requires great programming knowledge.

Hopefully the SF-SMB(R) will be used to foster investigations on non-conventional strategies for the simulated moving bed research.

7.7. References

1. Sá Gomes, P.M.d., *Advances in simulated moving bed: new operating modes; new design methodologies; and product (FlexSMB-LSRE ®) development.*, in *Chemical Enginnering Department*. 2009, Univeristy of Porto: Repositório Aberto da Universidade do Porto.
2. Faria, R.P. and A.E. Rodrigues, *Instrumental aspects of Simulated Moving Bed chromatography.* J. Chromatogr. A, 2015. **1421**: p. 82-102.
3. Migliorini, C., M. Mazzotti, and M. Morbidelli, *Simulated moving-bed units with extra-column dead volume.* AIChE Journal, 1999. **45**(7): p. 1411-1421.
4. Lim, Y.-I. and S.K. Bhatia, *Effect of dead volume on performance of simulated moving bed process.* Adsorption, 2011. **17**(1): p. 109-120.

Chapter 8

Experimental Validation of Solketal Synthesis on the SF-SMB(R)

8.1. Introduction

The Simulated Moving Bed Reactor (SMBR) is a Process Intensification strategy that combines chemical reaction and separation by adsorption in a single unit. The purely separative Simulated Moving Bed (SMB) is already an intensive mass transfer device, and the technology was upgraded by adding a reaction process, originating this multifunctional reactor. The SMBR overcomes the limitations of both reaction and separation process, surpassing the chemical equilibrium and avoiding the formation of azeotropes. By removing one of the reaction products, one can prevent parallel reactions and obtain purer and more concentrated outlet streams, which diminishes the use of desorbent and downstream separation costs [1]. The process is beneficial for thermodynamically limited reactions, such as the solketal synthesis from glycerol and acetone, because it enables the equilibrium shift in favour of product formation by adsorbing one of the reaction products [2].

The SMBR was developed as the practical implementation of the True Moving Bed Reactor (TMBR), a more efficient process derived from traditional batch chromatography. The movement of the solid enhances the separation: as the fluid phase moves in one direction, carrying the less retained component, which is removed in the raffinate stream, the solid phase moves in the opposite direction, carrying the more retained one, in turn, removed in the extract stream. This operation enhances the productivity by maximizing the separation driving forces and the use of the stationary phase and minimizing the desorbent consumption [3]. Besides, it enables much more difficult separations that, otherwise, with the traditional chromatography, could not be accomplished [4].

The downside of the TMB operation is the movement of particles inside the columns, which could lead to equipment damage and particle breakage due to abrasion and prevent the satisfactory desorption of the adsorbed species. The continuous counter-current chromatography was made possible by the development of the SMB, which simulates the

movement of the stationary phase by periodically shifting the inlet and outlet ports by one column in the direction of the fluid flow in a series of columns packed with the adsorbent [5]. The positions of the four streams set the borders between the unit's sections (as seen in Figure 8.1), each operating at specific flow rates and where distinct processes occur.

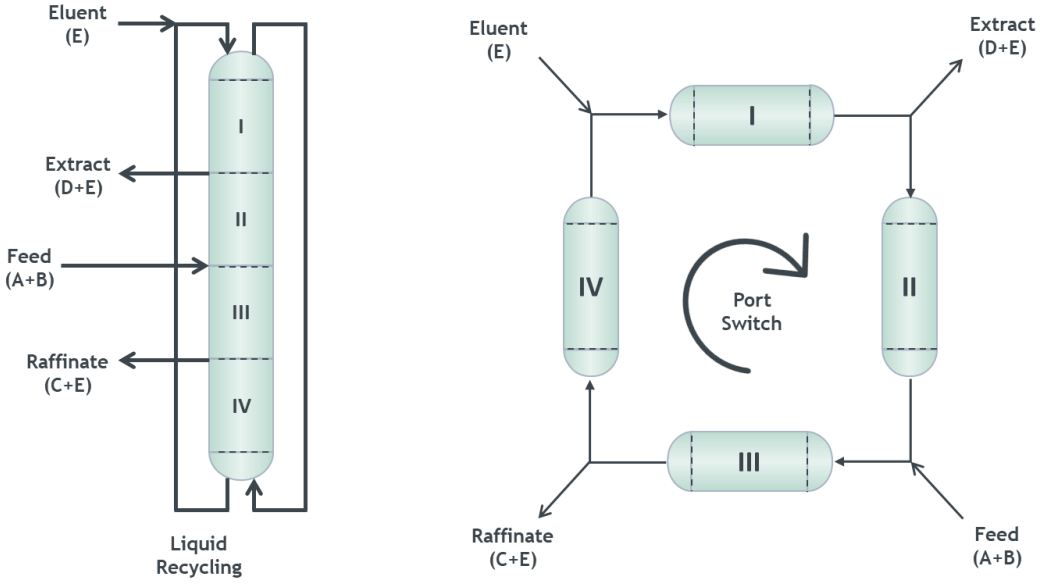

Figure 8.1. Scheme of a) a TMBR and b) an SMBR for the reaction A+B⇋C+D.

In the scheme, species A and B are the reactants, and E is the eluent. Product C is the least retained species, and product D is the most retained. For the correct operation of the SMBR, in Section I, D must be carried by the liquid phase for the appropriate adsorbent regeneration. In Sections II and III, reactants A and B are converted, and D must travel with the solid to avoid contamination of the raffinate stream and to be collected in the extract port while C must move in the opposite direction, that is, it must be carried by the fluid phase so it can be collected in the raffinate port. Finally, in Section IV, neither C nor D should be present in the desorbent for its recovery.

The initial step in the application of SMBR was made by Hashimoto et al. in 1983 for producing high fructose syrup in a process where reaction and separation occurred in different columns [5, 6]. Since then, numerous alternatives have been proposed for optimizing and

changing the original SMBR, broadening the possible application spectrum of this technology. It has been studied for the production of green fuels and solvents, as diethylacetal (DEE), dimethylacetal (DME), dibutylacetal (DBE), ethyl lactate (EL), glycerol ethyl acetal (GEA) [7-9], in the sugar industry for the sucrose inversion and glucose isomerization, in the petrochemical industry for the isomerization and separation of xylenes [2, 10].

Considering the previous cases of success of the SMBR for equilibrium-limited reactions, it was encouraging to test this technology for the first time for solketal synthesis. This was supported by the promising sorption enhancement reaction results obtained in Chapter 3 when testing the fixed-bed adsorptive reactor (FBAR) packed with Amberlyst-35. Due to the numerous degrees of freedom an SMBR process has, defining the optimal design and operating conditions is a demanding step. The novel optimization process developed in Chapter 4, based on the Equilibrium Theory and with the objective function of maximizing the productivity, was used to define the optimal column configuration, time switch and flow rates. In the present Chapter, the proof-of-concept of solketal synthesis in the SMBR was attained by performing experiments under the defined optimal operating conditions in the lab-scale SF-SMB(R). Therefore, the main objectives of Chapter 8 are validating the phenomenological model developed and thoroughly explained in Chapter 4 and testing and validating the novel SF-SMB(R) explained in Chapter 7.

8.2. Experimental Description

8.2.1. Materials and Chemicals

The chemicals selected to perform the adsorption and sorption enhanced reaction experiments in the fixed-bed reactor were glycerol (>99%), purchased from Sigma-Aldrich, acetone (>99%), purchased from Fisher Chemicals, solketal (>97%), purchased from VWR International and ethanol (>99%), purchased from Panreac-AppliChem. The water used in this work was purified in the LSRE-LCM laboratories. Additionally, methanol (>99%) purchased

from VWR International was used as washing solvent for the analytical method and blue dextran with a molecular weight of 2,000,000 purchased from Sigma-Aldrich was used as tracer.

Amberlyst-35, a highly acid macroreticular ion exchange resin composed by a styrene divinylbenzene polymeric matrix functionalized with sulfonic groups, was used as catalyst and adsorbent. It was purchased from Dow Chemical Company and its main characteristics are presented in Table 8.1 [11].

Table 8.1. Amberlyst-35 physicochemical properties [12].

Property	Value
Name	Amberlyst™ 35WET
Acidity ($eq \cdot kg^{-1}$)	≥ 5.2
Particle Diameter (μm)	700 – 950
Average pore diameter (nm)	30
Particle porosity	0.396
Tortuosity	4.1
Surface area ($m^2 \cdot g^{-1}$)	50
Solid density ($kg \cdot m^{-3}$)	800

8.2.2. Analytical Methods

The samples collected were analysed by Gas Chromatography (DANI Master GC) equipped with flame ionization (FID) and thermal conductivity detector (TCD) at least in duplicate. The column used to separate the compounds was the silica capillary column PoraBONDQ (25 m, 0.53 mm i.d., film thickness of 10 μm) in which Helium N50 was used as the carrier gas at a flowrate of 8 $ml.min^{-1}$. The linear velocity was set to 30 $cm.s^{-1}$ and the sample injection volume was 1.0 μL, with a split ratio of 20. The temperature of the injector and of the detectors was set to 573 K. The initial column temperature was 423.15 K, followed immediately by a temperature

increase at 5 K·min^{-1} until 553.15 K and subsequently held constant for 1 min. Methanol is used as the washing solvent.

8.2.3. Experimental Set-up and Procedure

Hydrodynamic Study

In the hydrodynamics study, 200 μL of a Blue Dextran solution (5 g·L^{-1}) were injected in each fixed-bed column for its characterization through tracer experiments. In previous works within the same conditions, it has been proven that there is no dependence between the bed porosity or the Peclet number and the flowrate, therefore only injections at 5.0 mL·min^{-1} were performed [12]. Water was used as eluent and the outlet concentration history was recorded with a UV-Vis detector (Gilson, model 115) at 300 nm. At least two runs were performed for each column to check the space time of the experimental curves and the bulk parameters reproducibility (Peclet number and bed porosity).

SMBR Experiments

The SMBR experiments were performed in the SF-SMB(R) assembled at LSRE-LCM in the scope of the present thesis (details regarding its construction are available in Chapter 7). The unit is constituted of eight stainless steel chromatographic columns (0.15 m length x 0.02 m internal diameter) packed with Amberlyst-35. As stated in Chapter 3, solketal synthesis is mostly limited by temperature-dependent phenomena (reaction rate, adsorption selectivity, mass transfer), reaching the best performance at 303K. An isothermal operation is guaranteed by keeping all the columns isolated inside a polycarbonate case. The columns are connected in series and the system can withstand up to 363 K and 200 bar. The characteristics of the SMBR columns are shown in Table 8.2.

Table 8.2. SF-SMB(R) average column characteristics.

Property	Value
Column length (cm)	15
Column internal diameter (cm)	2.12
Solid dry weight (A-35, g)	25.9
Bulk density ($g.cm^{-3}$)	0.39

Three HPLC pumps (Knauer BlueShadow 40P) promote the feed, eluent and recycle flowrates. The feed was constituted of acetone-to-glycerol molar ratio of 1.0 diluted in 50% of ethanol, on a molar basis, to overcome the miscibility issues between acetone and glycerol. The eluent was composed of pure ethanol. Initially, all columns are saturated with ethanol and special care was taken to purge the feed line to avoid asymmetries and discrepancies between the mathematical model and the experimental results. The experiments were performed in open loop.

Based on the simulation results presented in Chapter 4, the column configuration selected was 1-2-4-1 to provide the unit with the largest reaction and solketal separation are possible. The control and automation software receives the inputs of column configuration, eluent, extract, feed and recycle flowrates and BPR value and actuates the pneumatic valves and the control valves to ensure the unit operates at the values set by the user. A manual six-port sampling valve is located between the eight and the first columns to enable internal concentration profiles sampling collection. This is the only manual valve present in the entire system once the unit and the control and automation software were designed and built aiming to minimize the interaction of the user with the physical equipment.

8.3. Modelling Studies

8.3.1. Real SMBR Modelling and Design

The optimization of solketal synthesis in the SMBR (Chapter 4) was performed considering the TMBR model, due to the lower computational effort the latter requires. The equivalence between these models is as accurate as larger the number of columns and shorter the time switch, therefore, for solketal synthesis in the SF-SMB(R), the equivalence between the TMBR and the SMBR is particularly challenging because the number of columns is limited to eight, and the time switch is high due to the reaction and separation limitations.

The optimal point in terms of productivity that also assures an appropriate equivalence between the models was achieved for the point with a SF of 40% in Section I and 15% in Section IV, using a correction factor of 30% for the time switch. Such correction factor must be used due to the limitation of the model to describe reactive systems, which is aggravated by the fact that the reaction between glycerol and acetone to produce solketal is highly limited thermodynamically (more details regarding this particularity of the model can be found in Chapter 4 – Section 4.5). By specifying the safety factor, one defines the limit flowrate ratios between the liquid and the solid phases in the desorbent and adsorbent regenerations sections (Sections I and IV, respectively), estimated by the well-known Equilibrium Theory.

$$\gamma_I^{TMBR} > \frac{1-\varepsilon_b}{\varepsilon_b}\left[\varepsilon_p + (1-\varepsilon_p)\frac{q(C_{Water})}{C_{Water}}\right] \tag{8.1}$$

$$\begin{aligned}\frac{1-\varepsilon_b}{\varepsilon_b}\left[\varepsilon_p + (1-\varepsilon_p)\frac{q(C_{Solketal})}{C_{Solketal}}\right] < \gamma_{II}^{TMBR} < \gamma_{III}^{TMBR} \\ < \frac{1-\varepsilon_b}{\varepsilon_b}\left[\varepsilon_p + (1-\varepsilon_p)\frac{q(C_{Water})}{C_{Water}}\right]\end{aligned} \tag{8.2}$$

$$\gamma_{IV}^{TMBR} < \frac{1-\varepsilon_b}{\varepsilon_b}\left[\varepsilon_p + (1-\varepsilon_p)\frac{q(C_{Solketal})}{C_{Solketal}}\right] \tag{8.3}$$

$$\gamma_1^{SF} = (1+SF)\cdot\gamma_1 \tag{8.4}$$

$$\gamma_4^{SF} = \frac{1}{(1+SF)} \cdot \gamma_4 \tag{8.5}$$

The mathematical model developed in the thesis is comprehensive and accounts for the mass transfer resistances. Nevertheless, it does not consider real SMBR particularities, as tubing and equipment dead volumes, bed voids (due to shrinking of the adsorbent), delays/asymmetries in the control system response, equipment limitations, and fluctuations in the equipment normal operation. An extensive description on the dead volumes present on the SF-SMB(R) and the detailed explanation on their impact on the overall performance of the unit is presented in Chapter 7 (Section 7.2.2.).

The numerical solution for the model equations were performed using the software General PROcess Modelling System (gPROMS) version 7.0.7. The partial differential and algebraic equations were solved using a method of Orthogonal Collocation in Finite Elements (OCFEM) and discretizing the axial dimension of the fixed-bed column in 30 finite elements with two interior collocation points in each finite element. An integrated differential-algebraic equation solver (DASOLV) was used to solve the system of ordinary differential equations in time.

8.3.2. Definition of the Operating Parameters

As mentioned in the previous section, the optimal point in terms of productivity for the SF-SMB(R) is achieved by using a SF of 40% in Section I and 15% in Section IV. At this point, it is possible to achieve a purity of 97% for both raffinate and extract streams. The time switch is 33.4 min, which would require 4.5 hours to complete a cycle. Considering the process requires at least 14 cycles to reach the cyclic steady state (accordingly to the simulations), one would need at least three days to complete an experiment.

A common strategy to reduce the time switch of SMB experiments is to use higher flowrates, this way, the ratio between the liquid and the solid phases interstitial velocities (γ_j) is kept the same and, theoretically, so is the separation. However, this is not valid for reactive-separative processes because it is necessary to assure a sufficient residence time inside the columns for the reactants to contact the catalyst and form the products. Furthermore, increasing the flowrates would make the pressure drop even higher, as discussed in the previous section.

Since the main goal of the SF-SMB(R) experiment is to validate the model developed, to avoid wasting material and immaterial resources, it was decided to reduce the purity criterion of the extract and raffinate streams to 85% with the purpose of reducing the time switch of the experiment. The reactive separation regions (RSR) are determined by running an algorithm that sequentially tests the purity criterion resultant of $\gamma_2 \times \gamma_3$ combinations (for a fixed $\gamma_1 \times \gamma_4$ pair). If the purity criterion is met, the value is registered and γ_3 increments, if not, γ_3 is maintained and γ_2 increments. This results in a region that is delimited by the set purity criterion and inside of which all the operation points result in the appropriate extract and raffinate purity.

Since the time switch influences all the flowrates inside the unit, each time switch has an RSR. Therefore, RSRs were drawn for several time switches and the one selected was 8 minutes, because this is the lower value possible that still results in a considerable RSR. The resulting RSR is presented in Figure 8.2:

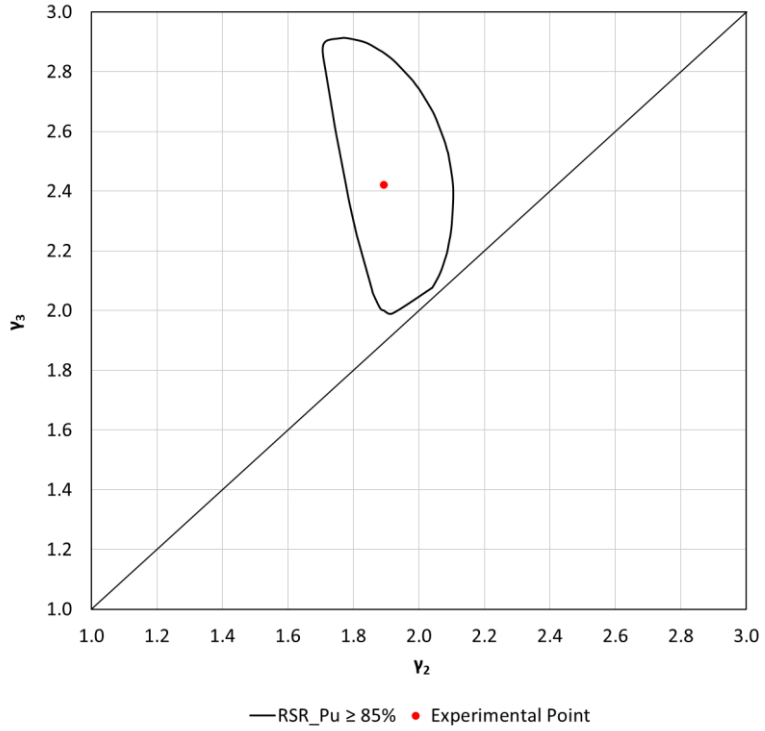

Figure 8.2. RSR of the SMBR, with a 1-2-4-1 configuration and a SF of 40% applied to Section I and 15% to Section IV, at 303 K, and feeding equimolar amounts of glycerol and acetone diluted in 50% of ethanol (t^* = 8 min). Purity criteria for the outlet streams ≥ 85%.

It was selected an operational point in the middle of the RSR to guarantee that the purity criteria would still be met despite eventual deviations on the pump operation that would generate flowrate deviations. Table 8.3 summarizes the main operational parameters of the selected point presented in Figure 8.2.

Table 8.3. SF-SMB(R) experimental operation conditions. The set values are presented between brackets.

Property	Value
Column configuration	1-2-4-1
Time switch (min)	8
Temperature (K)	313
Eluent molar fraction	1 (Ethanol)
Eluent flowrate ($mL.min^{-1}$)	17.60
Feed molar fraction	1:1:2 (Acetone:Glycerol:Ethanol)
Feed flowrate (mL.min-1)	1.43 (1.40)
Raffinate flowrate (mL.min-1)	2.87 (2.70)
Extract flowrate (mL.min-1)	16.16 (16.30)
Recycle flowrate (mL.min-1)	3.67 (3.80)

It is relevant to mention that the purity of the recycle stream is a crucial aspect for the correct operation of the SF-SMB(R). Therefore, since it was the first time operating the unit, to verify that the eluent regeneration was satisfactory and robust to the eventual deviation on the pump flowrates, it was decided to collect this stream at the end of every cycle to analyse its behaviour.

8.4. Solketal synthesis in the Conventional SMBR

The first step to prepare the unit for the synthesis experiments was performing the hydrodynamics study to estimate the values of Peclet and bed porosity through tracer experiments. The procedure is described in Section 8.2.3. and a more detailed description, with the calculations, can be found in Chapter 3. The average bed porosity is 0.408 and the average Peclet number is 172, considering all the columns.

For the synthesis of solketal in the SF-SMB(R), an equimolar mixture of acetone and glycerol diluted in ethanol was fed to the columns pre-saturated with ethanol. It was explained

previously that, despite being detrimental to almost every reactive system to dilute the reactants, it is necessary for the mixture of acetone and glycerol due to their limited solubility and due to the high viscosity of glycerol, which would certainly hamper the pumping and cause disturbances on the flow inside the columns.

The outlet concentration histories of the extract and raffinate streams are presented in Figure 8.3:

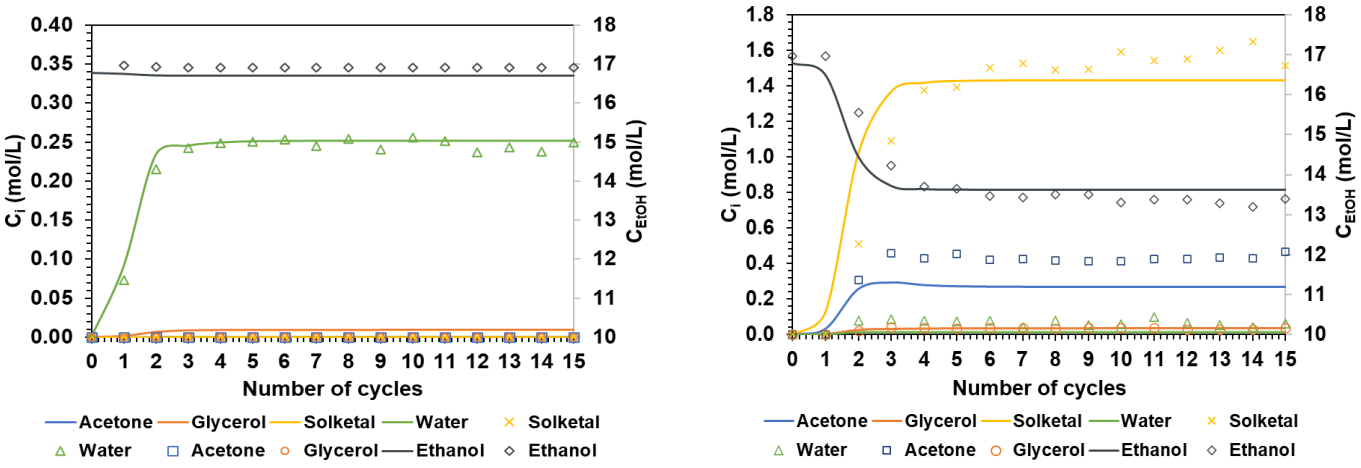

Figure 8.3. Extract (left) and raffinate (right) experimental points and modelled concentration histories (lines).

In Figure 8.3, the theoretical values were calculated with the SF-SMB(R) mathematical model presented in Chapter 4. As expected, solketal is the main compound in the raffinate stream and water is the predominant compound in the extract stream, both in eluent free basis. The mathematical model predicts relatively well the outlet concentration histories for solketal synthesis on the SF-SMB(R). It was possible to obtain R^2 of 0.93 for the Raffinate Outlet and 0.88 for the Extract. The oscillations observed in the experimental concentration histories may be induced either by operating flow rates fluctuations occurred during the experimental runs or by errors associated with gas chromatography analysis. The steady state, necessary to validate the experimental data, was achieved experimentally after the eighth cycle; then, it was possible

to collect the internal concentration profile. Figure 8.4 exhibits the internal concentration profile obtained in the fifteenth cycle, the last experimental cycle.

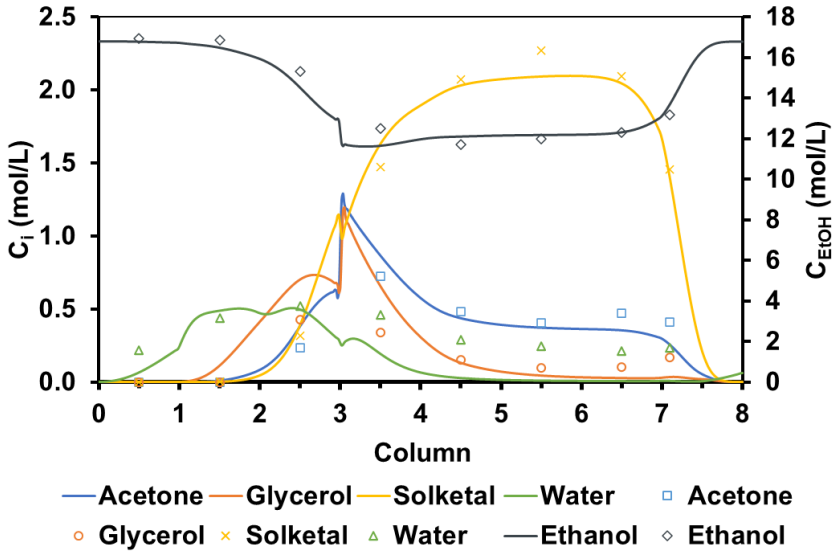

Figure 8.4. Experimental and simulated concentration profiles at the middle of the switching time (4 min) and the cyclic steady state (15th cycle) at 313 K.

The mathematical model predicts relatively well the outlet concentration histories and the internal concentration profile for solketal synthesis in the SF-SMB(R). The model predicts well the water behaviour in the extract stream. As for glycerol, the main contaminant in this stream, it is not detected because it is below the GC detection limit. The model, however, predicts a lower acetone concentration outlet in the raffinate stream and a lower water concentration in the internal concentration profile. The performance parameters obtained experimentally are presented in the following table:

Table 8.4. SF-SMB(R) experimental performance parameters. The estimated values from the model are presented between brackets.

Performance Parameter	Value
Productivity ($kg_{solk}\, L_{Ads}^{-1} s^{-1}$)	3.2 (3.5)
Desorbent Consumption ($L_{des.}\, kg^{-1}_{solk}$)	38.4 (29.1)
Raffinate Purity	75.7% (87%)
Extract Purity	100% (90%)
Conversion	83% (89%)

In terms of performance parameters, the model predicts very well the productivity and the conversion, but it fails slightly to predict the Desorbent Consumption. As mentioned, the purity detected in the Extract stream is higher because all the other compounds are present in amounts below the Gas Chromatography detection limit. As for the Raffinate stream, acetone presence affected the purity. This issue is carefully detailed in the following paragraphs.

By analysing the raffinate stream outlet history, one can conclude that the experimental concentration fronts are slightly more dispersed than the model prediction. It was possible to obtain a better fit between the experimental data and the model when a lower Peclet number was used in the model (80, instead of 172 estimated by the tracer experiments performed in each column individually).

There are several reasons that can contribute to a misleading estimate of the Peclet number. The dead volume introduced by the check valves (discussed Section 8.3.1. is critical, considering where they are located, and corresponds to 4.5% of the total dead volume, which is sufficient to promote the dispersion of the concentration fronts. Additionally, the columns were packed with water, the compound in which Amberlyst-35 is at its maximum swelling. When in contact with the reactional mixture, Amberlyst-35 shrinks, generating an additional dead volume.

A slight asynchronicity on the opening and closing of the on/off valves was observed when the switch occurs, which leads to an instability of the outlet flowrates. As soon as the valves assume the new positions, the system is supposed to quickly reach the stability. However, the difference of milliseconds between the opening and closing of the valves is enough to cause a pressurization (or depressurization) on the SF-SMB(R) (black continuous line on Figure 8.5). The pressurization leads the outlet flowrates to change (Figure 8.6 and Figure 8.7), and the system actuates to return to the set point, causing an overall instability and overcompensation on the control system, that often does not reach the steady state even after the entire switching time.

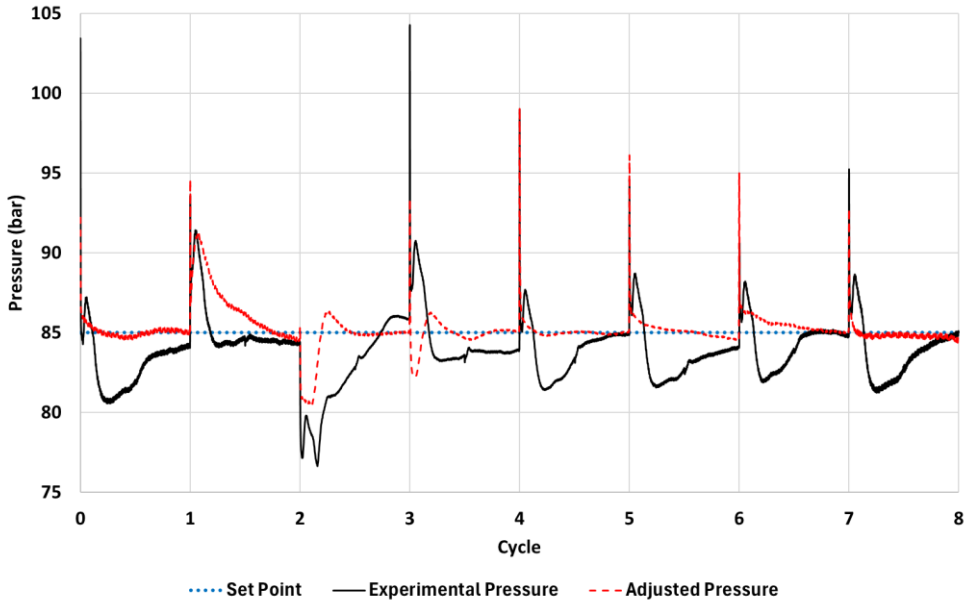

Figure 8.5. Experimental pressure over a cycle before and after the control system adjustments (offset of 15 seconds after the switch – measured by BPR at the recycle line).

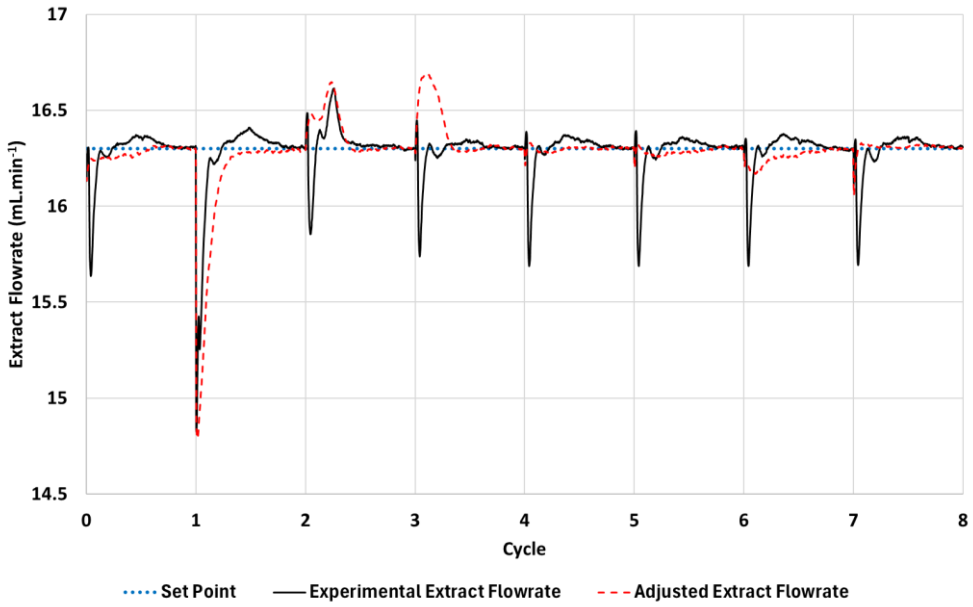

Figure 8.6. Experimental extract flowrate over a cycle before and after the control system adjustments (offset of 15 seconds after the switch – measured by MFM at the extract line).

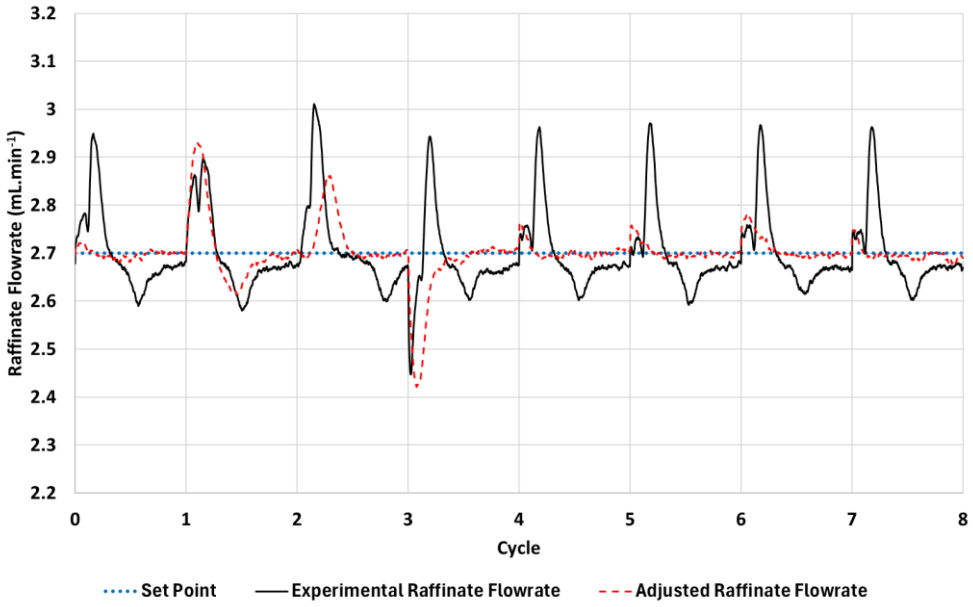

Figure 8.7. Experimental raffinate flowrate over a cycle before and after the control system adjustments (offset of 15 seconds after the switch – measured by MFM at the raffinate line).

It can be observed in Figure 8.7 that the raffinate flowrate increases by approximately 10% on the event of the switch (black continuous line), and this effect lasts for approximately one third of the switching time. Such increase in the raffinate flowrate displaces the compounds

concentration fronts on the direction of the fluid flow and reduce the reactants contact time with each other and with the stationary phase. Considering that the reaction between acetone ang glycerol is thermodynamically limited and that acetone has lower selectivity towards the stationary phase than glycerol, the increase in the raffinate flowrate may justify the slightly higher amount of acetone on this outlet collection port.

After a thorough observation of the actuation of the control valves, it was verified that the system would indeed quickly return to its set pressure and that what was impairing this behaviour was the overcompensation of the raffinate and extract flowrates by its correspondent control valves. Therefore, to overcome the limitation of the control system, a new Driver Virtual Instrument was developed aiming to introduce a time offset between the switching and the start of the actuation of the control valves. Delaying their actuation enables the system to return to the stability by itself. The comparisons of the responses with a time offset of 15 seconds and the experimental measurements are presented in Figure 8.5 to Figure 8.7. It can be observed that this change greatly improves the response of the control system (represented by the red dashed line) both because the measured value reaches more rapidly the set point and because the oscillations are smaller in magnitude.

8.5. Conclusion

The main objectives of this Chapter were validating experimentally the SF-SMB(R) (physical equipment and automation and control software) for liquid phase systems and validating the model developed with the experimental data collected in Chapter 4 for describing solketal synthesis on the SMBR. Since the Conventional SMBR was the base-case of this Thesis, it was decided to validate the model with this operating strategy, despite being the one that is the most limited in terms of performance. The experimental point was selected based on the Reactive Separation Region with a safety factor of 40% for Section I and 15% for Section

IV, with a purity constraint of 85% for both Extract and Raffinate streams and a time switch of 8 minutes. The experiments were performed at 303 K, by feeding even amounts of acetone and glycerol diluted in 50% of ethanol (for promoting miscibility of the reactants).

The mathematical model developed in the Thesis accounts for mass transfer resistances, but it does not consider real SMBR particularities, as tubing and equipment dead volumes, bed voids, delays/asymmetries in the control system response, equipment limitations, and fluctuations in the equipment normal operation. The most effective way of reducing discrepancies between the mathematical model and the real operation is planning each detail of the unit since the ideation of the project. The SF-SMBR was designed and built avoiding asymmetries and tube dead volumes, however equipment fluctuations and delays in the control system response are factors that are difficult to predict and control, therefore discrepancies between the experimental data and the mathematical model predictions may occur. Nevertheless, the model was able to predict satisfactorily the behaviour of solketal synthesis on the SMBR, both in terms of internal concentration profiles, outlet concentrations histories and performance parameters. The system was able to achieve a productivity of 3.2 $kg_{Solk} \cdot L_{Ads}^{-1} \cdot day^{-1}$ with a DC of 38.4 $L_{Desorbent} \cdot kg_{Prod}^{-1}$. This is below the range achieved for similar systems; however this was already expected according to the simulation studies reported in Chapter 4. That is what justifies implementing the two non-conventional strategies developed under the scope of this Thesis, Multifeed SMBR and the ModiCon SMBR.

The main difference between the model and the experimental data, and what impairs the most the performance of the SF-SMBR, is the higher concentration of acetone at the raffinate outlet. It was observed during the experiment that the slight asynchronicity on the opening and closing of the on/off valves when the switch occurs leads to an overall instability of the outlet flowrates. The system is robust to control such variations, the main issue was the overcompensation of the control system due to all valves actuating at the same time. It was necessary to implement

a modification on the control system to achieve a faster response to the periodic instability caused by the switch, and such modification led to a reduction on both the control response time and the amplitude of the response.

8.6. Notation

Abbreviations

gPROMS	General PROcess Modelling System
OCFEM	Orthogonal Collocation in Finite Elements
DASOLV	Differential-algebraic equation solver
SF	Safety factor

Symbols

Q	Flowrate	L min^{-1}
$\bar{Q}$	average flowrate	L min^{-1}
t^*	time switch	s
V	Volume	$cm.s^{-1}$

Greek Letters

γ	Ratio between the liquid and the solid interstitial velocities

Subscripts/Superscript

j	Section
DV	Dead Volume

8.7. References

1. Faria, R., N. Graça, and A. Rodrigues, *Green Fuels and Fuel Additives Production in Simulated Moving Bed Reactors*, in *Intensification of Biobased Processes*, Andrzej Górak and A. Stankiewicz, Editors. 2018, The Royal Society of Chemistry. p. 145-165.
2. Rodrigues, A.E., C.S.M. Pereira, M. Minceva, L.S. Pais, A.M. Ribeiro, A. Ribeiro, M. Silva, N. Graça, and J.C. Santos, *Simulated Moving Bed Technology: Principles, Design and Process Applications*. 2015: Elsevier Science.
3. Nishizawa, H., K. Tahara, S. Miyamori, Y. Motegi, T. Shoji, and Y. Abe, *True moving bed chromatography: solid–liquid multi-stage counter-current extraction.* J. Chromatogr. A, 1999. **849**(1): p. 61-69.
4. Faria, R.P. and A.E. Rodrigues, *Instrumental aspects of Simulated Moving Bed chromatography.* J. Chromatogr. A, 2015. **1421**: p. 82-102.
5. Rodrigues, A.E., Madeira, Luís Miguel, Wu, Yi-Jiang, Faria, Rui, *Sorption Enhanced Reaction Processes*. Sorption Enhanced Reaction Processes. 2017.
6. Hashimoto, K., S. Adachi, H. Noujima, and Y. Ueda, *A new process combining adsorption and enzyme reaction for producing higher-fructose syrup.* Biotechnology and Bioengineering, 1983. **25**(10): p. 2371-2393.
7. Pereira, C.S.M., V.M.T.M. Silva, and A.E. Rodrigues, *Fixed Bed Adsorptive Reactor for Ethyl Lactate Synthesis: Experiments, Modelling, and Simulation.* Separation Science and Technology, 2009. **44**(12): p. 2721-2749.
8. Faria, R.P.V., C.S.M. Pereira, V.M.T.M. Silva, J.M. Loureiro, and A.E. Rodrigues, *Glycerol valorisation as biofuels: Selection of a suitable solvent for an innovative process for the synthesis of GEA.* Chem. Eng. J. (Amsterdam, Neth.), 2013. **233**: p. 159-167.
9. Pereira, C.S.M., P.S. Gomes, G.K. Gandi, V.M.T.M. Silva, and A.E. Rodrigues, *Multifunctional Reactor for the Synthesis of Dimethylacetal.* Industrial & Engineering Chemistry Research, 2008. **47**(10): p. 3515-3524.
10. Agrawal, G., J. Oh, B. Sreedhar, S. Tie, M.E. Donaldson, T.C. Frank, A.K. Schultz, A.S. Bommarius, and Y. Kawajiri, *Optimization of reactive simulated moving bed systems with modulation of feed concentration for production of glycol ether ester.* Journal of Chromatography A, 2014. **1360**: p. 196-208.
11. Moreira, M.N., R.P.V. Faria, A.M. Ribeiro, and A.E. Rodrigues, *Solketal Production from Glycerol Ketalization with Acetone: Catalyst Selection and Thermodynamic and Kinetic Reaction Study.* Ind. Eng. Chem. Res., 2019. **58**(38): p. 17746-17759.
12. Moreira, M.N., I. Corrêa, A.M. Ribeiro, A.E. Rodrigues, and R.P.V. Faria, *Solketal Production in a Fixed Bed Adsorptive Reactor through the Ketalization of Glycerol.* Ind. Eng. Chem. Res., 2020. **59**(7): p. 2805-2816.

Chapter 9

Conclusions and Perspectives

9.1. General Conclusions

The Simulated Moving Bed Reactor (SMBR) has proven to be an outstanding Process Intensification strategy to produce green fuels and solvents, due to its capacity of combining reaction and adsorption in smaller and more efficient units. Although it has been topic of numerous investigations, there is still room for innovation in terms of new products and new modes of operation. In this Thesis, both approaches were followed: a new green fuel additive was produced, solketal, and the limitation of the conventional operation was overcome by two new non-conventional operating strategies, the Multifeed and the ModiCon SMBR. For that, the fundamental adsorption data was collected in a fixed-bed column, where studies of the sorption-enhanced reaction were also performed. Amberlyst-35 was the stationary phase for all the experiments. After that, the phenomenological model was developed, together with a novel optimization strategy applied to find the best operating condition for the SMBR, which was also used to find the optimal point of the Multifeed SMBR. The proof-of-concept was performed in the new unit built under the scope of the Thesis, the SF-SMB(R). More details on the conclusions taken from these tasks are presented as follows.

9.1.1. Fixed-bed Adsorptive Reactor

The implementation of the SMBR relies in the determination of the adsorption equilibrium data of the species with the adsorbent. For assessing these data, adsorption equilibrium curves were obtained through the Frontal Analysis Methodology. Experiments were performed at 303K and 323K. The model that describes the collected data is the Langmuir competitive adsorption model.

The results demonstrate that water has the strongest affinity to Amberlyst-35, followed by glycerol, acetone, and, lastly, solketal. This was a promising conclusion for producing solketal

by a sorption enhanced technology. Along with the adsorption enthalpies estimated through the model, it is also possible to confirm the exothermic nature of the process.

Reactive experiments on the adsorptive fixed-bed at 303 K and 323 K led to conclude that at higher temperatures, the sorption enhancement is higher due to the better mass transfer and favoured selectivity. Nonetheless, there was only a marginal difference on the maximum conversion for both temperatures and the steady state conversion is higher for 303 K, as expected for exothermic reactions. Another important output of the study is the validity of the mathematical models developed for the adsorption and for the sorption enhanced reaction.

9.1.2. Process Intensification on a Conventional SMBR

The novel optimization methodology developed in the Thesis reduces substantially the computational effort, and the time required to obtain the optimal operational parameters compared to other design/optimization techniques, as determination of the Reactive Separation Region (RSR). Since it is based on the True Moving Bed Reactor design, its reliability is limited for units with small number of columns and high time switch.

The best performing configuration is 1-2-4-1, with a productivity, 0.936 $kg_{Solk} \cdot L_{Ads}^{-1} \cdot day^{-1}$, and DC of 22.68 $L_{Desorbent} \cdot kg_{Prod}^{-1}$. From the sensitivity analysis to the SF, the combination that achieves the highest productivity in the studied range is 40% in Section I and 10% in Section IV. At this point, the productivity is 1.086 $kg_{Solk} \cdot L_{Ads}^{-1} \cdot day^{-1}$ and the DC is 26.24 $L_{Desorbent} \cdot kg_{Prod}^{-1}$. Solketal synthesis in the SMBR with Amberlyst-35 performs poorly due to the reaction thermodynamic limitation, the high diffusion time of the species in the solid phase, the high difference in the selectivity of acetone and glycerol with the solid, which makes them get separated shortly after being fed, and the similar affinity of acetone and solketal, which makes the raffinate stream prone to contamination.

9.1.3. Non-conventional Simulated Moving Bed Reactor: Multifeed SMBR

The Multifeed SMBR is a non-conventional operation strategy proposed to overcome the mentioned challenges of glycerol reaction with acetone in the Conventional SMBR. By introducing one more feed stream, the countercurrent contact between the reactants is promoted and the separation of solketal and acetone is improved.

The two-step optimization developed in Chapter 4 was used to estimate the best set of operational conditions of the Multifeed SMBR. The best configuration is 1-1-1-4-1 because it maximizes the number of columns in Section IIIB, where most of the reaction and the separation of acetone and solketal takes place. From the sensitivity analysis to the SF, the combination that achieves the highest productivity in the range studied is 40% in Section I and 10% in Section IV. At this point, the productivity is 7.35 $kg_{Solk} \cdot L_{Ads}^{-1} \cdot day^{-1}$, with a DC of 5.08 $L_{Desorbent} \cdot kg_{Prod}^{-1}$. This is in the range of productivities reported for similar processes and proves that solketal can be produced by a continuous chromatographic reactor.

9.1.4. Non-conventional Simulated Moving Bed Reactor: ModiCon SMBR

Another proposed alternative to improve the performance of the SMBR was the ModiCon SMBR. This strategy promotes the countercurrent contact between the reactants to improve the reaction and keep acetone concentration front further apart from the raffinate collection port. Since this is a dynamic operation, the optimization developed in Chapter 4 could not be used. Instead, the optimization was based on the "Reactive-Separation Volumes" methodology.

The optimal combination of SFs is 70% in Section I and 20% to Section IV with a time switch of 15.42 min (85% from the optimum of the Multifeed SMBR). At this optimal point, the productivity is 9.69 $kg_{Solk} \cdot L_{Ads}^{-1} \cdot day^{-1}$ with a DC of 6.76 $L_{Desorbent} \cdot kg_{Prod}^{-1}$. This indicates an increase in productivity of 38% compared to the Multifeed, with a cost of an increase of 35%

in the desorbent consumption. Nevertheless, the reactants consumption decreases by 12%, demonstrating it is more advantageous to operate the ModiCon than the Multifeed SMBR.

9.1.5. Assembly of the Supercritical Fluid Simulated Moving Bed Reactor – SF-SMB(R)

The SF-SMB(R) was built to be as versatile and robust as possible. Therefore, the distributed valve strategy was selected because the additional degrees of freedom provide the unit with the ability of operating with diverse number of columns, zones, and streams, zone bypass operation and independent ports switching.

The control and automation of the unit is performed by a LabVIEW program developed for this purpose. Through a friendly interface the user can define the operating parameters and monitor the process variables, minimizing the need to interact with the physical equipment. Efforts were made to minimize the dead volumes inside the unit by resorting to technical dimensional drawings to analyse several hypothetical configurations. The SF-SMB(R) can handle the temperature and pressure required for supercritical systems, and all the adjacent equipment and valves necessary to assure a safe operation.

9.1.6. Experimental Validation of Solketal Synthesis on the SF-SMB(R)

The proof-of-concept of solketal synthesis on the SMBR was performed in the SF-SMB(R) also with the purpose of validating this new unit for liquid phase operations. The Conventional SMBR was tested, and the experimental point was selected based on the RSR with a safety factor of 40% for Section I and 15% for Section IV, with a purity constraint of 85% for both Extract and Raffinate streams and a time switch of 8 minutes. The experiments were performed at 303 K, by feeding even amounts of acetone and glycerol diluted in 50% of ethanol.

The mathematical model predicts satisfactorily the behaviour of solketal synthesis on the SMBR, both in terms of internal concentration profiles, outlet concentrations histories and performance parameters. The system was able to achieve a productivity of 3.2 $kg_{Solk} \cdot L_{Ads}^{-1} \cdot day^{-1}$

with a DC of 38.4 $L_{Desorbent} \cdot kg^{-1}_{Prod}$. The discrepancies between the model and the experimental data are mainly caused by equipment fluctuations and delays in the control system response. Adaptations to the control system were performed to improve the response of the control valves. Nevertheless, the productivity is below the range achieved for similar systems, which was already expected according to the simulation studies reported in Chapter 4. That is what justifies implementing the two non-conventional strategies proposed, the Multifeed SMBR and the ModiCon SMBR.

9.2. Suggestion of Future Work

Although most of the initial objectives have been successfully accomplished, some new lines of research are open for future work. Some suggestions are proposed in the following paragraphs.

One of the most relevant topics studied in this Thesis was the Multifeed SMBR, since it has never been investigated for reactive systems. Even for purely separative systems, the literature regarding the implementation of SMB processes with extended or reduced number of columns is scarce. Promising results were obtained through the simulations performed in this Thesis for the synthesis of solketal, since it was demonstrated that the Multifeed SMBR was capable of increasing the productivity by 6.5 times, while reducing the desorbent consumption by 5.6 times. Nonetheless, since this is a new process, it still raises some concerns about the validity of the optimization process, that is based on the True Moving Bed Reactor, for describing the real unit. The proof-of-concept for this operation should be performed, as the Conventional SMBR was. In line with this suggestion of future work, the proof-of-concept of the ModiCon SMBR should also be performed.

To ascertain the suitability of the SMBR for the industrial production of solketal, an integrated industrial facility should be developed, with all the pre-treatment for crude glycerol,

and all the post-treatment for the SMBR outlet streams. This should be accompanied by an extensive economic evaluation that considers the feedstocks, consumables, product market value and operational costs. One of the greatest advantages of the SMBR for solketal production is its low environmental impact, especially considering the traditional production route, that is in batch and catalysed by strong homogeneous acids. It would be interesting to present the SMBR process as a more appealing solution by comparing both production routes in terms of environmental impacts through a Life Cycle Assessment.

The SF-SMB(R) is the most relevant physical output of the present Thesis. It was designed and built having in mind the flexibility of operating with several non-conventional strategies. It is a robust unit that can handle a broad set of operational conditions in terms of pressure, flowrate and temperature. Considering all the material and immaterial resources that were invested in the unit, it should be extensively explored for new systems, new operating strategies, and by new Master's and PhD students.

Finally, supercritical synthesis and separations must be further investigated in the SF-SMB(R). Systems that involve supercritical fluids are very sensitive to temperature and pressure variations, and time and focus must be invested in understanding the effect of these parameters on the overall unit performance. The work should begin by defining an appropriate system in which all the compounds are sufficiently miscible in the selected supercritical fluid. Butyl acetate from methyl acetate (from the polyvinyl alcohol industry) and butanol is a strong candidate, once all the compounds are miscible with supercritical carbon dioxide and this system has been previously investigated. Nonetheless, the stationary phase must still be studied, considering the catalytic activity and the adsorption equilibrium, the fundamental reaction and adsorption data must still be gathered, the mathematical model that takes into consideration the supercritical properties must still be developed and, eventually, the proof-of-concept of this synthesis will be performed.

APPENDIX A: Reaction equilibrium and kinetic data

The experimental equilibrium and kinetic data were obtained in a batch reactor with a temperature range of 303-323K and pressure of 8 bar. There were used 2 g of dry catalyst (Amberlyst-35), in a glass-jacketed reactor (model Buchiglaususter – Germany), with a maximum capacity of 1 dm^3. The experiments were performed with equimolar amounts of the reactants diluted in 50% of ethanol to promote the complete miscibility of the reactants. The catalyst was placed in the basket located out of the liquid. The experiment started when the basked is immersed in the liquid and the stirrer is switched on.

The experiments for the determination of the thermodynamic and kinetic parameters lasted enough so that there were no more variations in the bulk composition, which indicates the equilibrium was reached. The average final experimental composition at the three temperatures tested are presented in

Table A**.1**.

Table A.1. Equilibrium composition expressed in molar fraction.

T (K)	Acetone	Glycerol	Solketal	Water	Ethanol
303	0.129	0.128	0.121	0.121	0.500
313	0.138	0.137	0.112	0.112	0.499
323	0.141	0.139	0.110	0.110	0.499

The equilibrium constant was determined through Equation A.1, in terms of the activities, and considering the final composition of the reactor operated under isothermal conditions.

$$K_{eq} = \frac{a_{solk}a_{water}}{a_{acetone}a_{glycerol}} = \frac{x_{solk}x_{water}}{x_{acetone}x_{glycerol}} \frac{\gamma_{solk}\gamma_{water}}{\gamma_{acetone}\gamma_{glycerol}} \quad \text{(A.1)}$$

The activity coefficients were determined by the UNIFAC method [1]. The parameters required for the estimation of these coefficients, namely relative molecular volume and surface area of pure components and the interaction parameters are presented in It is not
the activity of the eluent, ethanol, is not considered on the estimation of the reactior
constant, however it must be considered on the estimation of the activity coefficients of the compounds.

Table A.2 and Table A.3, respectively. It is noteworthy that the activity of the eluent, ethanol, is not considered on the estimation of the reaction equilibrium constant, however it must be considered on the estimation of the activity coefficients of the compounds.

Table A.2. Relative molecular volume, and surface area of the subgroups of the pure species [1].

Composto	Name	Group	Subgroup	vi	Rk	Qk
Acetone	CH3 (end group of chain)	1	1	1	0.9011	0.848
	CH3CO	9	19	1	1.6724	1.448
Glycerol	CH2 (middle group of chain)	1	2	2	0.6744	0.540
	CH (middle group of chain)	1	3	1	0.4469	0.228
	OH	5	15	3	1.000	1.200
Water	H2O	7	17	1	0.9200	1.400
Solketal	CH3 (end group of chain)	1	1	2	0.9011	0.848
	CHO	10	21	1	0.6908	0.468
	CH2O	13	26	1	0.9183	0.780
	C (bonded to 4 other C)	1	4	1	0.2195	0
	CH2 (middle group of chain)	1	2	1	0.6744	0.540
	OH	5	15	1	1.0000	1.200
Ethanol	CH3 (end group of chain)	1	1	1	0.9011	0.848
	CH2 (middle group of chain)	1	2	1	0.6744	0.540
	OH	5	15	1	1.0000	1.200

Table A.3. Interaction parameters [1].

a_{mn}	1	5	7	9	10	13

1	0	986.5	1318	476.4	677	251.5
5	156.4	0	353.5	84	-203.6	28.06
7	300	-229.1	0	-195.4	-116	540.5
9	26.76	164.5	472.5	0	-37.36	-103.6
10	505.7	529	480.8	128	0	304.1
13	83.36	237.7	-314.7	191.1	-7.838	0

The estimated activity coefficients are presented in

Table A.**4**.

Table A.4. Activity coefficients for the equilibrium composition.

T (K)	Acetone	Glycerol	Solketal	Water	Ethanol
303	1.816	1.356	0.824	1.148	1.081
313	1.796	1.330	0.850	1.201	1.075
323	1.776	1.303	0.879	1.255	1.069

The equilibrium constant can also be expressed in terms of the reaction standard Gibbs free energy, ΔG^0, and temperature, T, known as the Van't Hoff law (Equation A.2):

$$K_{eq} = e^{\Delta G^0/RT} \tag{A.2}$$

The reaction standard Gibbs free energy, in turn, can be expressed in terms of the standard entropy, ΔS^0, and the standard enthalpy, ΔH^0 (Equation A.3). Combining both equations, a linear correlation, $\ln K_{eq}$ vs $1/T$ (K^{-1}), is obtained (Equation A.4).

$$\Delta G^0 = \Delta H^0 - T\Delta S^0 \tag{A.3}$$

$$\ln K_{eq} = \frac{\Delta S^0}{R} + \frac{\Delta H^0}{R}\frac{1}{T} \tag{A.4}$$

The standard enthalpy and Gibbs free energy could then be predicted, and the estimated values were −20.1 ± 1.1 kJ mol^{-1} and 1.4 ± 0.1 kJ mol^{-1}, respectively.

References

1. Fredenslund, A., J. Gmehling, and P. Rasmussen, *Chapter 4 - The Unifac Group-Contribution Method*, in *Vapor-liquid Equilibria Using Unifac*, A. Fredenslund, J. Gmehling, and P. Rasmussen, Editors. 1977, Elsevier. p. 27-64.

APPENDIX B: Main Information of the components of the SF-SMB(R)

Columns	
Manufacturer/Reference:	Alltech ® Stainless Steel Preparative Column / Model 96520
Capacity:	38mL
Max. operating pressure:	550 bar
Max. operating temperature:	100ºC
Material	316 Stainless Steel, PEEK
Typical Use:	Prep HPLC Columns
Material:	316 Stainless Steel, PEEK

Sampling Filter	
Suppliers/Reference:	PARALAB/ FIL0075
Pore size:	10 μm
Max. differential operating pressure:	70 bar
Max. operating temperature:	200 ºC

Two-way valves	
Manufacturer/Reference:	VICI-valco, Switzerland/ EMT6CSD12UW
Max. operating pressure:	690 bar
Max. operating temperature:	100 ºC
Max actuating pressure:	2.75 – 4.10 bar
Connection:	1/16"

Feed Container	
Manufacturer/Reference:	N.A.
Capacity:	1 L
Max. operating pressure:	15 bar

Max. operating temperature:	200 ºC
Bottom type:	Conical
Connections:	1/4'' NPT (Top: Female; Bottom: Male)
Valves:	1/2'' Globe (Top) / 1/4'' Globe (Bottom)
External jacket:	Yes

HPLC pumps	
Manufacturer/Reference	Knauer/BlueShadow 40P
Supplier	VWR
Flow rate range	0.001 - 50 ml/min
Flow rate increment	0.001 ml/min
Maximum delivery pressure	350 bar
Liquid temperature range	4−60 °C
Pump head materials	Stainless Steel
Wetted materials	GFP (graphite fiber reinforced PTFE), sapphire, ruby, PEEK, stainless steel, Zirconium oxide
Power supply	100 - 240 V; 50 - 60 Hz; Maximum power consumption 40 Watt

Relief Valve (SS-4R3A)	
Manufacturer Reference:	46.20005.0000 / 46.20006.0000
Max. pressure:	10 bar / 12 bar
Connections:	1/4'' NPT Male

Thermocouple (Type K)	
Supplier/Reference:	RS Amidata / 397-1264
Sensor type:	K (Nickel Chromium/Nickel Aluminium)
Element/Hot junction:	Single Element / Junction insulated from sheath
Sheath:	Stainless Steel 310
Connections:	1 m PFA Teflon flat pair cable (IEC 584)
Temperature range:	-40 to 750 ºC

Pressure Transducer	
Manufacturer/Reference:	Schaevitz Sensors / 1263-0103
Pressure range:	0 to 15 bar
Accuracy:	0.03 bar
Max. operating pressure:	75 bar
Working temperature range:	-20 to 80 ºC
Output:	5 VDC
Current:	0 to 5 mA
Frequency response:	2 kHz
Power Supply:	18 – 32 VDC

Coriolis flow meter Brockhorst mini-CORI FLOW M14-AGD-11-0-S	
Manufacturer/Reference:	Bronkhorst B.V., Netherlands
Supplier	STV Lda., Portugal
Max. operating pressure	200 bar
Temperature range:	0 to 70 ºC
Temperature stability:	0.01 ºC
Flowrate range - Liquid	0 – 30 kg/h
Mass flow accuracy	± 0,2% of rate
Pump maximum pressure:	0.4 bar
Pump maximum flow:	20 L/min
Heater Power:	2.3 kW
Power Supply:	230 V

NI USB-6001 Multifunctional DAQ	
Manufacturer/Reference:	National Instruments / NI USB-6001
Analog Input – Single-Ended Channels:	8
Analog Input – Differential Channels:	4
Analog Input – Resolution:	14-bit
Analog Input – Voltage Range:	-10 to 10 V
Analog Input – Overvoltage protection:	-30 to 30 V
Analog Input - Typical Voltage Accuracy:	6 mV
Analog Input - Max. Voltage Accuracy:	26 mV
Analog Input – System noise:	0.7 mVrms
Analog Input – Maximum Sample Rate:	20 kS/s
Analog Output – Number of Channels:	2
Analog Output – Resolution:	14-bit
Analog Output – Voltage Range:	-10 to 10 V
Analog Input – Typical Voltage Accuracy:	9.1 mV
Analog Input – Max. Voltage Accuracy:	34 mV
Analog Output – Update Rate:	5 kS/s
Analog Output – Output Current Drive:	-5 to 5 mA
Digital I / O – Bidirectional Channels:	13
Digital I / O – Logic Levels:	TTL
Digital Input – Type:	Sinking/Sourcing
Digital Input – Max. Voltage Range:	0 to 5 V
Digital Input – Overvoltage protection:	-20 to 20 V
Digital Output – Type:	Sinking/Sourcing
Digital Output – Current Drive Single:	8.5 mA
Digital Output – Current Drive All:	102 mA
Digital Output – Max. Voltage Range:	0 to 5 V
Counters:	1
Max. source frequency:	5 MHz
Size:	32-bit
Timebase Accuracy:	-100 ppm to 100 ppm
Triggering:	Digital

NI USB-6008 Multifunctional DAQ	
Manufacturer/Reference:	National Instruments / NI USB-6008
Analog Input – Single-Ended Channels:	8
Analog Input – Differential Channels:	4
Analog Input – Resolution:	12-bit
Analog Input – Voltage Range:	-10 to 10 V
Analog Input – Overvoltage protection:	-35 to 35 V
Analog Input - Typical Voltage Accuracy:	14.7 mV
Analog Input - Max. Voltage Accuracy:	138 mV
Analog Input – System noise:	5 mVrms
Analog Input – Maximum Sample Rate:	10 kS/s
Analog Output – Number of Channels:	2
Analog Output – Resolution:	12-bit
Analog Output – Voltage Range:	0 to 5 V
Analog Input – Typical Voltage Accuracy:	7 mV
Analog Input – Max. Voltage Accuracy:	36.4 mV
Analog Output – Update Rate:	5 kS/s
Analog Output – Output Current Drive:	5 mA
Digital I / O – Bidirectional Channels:	12
Digital I / O – Logic Levels:	TTL, LVTTL, CMOS
Digital I / O – Max. Voltage Range:	-0.5 V to 5.8 V (with respect to GND)
Digital Input – Type:	Sinking/Sourcing
Digital Input – Overvoltage protection:	-20 to 20 V
Digital Output – Type:	Sinking/Sourcing
Digital Output – Current Drive Single:	8.5 mA
Digital Output – Current Drive All:	102 mA
Counters:	1
Max. source frequency:	5 MHz
Size:	32-bit
Timebase Accuracy:	100 ppm
Triggering:	Digital

NI USB-6501 Multifunctional DAQ	
Manufacturer/Reference:	National Instruments / NI USB-6501
Digital I / O – Bidirectional Channels:	24
Digital I / O – Voltage Range:	0 to 5 V
Digital I / O – Logic Levels:	TTL
Digital Logic Levels – Current Drive Single:	8.5 mA
Digital Logic Levels – Current Drive All:	65 mA
Counters:	1
Max. source frequency:	5 MHz
Size:	32-bit
Triggering:	Digital

cDAQ-9171 CompactDAQ Chassis with a NI 9212	
Manufacturer/Reference:	National Instruments / NI 9212
Number of differential channels:	8
ADC resolution:	24 bits
Input range:	±78.125 mV
Overvoltage protection:	-30 to 30 V
Common-mode range:	±30 V (Channel-to-USB Ground)
Common-mode rejection ratio (0 to 1000 Hz):	>145 dB (Common-to-USB ground)
Noise rejection (50/60 Hz):	>80 dB
Temperature measurement ranges :	J, K, R, S, T, N, E, and B
Conversion time (50/60 Hz):	140 and 120 ms
Max. Sampling rate:	7.1 and 8.3 samples/s
Max. Cold-junction compensation accuracy:	0.60 °C (-20 to 65 ºC)
Cold-junction compensation resolution:	0.06 °C
Overvoltage protection:	30 V max. between TC+ and TC–

Five port solenoid valve SMC – SY 3A00-5U1	
Manufacturer/Reference:	SMC
Seals material:	Rubber
Valve type:	4 Position Dual 3 Port Valve N.C./N.C.
Fluid:	Air
Operating pressure range:	0.2 to 0.7 MPa
Operating temperature range:	-10 to 50 °C
Rated Voltage:	24VDC
Other specifications:	With light/surge voltage suppressor. Non-polar type

Control Valve RC200	
Manufacturer/Reference:	Badger Meter
Body material:	Stainless Steel
Seals material:	PTFE
Valve type:	On/Off
Connection:	NPT-internal thread
Max. operating temperature:	530 ºC
Power Supply:	230 VAC 50 Hz to 24 VDC

TEIP11-PS signal converter	
Manufacturer/Reference:	ABB
Signal input	4 to 20 mA
Signal Output	0.2 to 1 bar (3 to 15 psi)
Maximum supply pressure	2 bar
Ambient temperature	−40 to 85 °C

Back pressure regulator (EL-PRESS P-522C)	
Manufacturer/Reference:	Swagelok / SS-41GXS1
Body material:	Stainless Steel
Valve type:	3-way
Connection:	1/8 Swagelok fitting
Flow Coefficient:	0.8 L/min
Max. differential operating pressure:	172 bar
Max. operating temperature:	148 ºC

Pressure transducer (TE Conectivity, U5272)	
Manufacturer/Reference:	Swagelok / SS-41GXS1
Body material:	Stainless Steel
Valve type:	3-way
Connection:	1/8 Swagelok fitting
Flow Coefficient:	0.8 L/min
Max. differential operating pressure:	172 bar
Max. operating temperature:	148 ºC

DIN rail power supply 24VCD 5A Lyte series (DRL-24V120W1AA)	
Manufacturer/Reference:	DELTA/ DRL-24V120W1AA
Operating mode:	switched
Input voltage:	100. 240Vac (-15% + 10%)
Output voltage:	24VDC (+/- 2%)
Nominal output current:	5 A
Rated output power:	120W
Overcurrent and short-circuit limitation:	Yes, self-alarming
Working environment:	-20 to 75 ºC

APPENDIX C: Electrical scheme of the SF-SMB(R)

FO186

Electrical Scheme

POWER LINE SPECIFICATIONS	
Voltage	230 VAC 1Ph+N+E
Frequency	50 Hz
Max. Current	10 A
Auxiliary Voltage	24VDC

REV.	DATE	NAME	APPROVED ON	APPROVED BY	CHANGES
0	09/02/2023	Renato Vieira	19/04/2023	Miguel Mota	

paralab

Paralab
Rua Dr. Joaquim Manuel Costa 946, B
4420-437 Valbom
Gondomar

CREATED BY: Renato Vieira

CREATED ON: 09/02/2023

S/N:

SCALE 1 / 1

REVISION 0

PAGE 01

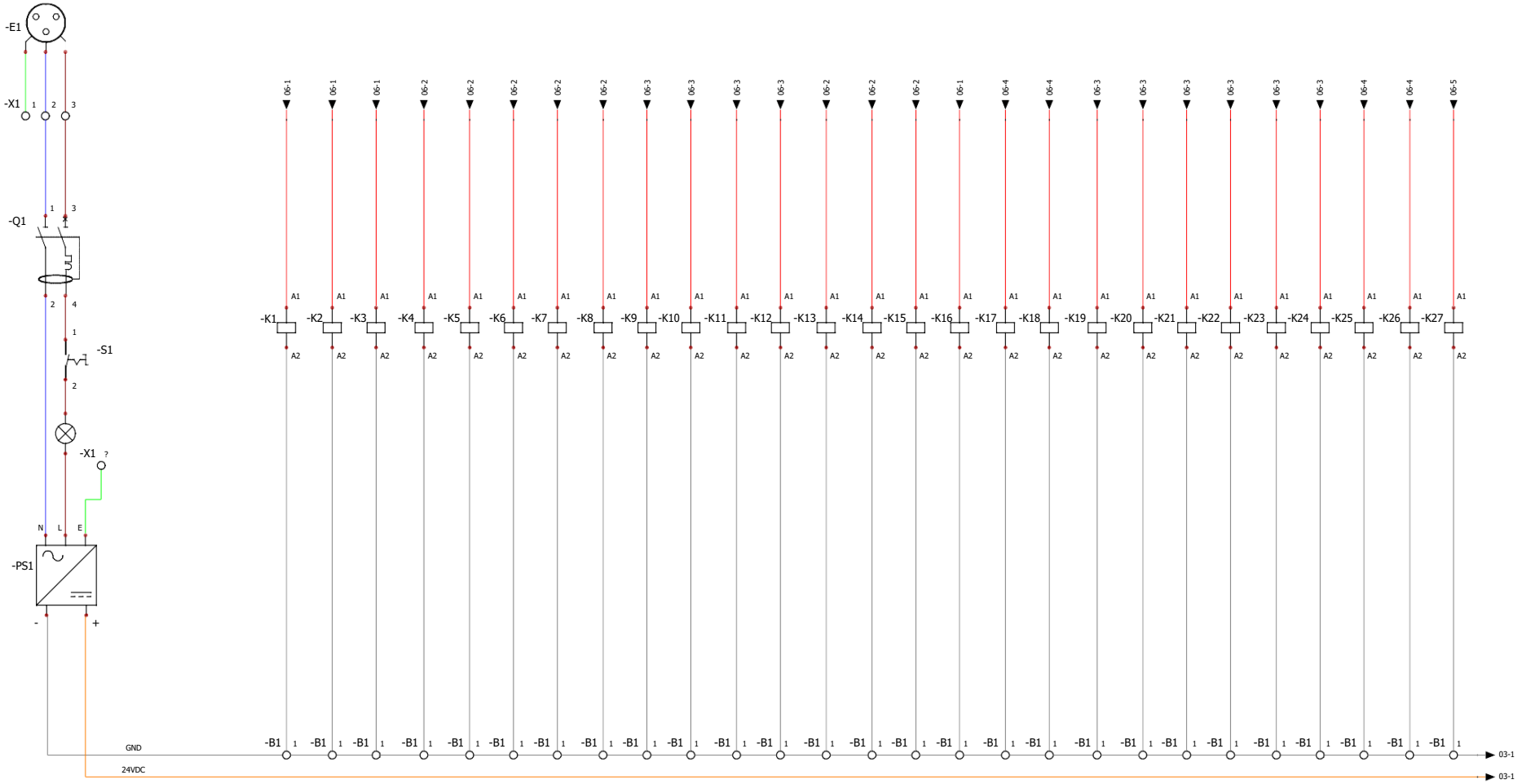

Paralab Rua Dr. Joaquim Manuel Costa 946, B 4420-437 Valbom Gondomar	Electrical Scheme FO186				SCALE 1 / 1
		0	19/04/2023	Renato Vieira	REVISION 0
		REV.	DATE	NAME	CHANGES
	S/N:	LOCATION: +L1 Main electrical closet	APPROVED BY: Miguel Mota	APPROVED ON:	PAGE 02

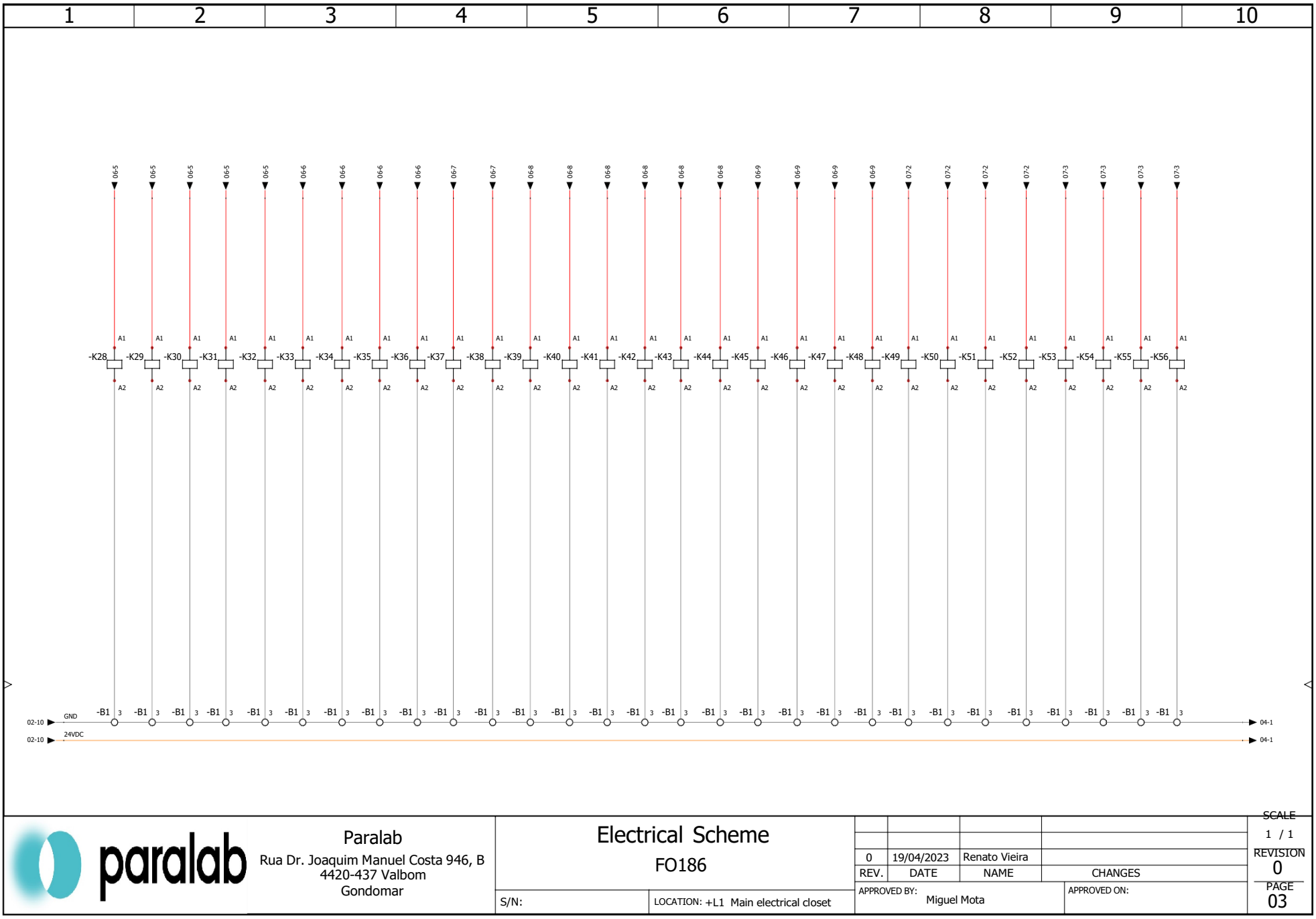
1
2
3
4
5
6
7
8
9
10
-K28 -K29 -K30 -K31 -K32 -K33 -K34 -K35 -K36 -K37 -K38 -K39 -K40 -K41 -K42 -K43 -K44 -K45 -K46 -K47 -K48 -K49 -K50 -K51 -K52 -K53 -K54 -K55 -K56
A1
A2
-B1
GND
24VDC
02-10
04-1
Paralab
Rua Dr. Joaquim Manuel Costa 946, B
4420-437 Valbom
Gondomar
Electrical Scheme
FO186
S/N:
LOCATION: +L1 Main electrical closet
0
19/04/2023
Renato Vieira
REV.
DATE
NAME
CHANGES
APPROVED BY:
Miguel Mota
APPROVED ON:
SCALE
1 / 1
REVISION
0
PAGE
03

1	2	3	4	5	6	7	8	9	10

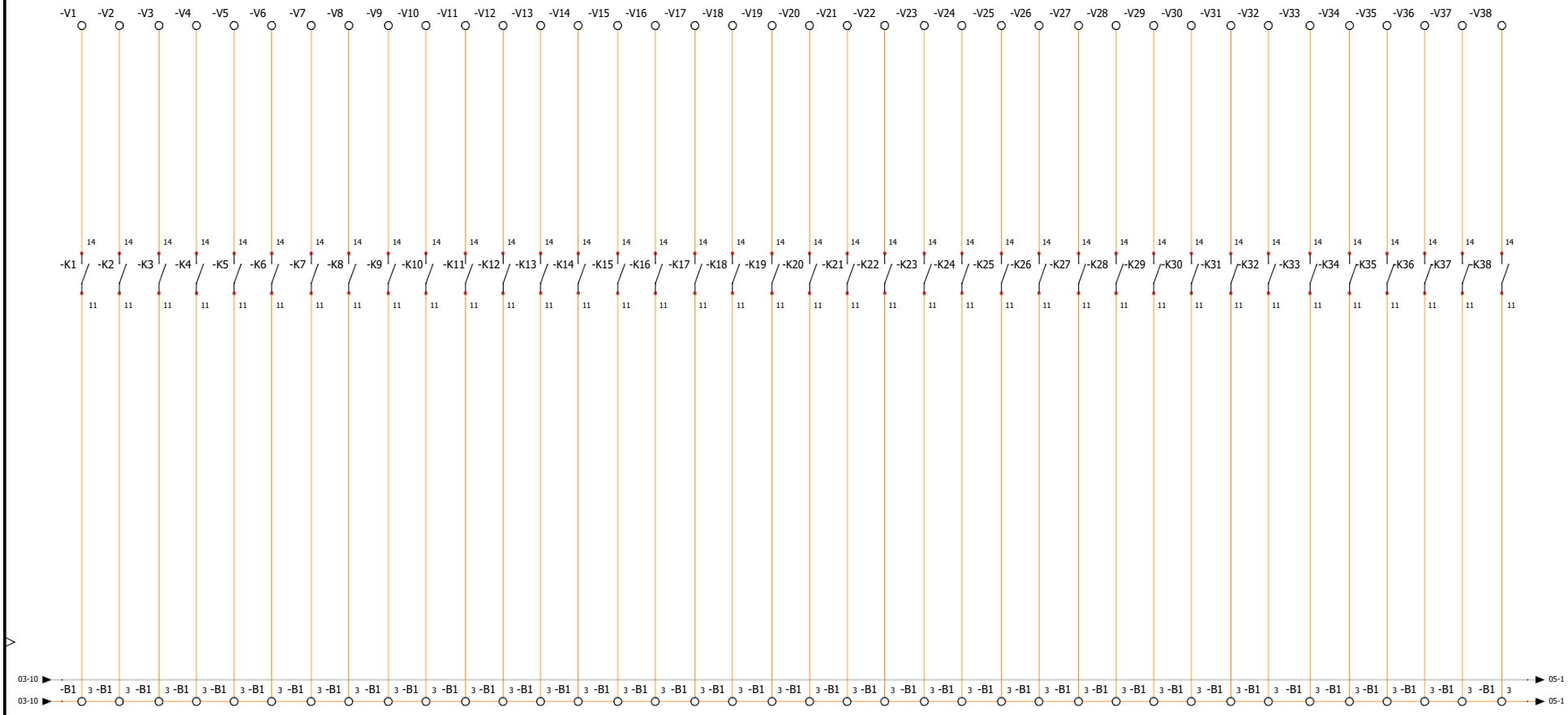

paralab	Paralab Rua Dr. Joaquim Manuel Costa 946, B 4420-437 Valbom Gondomar	Electrical Scheme FO186			SCALE 1 / 1
			0	19/04/2023 Renato Vieira	REVISION 0
			REV.	DATE NAME	CHANGES
		S/N:	LOCATION: +L1 Main electrical closet	APPROVED BY: Miguel Mota	APPROVED ON:
					PAGE 04

1	2	3	4	5	6	7	8	9	10

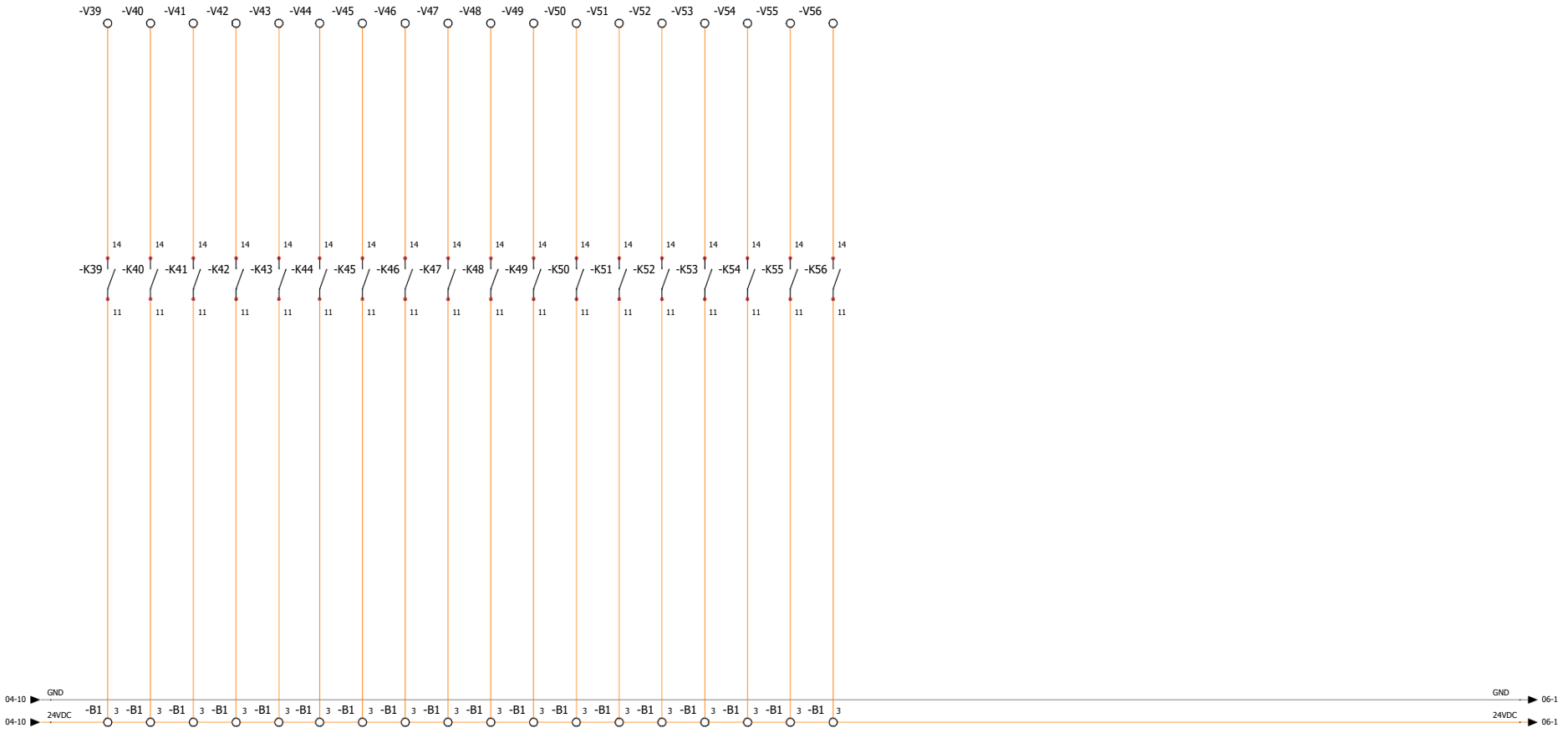

Paralab Rua Dr. Joaquim Manuel Costa 946, B 4420-437 Valbom Gondomar	Electrical Scheme FO186				SCALE 1 / 1
		0	19/04/2023	Renato Vieira	REVISION 0
		REV.	DATE	NAME	CHANGES
	S/N:	LOCATION: +L1 Main electrical closet	APPROVED BY: Miguel Mota	APPROVED ON:	PAGE 05


1
2
3
4
5
6
7
8
9
10
NI 6501
NI 6008
NI 6001-01
LEFT VIEW
RIGHT VIEW
Paralab
Rua Dr. Joaquim Manuel Costa 946, B
4420-437 Valbom
Gondomar
Electrical Scheme
FO186
S/N:
LOCATION: +L1 Main electrical closet
REV.
DATE
NAME
CHANGES
0
19/04/2023
Renato Vieira
APPROVED BY:
Miguel Mota
APPROVED ON:
SCALE
1 / 1
REVISION
0
PAGE
06

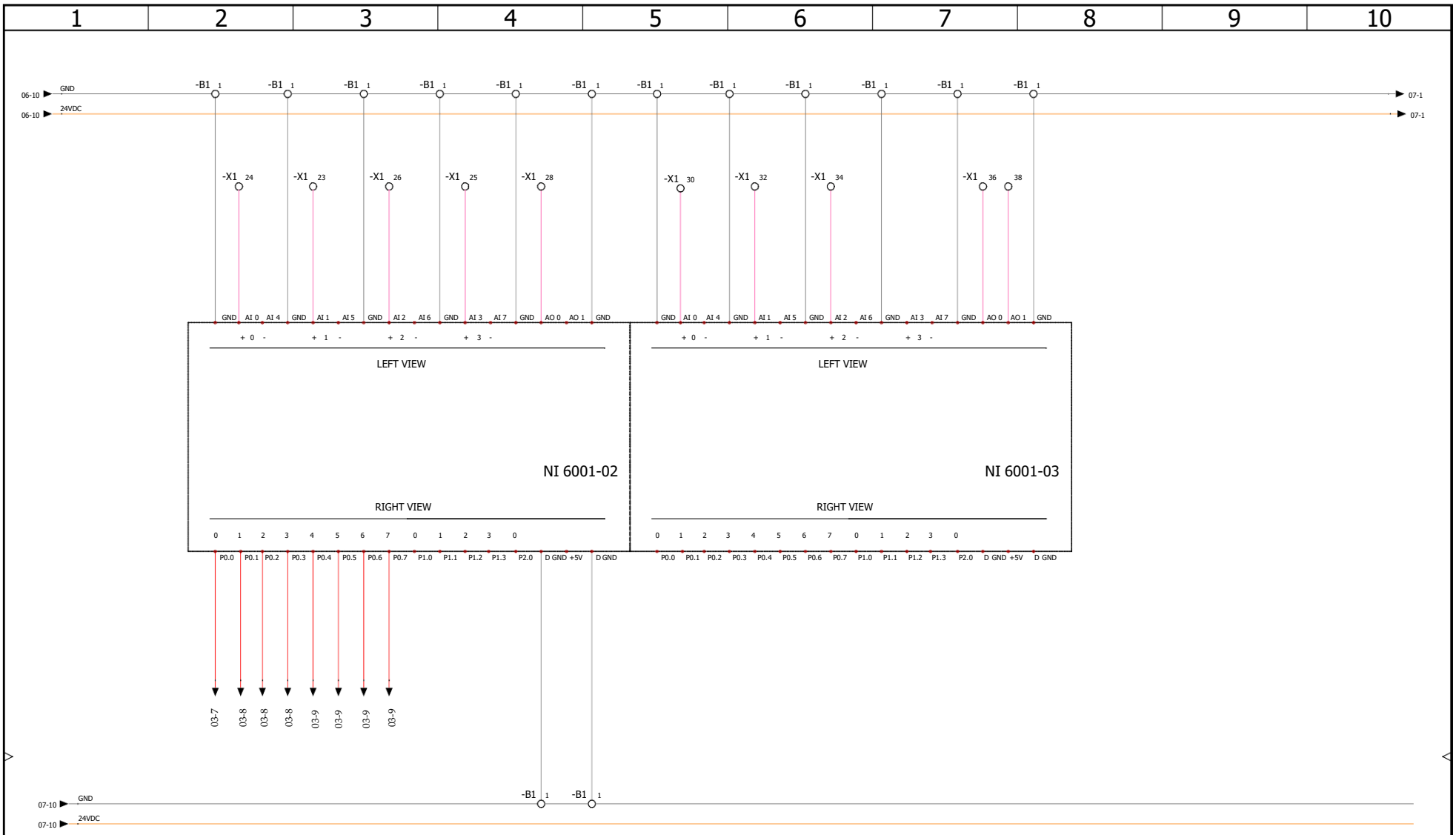

paralab	Paralab Rua Dr. Joaquim Manuel Costa 946, B 4420-437 Valbom Gondomar	Electrical Scheme FO186		SCALE 1 / 1
			0 19/04/2023 Renato Vieira	REVISION 0
			REV. DATE NAME CHANGES	
		S/N:	LOCATION: +L1 Main electrical closet	APPROVED BY: Miguel Mota APPROVED ON:
				PAGE 07

1	2	3	4	5	6	7	8	9	10

External Terminal Connections

Nº	Line Type	Description	Shunt	Nº	Line Type	Description	Shunt	Nº	Line Type	Description	Shunt
1	Neutral	Power Input	-	47	Output	BPR					
2	Phase	Power Input	-	48	---	---					
3	GND	24v bus	-	49	Input	MFC 1					
4	24V	24v bus	-	50	Input	MFM					
5	GND	24v bus	-	51	Input	BPR					
6	24V	24v bus	-	52	Input	MFC 2					
7	GND	24v bus	-	53	Output	MFC 2					
8	24V	24v bus	-	54	Output	MFC 1					
9	GND	24v bus	-								
10	24V	24v bus	-								
11	GND	24v bus	-								
12	24V	24v bus	-								
13	GND	24v bus	-								
14	24V	24v bus	-								
15	GND	24v bus	-								
16	24V	24v bus	-								
17	GND	24v bus	-								
18	24V	24v bus	-								
19	analog	Pressure transducer	-								
20	analog	Pressure transducer	-								
21	analog	Pressure transducer	-								
22	analog	Pressure transducer	-								
23	analog	Pressure transducer	-								
24	analog	Pressure transducer	-								
25	analog	Pressure transducer	-								
26	analog	Pressure transducer	-								
27	---	---	-								
28	---	---	-								
29	---	---	-								
30	---	---	-								
31	---	---	-								
32	---	---	-								
33	---	---	-								
34	---	---	-								
35	---	---	-								
36	---	---	-								
37	---	---	-								
38	---	---	-								
39	24v	MFM	-								
40	GND	MFM	-								
41	24v	MFC 1	-								
42	GND	MFC 2	-								
43	24V	MFC 2	-								
44	GND	BPR	-								
45	24v	BPR	-								
46	Output		-								

Paralab
Rua Dr. Joaquim Manuel Costa 946, B
4420-437 Valbom
Gondomar

Electrical Scheme
FO186

S/N:
LOCATION: +L1 Main electrical closet

REV.	DATE	NAME	CHANGES
0	19/04/2023	Renato Vieira	

APPROVED BY: Miguel Mota
APPROVED ON:

SCALE 1 / 1
REVISION 0
PAGE 08